DISSERTATION

SUBMITTED TO THE
COMBINED FACULTIES FOR THE NATURAL SCIENCES AND FOR MATHEMATICS
OF THE RUPERTO-CAROLA UNIVERSITY OF HEIDELBERG, GERMANY

FOR THE DEGREE OF
DOCTOR OF NATURAL SCIENCES

PRESENTED BY

FRANZISKA MARIA ZICKGRAF, M.Sc.
BORN IN: SPEYER, GERMANY

ORAL-EXAMINATION: 28.09.2018

SPDEF IS A MEDIATOR OF TUMORIGENICITY IN SSEA1^{-} TUMOR-INITIATING CELLS IN HIGH-GRADE SEROUS OVARIAN CANCER

REFEREES:

PROF. DR. ANDREAS TRUMPP

PROF. DR. THOMAS HOFMANN

oîda ouk eidōs

"*Ich weiß, dass ich nicht weiß*."

Sokrates

ABSTRACT

High Grade Serous Ovarian Adenocarcinoma (HGSOC) is a highly aggressive disease with poor prognosis and the leading cause of gynecological tumor-related deaths. The poor prognosis is related to the fact that already during early stages tumor cells start to spread into the peritoneum. This metastatic spread and the colonization of organs located within the peritoneum are the biggest problems with regard to therapy of HGSOC. Tumors often consist of a functionally heterogeneous population of cancer cells with distinct features. Subsets of tumor cell populations are able to promote tumor progression, metastatic spread and colonization, as well as outgrowth of tumor cells at distant organs. Therefore, the identification and targeting of so-called tumor-initiating cells is crucial. Knowledge about the intrinsic features of tumor-initiating cells and targeting them may ultimately lead to tumor regression and improved patient survival. However, no conclusive evidence about markers for a tumor-initiating population has been provided so far and even less is understood regarding the molecular mechanisms driving tumor-initiating cancer cell populations in HGSOC.

My work shows that Stage Specific Embryonic Antigen 1 negative ($SSEA1^-$) cells are enriched for tumor-initiating abilities in human HGSOC. Furthermore, $SSEA1^-$ cells can give rise to both $SSEA1^-$ and $SSEA1^+$ cells whereas $SSEA1^+$ cells only give rise to $SSEA1^+$ cells demonstrating a hierarchical organization with $SSEA1^-$ cells being on top. Gene expression profiling demonstrated an enrichment of the transcription factor SAM-pointed ETS domain-containing factor (SPDEF) in $SSEA1^-$ cells. Lentiviral knockdown of SPDEF impaired *in vivo* tumor growth and *in vitro* colony formation, whereas overexpression of SPDEF resulted in increased colony formation *in vitro* and tumor formation *in vivo*. Strikingly, also $SSEA1^+$ cells acquired the capacity to initiate tumors *in vivo* and form colonies *in vitro* after SPDEF expression was re-introduced. I also show, that SPDEF negatively regulates the expression of the transcription factor Forkhead box protein A2 (FOXA2). FOXA2 overexpression resulted in decreased tumor-promoting capacity in an *in vivo* tumor formation assay.
Based on these results, I propose that the transcriptional programs modulated by SPDEF, as well as those genes changed due to suppressed FOXA2 target gene transcription, lead to increased survival, clonogenicity and stemness of $SSEA1^-$ $SPDEF^{high}$ $FOXA2^{low}$ cells and may therefore promote ovarian cancer tumor initiation and metastatic spread.

In summary, the data I generated indicate that SSEA1$^-$ cells represent a cellular subpopulation with increased tumor-initiating ability in HGSOC. These cells express higher levels of SPDEF, which exerts its tumorigenic potential by suppressing FOXA2 expression. Developing SPDEF inhibitors might be promising to target the SSEA1$^-$ tumor-initiating population and might ultimately lead to tumor regression and improved patient survival.

ZUSAMMENFASSUNG

Das Hochgradig Seröse Ovarialkarzinom (HGSOC) ist eine äußerst aggressive Erkrankung mit schlechter Prognose und die führende Ursache gynäkologischer, tumorassoziierter Letalität. Tumorzellen metastasieren bereits sehr früh im Laufe der Erkrankung. Diese frühe metastatische Ausbreitung und die Besiedlung von Organen im Peritoneum stellen das größte klinische Problem in der Behandlung des HGSOC dar. Tumore bestehen oft aus einer heterogenen Population von verschiedenartigen Tumorzellen, von denen nur bestimmte Zellen in der Lage sind die Tumorprogression und Metastasierung zu initiieren. Daher ist die Identifizierung solcher tumorinitiierenden Zellen von größter Bedeutung. Wissen über die intrinsischen Eigenschaften dieser tumorinitiierenden Zellen und die Entwicklung von Medikamenten gegen diese, könnten letztendlich zu einer Tumorregression und verbessertem Patientenüberleben führen. Für das humane HGSOC wurden jedoch bisher keine Daten hinsichtlich Oberflächenmolekülen, die eine funktionelle tumorinitiierende Population charakterisieren, publiziert. Weiterhin ist noch weniger über die molekularen Mechanismen, die die tumorinitiierenden Zellen im Ovarialkarzinom auszeichnen, bekannt.

Die Ergebnisse meiner Arbeit zeigen, dass Zellen, die keine Expression des Stadiums-spezifische Embryonalen Antigens 1 ($SSEA1^-$) zeigen, für tumorinitiierende Zellen im HGSOC angereichert sind. Des Weiteren generieren $SSEA1^-$ Zellen sowohl wiederum $SSEA1^-$ als auch $SSEA1^+$ Zellen, $SSEA1^+$ hingegen ausschließlich $SSEA1^+$ Zellen. Dies zeigt den hierarchischen Aufbau des HGSOC mit $SSEA1^-$ Zellen an der Spitze. Genexpressionsanalysen zeigten eine Überexpression des Transkriptionsfaktors SAM-pointed ETS-Domäne-enthaltender Faktor (SPDEF) in $SSEA1^-$ Zellen. Die lentivirale Inhibition der SPDEF Expression beeinträchtigt die *in vitro* Kolonienbildung und das Tumorwachstum *in vivo*. Die Überexpression von SPDEF hingegen resultierte in einer gesteigerten Kolonienbildung *in vitro* und Tumorbildung *in vivo.* Durch die Überexpression von SPDEF in weniger aggressiven $SSEA1^+$ Zellen konnten wir deren Fähigkeit, Tumore zu initiieren und Kolonien zu formen, massiv erhöhen, was zeigt, dass SPDEF alleine ausreicht um die Tumorigenizität zu steigern. Des Weiteren konnten wir zeigen, dass SPDEF den Transkriptionsfaktor Forkhead Protein A2 (FOXA2) negativ reguliert. Die Überexpression von FOXA2 selbst zeigte ein tumorsuppressives Potential.

Basierend auf meinen Ergebnissen propagiere ich hiermit ein Modell, das durch die Induktion oder Repression von durch SPDEF regulierten Genen, sowie durch die durch FOXA2 veränderte Genexpression, zu einem verbesserten Überleben und einer erhöhten Klonogenizität von SSEA1^{-} SPDEF^{hoch} FOXA2^{niedrig} Zellen führt, und dadurch, zur Initiierung von Eierstockkrebs und dessen Metastasierung.

Zusammengefasst lässt sich sagen, dass ich SSEA1^{-} Zellen als tumorinitiierende Ovarialkarzinomszellen entdeckt und funktionell charakterisiert habe. Diese Zellen produzieren mehr SPDEF und dieser Transkriptionsfaktor übt seine pro-tumorigene Funktion durch die Reduktion der FOXA2 Expression aus. Eine zielgerichtete Therapie, die gegen SSEA1^{-} Ovarialkarzinomszellen gerichtet ist, könnte durch die Entwicklung von SPDEF Inhibitoren möglich sein. Diese Blockade von SPDEF könnte zu einer Tumorregression und möglicherweise zu einem verlängerten Überleben von Patienten mit Ovarialkarzinom führen.

CONTENTS

1. INTRODUCTION

1.1 Ovarian Cancer

1.1.1 General

High grade serous ovarian cancer (HGSOC) is among the most malignant solid tumors and the leading cause of gynecological-cancer associated deaths. Five-year overall survival rate is 47 % and drops to only 29 % when the tumor is also located at distant sites (Siegel *et al.,* 2018). While only 15 % of all ovarian tumors are only localized to the ovary, the vast majority of tumors (60 %) are also situated at distant organs. This can be explained by the late diagnosis of the disease.

Risk factors of ovarian cancer include number of ovulatory cycle, advanced age, positive familial background for ovarian, breast or uterine tumors, as well as hereditary mutations of BRCA1/2, TP53 or mismatch repair genes (Romero and Bast 2012). A positive factor preventing the development of ovarian cancer is the use of oral contraceptives (Matulonis *et al.,* 2016).

1.1.2 Pathophysiology

Although once considered as a single disease, different subtypes of ovarian cancer can now be diagnosed based on their tissue origin. Different histotypes resemble epithelial cells of cervical glands (mucinous type), endometrium (endometrioid type), vaginal rests (clear cell type) or fallopian tube (serous type) (Romero *et al.,* 2012). An overview of the histological subtypes is given in figure 1. These histotypes have been linked to expression of the HOX genes HOXA9, HOXA10 and HOXA11 which normally regulate gynecological differentiation (Cheng *et al.,* 2005).

Ovarian cancer can further be distinguished into low-grade and high grade ovarian cancer. Low-grade cancers include mucinous, clear cell, endometrioid and serous cancers, whereas high-grade ovarian cancers are of the serous, endometrioid and undifferentiated types (Romero *et al.,* 2012). Low grade tumors carry mutations in KRAS, BRAF and PIK3CA, as well as microsatellite instability, loss of heterozygosity on chromosome Xq and amphiregulin expression (Bast *et al.,* 2009). However, high-grade serous ovarian tumors are characterized by TP53 aberrations and eventually BRCA1 and BRCA2, as well as loss of heterozygosity on chromosomes 7q and 8q (Bast *et al.,* 2009).

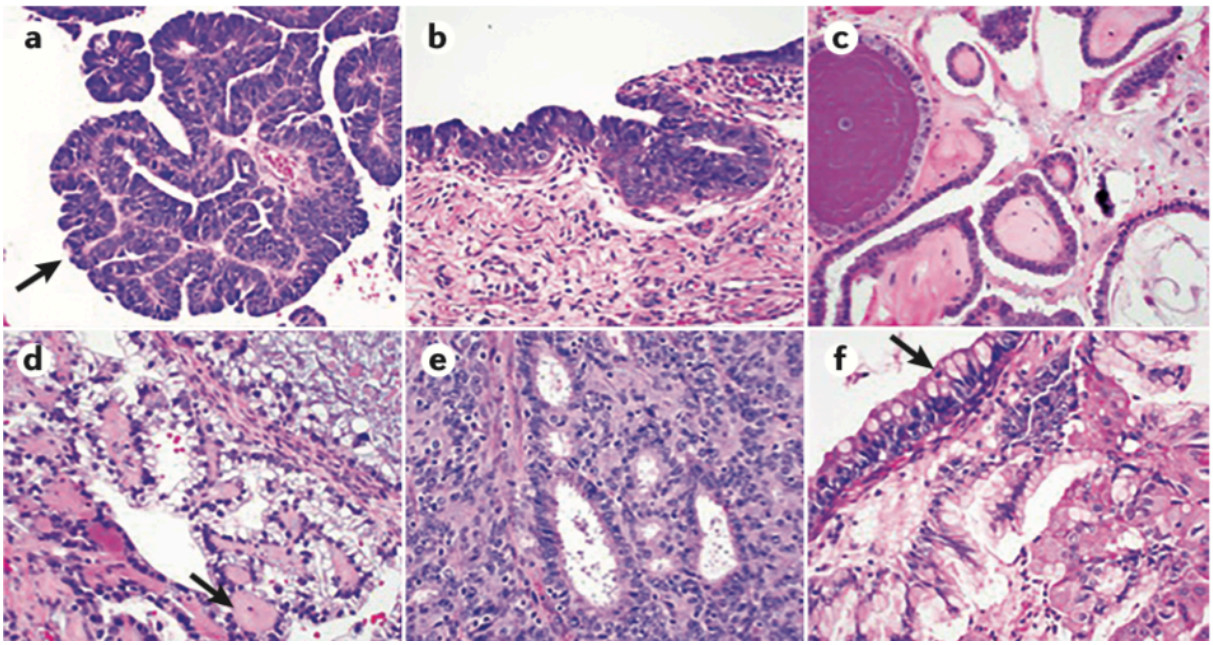

Figure 1: Histological subtypes of ovarian cancer.
(a) High-grade serous ovarian carcinoma is characterized by atypia, high nuclear-to-cytoplasmic ratio and many mitoses. The arrow depicts papillary architecture. (b) Serous tubal intraepithelial lesions are similar to HGSOC with severe atypia, many mitoses and lack of polarity. (c) Low-grade serous ovarian carcinoma also shows papillary architecture, but mild atypia and a low nuclear-to-cytoplasmic ratio. (d) Clear-cell carcinoma is characterized by large atypical tumor cells. The arrow depicts the characteristic stromal hyalinization. (e) Endometrioid adenocarcinoma is defined by gland formation and nuclear atypia. (f) Mucinous adenocarcinoma show mucin-filled cells. The arrow indicates goblet cell forms present. Figure was adapted from (Matulonis *et al.,* 2016).

Ovarian tumors spread through blood and lymphatic vessels and metastasize to distant organs including the liver, lung and brain. Due to the original location of ovarian tumors, they spread into the abdominal cavity and form small tumor nodules on the omentum and peritoneum during early stages of the disease (Romero *et al.,* 2012). Ovarian tumors are staged according to the scheme depicted in table 1.

Table 1: Staging of ovarian cancer.
Table was adapted and modified from (Matulonis *et al.,* 2016).

FIGO stage	Description	TNM stage
I	Tumor confined to ovaries or fallopian tubes	T1
IA	Tumor limited to one ovary (with ovarian capsule intact) or fallopian tube; no tumor on ovarian or fallopian tube surface; no malignant cells in the ascites or peritoneal washings	T1a
IB	Tumor limited to both ovaries (with ovarian capsules intact) or fallopian tubes; no tumor on ovarian or fallopian tube surface; no malignant cells in the ascites or peritoneal washings	T1b
IC	Tumor limited to one or both ovaries or fallopian tubes, with any of the following C substages: • IC1: surgical spill intraoperatively • IC2: capsule ruptured before surgery or tumor on ovarian or fallopian tube surface • IC3: malignant cells in the ascites or peritoneal washings	T1c
II	Tumor involves one or both ovaries, or the fallopian tubes with pelvic extension below the pelvic brim or primary peritoneal cancer (Tp)	T2
IIA	Extension and/or implants of tumor on uterus and/or fallopian tubes and/or ovaries	T2a
IIB	Extension of tumor to other pelvic intraperitoneal tissues	T2b
III	Tumor involves one or both ovaries, the fallopian tubes, primary peritoneal cancer with cytologically or histologically confirmed spread to the peritoneum outside the pelvis and/or metastasis to the retroperitoneal lymph nodes	T3
IIIA	Metastasis to the retroperitoneal lymph nodes with or without microscopic peritoneal involvement beyond the pelvis IIIA1: positive retroperitoneal lymph nodes only (pathologically proven) • IIIA1(i): metastasis up to 10 mm in greatest dimension • IIIA1(ii): metastasis >10 mm in greatest dimension	T1, T2, T3aN1
	IIIA2: microscopic extrapelvic (above the pelvic brim) peritoneal involvement with or without positive retroperitoneal lymph nodes	T3a/T3aN1
IIIB	Macroscopic peritoneal metastasis beyond the pelvis up to 2 cm in greatest dimension, with or without metastasis to the retroperitoneal lymph nodes	T3b/T3bN1
IIIC	Macroscopic peritoneal metastasis beyond the pelvis >2 cm in greatest dimension, with or without metastasis to the retroperitoneal lymph nodes	T3c/T3cN1
IV	Distant metastasis excluding peritoneal metastases • IVA: pleural effusion with positive cytology • IVB: parenchymal metastases and metastases to extra-abdominal organs (including inguinal lymph nodes and lymph nodes outside of the abdominal cavity)	AnyT,anyNorM1

1.1.3 Treatment and surgery

Treatment of ovarian cancer at early stages of the disease aims at curing and includes surgery. At later stages of the disease, cytoreductive surgery is used to reduce the tumor burden (Matulonis *et al.,* 2016). Although, the five-year survival rate has been improved by surgery, the long-term survival of patients is still low due to the heterogeneity of the disease (Bast *et al.,* 2009).

About 70 % of patients initially benefit from platinum- (carboplatin and cisplatin) and taxane-based (paclitaxel and docetaxel) chemotherapy after surgery; however some drug-resistant cells survive and remain dormant which leads to recurrence of ovarian tumors (Bast *et al.,* 2009). Patients with advanced ovarian cancer having undergone platinum-and taxane-based chemotherapy have a median overall survival of five years (Ozols *et al.,* 2003). Despite initial response, the majority of patients relapse and only 29 % survive longer than five years (Siegel *et al.,* 2018). Second-line chemotherapeutic treatments besides platinum- and taxane-based chemotherapy include anti-angiogenic agents and poly (ADP-ribose) polymerase (PARP) inhibitors. Immunological therapies are also currently under investigation (Matulonis *et al.,* 2016). Further agents applied include doxorubicin, topotecan, etopside and gemcitabine (ten Bokkel Huinink *et al.,* 1997, Rose *et al.,* 1998, Gordon *et al.,* 2001, Ferrandina *et al.,* 2008).

Targeted therapies are of increasing importance in the treatment of cancers. Unfortunately, no effective targeted therapy to treat ovarian tumors has been approved to date. A clinical phase III trial of the VEGF inhibitor bevacizumab showed an overall survival advantage of only 2 weeks, but approximately 4 months of increased progression-free survival (Perren *et al.,* 2011, Oza *et al.,* 2015). For a subset of patients, namely BRCA1/2 mutant-bearing patients, the targeted agents olaparib, niraparib and rucaparib, which are PARP inhibitors, have recently been approved (Coleman *et al.,* 2017, Pujade-Lauraine *et al.,* 2017, Konstantinopoulos PA *et al.,* 2018). Median progression-free survival was increased for 14 months for the olaparib treatment arm compared to placebo (Pujade-Lauraine *et al.,* 2017). Other targeted therapies under investigation include the c-Kit and PDGFR inhibitor masatinib, the PD-1 inihbitor pembrolizumab, the mTOR inhibitor temsorilimus and the c-Met and VEGFR2 inhibitor cabozantinib (U.S. National Library of Medicine 2018).

Further research is necessary to identify key signaling molecules in ovarian cancer and to design targeted agents against these. In this context, substratification of patients based on molecular markers will be crucial.

1.1.4 Key signaling pathways, genetic alterations and molecular subtypes

Ovarian cancer is a remarkably heterogeneous disease, both at the molecular and cellular level (Bast *et al.,* 2009). Most ovarian cancers (96 %) harbor mutations in the tumor suppressor gene *TP53* (Cancer Genome Atlas Research 2011). *BRCA1* (5%) and *BRCA2* (5%) mutations are further common genetic abnormalities found in ovarian cancer patients. Patients with inherited DNA repair defects possess a high lifetime risk of developing ovarian cancer depending on the defect (*BRCA1* 30-60%, *BRCA2* 15-30%) (Bast *et al.,* 2009). Other mutated genes with a frequency of less than 5 % that have been implicated in ovarian cancer include *NF1, RB1, LRP1B, SETD2, CDK12, KMT2A* and *ARID1A* (International Cancer Genome *et al.,* 2010, Cancer Genome Atlas Research 2011). Further genetic abnormalities in ovarian cancers are summarized in table 2.

Table 2: Genetic abnormalities in ovarian cancer.
Table was adapted from (Bast *et al.,* 2009). NA = not applicable, ND = not determined.

event	effect	Chromosome	Gene
Gene amplification	Activation	1q22, 3q26, 5q31, 8q24, 19q, 20p, 20q13.2	*RAB25, PRKCI, EVI1, PIK3CA, FGF1, MYC, PIK3R1, AKT2, ND, AURKA*
Gene deletion	Inactivation	4q, 5q, 16q, 17p, 17q, Xp and Xq	ND
Mutation	Activation	NA	*KRAS* (15%), *BRAF* (12%), *CTNNB1* (12%), *CDKN2A* (10%), *APC* (9%), *PIK3CA* (8%), *KIT* (7%) and *SMAD4* (7%)
Hypomethylation	Activation	NA	*IGF2* and *SAT2*
Loss of heterozygosity	Inactivation	17p13 and 17q21 (in 50% of cases or more) 1p, 3p, 5q, 5q, 6q, 7q and 8q (in fewer than 30% of cases)	*ARHI*, *PEG3, PLAGL1, RPS6KA2, TP53, BRCA1, BRCA2, PTEN, OPCML* and *WWOX*
Mutation	Inactivation	NA	*TP53* (62%), *BRCA1* (5%), *BRCA2* (<5%) and *PTEN* (3–8%)
Promoter methylation	Inactivation	NA	*ARHI, DAPK1, CDH13, MLH1, ICAM1, PLAGL1, DNAJC15, MUC2, OPCML, PCSK6, PEG3, CDKN2A, CDKN1A, RASSF1, SOCS1, SOCS2, PYCARD* and *SFN*

In ovarian cancers, more than 7 signaling pathways are activated in > 50 % of tumors (Bast *et al.,* 2009). Besides defects in homologous recombination, *FOXM1* (84 %) and *NOTCH* (22 %) signaling pathways have been implicated in serous ovarian cancer pathophysiology. *RB1* and *PI3K/RAS* pathways were further altered in 67 % and 45 % of serous ovarian cancer samples, respectively (Cancer Genome Atlas Research 2011). Further pathways implicated in the disease progression include *JAK2-STAT3* signaling driven by autocrine IL6 which is overexpressed in most ovarian cancers (Rosen *et al.,* 2006). NF-κB transcription factor network is another signaling pathway which is overexpressed in > 50 % of ovarian cancers. Activation of NF-κB signaling (figure 2) upregulates anti-apoptotic genes and growth-promoting cytokines to support ovarian cancer progression (Samanta *et al.,* 2004, Lin *et al.,* 2007, Matulonis *et al.,* 2016). Lysophosphatic acid is produced by the phosphodiesterase D and binds to the G-protein –linked receptors LPAR2 and LPAR3, thereby promoting primary tumor growth and metastasis (Murph *et al.,* 2006). The LPA signaling pathway is activated in about 90 % of ovarian cancers (Bast *et al.,* 2009). Further signaling pathways that have been implicated in ovarian cancer pathogenesis include Hedgehog, WNT and TGF-β signaling (figure 2) (Schmid *et al.,* 2011, Szkandera *et al.,* 2013, Basu *et al.,* 2015).

In addition to molecular aberrations and defective signaling pathways, four transcriptional subtypes (mesenchymal, differentiated, immunoreactive and proliferative) have been identified based on transcriptional profiling. Furthermore, four promoter methylation subtypes and three microRNA subtypes within serous ovarian cancer have been characterized (Cancer Genome Atlas Research 2011). Another study showed an association of the mesenchymal subtype with a microRNA-regulated network and linked this to poor overall survival (Yang *et al.,* 2013).

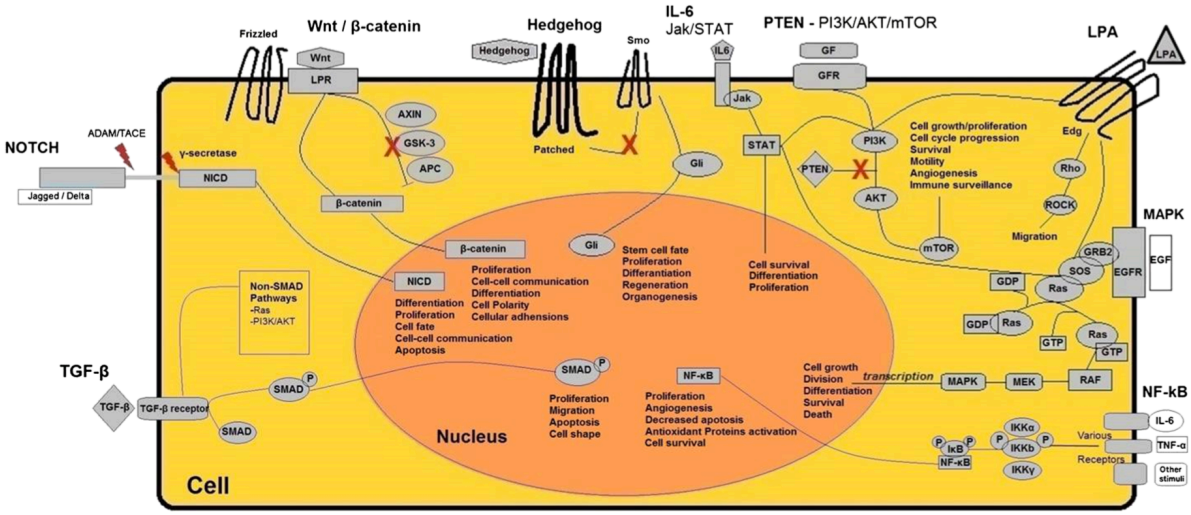

Figure 2: Key signaling pathways implicated in the progression of ovarian cancer.
The main signaling pathways in ovarian cancer are PI3K-RAS, NF-κB, LPA, JAK-STAT, NOTCH and FOXM1 signaling. Besides, Hedgehog, WNT and TGF-β signaling have been implicated in the pathogenesis of ovarian cancer. Figure was adapted from (Kotsopoulos *et al.,* 2014).

1.1.5 Disease models

Models of ovarian cancer include genetically-defined mouse models, as well as xenografts and cell lines. Since the cell of origin of epithelial ovarian cancer is still not clear, the limited knowledge about ovarian cancer etiology has subsequently resulted in a limited development of genetically-defined mouse models. Although the fallopian tube and the ovarian surface epithelium (OSE) are considered as tissue of origin for epithelial ovarian tumors (Dubeau 1999, Kurman and Shih Ie 2008, Morin and Weeraratna 2016), no promoters that specifically drive transgene expression and the disease have been identified so far. However, up to 60 % of patients with epithelial ovarian cancer also present with serous intraepithelial carcinoma lesions (STIC) in their fallopian tubes, linking theses lesions to epithelial ovarian cancer (Kindelberger *et al.,* 2007).

The first described genetically-defined mouse model of epithelial ovarian cancer used the avian retroviral receptor system (TVA) and the keratin-5 and β-actin promoters. While the keratin-5 promoter restricted expression of TVA to the OSE, the β-actin promoter led to its expression within the whole ovary (Orsulic *et al.,* 2002). These mice were then crossed with $p53^{-/-}$ null mice. Both mouse models could then be infected with oncogenes in a retroviral

system. The mice with either the keratin-5 or β-actin promoters gave rise to tumors, concluding that the OSE was the tissue of origin for epithelial ovarian cancer (table 3).
Another mouse model was engineered using the Müllerian promoter MISIIR to express the SV40 T antigen. The MISIIR is mainly expressed in the OSE but also the fallopian tube. These mice developed tumors at the age of 6 to 13 weeks (Connolly *et al.,* 2003). Other genetically-defined mouse models are summarized in table 3.

Table 3: Genetically-defined mouse models of epithelial ovarian cancer.
The table was adapted and modified from (Fong and Kakar 2009)

promoter	targeted gene	tumorigenesis	reference
keratin-5 or β-actin	TVA, $p53^{-/-}$, oncogenes	yes	(Orsulic *et al.,* 2002)
MISIIR	SV40TAg	yes	(Connolly *et al.,* 2003)
AdCRe	$p53^{-/-}$ & $Rb^{-/-}$,	yes	(Flesken-Nikitin *et al.,* 2003)
AdCre	Kras & $Pten^{-/-}$	yes	(Dinulescu *et al.,* 2005)
AdCre	$Pten^{-/-}$ & $APC^{-/-}$	yes	(Wu *et al.,* 2007)
FSHR	Cre, $Brca1^{-/-}$	no	(Chodankar *et al.,* 2005)
AdCre	$Brca1^{\Delta 5\text{-}13}$	no	(Clark-Knowles *et al.,* 2007)
MISIIR	Pttg	no	(El-Naggar *et al.,* 2007)
MISIIR	Pik3ca	no	(Liang *et al.,* 2009)

A different approach of studying ovarian cancer lies in the xenotransplantation of pieces of primary ovarian patient tumors into NSG mice that are non-obese diabetic mice with severe combined immunodeficiency (NOD/SCID) and are also deficient for NK cells (NOD/SCID Il $2rg^{-/-}$) (Greiner *et al.,* 1995, Ito *et al.,* 2002). The advantage of xenograft models lies in the preservation of tumor heterogeneity both when transplanted into NSG mice in which the patient characteristics are contained and stromal-tumor cell interactions are reflected, as well as in cell culture when cultured under CSC conditions allowing tumor progression to be adequately studied. However, xenograft models are space-occupying and are not feasible regarding large-scale drug screens. Thus, cell lines established from ovarian cancers are used. However, these are mostly cultured under FCS conditions resulting in the loss of heterogeneity of the original tumor in most of the cell lines. Additionally, morphological

characteristics are often lost when these cell lines are xenotransplanted into NSG mice (Lee *et al.,* 2006).

Due to these reasons, our lab established a patient-matched xenograft model of primary tumors. The HGSOC xenograft model used in this thesis was established by Wagner *et al.* and myself (Wagner 2013). This model is comprised of primary tumor pieces, matched patient-derived xenografts, resulting in established patient-matched serum-free cell cultures under CSC conditions. The patient-derived xenografts were established by transplanting pieces of primary tumors subcutaneously into NSG mice in order to expand the tumor material. The outgrowing tumors were then further digested so that a single cell suspension was obtained. From this, a serum-free cell line was established under CSC conditions. To prove that the established cell line is tumorigenic, the cells were again injected s.c. into NSG mice and assessed for tumor outgrowth (figure 3 a). The model was established in order to preserve the heterogeneity of the original patient tumors, both in the xenografted tumors but also in cell culture. To preserve the cellular heterogeneity under cell culture conditions, cells were cultured without FCS and in a CSC medium with few, well-defined factors considered to retain stemness (3.1.5). When xenografting the primary patient tumor pieces, the cellular heterogeneity, as well as characteristic markers of ovarian tumors, cancer antigen 125 (CA125) and Wilms tumor 1 (WT1) were preserved (figure 3 b). However, when xenografting SKOV3 cells, no heterogeneity and no expression of CA125 and WT1 could be detected (figure 3 b).

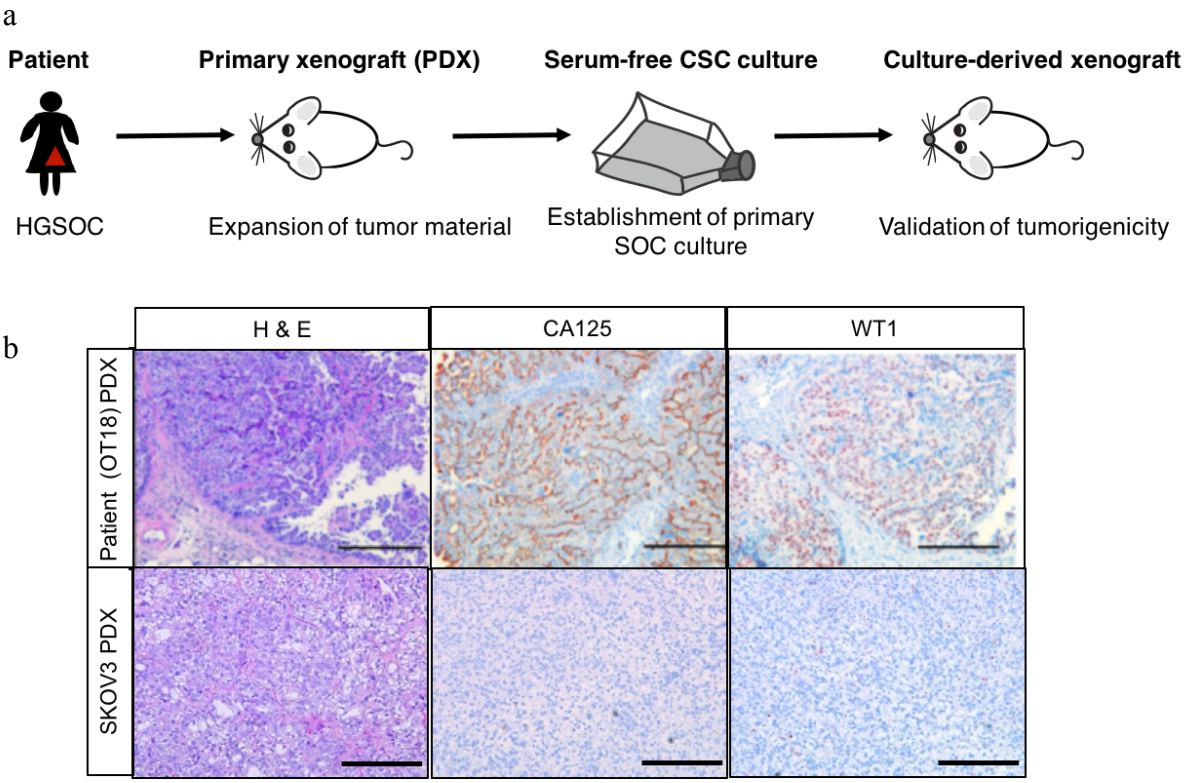

Figure 3: Patient-matched xenograft model of high-grade serous ovarian cancer.
(a) A patient-derived model of HGSOC was established by transplanting pieces of primary tumors s.c. into NSG mice in order to expand the tumor material. The outgrowing tumors were then further digested in that a single cell suspension was obtained. From this, a serum-free cell line was established under CSC conditions. To prove that the established cell line is tumorigenic, the cells were again injected s.c. into NSG mice and assessed for tumor outgrowth. (b) Comparison of patient-derived xenografts (PDX) of patient OT18 and the conventional SKOV3- cell line regarding histology and the expression of the ovarian cancer-associated markers CA125 and WT1, which can only be detected in the OT18-derived xenograft. Scale bar denotes 100 µm Immunohistochemical stainings were adapted and modified from (Wagner 2013).

1.2 Tumor heterogeneity

1.2.1 Cancer heterogeneity

Cancer has long been considered as one disease and to consist of a homogeneous population of cells. Tumor progression itself was perceived as accumulation of genetic aberrations (Foulds 1954, Nowell 1976). However, tumors consist of a heterogeneous population of cells which differ regarding their molecular aberration, morphology, differentiation status and activation of signaling pathways.

Key issues in the field address the question whether tumor subtypes arise due to different cells of origin giving rise to heterogeneous populations of cells or whether the subtypes evolve

from a single cell. The molecular differences and mechanisms leading to tumor heterogeneity are still largely unknown. Tumors can be heterogeneous due to intratumoral or intertumoral heterogeneity. Intertumoral heterogeneity, variability of tumor cells arising from the same tissue of origin, is considered to evolve due to different tumor-initiating cells or a single cell undergoing different oncogenic events between tumors. Intratumoral heterogeneity arises due to a single cell undergoing various oncogenic changes and thus, giving rise to different tumor subtypes within a tumor (Visvader 2011).

In addition, the microenvironment of the tumor cells contributes to inter- and intratumoral heterogeneity due to interaction of immune, stromal, endothelial and other cell types with the cancer cells (Tlsty and Coussens 2006, Polyak *et al.,* 2009). Further, the existence of cancer stem cells (CSC) and their evolution during tumor progression contributes to tumor heterogeneity (Visvader and Lindeman 2012, Beck and Blanpain 2013).

However, none of these mechanisms contributing to tumor heterogeneity is exclusive. Moreover, all of them act together and form a complex network of interacting cells which ultimately, drives tumor progression. Taken together, cancer is today perceived as many different diseases which should be also treated in a targeted manner.

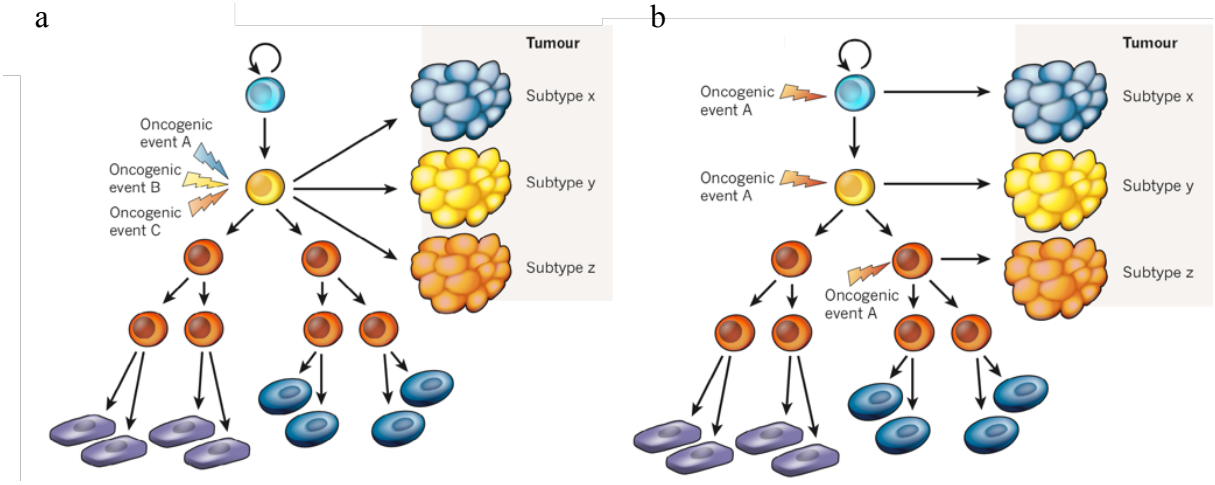

Figure 4: Models of intertumoral heterogeneity.
(a) In the genetic mutation model, different oncogenic events in a cell give rise to different tumor subtypes. (b) Different cells of origin within a hierarchy give rise to different tumor subtypes. Figure was adapted from (Visvader 2011).

1.2.1 Cell of origin

The cell of origin of cancer is assumed to be a cell which obtains tumorigenic capacities due to multiple genetic and epigenetic events and gives rise to a clonal population of cancer cells which further evolve during tumor progression and build a heterogeneous tumor.

The cell of origin of a tumor is not necessarily a cancer stem cell, it can also be a normal tissue cell which acquired tumorigenic capacities. Cancer stem cells however, can arise later during tumor progression from the initial cell of origin. Thus, a cell of origin of a tumor can either be a normal tissue cell which acquired tumorigenic characteristics or a stem cell which acquired tumor-promoting characteristics (Visvader 2011).

It is thought that epithelial ovarian cancer arises from the ovarian surface or from subsurface or cortical inclusion cysts (Feeley and Wells 2001, Bast *et al.,* 2009). Also, the lining of the fallopian tube, deposits of endometriosis or the surface of the peritoneal cavity have been considered as the tissue of the cell of origin of ovarian cancer (Bast *et al.,* 2009).

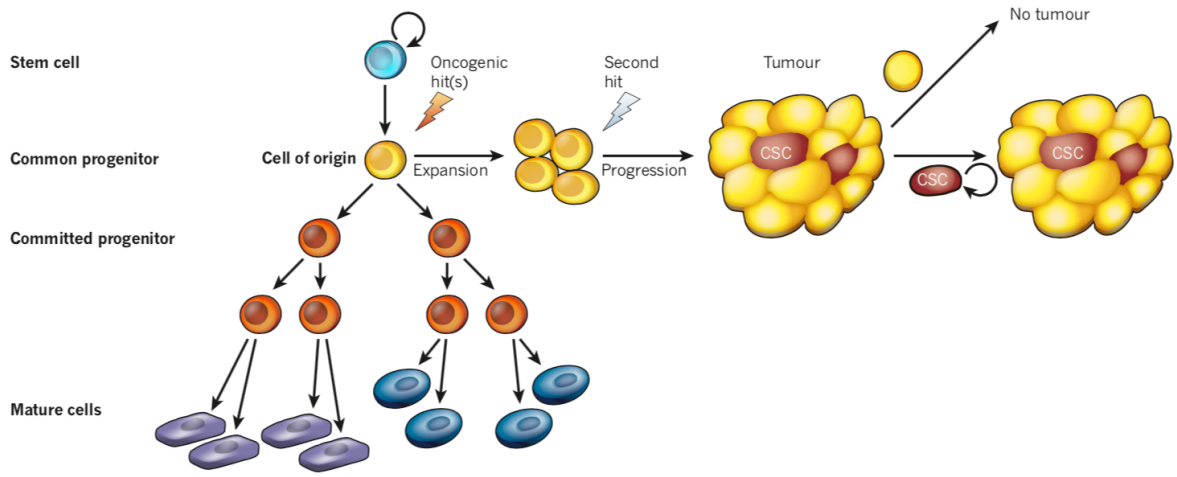

Figure 5: The cell of origin model and the evolution of cancer stem cells.
Tissues are organized in a hierarchical way (left). The cell of origin of a tumor can be either a normal tissue cell which acquired tumorigenic characteristics or a stem cell which acquired tumor-promoting characteristics. Tumor cells derived from tissue progenitor cells (yellow) gave rise to a tumor and with tumor progression, gained oncogenic capacities leading to the development of a cancer stem cell (CSC, red). In this model, only CSC can maintain the tumor, other tumor cells are not able of sustaining tumorigenesis (right). Figure was adapted from (Visvader 2011).

1.2.2 Cancer stem cells

Similar to the clonal evolution theory (Nowell 1976) which implies that genetic and epigenetic changes arise in tumor cells and confer a growth advantage for them, the cancer stem cell (CSC) theory says that tumor cells are organized in a hierarchical way in such that only a small subset of cells is responsible for sustaining tumorigenesis. These cells give rise to the cellular heterogeneity of the tumor and establish its phenotype (Visvader *et al.,* 2012).

CSC exhibit self-renewal, differentiation and stemness features, but they are not necessarily derived from transformation of a normal tissue stem cell. CSC can originate from a normal cell that acquired stem cell features over time. Moreover, tumors may harbor multiple genetically distinct CSC subpopulations and thus, different phenotypes. The phenotype of CSC may also vary between patients. In addition, metastatic CSC can evolve from primary CSC. A tumor can itself also undergo reversible phenotypic changes (Visvader *et al.,* 2012).

CSC exist in various tumors. The first evidence for CSC has been demonstrated by Dick and colleagues (Bonnet and Dick 1997). Dick *et al*. showed that $CD38^-$ / $CD34^+$ cells are the leukemic stem cells and thus compromise the tumorigenic population in acute myeloid leukemia. Further CSC have been identified in other tumor entities. In glioblastoma, $CD133^+$ cells have been shown to possess increased self-renewing potential (Singh *et al.,* 2003). In breast tumors, $CD44^+$ / $CD24^-$ cells have been identified as the tumor-initiating population which could also be serially passaged and gave rise to new tumors (Al-Hajj *et al.,* 2003). Other tumors in which CSC have been identified include prostate cancer ($CD133^+$ / $CD44^+$ / integrin $\alpha2\beta1^{high}$) (Collins *et al.,* 2005) and melanoma ($CD271^+$) (Boiko *et al.,* 2010). However, CSC do not account for functional heterogeneity in all tumors.

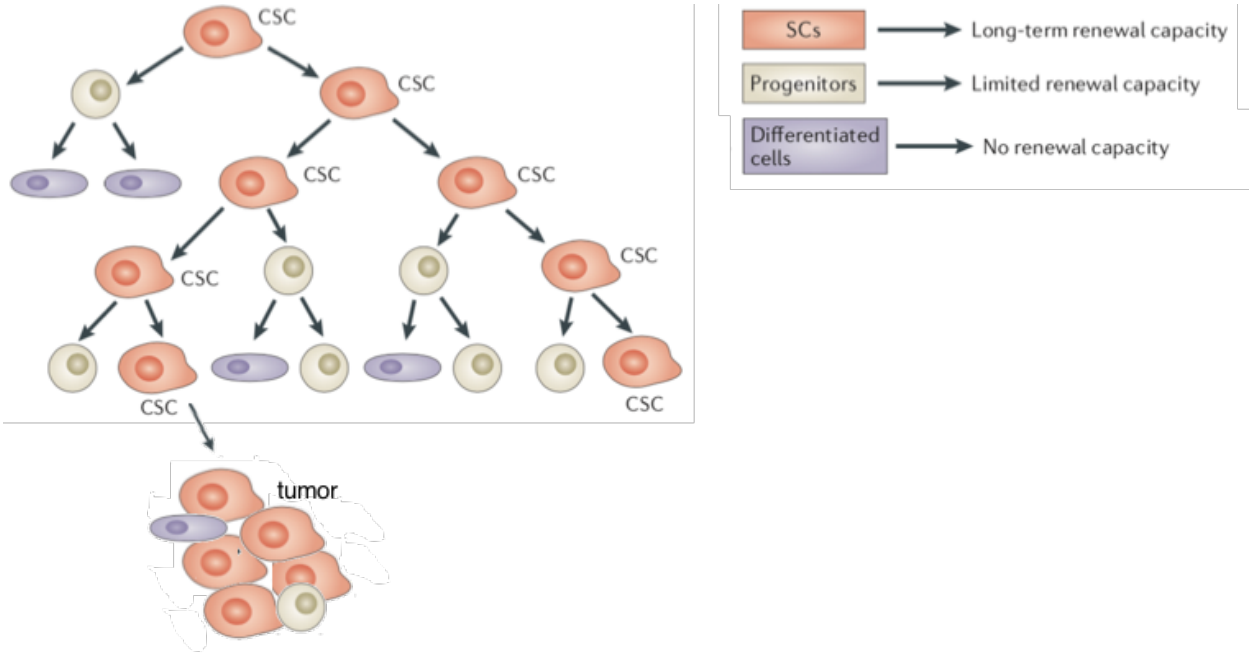

Figure 6: The Cancer stem cell model.
Tumors are organized in a hierarchical way and only a subset of tumor cells can give rise to new tumors. At the top of the hierarchy, a cancer stem cell (CSC, red) resides which gives rise to progenitor cells (purple) with limited self-renewal capacity and eventually, to terminally differentiated cells (beige). The CSC itself also possesses a long-term self-renewal capacity and maintains tumor growth. Figure was adapted and modified from (Beck *et al.,* 2013).

1.2.3 Cancer stem cells in ovarian cancer

In ovarian cancer, there is limited evidence for CSC (Bast *et al.,* 2009). It has been reported that the surface molecule CD44 enriched for tumors with increased metastatic potential and drug-resistance (Gao *et al.,* 2015). Further, Meng *et al.* showed that $CD44^+$ / $CD24^-$ cells contain an increased number of CSC (Meng *et al.,* 2012). Also, as few as 100 $CD44^+$ $CD117^+$ cells initiated tumors in xenograft models, whereas 10^5 $CD44^-$ $CD117^-$ could not (Zhang *et al.,* 2008). Other studies showed that $CD44^+$ $MYD88^+$ cells possess tumor-initiating activity, chemoresistance and constitutive NF-κB signaling as compared to $CD44^-$ $MYD88^-$ (Alvero *et al.,* 2009). Moreover, CD133 expression correlated with decreased survival and decreased response to chemotherapy (Zhang *et al.,* 2012). Further markers that have been implicated as potential CSC markers include ALDH1A1 and CD117 (Lupia and Cavallaro 2017). The known putative CSC markers in ovarian cancer are summarized in table 4.

Table 4: Ovarian cancer stem cell markers.
The table was adapted and modified from (Lupia *et al.,* 2017).

marker	biological function	Lowest number of tumorigenic CSC
CD24	Transmembrane glycoprotein. Activates STAT3. Stemness, cell adhesion, metastasis	5000
CD44	Hyaluron receptor. Stimulates EGFR-RAS-ERK. Cell proliferation, differentiation, chemoresistance	100 ($CD44^+$ / $CD117^+$)
CD117	Receptor tyrosine kinase. Regulates PI3K/AKT, RAS/ERK, Src and JAK/STAT pathways. Cell signaling, apoptosis, cell differentiation proliferation, cell adhesion.	1000
CD133	Transmembrane glycoprotein. PI3K/AKT pathway. CSC maintenance, tumor formation, chemoresistance.	100
ALDH1A1	Aldehyde dehydrogenase enzyme. CSC maintenance	-

1.3 Glycans

It is still unclear how stem cells maintain their self-renewal and, especially in the case of cancer stem cells, tumor-initiating capacities. Post-translational modifications of proteins as phosphorylation, sumoylation, methylation, acetylation, ubiquitination and glycosylation among other mechanisms have been considered to play a role in the maintenance of stemness (Wang *et al.,* 2014). These modifications change the function of proteins (Haltiwanger 2002) and extend it beyond gene expression in that a tighter control of pluripotency, reprogramming and differentiation is possible (Wang *et al.,* 2014).

Glycans – oligosaccharides – are attached to proteins and lipids and form a glycocalyx on the cell surface but are also attached to intracellular proteins (Lanctot *et al.,* 2007). Glycans are generated by many enzymes including glycosyltransferases, fucosyltransferases and many others. Aberrant glycosylation is defined as a loss of expression, an excessive glycosylation or truncated forms of glycans and sometimes also the appearance of new glycosylated structures (Varki *et al.,* 2015).

Glycans can isolate specific stem cell lineages. SSEA3, SSEA4, TRA1–60 and TRA1–81 are expressed in embryonic stem cells (Lanctot *et al.,* 2007, Varki *et al.,* 2015) and SSEA1 has been shown to be expressed in glioblastoma tumor-initiating cells (Son *et al.,* 2009).

It has further been demonstrated that O-GlcNac of Oct4 and Sox2 in mouse embryonic stem cells enhances the transcriptional activity of these genes and thus, the increased transcription of pluripotency-related genes (Jang *et al.,* 2012).

Glycosylation plays a role in many cellular processes including signal transduction (Haltiwanger 2002), cell-cell interactions (Fogel *et al.,* 2010), immune responses (Rudd *et al.,* 2001, Marth and Grewal 2008), protein structure (Balog *et al.,* 2010), regulation of pluripotency, embryonic development (Yan *et al.,* 2010) and also cancer development (Varki *et al.,* 2009, Wang *et al.,* 2014, Varki *et al.,* 2015). For example, Notch signaling has been described to be tightly regulated by glycosylation. The addition of fucose and N-acetylglucosamine residues to Notch enables binding of its ligands delta and serrate thereby modulating Notch signaling and also cell fate determination (Moloney *et al.,* 2000, Moloney *et al.,* 2000, Yang *et al.,* 2005).

Differential expression of fucosyltransferases and N-acetylglucosaminyltransferases have been implicated in either promoting tumors or suppressing tumor progression (Varki *et al.,* 2015). In colorectal cancer cell lines, suppression of fucosylation of TGFβ receptors type 1 led to inhibition of downstream phosphorylation and inihbition of invasion and migration, as well as inhibition of EMT (Hirakawa *et al.,* 2014). Further, sialyation and fucosylation of EGF receptors has been demonstrated to suppress its dimerization and phosphorylation, thus inhibiting downstream signaling and invasion of lung cancer cells (Liu *et al.,* 2011).

However, inhibition of ST6GalI-mediated sialylation in colon cancer cells has been shown to increase tumor cell proliferation *in vitro* and *in vivo* and further increased the effect of the EGFR-inhibitor gefitinib (Park *et al.,* 2012). In ovarian cancer, however, increased ST6GalI expression increased EGFR activation and protected against gefitinib-induced cell death (Britain *et al.,* 2018).

1.4 Stage-specific embryonic antigen 1 (SSEA1)

Stage-specific embryonic antigen 1 (SSEA1), also called Lewis X or CD15 (figure 7), is a carbohydrate structure consisting of galactose β1→4-linked and fucose α1→3-linked to N-acetylglucosamine (Galβ1→4[Fucα1→3]GlcNAcβ1]) (Gooi *et al.,* 1981, Hakomori *et al.,* 1981). The SSEA1 epitope can be further modified by fucosylation, sialyation or sulfation (Hennen 2011, Varki *et al.,* 2015).

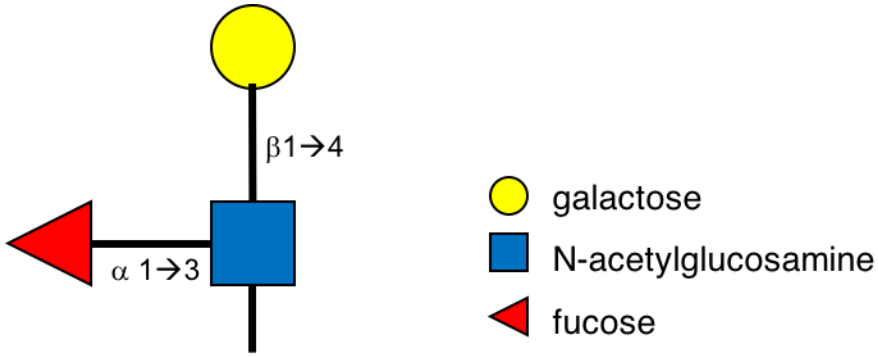

Figure 7: Structure of SSEA1.
SSEA1 consists of galactose (yellow) β1→4-linked and fucose (red) α1→3-linked to N-acetylglucosamine (blue) (Galβ1→4[Fucα1→3]GlcNAcβ1]).

SSEA1 is a carbohydrate structure which is carried by glycoproteins and glycolipids. Because of SSEA1 being a sugar structure, it is not defined by a gene but synthesized by various enzymes including fucosyltransferases 4 and 9 (FUT4, FUT9) (Nakayama *et al.,* 2001). Activation of glycosyltransferases and glycosidases seems to regulate SSEA1 expression (Knowles *et al.,* 1982).

SSEA1 was defined by the epitope detected by a monoclonal antibody derived by fusion of mouse myeloma cells with spleen cells from a mouse immunized with F9 teratocarcinoma cells (Solter and Knowles 1978). SSEA1 is an embryonic stage-specific antigen first detected on blastomeres of the 8-cell stage in mice (Solter *et al.,* 1978). It is further expressed on embryonal carcinomas (Solter *et al.,* 1978), as well as other tumors like hepatocellular or colorectal tumors derived from initially SSEA1$^+$ non-neoplastic tissues and tissues initially negative for SSEA1, like breast and ovarian tissue (Knowles *et al.,* 1982, Fox *et al.,* 1983). In humans, SSEA1 is expressed on differentiated cells including myeloid and epithelial cells (Arber and Weiss, 1993). While it is absent in mouse differentiated cells, it is, however, expressed on human differentiated cells originating from various tissues such as the nervous system, the urinary or digestive tract, but again absent in human pluripotent embryonic cells and stem cells (Solter *et al.,* 1978, Fox *et al.,* 1983, Wright and Andrews 2009). The only exception are human neural stem cells (Hennen *et al.,* 2011, Yanagisawa 2011). A list of proteins identified to be modified with SSEA1 is given in table 5. However, the identification of proteins modified with SSEA1 depends on tissue type and the antibody clone used.

SSEA1 can impact growth factor signaling, adhesion and cell migration. Depending on the cell type, different functions of SSEA1 have been described (Hennen 2011). It has been described that SSEA1 promotes the migration of neural stem progenitor cells and that this

effect is mediated by SSEA1 carried on β1-integrins (Yanagisawa *et al.,* 2005). Dvorak *et al.* showed that a large excess of extracellular SSEA1 prevents the mitogenic effect of FGF2 in embryonic stem cells by promoting the oligomerization of FGF2. Further, the authors show that phospholipase C γ is activated by both SSEA1 and FGF2. Ultimately, the authors claim that SSEA1 may act as a negative regulator of FGF-2induced embryonic stem cell proliferation (Dvorak *et al.,* 1998). Capela *et al.* show that SSEA1-containing molecules bind to Wnt1 in mouse neural progenitor cells and thus, may present this molecule and other growth factors important for self-renewal and growth (Capela and Temple 2006).
Regarding the function of SSEA1 in cancer, Son *et al*. showed that SSEA1 is a marker for tumor-initiating cells in human glioblastoma (Son *et al.,* 2009). It has further been shown that human cells can gain tumorigenic potential through de-differentiation and that these cells are positive for SSEA1 (Scaffidi and Misteli 2011).

Table 5: SSEA1-carrier proteins.
Table was adapted and modified from (Hennen 2011).

protein	cell type	antibody	reference
β1-integrin	neural stem progenitor cells	AK97	(Yanagisawa *et al.,* 2005)
LAMP-1	mouse neural stem cells	AK97	(Yagi *et al.,* 2010)
Phosphacan	rat brain	FORSE-1	(Allendoerfer *et al.,* 1999)
L1CAM	postnatal mouse brain	487	(Streit *et al.,* 1990)
RPTPβζ	rat brain	73-30	(Nishiwaki *et al.,* 1998)
Astrochondrin	postnatal mouse brain	487	(Streit *et al.,* 1993)
CD24	postnatal mouse brain	487	(Lieberoth *et al.,* 2009)
Synapsin 1	bovine brain	487	(Wang *et al.,* 2011)
Tenascin C	mouse brain	5750, 487	(Hennen 2011)
LRP1	mouse brain	5750, 487	(Hennen 2011)
Thy-1	thymus, adult rat brain	487	(Streit *et al.,* 1996)
C2	colon cancer	258-1276	(Rho *et al.,* 2014)
C4B / C4A	colon cancer	258-1276	(Rho *et al.,* 2014)
CD27	colon cancer	258-1276	(Rho *et al.,* 2014)

CD59	colon cancer	258-1276	(Rho *et al.,* 2014)
CD97	colon cancer	258-1276	(Rho *et al.,* 2014)
COL18A1	colon cancer	258-1276	(Rho *et al.,* 2014)
COL1A1	colon cancer	258-1276	(Rho *et al.,* 2014)
COL4A3	colon cancer	258-1276	(Rho *et al.,* 2014)
CTSD	colon cancer	258-1276	(Rho *et al.,* 2014)
DCD	colon cancer	258-1276	(Rho *et al.,* 2014)
DEFA1	colon cancer	258-1276	(Rho *et al.,* 2014)
EFNA5	colon cancer	258-1276	(Rho *et al.,* 2014)
F5	colon cancer	258-1276	(Rho *et al.,* 2014)
FBLN2	colon cancer	258-1276	(Rho *et al.,* 2014)
FCGR2A	colon cancer	258-1276	(Rho *et al.,* 2014)
IL10	colon cancer	258-1276	(Rho *et al.,* 2014)
IL2RA	colon cancer	258-1276	(Rho *et al.,* 2014)
KRAS	colon cancer	258-1276	(Rho *et al.,* 2014)
LAMB1	colon cancer	258-1276	(Rho *et al.,* 2014)
LIFR	colon cancer	258-1276	(Rho *et al.,* 2014)
NPY	colon cancer	258-1276	(Rho *et al.,* 2014)
PDIA3	colon cancer	258-1276	(Rho *et al.,* 2014)
SERPINE1	colon cancer	258-1276	(Rho *et al.,* 2014)
SHBG	colon cancer	258-1276	(Rho *et al.,* 2014)
SPARC	colon cancer	258-1276	(Rho *et al.,* 2014)
CD71 (TFRC)	colon cancer	258-1276	(Rho *et al.,* 2014)
TGFA	colon cancer	258-1276	(Rho *et al.,* 2014)
VWF	colon cancer	258-1276	(Rho *et al.,* 2014)
WISP2	colon cancer	258-1276	(Rho *et al.,* 2014)
WNT7B	colon cancer	258-1276	(Rho *et al.,* 2014)

1.5 SAM pointed domain-containing ETS transcription factor (SPDEF)

SAM pointed domain-containing ETS transcription factor (SPDEF) is a transcription factor of the 28 member containing ETS family of transcription factors with an 85 kDa DNA-binding ETS domain. Originally, the first ETS gene has been shown to be a viral oncogene of the avian transforming retrovirus E26 (Sharrocks 2001, Mahajan 2016). The ETS domain of SPDEF consists of a variant of the winged helix-turn-helix motif which contains three α helices and four β sheets. This structure specifically binds to the 5'-GGAA/T-3' DNA sequence (Sizemore *et al.,* 2017). However, it has been shown that SPDEF preferentially binds to the GGAT motif instead of the GGAA motif which is preferred by other ETS-family members (Oettgen *et al.,* 2000). SPDEF further contains a pointed (PNT) domain (figure 8) which is a helical bundle and is important for dimerization and transcriptional repression (Lacronique *et al.,* 1997, Kim *et al.,* 2001, Sizemore *et al.,* 2017).

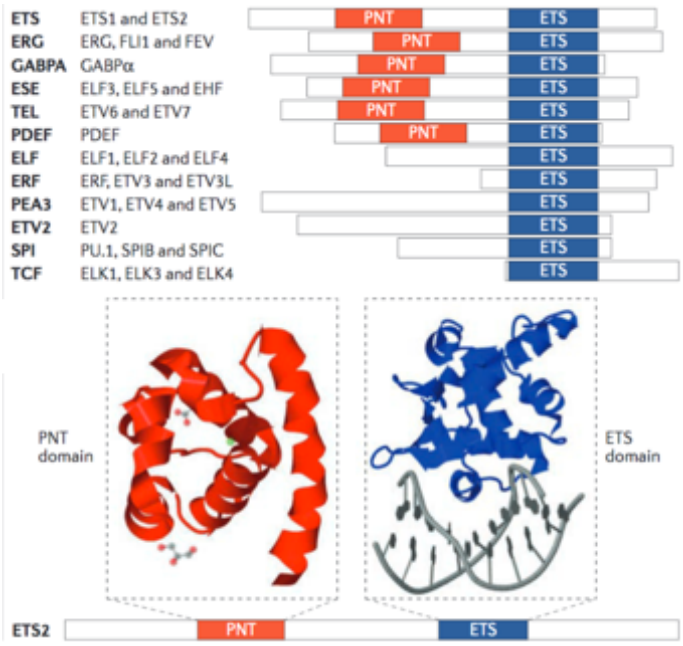

Figure 8: Protein structure of ETS proteins.
Figure adapted from (Sizemore *et al.,* 2017).

The expression of SPDEF is restricted to epithelial cells and has been found in prostate, colon, gastric, ovary and airway epithelium (Mahajan 2016).

Post-translational modifications of ETS proteins change their stability, DNA binding ability, cellular localization and interaction with other proteins (Sharrocks 2001). Thus, they can activate or repress transcription of target genes in order to regulate cell growth, apoptosis or

development (Oikawa and Yamada 2003). ETS-family members have been shown to be downstream targets of RAS-MAPK signaling (Sharrocks 2001, Oikawa *et al.,* 2003). For SPDEF, specifically, a MAPK phosphorylation site at T50 has been demonstrated (Gunawardane *et al.,* 2005). Further phosphorylation sites of SPDEF that have been reported but not validated include a PI3K site, a protein kinase C, an AKT and a tyrosine kinase consensus sequence (Mahajan 2016). Besides being a downstream target of RAS-MAPK signaling, SPDEF, specifically, was identified as a downstream target of estrogen signaling in mammary epithelial progenitor as well as luminal epithelial breast cancer cells (Buchwalter *et al.,* 2013). Further, androgen receptor inactivation has been demonstrated to reduce SPDEF expression (Tsai *et al.,* 2018). Other studies showed that SPDEF is a downstream target of ATOH1 (Atonal homolog 1) in the intestine and at the same time a co-regulator of ATOH1 (Lo *et al.,* 2017). Also, the STAT signaling pathway has been implicated to play a role in SPDEF regulation. Yu *et al.* showed that STAT6 repression inhibited SPDEF expression in human airway epithelial cells (Yu *et al.,* 2010).

Numerous genes have been identified as target genes of SPDEF in various cell types (Mahajan 2016). A summary of the target genes is given in table 6. SPDEF has been shown to interact directly with the DNA-binding domain of the androgen receptor and enhances expression of the prostate-specific antigen (PSA). Besides, it also induces expression of the PSA independently of the androgen receptor (Oettgen *et al.,* 2000). In prostate cancer cells, loss of SPDEF induced TGFBI expression and promoted EMT and bone metastasis (Chen *et al.,* 2017). Further, in prostate cancer, chemokine C-C motif ligand 2 (CCL2) has been described to be another target gene of SPDEF and to be repressed by it. Upon knockdown of SPDEF, CCL2 was expressed and epithelial-to-mesenchymal transition induced (Tsai *et al.,* 2018). In colorectal cancer, SPDEF expression induced a quiescent state and inhibited intestinal tumorigenesis by inhibiting the transcriptional activity of β-catenin via protein-protein interactions (Lo *et al.,* 2017). The authors of the study further propose that when SPDEF is absent, cell cycle genes and stem cell genes are expressed by β-catenin. However, when SPDEF is expressed, its binding to β-catenin disrupts binding of TCF1 and TCF3 and shifts expression to only stem cell-related genes, thereby inducing quiescence (Fingleton 2017, Lo *et al.,* 2017).

Deregulation of ETS expression or fusion of ETS proteins with JAK2 are involved in the development of leukemia and have been shown to play a role in other solid tumors

(Lacronique *et al.,* 1997, Kim *et al.,* 2001, Buchwalter *et al.,* 2013). In colon cancer, however, SPDEF expression has been described as a negative regulator of cell growth and migration (Moussa *et al.,* 2009).

In normal tissues, SPDEF expression defines lineages and is involved in differentiation processes. It has been implicated in regulating intestinal differentiation, as well as differentiation of goblet and Paneth cells (Gregorieff *et al.,* 2009, Fingleton 2017).

Further, expression of ETS proteins was implicated in metastasis and invasion (Gallego-Ortega *et al.,* 2015, Heo *et al.,* 2015, Sizemore *et al.,* 2017).

The role of SPDEF in ovarian cancer is unknown. Regarding the tumor-promoting or suppressive role of SPDEF in ovarian cancer, rare data are available. Rodabaugh *et al.* report that SPDEF is overexpressed in about 30 % of serous epithelial ovarian cancers. In normal ovary and benign serous cystadenomas, SPDEF expression was completely absent (Rodabaugh *et al.,* 2007). Other data reported that SPDEF is expressed in 71 % of ovarian tumors (Ghadersohi *et al.,* 2004). In another study, however, the highest levels of SPDEF expression have been found in normal ovarian tissue, followed by stage Ia and IIb tumors (Ghadersohi *et al.,* 2008). Besides, the authors claim that overall survival of patients with $SPDEF^{high}$ tumors was significantly longer. Also, expression of SPDEF in SPDEF-negative tumors inhibited tumor cell growth and induced apoptosis (Ghadersohi *et al.,* 2008).

Table 6: SPDEF target genes in various cancers.
The table was adapted and modified from (Mahajan 2016).

gene	main function	tissue type	major finding	reference
PSA	screening tool for prostate cancer		SPDEF binds to PSA promoter & induces gene expression	(Oettgen *et al.,* 2000)
MMP9 / MMP7	tumor progression, stromal remodeling, metastasis	breast and prostate cancer cell line	SPDEF is negative regulator	(Steffan *et al.,* 2016)
Survivin	inhibitor of apoptosis	breast, ovarian and prostate cancer	Survivin is a transcriptional target of SPDEF	(Ghadersohi *et al.,* 2007, Turner *et al.,* 2011)
uPA / uPAR	invasion and	breast	SPDEF downregulates	(Kruger *et al.,*

	metastasis	cancer cell line	uPA and upregulates uPAR	2000, Turner *et al.,* 2008, Turner *et al.,* 2011)
Maspin	tumor suppressor	breast, prostate and lung cancer	SPDEF induces maspin expression which decreases invasion and metastasis	(Feldman *et al.,* 2003, Kim *et al.,* 2004, Mahajan *et al.,* 2013)
p21	cell cycle regulator	breast cancer cell line	SPDEF overexpression increases p21	(Schaefer *et al.,* 2010)
p62	apoptosis and autophagy	breast cancer cell line	SPDEF upregulates p62	(Thompson *et al.,* 2003)
Slug	EMT regulator	breast and prostate cancer cell line	SPDEF reduces SLUG expression and thereby inhibits invasion and migration	(Steffan *et al.,* 2016)
VASP	inhibits migration, cytoskeletal remodeling	breast cancer cell line	VASP is a putative target gene of SPDEF	(Turner *et al.,* 2008)
LASP1	cytoskeletal reorganization	breast cancer cell line	-	(Turner *et al.,* 2008, Frietsch *et al.,* 2010)
Stathmin	microtubule dynamics	prostate cancer cell line	SPDEF downregulates stathmin and thereby inhibits prostate cancer	(Sabherwal *et al.,* 2012)
HOXB13	invasion	prostate cancer cell line	HOXB13 suppresses SPDEF expression	(Kim *et al.,* 2014)
DNA methylation	hypo- or hypermethylation	breast and prostate cancer cell line	methylation inhibition increased SPDEF expression	(Sabherwal *et al.,* 2013)
FOXM1	-	prostate cancer	SPDEF negatively regulates FOXM1 thereby inihibiting tumorigenesis	(Cheng *et al.,* 2014)

1.6 Forkhead box protein A2 (FOXA2)

Forkhead box protein A2 (FOXA2) is a transcription factor belonging to the forkhead box (FOX) transcription factor superfamily (Katoh and Katoh 2004). Forkhead box proteins contain a 110 amino acid motif that is required for DNA binding of the transcription factor (Weigel and Jackle 1990). FOXA2 shares 95 % sequence identity with FOXA1 and is also an important paralog of FOXA1 (Friedman and Kaestner 2006).

It has been shown, that FOXA2 contains an AKT2/PKB phosphorylation site which is proposed to be responsible for nuclear localization of FOXA2 (Wolfrum *et al.,* 2003, Wolfrum *et al.,* 2004). Further, FOXA2 expression has been shown to be induced by sonic hedgehog in the neural tube (Sasaki *et al.,* 1997).

FOXA2 is required for many developmental and differentiation processes including formation of the nervous system, endoderm-derived structures, the notochord and embryonic development (Friedman *et al.,* 2006). It further controls lipid homeostasis and regulates target genes as enzymes involved in glucose metabolism (Wolfrum *et al.,* 2004, Friedman *et al.,* 2006).

In cancer, FOXA2 has been mainly considered as a tumor suppressive transcription factor. In pancreatic cancer, deletion of FOXA2 resulted in increased invasion and *in vivo* tumor growth, thereby supporting the role of FOXA2 as a tumor suppressor (Wolfrum *et al.,* 2003). Besides, in glioma cells, expression of FOXA2 suppressed proliferation, migration and invasion of the cells and attenuated *in vivo* tumor growth (Ding *et al.,* 2017). Moreover, FOXA2 has been demonstrated to abrogate cell proliferation and migration in gastric cancer (Li *et al.,* 2017). In lung cancers, FOXA2 reduced invasion and suppressed TGF-β induced EMT and thereby suppressed metastasis (Tang *et al.,* 2011).

Regarding a tumor-promoting or suppressive role of FOXA2 in ovarian cancer, no publications are available so far.

2. AIM OF DISSERTATION

High grade serous ovarian cancer (HGSOC) is a lethal disease and among the most malignant tumors. Tumor cells spread into the peritoneum during the early stages of the disease. This metastatic spread and the colonization of the organs in the peritoneum are the major problems for the treatment of HGSOC. Since tumors consist of a heterogeneous population of cells of which only some are able to drive the colonization and outgrowth of tumor cells at distant organs, the identification of these tumor-initiating cells is crucial. Targeting tumor-initiating cells may ultimately lead to regression of the tumor and prevention of metastatic spread. However, in order to target tumor-initiating cells, the molecular mechanisms responsible for their tumorigenic properties have to be identified.

So far, there is no conclusive evidence for the existence of tumor-initiating cells in HGSOC and above all, even less is known about their molecular mechanisms driving tumorigenesis (Zhang *et al.,* 2008, Alvero *et al.,* 2009, Meng *et al.,* 2012, Zhang *et al.,* 2012, Gao *et al.,* 2015, Lupia *et al.,* 2017). Further, few targeted therapies are available to treat patients (Perren *et al.,* 2011, Pujade-Lauraine *et al.,* 2017). Hence, research about tumor-initiating cells and their molecular mechanisms is necessary.

The aim of this dissertation is to identify tumor-initiating cells in HGSOC that promote metastatic spread based on surface marker expression. These shall be specified by discriminating functionally different subpopulations within the tumor bulk. Further, the underlying molecular mechanisms rendering tumor-initiating cells more tumorigenic than the bulk of the tumor will be analyzed.

The analysis of the molecular drivers of tumorigenesis in tumor-initiating ovarian cancer cells may hereafter lead to the development of new targeted therapies to ultimately improve patient survival.

3. MATERIAL AND METHODS

3.1 Material

3.1.1 Equipment

Aria I and III	Beckmann Coulter
balance	Acculab
Bioanalyzer 2100	Agilent Technologies
centrifuge 5810R	Eppendorf
Chemidoc Imaging system	Biorad
freezer	Liebherr
fridge	Liebherr
gel electrophoresis device	Biorad
heatblock	HLC
ice machine	Hoshizaki
incubator Heracell 240i	Thermo Fisher
IVIS Spectrum In Vivo Imaging System	Perkin Elmer
laminar flow hood Safe2020, HeraSafe KS	Thermo Fisher
LSR II	Beckmann Coulter
LSR Fortessa	Beckmann Coulter
microcentrifuge 5415D	Eppendorf
microscope PrimoVert	Zeiss
Mr. Frostie	Nalgene
Nanodrop 1000	Thermo Fisher
Neubauer chamber	Brand
pipettes 2.5 µl, 20 µl, 200 µl, 1000 µl	Eppendorf
pipette boy	Integra
racks	eBiosciences
rocker	Stuart
shaking incubator Multitron	Infors HT
spectrophotometer Spectramax M5	Molecular Devices
Thermocycler	Biometra
Trans-Blot Turbo system	Biorad
Viia 7 qPCR machine	Life Technologies
vortexer Vortexgenie 2	Scientific Industries
water bath TW20	Julabo

3.1.2 Consumables

autoclavable bags	#09.302.0020	Nerbe Plus
cell culture flask T75	#90076	TPP
cell culture flask T150	#90151	TPP
cell scraper	#99003	TPP
cover slips	-	Menzel
Criterion TGX Precast Protein gel	#5671081	Biorad
cryotubes	#375418	Thermo Scientific
eppis 1.5 ml	#2025-11-28	Eppendorf
eppis 2.0 ml	#2025-08-28	Eppendorf

FACS tubes	#55.1579	Sarstedt
filter bottles 250 ml	#99250	TPP
filter bottles 500 ml	#99500	TPP
filter bottles 1000 ml	#99950	TPP
filter bottles 250 ml, 0.45 µm	#SCHVU02RE	Millipore
gloves	#XC INT S	Microflex
microscope slides	-	Engelbrecht
Multiwell deep well plates, 96-well	#737-2515	Eppendorf
parafilm	PM-996	Bemis
Pasteur pipettes	-	WU Mainz
PRIMARIA flasks T25	#353808	Corning
PRIMARIA flasks T75	#353810	Corning
PRIMARIA plates 6-well	#353846	Corning
PRIMARIA plates 24-well	#353847	Corning
PRIMARIA plates 96-well	#353872	Corning
PVDF membrane	#1704157	Biorad
qPCR plates, 386 wells	#AB1384	Thermo Fisher
qPCR seal	#4ti-0560	4titude
scalpels	#02.001.30.010	Feather
Serological pipettes 2 ml	#357507	Corning
Serological pipettes 5 ml	#357543	Corning
Serological pipettes 10 ml	#357551	Corning
Serological pipettes 25 ml	#357525	Corning
Serological pipettes 50 ml	#357550	Corning
tips 20 µl	#S1120-1810	Starlab
tips 200 µl	#S1120-8810	Starlab
tips 1000 µl	#S1122-1830	Starlab
Trans-blot Turbo transfer stacks	#1704157	Biorad
tubes 15 ml	#91015	TPP
tubes 50 ml	#431720	Greiner
Ultra low attachment plates, 6-well	#CLS3471	Sigma
X ray films (Fuji)	#RX1824	Kisker

3.1.3 Chemicals

AlbuMAX I Lipid Rich BSA	#11020039	Thermo Fisher
albumin fraction V	#8076.4	Roth
buffer EB	#1014608	Qiagen
buffer TE	#1018499	Qiagen
carbenicillin	#A1491	AppliChem
crystal violet	#V5265	Sigma
DMSO	#D2650	Sigma
Dulbecco's Phosphate Buffered Saline	#D8537	Sigma
EDTA	#E6758	Sigma
ethanol, 100 %	#E/0650DF/C17	Fisher Chemical
formalin, 10 %	#HT501128	Sigma
glutaraldehyde	#G6257	Sigma
LB broth	#1.10285.0500	Merck Millipore
LB agar	#1.10283.0500	Merck Millipore

methanol	#32213	Sigma
RNase A	#1007885	Qiagen
RNase-free water	#10177979	Qiagen
Skim milk powder	#70166	Sigma
SOC medium	#15544-034	Invitrogen
sodium carbonate	#222321	Sigma
sodium acetate	#S8750	Sigma
TCEP	#77720	Thermo Fisher
Trizma base	#T1503	Sigma
trypan blue	#15250	Gibco
Tween	#P1379	Sigma
Ultrapure distilled water	#10977-035	Life Technologies
xylol	#33817	Sigma

3.1.4 Compounds and reagents

100 bp ladder	#15628050	Invitrogen
1 kb Generuler ladder	#SM0331	Thermo Fisher
accutase	#A1110501	Thermo Fisher
AEC substrate chromogen	#K3464	Dako
agarose	#A9414	Sigma
Antarctic Phosphatase buffer	#B0289	NEB
buffer NEB 3.1	#7203	NEB
Clarity Western ECL Blotting Substrate	#1705060	Biorad
Clarity Max Western ECL Substrate	#1705062	Biorad
Cryostor	#2874	Sigma
CutSmart buffer	#B7204S	NEB
D-luciferin firefly, potassium salt	#115144-35-9	Biosynth
DMEM/F12	#12634-010	Gibco
dNTPs	#R0191	Fermentas
ethidium bromide	#2218.1	Roth
Homemade *Taq* buffer	-	DKFZ
IMDM	#21980-032	Gibco
Restore Western Blot Stripping buffer	#21059	Thermo Fisher
RIPA buffer	#9806S	Cell Signaling
Spectra Multicolor Broad Range ladder	#26631	Thermo Fisher
T4 DNA ligase	#M0202S	NEB
T4 DNA ligase buffer	#B0202S	NEB
TAE buffer	#A1691,1000	AppliChem
Taqman Universal PCR master mix	#4324018	Thermo Fisher
Target retrieval solution, citrate pH 6	#S2369	Dako
10x TGS running buffer	#161-0772	Biorad
10x Trans-blot Turbo transfer buffer	#10026938	Biorad
Q5 Hot Star High Fidelity 2x master mix	#M0494S	NEB

3.1.5 Media and buffer

Cell culture media:

SOC Cancer Stem Cell Medium:

500 ml Advanced DMEM/F12	#12634-010	Invitrogen
25 ml Sterile H_2O Cell Culture Grade	#10977-035	Invitrogen
5 ml N2 Supplement	#17502048	Invitrogen
2 mM Glutamine	#25030-024	Gibco
500 µg L-glutathione, reduced	#G6013	Sigma
50 ng/ml hBasic FGF	#100-18B	Peprotech
20 ng/ml hEGF	#AF-100-15	Peprotech
10 ng/ml R^3 IGF	#I1271	Sigma
100 µM β mercaptoethanol	#21985-023	Invitrogen
5 µg/ml insuline	#12585014	Life Technologies
36 ng/ml Hydrocortisone	#H0888	Sigma
0,5 ng/ml ß-Estradiol	#E2758	Sigma
1 ml AlbuMAX I Lipid Rich BSA 30%	#11020039	Thermo Fisher
1.7 ml glucose (45%)	# G8769	Sigma
500 µl Trace Elements B	#25-022-CI	Corning
500 µl Trace Elements C	#25-023-CI	Corning
250 µl Trace Elements A	#25-021-CI	Corning
5 mM HEPES	#1563016	Invitrogen
2 µg/ml heparine	# H3149	Sigma
1 ml lipid mixture	#L0288	Sigma

COBG medium:

500 ml CO_2-independent medium	#18045-054	Gibco
1 % BSA	#11020039	Thermo Fisher
2 mM glutamine	#25030-024	Gibco

PEB buffer:

500 ml PBS	#D8537	Sigma
2 mM EDTA	#E6758	Sigma
1 % BSA	#11020039	Thermo Fisher

Bacterial media:

LB-medium (liquid):
25.0 g LB broth in 1 l purified water + 100 µg carbenicillin

LB-agar:
37.0 g LB agar powder in 1 l purified water + 100 µg carbenicillin

Western blotting buffers:

WB lysis buffer:

10x RIPA buffer	#9806S	Cell Signaling
100x AEBSF	#A8456	Sigma
100x Halt Protease Inhibitor Cocktail	#87786	Thermo Fisher
100x EDTA	#87786	Thermo Fisher

+ fill up with deionized H_2O

10x TBS buffer (2 l), pH= 7.5:
48.4 g TRIS-base, 160 g NaCl, 2 l purified water
adjusted to pH 7.5 with HCL/NaOH

1x TBS-T (10 l):
1l 10 x TBS buffer, 9 l purified water, 50 ml 20x tween

TBS-T + 5 % milk + 0.02 % sodium azide (1 l):
1 l 1x TBS-T, 50 g skim milk powder, 800 µl 25 % sodium azide

TBS-T + 5 % BSA +0.02 %sodium azide (1l):
1 l 1x TBS-T, 50 g BSA, 800 µl 25 % sodium azide

Buffer for cloning:

10x TAE buffer (1 l):
48.4 g TRIS base, 11.4 ml acetic acid (pH 17.4), 3.7 g EDTA disodium salt, volume was scaled to 1 l with purified water

Buffers for viral transduction:

2.5 M $CaCl_2$ (100 ml):
36.75 g $CaCl_2$ volume was scaled to 100 ml with purified water

2x HBS (500 ml):
8 g NaCl, 6.5 g HEPES, 1 mM Na2HPO4, pH was adjusted to 7.0 and sterile filtered through a 0.22 µM filter in order to determine the highest transfection-efficient HBS solution, the Na2HPO4 concentration was thereby gradually increased in a range from 1 mM to 2 mM in 0.2 mM steps and titrated on HEK 293T cells

3.1.6 Enzymes

Antarctic Phosphatase	# M0289	NEB
BamHI	# R0136L	NEB

EcoRI	#R3101S	NEB
homemade *Taq* polymerase	-	DKFZ
NotI	# R0189	NEB
T4 DNA ligase	# 2011A	Takara

3.1.7 Kits

Avidin / biotin blocking Kit	#SP-2001	Vector labs
BD Lyoplate Human Screening Panel	# 560747	BD
CellTiterBlue Kit	# G8088	Promega
Dako Real Detection System	#K5003	Dako
Dako Real Peroxidase-blocking solution	#S2023	Dako
High Capacity cDNA Kit	# 4368814	Applied Biosystems
HiSpeed Plasmid Maxi Kit	# 12662	Qiagen
miRNeasy Mini Kit	# 217004	Qiagen
Pierce BCA Protein assay Kit	#23225	Thermo Fisher
Pierce IP Kit	# 88805	Thermo Fischer
Qiaprep Spin Miniprep Kit	# 27104	Qiagen
Qiaquick Gel extraction Kit	# 28704	Qiagen
Qiaquick PCR purification Kit	# 28106	Qiagen

3.1.8 Antibodies

Table 7: List of antibodies.

antigen	fluoro-phor	species	clone	company	appli-cation	dilution
anti-human CD24	APC	mouse IgG2a	ML5	Biolegend #311118	FACS	1:100
anti-human CD44	APC	mouse IgG2b	G44-26	BD #559942	FACS	1:5
anti-human EPCAM	FITC	mouse IgG1	EBA-1	BD #347197	FACS	1:5
anti-human SSEA1	Alexa 647	mouse IgM	MC-480	Biolegend #125608	FACS	1:20
anti-human SSEA1	PE	mouse IgM	MC-480	eBiosciences #12-8813-42	FACS	1:20
anti-human SSEA1	V450	mouse IgM	MC-480	BD #561561	FACS	1:20
anti-human Ki67	-	mouse IgG1	MIB-1	Dako #M7240	IHC	1:200
anti-human SSEA1	-	mouse IgM	MC-480	Invitrogen #41-1200	IHC	1:1000
anti-human SPDEF	-	mouse IgG1	G10	Santa Cruz # SC-166846	WB	1:500
anti-human FOXA2	-	mouse IgG2a	-	Abcam ab60721	WB	1:500

anti-human Vinculin	-	Rabbit IgG	-	Cell Signaling #4650	WB	1:1000
Anti-rabbit IgG	HRP	Goat IgG	-	Southern Biotech #4030-05	WB	1:10,000
Anti-mouse IgG	HRP	Goat IgG	-	Southern Biotech #1010-05	WB	1:10,000
Anti-mouse IgG2a	HRP	goat IgG	-	Southern Biotech #1081-05	WB	1:10,000

Table 8: List of istopyes.

antigen	fluorophor	species	clone	company	application
isotype	V450	mouse IgM	G155-228	BD #560861	FACS
isotype	PE	mouse IgM	MM-30	Biolegend #401609	FACS
isotype	Alexa 647	mouse IgM	MM-30	Biolegend #401618	FACS
isotype	APC	mouse IgG2b	27-35	BD #555745	FACS
isotype	APC	mouse IgG2a	MOPC-173	Biolegend #400220	FACS
isotype	FITC	mouse IgG1	MOPC 21	BD #555748	FACS

3.1.9 Oligonucleotides

shRNA sequences: Dharmacon

pTRIPZ sh_SPDEF V3THS_376889	ACAGCATGTCAAAGTAGGA
pTRIPZ sh_FOXA2_1 V2TH2_86208	AAGAGGAGTTCATAATGGG
pTRIPZ sh_FOXA2_2 V2TH2_86209	ATTAATCGGACCCGAGACC
pTRIPZ sh_FOXA2_3 V3TH2_306420	TGAGGTCCATTTTGTGGGG
pTRIPZ sh_NS	CTTACTCTCGCCCAAGCGAGAG

Sequencing and cloning primer: Sigma

primer name	sequence	nmoles	purity
pIRES-RP	TATAGACAAACGCACACCG	0.05 nmol	HPLC
SPDEF_FW	AAATATGGATCCATGGGCAGCGCCAGCCCGGGT	0.05 nmol	HPLC
SPDEF_RV	AAAGCGGCCGCTCAGATGGGGTGCACGAACTGGT	0.05 nmol	HPLC
pTRIPZ_sh_FW	GGAAAGAATCAAGGAGG	0.05 nmol	HPLC

pLego_SFFV_FW	GAGCTCACAACCCCTCACTC	0.05 nmol	HPLC
FOXA2_FW	ATATGGATCCATGCACTCGGCTTCCAGTATG	0.05 nmol	HPLC
FOXA2_RV2	ATAGTGAATTCTTAAGAGGAGTTCATAATGGGC	0.05 nmol	HPLC
pEXA2_RV	AGCTCACTCATTAGGCACCCCAGGCTTTAC	0.05 nmol	HPLC

3.1.10 Taqman probes

EEF1A2	Hs00951278_m1	Thermo Fisher
FOXA2	Hs00232764_m1	Thermo Fisher
HIF1α	Hs00153153_m1	Thermo Fisher
HMGCR	Hs00168352_m1	Thermo Fisher
LRP3	Hs00233925_m1	Thermo Fisher
MUC1	Hs00159357_m1	Thermo Fisher
PPIA	Hs04194521_s1	Thermo Fisher
RARRES1	Hs00161204_m1	Thermo Fisher
SPDEF	Hs01026050_m1	Thermo Fisher
SREBF1	Hs01088691_m1	Thermo Fisher
YIPF1	Hs00219196_m1	Thermo Fisher

3.1.11 Plasmids

pCMV6-XL5 NM_021784.3 (FOXA2 coding sequence)	Origene
pCMV6-XL5 NM_012391.2 (SPDEF coding sequence)	Origene
pLegoiT2	kind gift from M. Falcone
pV2Luc	kind gift from S. Wagner
pFOXA2_inducible	kind gift from F. Geist

3.1.12 Viruses

FOXA2_OX
FOXA2_OX_ind
FOXA2_sh_86208
FOXA2_sh_86209
FOXA2_sh_306420
H2B-GFP
iT2
Luciferase
NS
SPDEF_sh_376889
SPDEF_OX

3.1.13 Bacterial Strains

STBL3 cells: Life Technologies
Genotype: F- *mcr*B *mrrhsd*S20(rB-, mB-) *rec*A13 *sup*E44 *ara*-14 *gal*K2 *lac*Y1 *pro*A2 *rps*L20(StrR) *xyl*-5 λ- *leumt*l-1

3.1.14 Cell lines

OC12, OC14, OC15, OC18, OC19, OC20

3.1.15 Mice

NOD.Cg-*Prkdcscid Il2rgtm1Wjl* (NSG) mice

3.1.16 Software

Ape Plasmid Editor 2.0.49.10	http://jorgensen.biology.utah.edu/wayned/ape/.com
Chipster 3.13	(Kallio *et al.,* 2011)
ELDA online tool	(Hu and Smyth 2009)
Fiji 2.0.0	(Schindelin *et al.,* 2012)
FlowJo 10.4	FloJo, LLC
gene ontology.org	(Ashburner *et al.,* 2000, The Gene Ontology 2017)
GraphPadPrism 7	GraphPad Software
KM-plotter online tool	(Gyorffy et al., 2012)
Living Image Software 4.4	Perkin Elmer
Nanodrop Software 3.6.0	Thermo Fisher
QuantStudio Real-Time PCR Software v1.3	Thermo Fisher
R 3.3.3	(R Core Team 2017)

3.2 Methods

3.2.1 Cell culture methods

3.2.1.1 General cell culture conditions

Cells were cultured in a humidified atmosphere in an incubator at 37° C with 5 % CO_2. All OC cell lines were maintained in FCS-free CSC – medium (3.1.5) which was changed every three days or if phenol red indicated a decrease in pH. Cell lines were tested for mycoplasma, squirrel monkey retrovirus and epstein-barr-virus as well as interspecies crosscontamination on a regular basis.

3.2.1.2 Primary *in vitro* and *in vivo* xenograft model system for serous ovarian cancer or cell lines

SOC (Serous Ovarian Cancer) cell lines were derived from patient-specific serous ovarian tumors and pieces thereof xenografted into NSG mice in order to expand the tumor material. Resulting tumors were digested into single cell suspensions and a cell culture in FCS-free CSC medium was established. Once the cell culture was established, the cells were again transplanted into mice in order to verify their tumorigenicity. Based on gene expression profiling, the cell lines were then characterized and classified according to one of the four subtypes mesenchymal, proliferative, differentiated and immunoreactive (1.1.5, 3.1.14 and 4.1).

HEK293T cells were cultured in IMDM medium + 10 % FCS and 2 mM L-glutamine.

3.2.1.3 Passaging of adherent cell lines

Cells were maintained under CSC conditions. Medium was aspirated of cells 80-90 % confluent and 3 ml accutase added per T75 flask. Cells were then put into the incubator and after cells had detached, 5 ml COBG-medium was used to collect the cell suspension, transferred to a 50 ml falcon and centrifuged for 5 min at 1200 rpm. Afterwards, the supernatant was discarded and the cells plated in a new T75 flask according to pre-defined splitting ratios (OC12: 1:20, OC14, OC18 and OC19: 1:3, OC15 and OC20: 1:5). Splitting was performed once a week (OC12, OC14, OC15) or every second week (OC18, OC19, OC20).

HEK293T cells were split weekly with 5 ml trypsin/EDTA in a 1:20 ratio and seeded in IMDM + 10 % FCS + 2mM L-glutamine.

3.2.1.4 Thawing of cells

Cells were thawed in a 37° C water bath, put into a 50 ml falcon and 10 ml CSC medium was slightly added to the cells. Cells were then centrifuged at 4° C, 1300 rpm for 5 min and the resulting supernatant was then discarded and cells plated into PRIMARIA flasks.

3.2.1.5 Freezing of cells and storage

In order to freeze SOC cells, cells were spun down and the pellet resuspended in 5 ml Cryostor freezing reagent. Cells were then aliquoted into eppis, put into a Mr. Frostie and frozen at -80° C. For long-term storage, cells were transferred into liquid nitrogen.

3.2.1.6 Determination of cell number and viability

In order to determine cell number, cells were resuspended with 1 ml medium. A 10 µl aliquot was then mixed with 90 µl of trypan blue solution and 10 µl thereof put into a Neubauer chamber. Viable cells in all four squares were counted and calculated according to the following formula:

$$\frac{cells}{ml} = \frac{cell\ number}{4}\ x\ 10^4\ x\ 10\ (dilution\ factor)$$

3.2.1.7 Seeding of cells

Cells were seeded for several assays including proliferation and colony-formation assays. The number of viable cells was determined and equal numbers of cells from a master mix were then seeded into PRIMARIA plates. Cell numbers differed between experiments and cell lines. If not indicate otherwise, 3200 cells per 6-well, 15.000 cells per 24-well and 50.000 cells per 6-well were seeded.

3.2.2 Cell biological methods

3.2.2.1 Transfection of HEK293T cells

Lentiviral particles were transduced in HEK293T cells. For lentiviral production, HEK293T cells were seeded in T150 flasks and incubated over night in that they reach 60-70 % confluency the next day. The next day, medium was changed and replaced with IMDM + 10 % heat-inactivated FCS supplemented with 25 µM chloroquine-containing medium. Then, a calcium-phosphate precipitate composed of a mix of 15 µg packaging plasmid pSPAX2, 6 µg of the envelope plasmid pMD2.G and 20 µg of the target DNA and water to fill up to 500 µl, as well as 50 µl 2.5 M $CaCl_2$ and 500 µl 2x HBS was prepared. The precipitate was then shaken vigorously, kept at RT for 5 min and then added to the pre-prepared chloroquine-containing media. Medium was then changed 8 h post-transfection.

3.2.2.2 Concentration of virus

The virus supernatant was harvested 24 h & 48 h post transfection. Supernatant was centrifuged for 10 min at 2000 g to remove debris. Afterwards, the supernatant was filtered through a 0.45 µM filter and if not directly used for ultracentrifugation, frozen at -80° C. For ultracentrifugation, supernatant was equally distributed into ultracentrifugation buckets and then centrifuged for 2 h at 25,000 rpm at 4 °C. After centrifugation, the SN was discarded, the liquid at the rim of the buckets removed with some wipes and the pellet resuspended in 1/500 volume of DMEM+F12 of the amount of starting supernatant. Then it was aliquoted in 10 ml fractions and frozen at –80° C.

3.2.2.3 Determination of viral titer

In order to determine the titer of the virus, 20,000 HEK cells were seeded per 12-well. The next day, one well was counted, the medium of the other wells was changed to IMDM + 10 % HIN-FCS + 10 µg/ml polybren and 10 µl of virus in 1:10 dilution steps added to the wells in duplicates. 14 h later, the medium was replaced by IMDM + 10 % HIN-FCS medium. 72 h post transduction, the cells were analyzed by flow cytometry regarding transfection efficiency and the virus titer calculated according to the following formula:

$$Titer\left(\frac{transducing\ units}{ml}\right) = number\ of\ cells\ seeded\ (count\ at\ day\ 1)\ x\ \frac{(\frac{\%\ of\ EGFP+\ cells}{100})}{volume\ of\ virus\ in\ ml}$$

3.2.2.4 Transduction of SOC cell lines

Prior to transduction, SOC cells were seeded in 6-wells so that they reach 50 % confluency the next day. Medium was then replaced by IMDM + 10 µg/ml polybren. Then, the SOC cells were transduced with virus at different MOIs (0.3, 1, 3). The required virus volume was calculated according to the following formula: $Viral\ particles = MOI\ x\ cell\ number\ seeded$ and $volume\ of\ virus\ [ml] = \frac{viral\ particles}{titer\ [\frac{transducing\ units}{ml}]}$. After 14 h, the medium was replaced with fresh CSC medium. The percentage of positively transduced SOC cells was determined 72 h post-transduction via FACS. Populations with around 30 - 50 % positive cells were used and further passaged.

3.2.2.5 Generation of stable knockdown and overexpression cell lines

In order to generate stable knockdown and overexpression cell lines, cell populations with an initial transduction efficiency of 30 – 50 % were further cultured. These were then flow cytometrically sorted into approximately 100 % pure populations, further cultured and as soon as enough cells had grown, cells were collected and frozen in aliquots.

3.2.2.6 Fluorescence activated cell sorting (FACS)

For fluorescence activated cell sorting (FACS), cells were washed and up to 10^6 cells were resuspended in 100 µl PEB buffer. Then, primary antibodies were added to the suspension in pre-titrated concentrations (3.1.8) and incubated for 30 min on ice protected from light. After another washing step and filtering, samples, as well as isotype and unstained controls were then recorded at a LSR II or a Fortessa (Beckman Coulter). Dead cells were excluded by propidium iodide staining.

FACS sorting experiments were performed at Aria I or III (Beckman Coulter) at the Imaging and Flow Cytometry Unit, DKFZ. Regarding SSEA1 expression, $SSEA1^+$ and $SSEA1^-$ cells were defined as the 10% of cells with the highest or lowest SSEA1 staining, respectively. Data analysis was performed with the FlowJo software.

3.2.2.7 5’-ethynyl-2’-deoxyuridine (EdU) assay

For cell cycle analysis, cells were incubated with 10 µM 5’-ethynyl-2’-deoxyuridine (EdU) for 1 h. Afterwards, cells were detached with accutase followed by staining with anti-SSEA1-

A647 antibody. Then, cells were washed with PBS + 1 % BSA and incubated with 100 µl click-it fixative for 15 min at RT, protected from light. After another washing step, the pellet was resuspended in 100 µl click-it saponin-based permeabilization and wash reagent and also incubated for 15 min. A master mix containing $CuSO_4$, Pacific Blue fluorescent dye azide and a reaction buffer additive was prepared according to the manufacturer's instructions. 500 µl were then added to the sample and incubated for 30 min at RT in the dark. After washing with click-it saponin-based permeabilization and wash reagent, the pellet was resuspended in 100 µl of the same buffer and 1 µl of 100 mg/ml ribonuclease A, as well as 2 µl of 1 mg/ml propidium iodide were added and incubated for 30 min. For flow cytometric analysis, the lowest flow rate was used and gating was performed as shown in figure 20 a.

3.2.2.8 Colony formation assay (adherent and sphere conditions)

Colony formation assays were performed by seeding a small number of cells (3,200 OC12 cells per 6-well, 800 OC12 cells per 24-well; 4,000 OC15 cells per 6-well, 12,000 OC18 cells per 6-well, 50,000 OC20 cells per 6-well) into 6- or 24-wells in triplicates. For the assay in adherent conditions, PRIMARIA plates were used, for sphere conditions ultra-low attachment plates were used. Cells were let grown for 7 or 14 days (OC12 or OC20, respectively). For the adherent colony-formation assay, medium was then removed, plates were washed with PBS and then wells were incubated with 1 ml of staining solution (0.5 % crystal violet, 6 % glutaraldehyde and filled up with H_2O) for 30 min. Then, the staining solution was removed, the wells were washed with H_2O and let dry. Afterwards, pictures of the stained colonies were taken and analyzed with a Fiji script regarding colony number and size (7.2). Regarding the assay in sphere conditions, spheres were manually counted under a microscope.

3.2.2.9 *In vitro* limiting dilution analysis

For in vitro limiting dilution analysis, cells were seeded in 1:2 dilution steps in octaplicates in 96-well plates. After 7 or 14 days of culture, every well was scored as positive or negative for the appearance of at least one colony. One colony was defined as to consist of at least six cells. The resulting scoring was then analyzed by ELDA limiting dilution analyses tool regarding frequency of stem cells.

3.2.2.10 Cell proliferation assay

Cell proliferation assays were performed by using the Cell Titer Blue kit. The added solution contains resazurin which is reduced by viable cells to resorufin which can then be measured by a different wavelength. Thus, the amount of resorufin correlates with the number of viable cells and is thereof a measure for proliferation.
For the assay, equal numbers of cells were seeded into 96-well plates (OC12: 1500 cells/well, OC20: 4000 cells/well). Every day 20 µl CellTiter Blue solution was added to the respective wells and the amount of resorufin was colorimetrically measured after 3 h at a wavelength of 590 nm with a spectrophotometer. Values were then normalized to day 0 measurements.

3.2.2.11 Wound scratch assay

For the wound scratch assay, cells were seeded in that they reach confluency the next day. Then, cells were incubated for 1 h with mitomycin. Afterwards, a scratch was made with a sterile tip and the medium was changed. At various time points (0 h, 8,5 h and 19 h) microscopic pictures of the scratch area were taken. Analysis of the size of the scratch area was then performed via Fiji.

3.2.3 Molecular Methods

3.2.3.1 RNA extraction

Extraction of RNA was performed with the miRNeasy Kit (Qiagen) according to the manufacturer's instructions. Measurement of RNA concentration was performed with the Nanodrop (Thermo Fisher) or via Bioanalyzer (Agilent Technologies).

3.2.3.2 cDNA preparation

For preparation of cDNA, 500 ng of RNA were used and transcribed into cDNA with the High Capacity cDNA Kit (Applied Biosystems) according to the manufacturer's instructions. Distilled water was then added to the reaction volume and filled up to 20 µl. Afterwards, reverse transcription was performed in a thermal cycler for 10 min at 25° C, 2 h at 37° C followed by 5 min at 85° C. Finally, the reaction volume was filled up to 50 µl with distilled water so that a cDNA concentration of 10 ng/µl was obtained.

3.2.3.3 Quantitative real-time PCR (qPCR)

Quantitative real-time PCR aims at quantifying the amount of transcribed mRNA in a cell. Total RNA was extracted using the miRNeasy Kit (Qiagen) and transcribed into cDNA with the High Capacity cDNA Kit (Applied Biosystems). Then, equal amounts of cDNA (10 ng) were incubated with 0.5 µl of the FAM-labeled target Taqman probe and 3.5 µl Taqman Universal master mix. Then, the qPCR was run at 50 °C for 2 min, 95 °C for 10 min, 95 °C for 15 sec, 60 °C for 1 min (40 cycles) at the Viia 7 Real-Time PCR System (Applied Biosystems). The Viia 7 software 1.1 was then applied for data acquisition and analysis. Normalization of the expression of the target gene was done against PPIA.

3.2.3.4 Cloning strategy

The plasmid overexpressing SPDEF was designed based on the LegoiT2 vector which was cut with *BamHI* and *NotI* in the multiple cloning site. The SPDEF coding sequence (accession number NM_012391.2) was amplified by the primers SPDEF_FW and SPDEF_RV, purified via gel extraction and ligated with the dephosphorylated LegoiT2 vector.
Regarding FOXA2 overexpression, the target sequence (accession number: NM_21784.4) was amplified with the primers FOXA2_FW2 and FOXA2_RV. The LegoiT2 vector was cut with *BamH1* and *EcoRI* and ligated with the amplified and purified FOXA2 coding sequence.
The inducible FOXA2 OX vector was generated by F. Geist based on the backbone of the inducible pTRIPZ non-silencing plasmid. Briefly, the shRNA sequence was cut by *AgeI* and *MluI* and the FOXA2 sequence (accession number: NM_21784.4) was inserted by Gibson cloning with restoration of the *AgeI* and *MluI* restriction sites.

3.2.3.5 Polymerase chain reaction (PCR)

For amplification of the coding sequences of SPDEF and FOXA2, a PCR was run. Therefore, the pCMV-XL5 NM_021784.3 (FOXA2 coding sequence) or pCMV6-XL5 NM_012391.2 (SPDEF coding sequence) plasmids, 10 µM of the respective primers SPDEF_FW and SPDEF_RV or FOXA2_FW2 or FOXA2_RV, as well as the Q5 Hot Star 2x master mix (NEB) and dNTPs (Fermentas) were used according to the manufacturer's instructions.
The PCR was run at 98° C for 30 sec, then 30 cycles of 98° C for 10 sec, 68° C for 30 sec and 72° C for 30 sec, as well as after the 30 cycles another 2 min at 72° C.

3.2.3.6 PCR clean-up

Purification of PCR fragments was performed with the Qiaquick PCR purification Kit (Qiagen) according to the manufacturer's instructions.

3.2.3.7 Restriction digest

Restriction digest of the LegoiT2 vector and the purified PCR *fragments* of the coding sequences of SPDEF and FOXA2 was done with *BamHI* and NotI for SPDEF and with *BamHI* and *EcoRI* for FOXA2 in NEB buffer 3.1 for 15 min at 37° C according to the manufacturer's instructions.

3.2.3.8 Dephosphorylation of LegoiT2

The dephosphorylation of the LegoiT2 vector for subsequent ligation was done with the Antarctic Phosphatase Kit (NEB) according to the manufacturer's instrcutions. Briefly, kit components were incubated with 5 µg of the LegoiT2 DNA for 15 min at 37° C and heat inactivated for 5 min at 70° C.

3.2.3.9 Gel extraction

Gel extraction was performed with the Qiaquick Gel extraction Kit (Qiagen) according to the manufacturer's instrcutions.

3.2.3.10 Ligation

For ligation of the dephosphorylated pLegoiT2 vector and the digested fragments of SPDEF or FOXA2 coding sequences, the DNA was incubated with T4 DNA ligase and T4 ligation buffer (Takara) for 1 h at RT followed by heat inactivation at 65° C for 15 min. Insert and vector DNA ratio for ligation was 3:1.

3.2.3.11 Transformation of competent bacteria

For transformation of chemocompetent STBL3 bacteria, bacteria were thawed on ice, the ligated vector was added without pipetting and incubated for 1 h on ice. Then, cells were put

in a waterbath at 42° C for 45 sec and afterwards put on ice for 2 min. Then 250 µl SOC medium was added & cells let shaken for 1 h at 37° C at 225 rpm. Afterwards, the mixture was plated on a pre-warmed LB plate containing 100 µg/ml carbenicillin and incubated over night at 37° C.

3.2.3.12 Colony-Polymerase Chain Reaction

In order to verify which bacterial colony on the LB agar plate contained the plasmid of interest, a colony PCR was performed. A master mix of 0.35 µl homemade Taq polymerase and 5 µl buffer (DKFZ), 1 µl dNTPs (10 mM, Fermentas), 2.5 µl DMSO (Sigma), as well as 2 µl forward and 2 µl reverse primers were mixed. Then, one colony was picked with a tip, first tipped on a second agar plate in order to conserve the colony for subsequent mini and maxi cultures, and second, put into the master mix. A PCR was then run for 1 min at 95° C, then 30 cycles of 1 min at 95° C, 90 sec at 60° C, 1 min at 72° C and after the cycles another 5 min at 72° C. After the PCR, the samples were loaded onto an agarose gel and analyzed regarding expected plasmid bands.

3.2.3.13 Agarose gel electrophoresis

Agarose gel electrophoresis is used to analyze the size of DNA fragments and to purify these. For gel electrophoresis, midi gels were prepared by mixing 300 ml TAE buffer and 3 g agarose and heating them in the microwave for 3 min. After the solution had cooled down a bit, 1 drop of ethidium bromide was added to the mixture and the solution was poured in a gel retainer. The samples were then mixed with 1 loading dye and loaded onto the gel together with a 1 kb or 100 bp ladder. The gel was run at 130 V for 1 h in TAE buffer and analyzed under UV light.

3.2.3.14 Cultivation of bacteria

Bacteria were cultured either in mini or maxi cultures. Therefore, a single bacterial colony was picked from a LB plate, added to 5 ml of LB medium containing 100 µg/ml carbenicillin and put in a shaker and cultured for 8 h at 37° C and 200 rpm. The mini was then used to inoculate a maxi culture (250 ml) which was again cultured in a shaker at 37° C over night.

3.2.3.15 Glycerol stock

For long-term storage of bacteria, a glycerol stock was made. Therefore, 700 µl of bacteria were mixed with 300 µl of sterile glycerol and then frozen at -80° C. For re-cultivation, a bit of the frozen bacteria was scraped with a scraper and streaked on a LB agar plate.

3.2.3.16 Plasmid purification

Plasmid purification aims at purifying plasmid DNA and is based on an alkaline lysis of bacterial cells followed by binding of DNA to a silica membrane in the presence of a high salt concentration. After several washing steps, the DNA is then eluted.
Purification of plasmid DNA was performed with the Qiaprep Spin Miniprep Kit (Qiagen) for mini cultures or the HiSpeed Plasmid Maxi Kit (Qiagen) for maxi cultures according to the manufacturer's instructions.

3.2.3.17 Determination of DNA concentration

The DNA concentration was measured by the Nanodrop at 260 nm and 280 nm. An optical density (OD) of 1 at 260 nm corresponds to 50 ng/µl dsDNA. The OD at 280 nm measures the protein contamination of the sample. The ratio between OD_{260}/OD_{280} gives the purity of the DNA concentration and should be between 1.8 and 2.

3.2.3.18 Ethanol precipitation of DNA

In order to obtain sterile DNA for lentivirus production, the purified plasmid DNA was further cleaned by ethanol precipitation. Therefore, 1 ml plasmid DNA was mixed with 100 µl 3 M NaAcetat at pH 5.2 (1:10), distributed to two eppis and 2 volumes of ice-cold ethanol were added, shaken in and put at -20° C for 5 min. Then, DNA was centrifuged for 15 min at 4° C at 15,000 rpm. The next steps were then performed at a laminar flow hood. The supernatant was discarded, then two volumes of 70 % ice-cold ethanol were added and the sample centrifuged for 15 min at 4° C at 15,000 rpm. Afterwards, the supernatant was again discarded. The sample was then let dry under the hood and finally, it was dissolved in 300 µl sterile TE buffer and the concentration adjusted to 1 µg/µl.

3.2.3.19 Sequencing

For sequencing of DNA fragments, DNA was diluted to a concentration of 30 – 100 ng/µl. The diluted DNA was then sent to GATC Biotech together with the respective sequencing

primer (10 µM). ”Single read sequencing“ was performed at GATC Biotech and the resulting sequencing data were analyzed the next day with regards to whether they contain the sequence of interest.

3.2.4 Biochemical methods

3.2.4.1 Cell lysis

For cell lysis, adherent cells were put on ice, washed twice with ice-cold PBS and lysis buffer containing 10x RIPA buffer, 100x AEBSF, 100x EDTA and 100x Protease Halt and Inhibitor cocktail in dH_2O (100 µl per 6-well, 700 µl per T75 PRIMARIA flask) was added and incubated for 5 min. Then, the cells were scraped, put into eppis and again incubated for 20 min on ice. Finally, the lysate was centrifuged at 14,000 rpm for 15 min at 4° C. After centrifugation, the supernatant (lysate) was put into a fresh tube and stored at -80° C.

3.2.4.2 Determination of protein concentration

Protein concentration was determined with the BCA assay (Thermo Fisher) according to the manufacturer’s instrcutions.

3.2.4.3 Sodium dodecyl sulfate polyacrylamide gel electrophoresis

SDS-PAGE (Sodium dodecyl polyacrylamide gel electrophoresis) separates proteins according to their molecular weight in the presence of β-mercaptoethanol and SDS. β-mercaptoethanol reduces the bisulfide bonds of proteins and SDS negatively charges proteins due to ist anionic charge and forces them to loose their native conformation by disrupting non-covalent bonds.
For SDS-PAGE, 10 µg of protein was incubated with 1x LDS buffer and 1x TCEP reducing agent and then heated for 10 min at 70° C. Denaturated proteins were then loaded onto a 4-12 % Bis-Tris gel and the Spectra Multicolor Broad Range ladder was used as a ladder. TGS buffer (Biorad) was used as a running buffer and the gel was run at 100 V for 1 h in a Biorad gel chamber.

3.2.4.4 Western blot

For immunoblotting, the gel chamber was broken and the gel put on top of a transfer stack soaked in Trans-blot Turbo transfer buffer (Biorad). On top of these, a PVDF membrane

which was preactivated in methanol for 1 min, and another transfer stack were laid. The blot was then run at 25 V for 10 min in the Trans-blot Turbo system (Biorad).
The membrane could further be activated by UV light in the Chemidoc Imaging system (Biorad) in order to validate equal loading of proteins and for further normalization of protein load. Blocking of the membrane was then performed with 5 % milk in TBS-T for 1 h.

3.2.4.5 Detection of proteins

For detection of proteins, primary antibodies were diluted in 10 ml of 5 % milk in TBS-T with 0.02 % sodium azide and phospho-antibodies were diluted in 5 % BSA in TBS-T with 0.02 % sodium azide. Antibodies were then added to the membrane and incubated at 4° C over night. The next day, the membrane was washed five times for 5 min with TBS-T and then incubated for 1 h with secondary anti-horseradish peroxidase-linked antibodies diluted 1: 10,000 in 5 % milk in TBS-T. Afterwards, the membrane was again washed five times for 5 min with TBS-T, probed with 5 ml of 1:1 diluted Clarity Western ECL Blotting Substrate solution or Clarity Max Western ECL Substrate solution (Biorad) and then developed in the Chemidoc Imaging system (Biorad) for various time points ranging from 1 sec to 30 min.

3.2.4.6 Re-probing of the blots.

For re-probing of blots, the blots were incubated with Restore Plus Western Blotting Stripping buffer (Thermo Fisher) for 10 min at RT. Afterwards, the membrane was washed twice in TBS-T and then blocked for 1 h with 5 % milk in TBS-T. Then, the next primary antibody was added and incubated over night at 4° C.

3.2.5 Immunohistochemistry

Immunohistochemical stainings were performed by Vanessa Vogel, Department of Pathology, University Clinic Heidelberg, and Ornella Kossi, HI-STEM/DKFZ Heidelberg.
Briefly, tumor specimens were fixed in 10 % formalin for 48 h, dehydrated with increasing ethanol concentrations, followed by xylene and subsequent embedding in paraffin. To perform immunohistochemical staining, slides were deparaffinized by xylol, followed by decreasing ethanol concentrations (100 %, 96 %, 70 %) and finally, water. For antigen retrieval, slides were cooked in a steam pot with citrate buffer pH 6.0 for 15 min, followed by cooling down for 30 min and rinsing with distilled water. Unspecific binding was then

blocked by using the Avidin/Biotin Blocking Kit according to the manufacturer's instructions. Then, the primary antibodies were incubated according to the concentrations in 3.1.8 in a volume of 200 µl for 30 min at room temperature followed by a rinsing step in PBS/0.5 % tween buffer and subsequent addition of the appropriate biotinylated secondary antibody using the Dako Real Detection System and incubation for 20 min at room temperature. Then, endogenoeus peroxidase was blocked for 5 min at room temperature followed by another washing step in PBS/0.5 % tween buffer. Afterwards, slides were incubated with horseradish-peroxidase for 20 min at room temperature, again rinsed with PBS/0.5 % tween and incubated with AEC substrate chromogen solution. Slides were monitored under the microscope for optimal incubation time determination. Then, the slides were counterstained with hematoxylin.

3.2.6 Mouse methods

3.2.6.1 Intraperitoneal and subcutaneous xenograft assays

Mice were intraperitoneally injected with tumor cells in a volume of 100 µl of CSC medium. For subcutaneous approaches, tumor cells in CSC medium were mixed with ice-cold matrigel in a 1:3 volume (matrigel : CSC) and then subcutaneously injected.
At the endpoint of the experiment, mice were euthanized and tumors taken out. Regarding mice that were intraperitoneally injected, mice were also euthanized and then 3 ml of PBS was injected into the abdomen and the mouse ascites including tumor cells was taken out with a syringe and flow cytometrically analyzed.
All mouse experiments followed German legal regulations and were before approved by the governmental review board of the state Baden-Wurttemberg (G17/12 and G235/16).

3.2.6.2 *In vivo* imaging

For bioluminescent imaging, mice were intraperitoneally injected with 250 µl of 15 mg / ml luciferin. Mice were anesthetized with a 1.8 flow rate of O_2 / 2.5 % isoflurane mixture for 6 min and then put into the IVIS Spectrum *In Vivo* Imaging System. Pictures, as well as photon flux measurements were recorded for various time points and total photon flux was analyzed by defining a region of interest across the abdomen of the mice.

3.2.7 Bioinformatic analyses

3.2.7.1 Gene expression analyses

Total RNA of FACS-sorted SSEA1$^+$ and SSEA1$^-$ cells, as well as total RNA of SPDEF overexpression, knockdown, iT2 and NS control cells cultured for 7 days with or without doxycycline were extracted using the miRNeasy Kit (Qiagen). Quality and quantity of RNA was measured via Nanodrop and Agilent 2100 Bioanalyzer. RNA was then subjected to the Genomics and Proteomics Core Facility, DKFZ, for gene expression profiling. The Illumina HT12v4 BeadChip technology was applied for expression profiling. Testing for statistically different genes was done with Chipster 3.13 software (Kallio *et al.,* 2011). Briefly, resulting raw data were quantile normalized and filtered with the coefficient of variation method (0.5). Differential gene expression was then performed with the empirical Bayes test with Benjamini-Hochberg correction for multiple testing (FDR < 0.05 and 0.1) or without (p-value 0.05, 0.01 and 0.001).

Gene expression data were hierarchically clustered by clustering the top 100 differentially expressed genes with average-linking method and manhattan distance using R software (R Core Team 2017). For clustering according to single patient background, batch effect removal was performed using the ComBat method (Johnson *et al.,* 2007). Principal component analyses were further conducted. To visualize differential gene expression, volcano plots were computed. R scripts for heatmaps, volcano plots and principal component analyses are given in 7.2.

3.2.7.2 Gene set enrichment analyses

Gene set enrichment analyses (GSEA) were performed on quantile normalized data. P values were computed using standard parameters with 1,000 permutations and corrected with the false-discovery rate method (Subramanian *et al.,* 2005).

3.2.7.3 Gene Ontology analyses

Gene ontology analyses (biological processes) for SSEA1$^+$ and SSEA1$^-$ cells were performed by analyzing all genes differentially enriched with a p-value of 0.1 in the respective population with the online tool at www.gene ontology.org (Ashburner et al., 2000, The Gene Ontology 2017). Top GO terms that were enriched with a FDR < 0.05 were chosen.

3.2.7.4 Kaplan-Meier overall survival analyses

Overall survival analyses were performed with the online tool "KMplotter" (Gyorffy *et al.,* 2012). Briefly, GSE23554, GSE9891, GSE26193 and GSE14764 datasets were chosen and analyses conducted by choosing the parameters "serous histology" and "auto select best cut-off". All other parameters were as default.

3.2.7.5 Gene signature calculation and overall survival analyses

For the generation of the 15-gene SPDEF target gene signature, the top 15 differentially expressed genes between OC12 iT2 and SPDEF OX samples (SLC16A9, HES4, RAB31, LRP3, EEF1A2, BAIAP2L2, UNC5A, RNF39, CRYAB, YIPF1, TSPAN9, PTGER2, RAP1GAP, MLPH, RARRES1) were taken, the z-score expression for these genes over all patients from the TCGA dataset (n = 420 patients) computed and finally, the sum over all genes calculated. Then, the lower 25 % and the upper 75 % quantile of the sum of the z-scores was assigned to death (1) or alive (0) events and a Kaplan-Meier curve calculated.

3.2.7.6 Correlation study

For correlation analyses of ESR and SPDEF, z-scores of gene expression data from a cohort of 535 patients of the TCGA dataset were used. Expression values were assembled in a correlation matrix and Spearman correlation as well as p-value were computed

3.2.7.7 Statistical analyses

Statistical analyses were performed with GraphPad Prism 7 software. The respective tests used are denoted in the figure legends. Statistical analyses for *in vitro* and *in vivo* limiting dilution analyses were performed with the ELDA online tool (Hu *et al.,* 2009). P-values < 0.05 were considered as statistically significant. Regarding GSEA, a FDR < 0.25 was considered as statistically significant. Differential gene expression analyses were performed with Chipster 3.13 software (Kallio *et al.,* 2011) by using the empirical Bayes test with Benjamini-Hochberg correction for multiple testing (FDR < 0.05 and 0.1) or without (p-value 0.05, 0.01 and 0.001).

4. RESULTS

4.1 Identification of tumor-initiating cells in HGSOC

The identification of tumor-initiating cells in high-grade serous ovarian cancer implies the utilization of a model which preserves the heterogeneity of the original patient tumors and retains the tumor-initiating cells. Therefore, Dr. Steve Wagner and me established patient-derived *in vitro* and *in vivo* models of HGSOC cell lines (1.1.5) which recapitulate the heterogeneity of the original tumor (Wagner 2013). The characteristics of patients and tumors, as well as thereof derived SOC cell lines are summarized in table 9.

Table 9: Characteristics of the patient-derived SOC cell lines.
Table was composed with data from (Wagner 2013, Jabs *et al.,* 2017). ND = not determined

SOC cell line	Origin	FIGO stage	Grade	TNM	Pathological disease	subtype	SNV or gene loss
OC12	tumor	IIIc	G3	TN1M1	serous adeno-carcinoma	mesenchymal	TP53
OC14	ascites	IV	G3	TN1M1	serous adeno-carcinoma	mesenchymal	TP53
OC15	ascites	IIIc	G3	TN1M1	serous adeno-carcinoma	immunoreactive	TP53
OC18	tumor	IIIc	G3	TN1M1	serous adeno-carcinoma	differentiated	TP53
OC19	tumor	IIIc	G3	TN1M1	serous adeno-carcinoma	proliferative	TP53, BRCA2
OC20	pleural effusion	IIIc	G3	TN1M1	serous adeno-carcinoma	proliferative	TP53, BRCA1
ASC211	ascites	IIIc	G3	TN1M1	serous adeno-carcinoma	ND	-
PE306	pleural effusion	IV	G2	TN1M1	serous adeno-carcinoma	ND	TP53

4.1.1 A surface marker screen reveals heterogeneously expressed molecules

Since we believe that phenotypic heterogeneity is also reflected in molecular and functional heterogeneity, Dr. Steve Wagner performed an antibody-based flow cytometric surface screen of the OC12 cell line in order to identify subpopulations of cells among the bulk tumor cells (Wagner 2013). We reanalyzed the screen data (figure 9) in order to identify populations which showed an up to 10 % positive expression of the respective surface molecule (yellow), positive and negative populations (red), a broad distribution of expression (green), no expression (white) or only positive populations (blue).

The expression of known markers of tumor-initiating cells like CD24 or CD44 (Meng *et al.,* 2012, Gao *et al.,* 2015) and emerging ones like CD151 (Wagner 2013) could be identified by our screen (figure 9). Further, surface molecules of stemness and pluripotency ((Lanctot *et al.,* 2007, Varki *et al.,* 2015)), such as SSEA3, SSEA4, TRA-1-60 and TRA-1-81, were also heterogeneously expressed.

However, since we were most interested in heterogeneous subpopulations and in identifying new markers of ovarian cancer-initiating cells, we focused on the surface molecules marked in red and yellow. Based on literature research, we decided to focus on SSEA1 / CD15 (Stage-specific embryonic antigen 1) and analyzed its role as a tumor-initiating marker.

Taken together, the reanalysis of the flow-cytometric surface marker screen identified subpopulations of SSEA1 positive and negative cells among OC12 ovarian cancer cells.

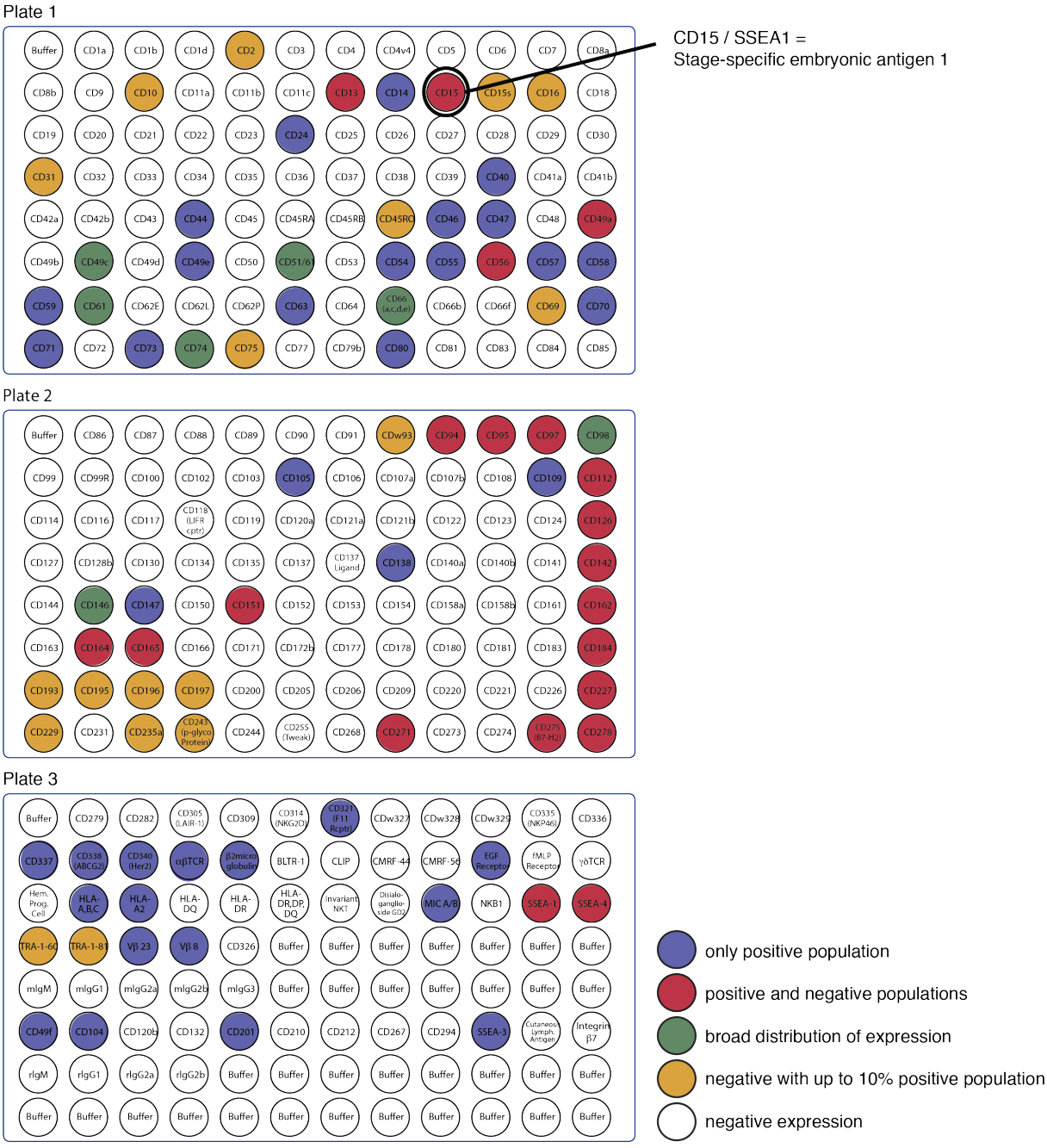

Figure 9: Expression of cell surface markers of the OC12 cell line as analyzed with the BD Lyoplate Human Cell Surface Marker Screening Panel.
Blue = all cells are positive for the respective marker, red = positive and negative populations exist, green = broad distribution of expression, yellow = mainly negative population but with up to 10% of total cells with positive expression, white = no expression. Data were generated by (Wagner 2013), but reanalyzed.

4.1.2 SSEA1 is heterogeneously expressed in primary OC cell lines, xenografts and patient samples of HGSOC

We confirmed the heterogeneous expression of SSEA1 in the OC12 and five other patient-derived ovarian cancer-cell lines OC14, OC15, OC18, OC19 and OC20 by FACS (figure 10). In all cell lines analyzed, we found a broad distribution of SSEA1 expression, with both highly positive and negative populations, varying from more than 90 % of $SSEA1^-$ cells (OC15) to more than 90 % of $SSEA1^+$ cells (OC18, OC20). In table 10, the expression of SSEA1 as analyzed by FACS at different passaging time points is shown.

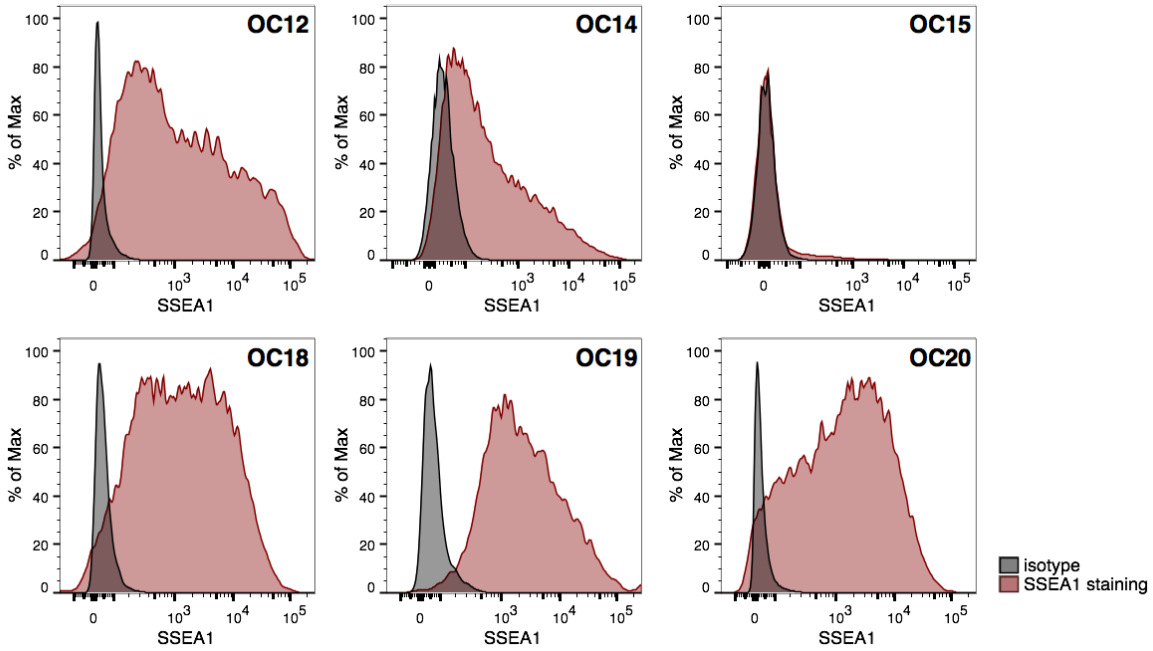

Figure 10: SSEA1 is heterogeneously expressed in different primary OC cell lines.
FACS analysis of cultured OC cell lines stained with anti-SSEA1 antibody (red) or control isotype (black).

Table 10: SSEA1 expression in OC cell lines at different passages as analyzed by FACS.

	experiment 1 [%]	passage	experiment 2 [%]	passage	experiment 3 [%]	passage
OC12	46	6	97	13	75	19
OC14	56	11	50	12	66	14
OC15	7	6	8	17	1	25
OC18	91	9	93	14	-	-
OC19	46	6	85	14	94	21
OC20	95	7	82	10	69	12

To confirm that SSEA1 is also remained *in vivo* and that it is also heterogeneously expressed, we further analyzed xenograft tumors and patient samples regarding SSEA1 expression.
We could detect a heterogeneous SSEA1 staining in xenografted tumors of 6 OC patients (figure 11). In order to confirm that the stained cells in the tumors are indeed of human origin, we verified this by co-staining for human Ki67 (figure 11, pink). In addition to the tumors displaying a heterogeneous expression of SSEA1 (figure 11, brown), the amount of positively stained cells seemed to correlate with the SSEA1 staining pattern of the OC cell lines. OC15 xenografts, for example, displayed nearly no $SSEA1^{+}$ staining which is in line with a nearly completely negative FACS staining for SSEA1 in the OC15 cell line (figure 10).

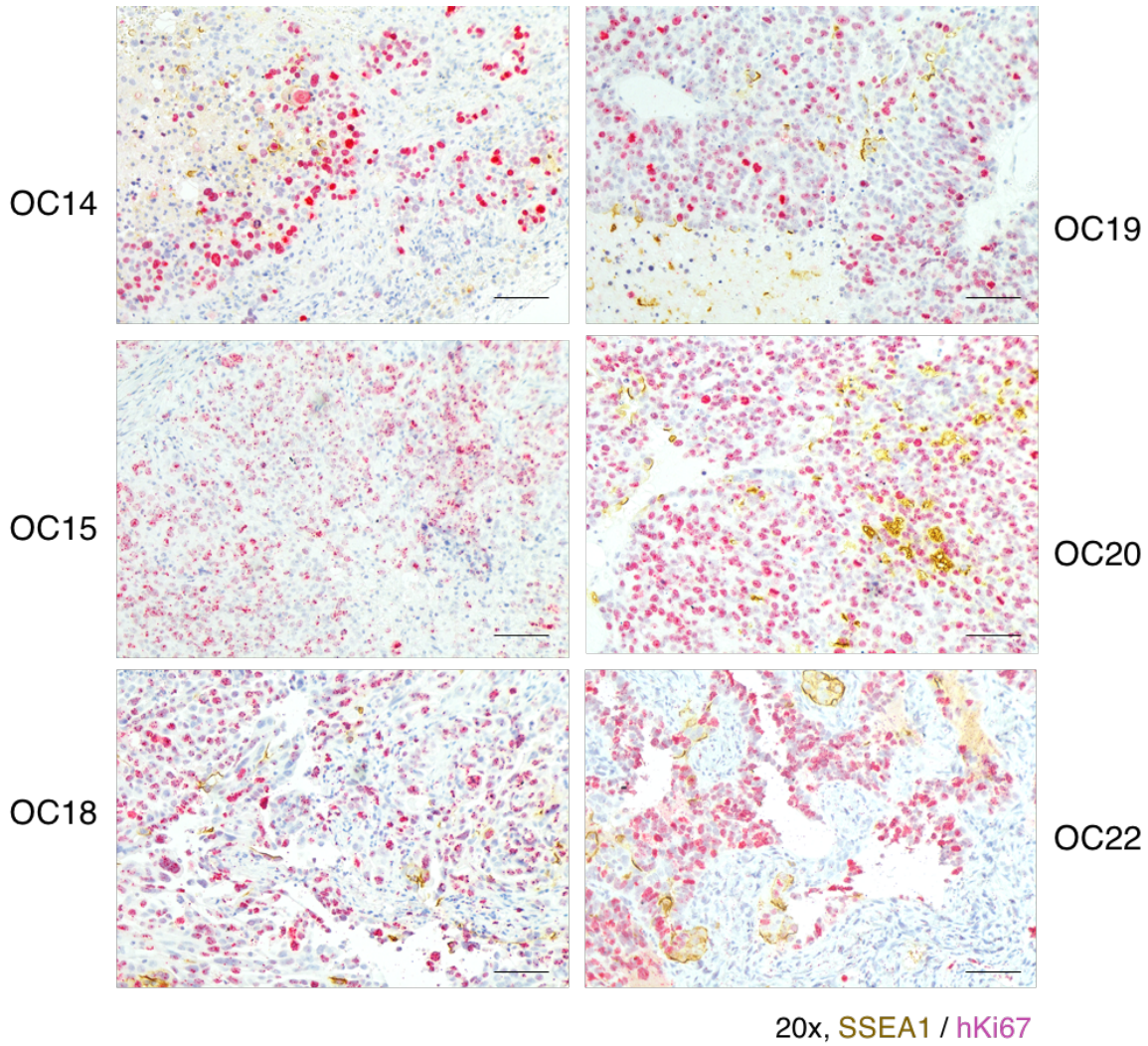

Figure 11: SSEA1 is expressed in xenografts of patient-derived OC lines.
SSEA1 expression (brown) was stained in xenograft tumors derived from patient-derived OC lines. In order to verify the human origin of the cells, a counterstaining with human Ki67 (pink) was performed. Scale bar denotes 100 µm.

We could further detect a heterogeneous expression of SSEA1 in primary patient samples. Patient-derived ascites further showed a heterogeneous expression for SSEA1 (figure 12 b). Besides, we also detected a heterogeneous expression of SSEA1 in primary patient tumors based on immunohistochemistry (figure 12 c).

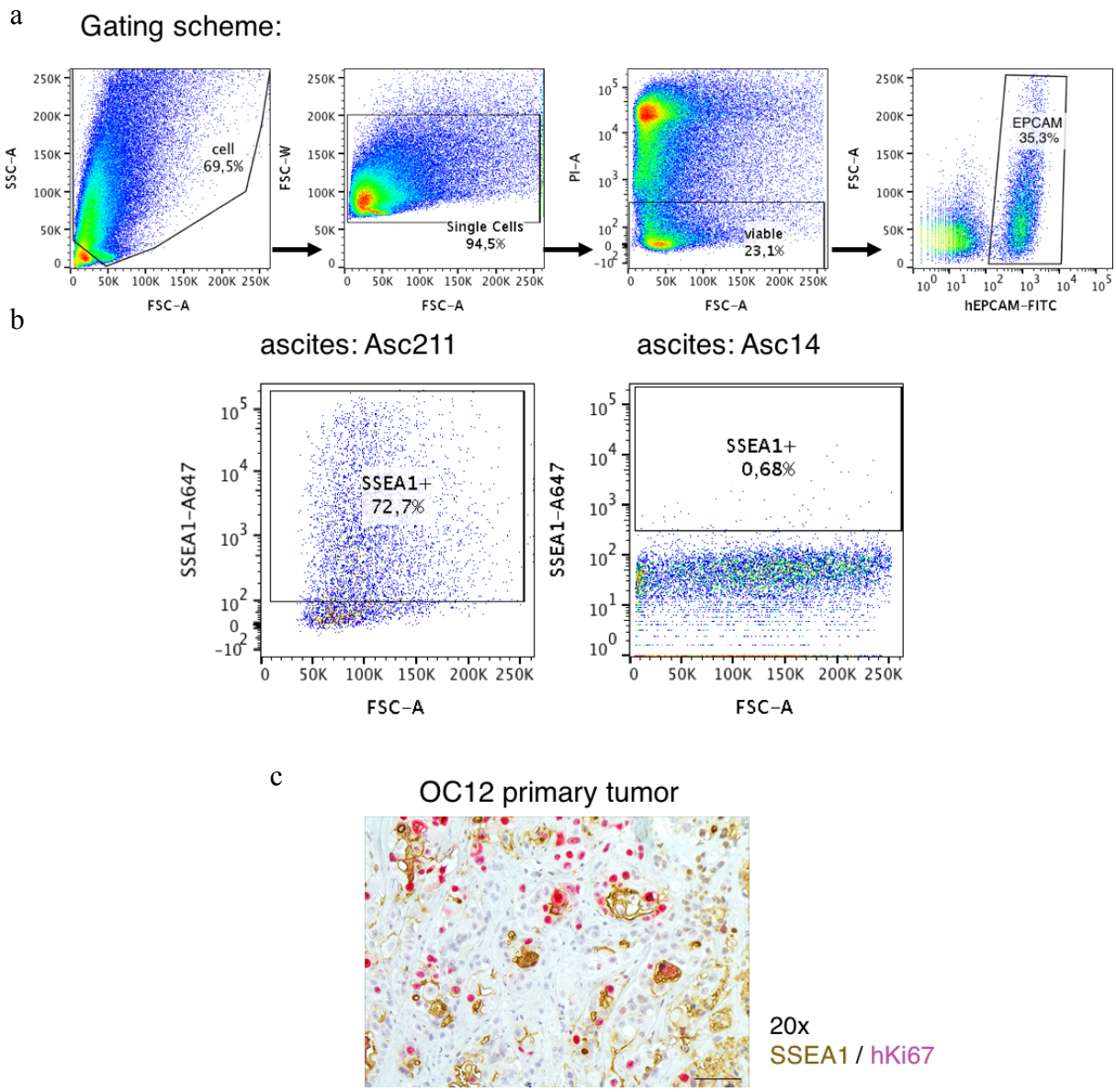

Figure 12: SSEA1 is heterogeneously expressed in ascites and primary tumors of patients.
(a) Gating scheme for FACS analysis of patient ascites samples regarding SSEA1 expression. (b) FACS-staining of patient-derived ascites of samples Asc211 and Asc14 for SSEA1. (c) Immunohistochemical staining of the primary tumor of patient OC12. Scale bar denotes 100 µm. EPCAM = epithelial cell adhesion molecule, FITC = fluorescein isothiocyanate, FSC = forward scatter, PI = propidium iodide, SSC = sideward scatter

4.2 SSEA1$^-$ cells define a tumor-initiating population in HGSOC

4.2.1 Functional characterization of SSEA1$^+$ and SSEA1$^-$ cells *in vitro*

4.2.1.1 The SSEA1 population is different from CD24 and CD44 populations

The cell surface molecules CD24 and CD44 have been identified as 'cancer stem cell' markers in various malignancies including ovarian cancer (Meng *et al.,* 2012, Gao *et al.,* 2015). In order to confirm that the SSEA1$^+$ and SSEA1$^-$ cell populations are unique populations different from those of CD24 and CD44, we performed a co-staining of SSEA1 and either CD44 (figure 13) or CD24 (figure 14) and analyzed the cell population by FACS. In all 6 OC cell lines, there was no correlation between the SSEA1 and CD24 or CD44 staining, respectively.

We hence concluded that the SSEA1$^+$ and SSEA1$^-$ populations are unique populations different from either CD24- or CD44-positive or negative populations.

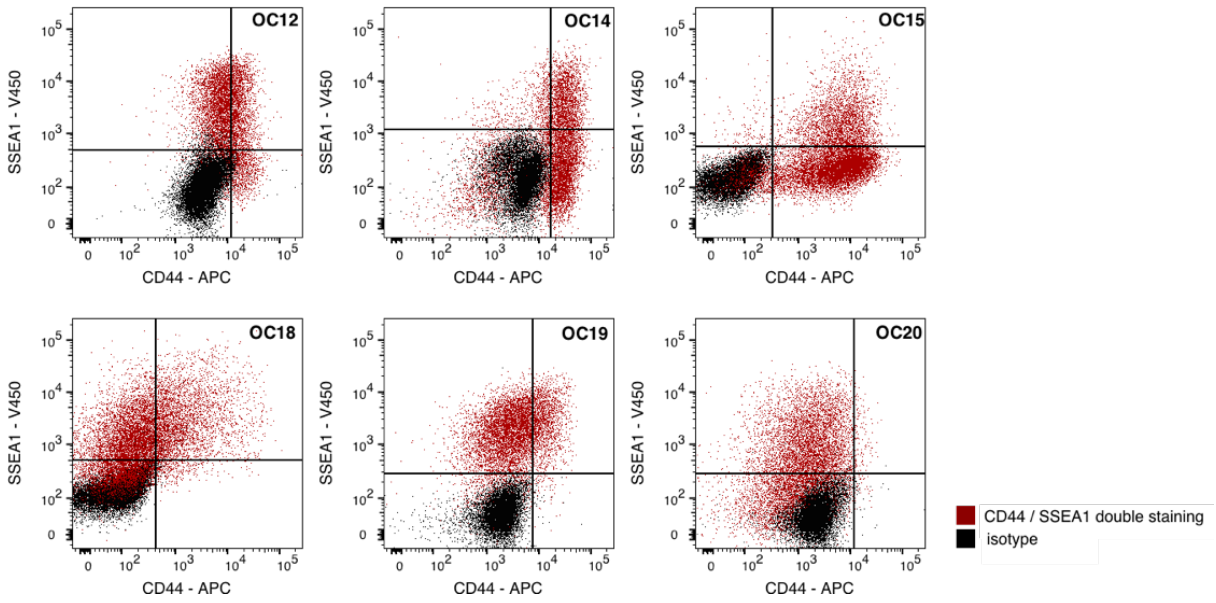

Figure 13: SSEA1 expression does not overlap with CD44 staining.
Flow cytometric analysis of the double staining of SSEA1-V450 and CD44-APC (red) and overlay with the respective isotype controls (black). APC = allophycocyanin.

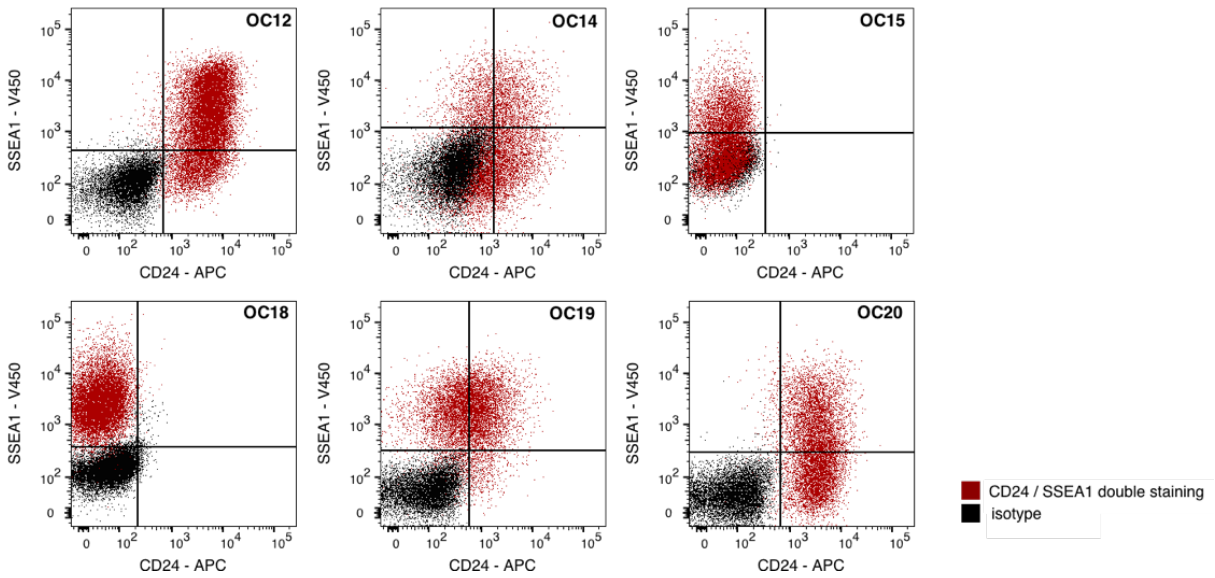

Figure 14: SSEA1 expression does not overlap with CD24 staining.
Flow cytometric analysis of the double staining of SSEA1-V450 and CD24-APC (red) and overlay with the respective isotype controls (black). APC = allophycocyanin.

4.2.1.2 SSEA1$^+$ and SSEA1$^-$ cells differ in size

Previous observations from histological and FACS stainings suggested that the SSEA1$^+$ and SSEA1$^-$ cells may differ in cell size. Thus, we analyzed the size of the SSEA1$^+$ and SSEA1$^-$ cells by comparing their forward and sideward scatter FACS profiles, respectively (figure 15a, c). The median fluorescence intensity was significantly lower regarding sideward ($p = 0.01$) and forward scatter ($p = 0.006$) profile in the SSEA1$^-$ population of all six OC lines (figure 15b, d).

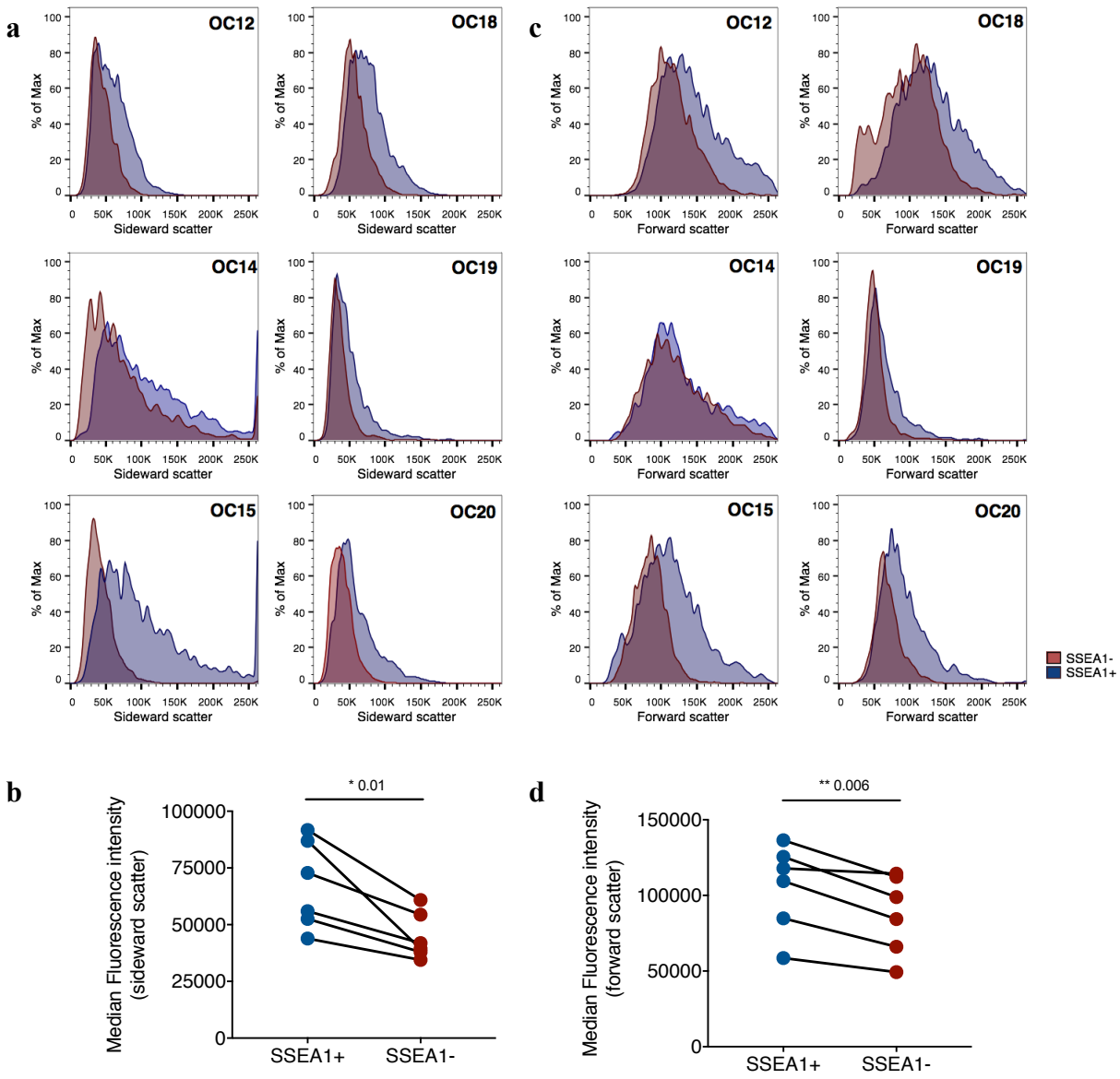

Figure 15: Sideward and forward scatter size distribution of SSEA1$^-$ and SSEA1$^+$ cells. FACS analysis of 6 OC cell lines regarding the size of SSEA1$^-$ (red) and SSEA1$^+$ (blue) cells as measured by their sideward (a) and forward scatter (c) distribution. (b, d) Quantification of the median fluorescence intensity of sideward and forward scatter of SSEA1$^+$ and SSEA1$^-$ cells. * $p < 0.05$, ** $p < 0.01$; paired, parametric, two-tailed t-test.

We further examined the sorted SSEA1$^-$ and SSEA1$^+$ cells under the microscope in order to assess different morphological characteristics.

We observed that the SSEA1$^+$ cells were bigger and contained more nuclei than the SSEA1$^-$ cells (figure 15), confirming the data from the FACS forward and sideward scatter analyses.

To sum up, we discovered that the SSEA1$^-$ and SSEA1$^+$ cells differ phenotypically regarding their size and growth characteristics.

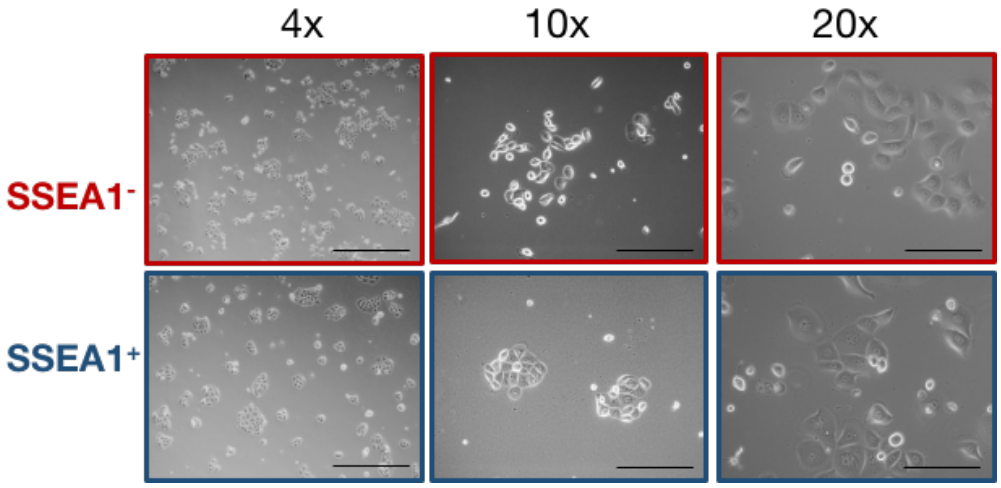

Figure 16: Representative images of FACS-sorted SSEA1$^-$ and SSEA1$^+$ cells.
The purity of the sorted cells was 79% and 90% for the SSEA1$^-$ and SSEA1$^+$ cells, respectively. Scale bar denotes 50 µm (20x), 100 µm (10x) and 250 µm (4x).

4.2.1.3 SSEA1$^+$ and SSEA1$^-$ cells do not differ regarding *in vitro* growth

In order to analyze the growth characteristics of SSEA1$^+$ and SSEA1$^-$ cells, we FACS-sorted SSEA1$^+$ and SSEA1$^-$ cells, seeded them into 96-well plates and assessed growth with the Cell Titer Blue (CTB) assay by measuring the reduction of resazurin to resorufin at various time points.

No growth differences were detected between SSEA1$^+$ and SSEA1$^-$ cells both in OC12 and OC20 cell lines (figure 17).

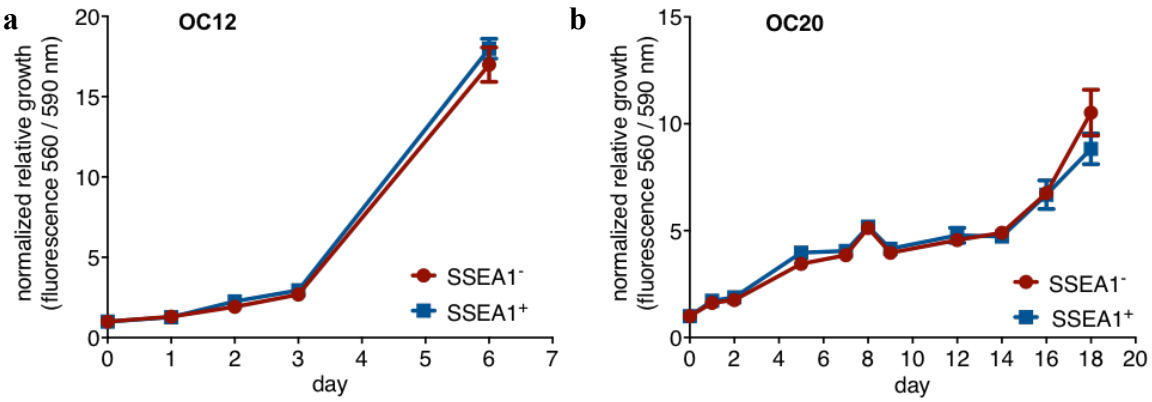

Figure 17: Growth curve of SSEA1$^-$ and SSEA1$^+$ cells *in vitro*.
Growth of FACS-sorted SSEA1$^-$ (red) and SSEA1$^+$ (blue) cells was measured via the Cell Titer Blue assay in OC12 (a) and OC20 cells (b). Mean ± SD.

4.2.1.4 SSEA1$^-$ cells give rise to SSEA1$^+$ cells *in vitro*

Since the expression of SSEA1 was heterogeneous in all OC cell lines tested *in vitro*, we wondered whether these are separate populations or whether SSEA1 expression is unstable and cells can convert SSEA1$^-$ to SSEA1$^+$ or vice versa.

To address this question, we transduced OC12 and OC19 cells with H2B-GFP, then stained for SSEA1, sorted the cells into SSEA1$^-$ H2B-GFP$^-$ and SSEA1$^+$ H2B-GFP$^+$ cells, mixed them in a 50:50 ratio and took them into culture (figure 18a, b and figure 19a). Cells were allowed to grow for 39 (OC12) or 14 days (OC19), followed by occasional splitting. At different time points (OC12: 7, 10, 17, 39 days; OC19: 1, 2, 3, 6, 14 days), parts of the cultured cells were again stained for SSEA1, analyzed by flow cytometry and the number of SSEA1$^+$ cells derived from initially either SSEA1$^-$ or SSEA1$^+$ cells was assessed (figure 18c and figure 19b). The origin of the initially either SSEA1$^+$ or SSEA1$^-$ cells could be tracked since they were additionally also either H2B-GFP$^-$ (SSEA1$^-$) or H2B-GFP$^+$ (SSEA1$^+$).

To exclude a potential effect of H2B-GFP, also SSEA1$^-$ H2B-GFP$^+$ and SSEA1$^+$ H2B-GFP$^-$ cells were sorted, mixed, taken into culture and the amount of SSEA1$^+$ cells derived from initially either SSEA1$^-$ or SSEA1$^+$ quantified (figure 18d, e and figure 19c, d).

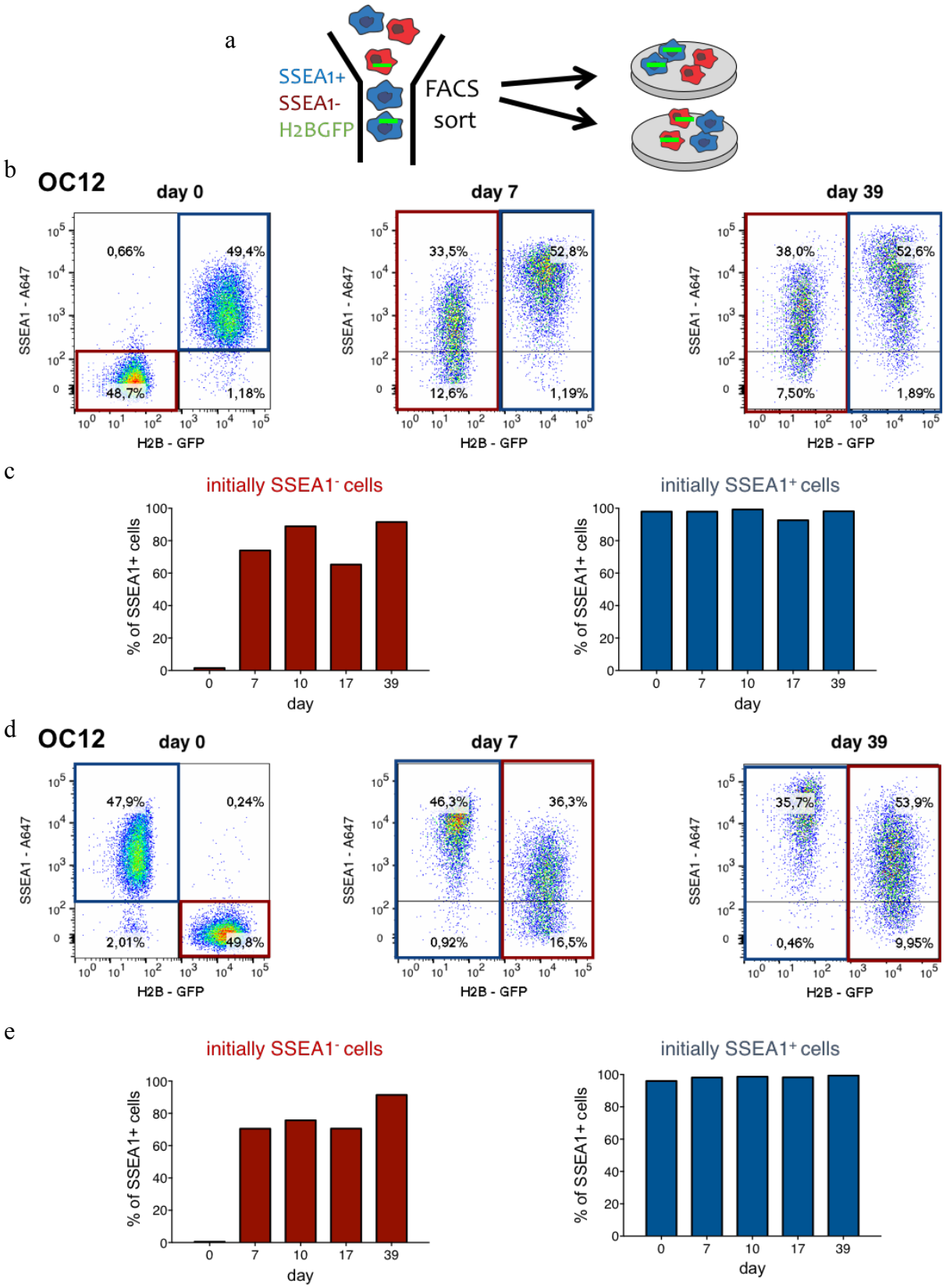

Figure 18: SSEA1$^-$ cells give rise to SSEA1$^+$ cells *in vitro* (OC12).
(a) Schematic overview of the experimental workflow to assess the plasticity of SSEA1$^-$ and

SSEA1$^+$ cells. (b) FACS-sorted, initially 99 % pure SSEA1$^-$ H2BGFP$^-$ (red) and initially 98 % pure SSEA1$^+$ H2BGFP$^+$ (blue) cells of OC12 were mixed in an approximately 50:50 ratio and cultured for 39 days. On day 7, 10, 17 and 39, the cells were stained for SSEA1 and the percentages of SSEA1$^+$ cells in the initially SSEA1$^-$ (red) and initially SSEA1$^+$ (blue) cells analyzed by flow cytometry and quantified (c). (d) FACS-sorted, initially 96 % pure SSEA1$^+$ H2B-GFP$^-$ (blue) and initially 99 % pure SSEA1$^-$ H2BGFP$^+$ (red) cells of OC12 were mixed in an approximately 50:50 ratio and cultured for 39 days. On day 7, 10, 17 and 39, the cells were stained for SSEA1 and the percentages of SSEA1$^+$ cells in the initially SSEA1$^-$ (red) and initially SSEA1$^+$ (blue) cells analyzed by flow cytometry and quantified (e). Horizontal lines in (c and d) depict the isotype staining cutoff. GFP = green fluorescent protein, H2B = histone 2 B

The number of FACS-sorted initially 98 % (OC12) and 98 % (OC19) pure SSEA1$^+$ H2B-GFP$^+$ cells, was stable over time in both the OC12 and OC19 cell lines. However, the amount of initially 99 % (OC12) and 94 % (OC19) pure SSEA1$^-$ H2B-GFP$^-$ cells decreased quickly and by day 7 (OC12) or 14 (OC19), respectively, more than 80 % of the cells became SSEA1$^+$ (figure 18b, c and figure 19a, b). It could be clearly verified that these cells were originally derived from the SSEA1$^-$ cells since they were still H2B-GFP$^-$.

The SSEA1$^+$ cells also retained their SSEA1 expression over time and the SSEA1$^-$ cells became positive when performing the experiment the opposite way, namely quantifying SSEA1$^+$ / SSEA1$^-$ cells derived from initially 99 % (OC12) and 93 % (OC19) pure SSEA1$^-$ H2B-GFP$^+$ or 96 % (OC12) and 97 % (OC19) pure SSEA1$^+$ H2B-GFP$^-$ cells, respectively (figure 18d, e and figure 19c, d).

Sorted SSEA1$^-$ and SSEA1$^+$ cells were also taken into culture individually and the emergence of SSEA1$^+$ cells was quantified. Just as in the mixed cultures, SSEA1$^-$ cells quickly gave rise to SSEA1$^+$ cells and the SSEA1$^+$ cell population was stable over time (data not shown).

We concluded, that solely SSEA1$^-$ cells are able to give rise to SSEA1$^+$ progenies. The phenotype of SSEA1$^+$ cells, however, stayed stable and SSEA1$^+$ cells could not give rise to SSEA1$^-$ ones. Taken together, these data indicate that SSEA1$^-$ cells sustain *in vitro* growth of tumor cells by generating SSEA1$^-$ and SSEA1$^+$ cells and may be further ahead in the cellular hierarchy than SSEA1$^+$ cells.

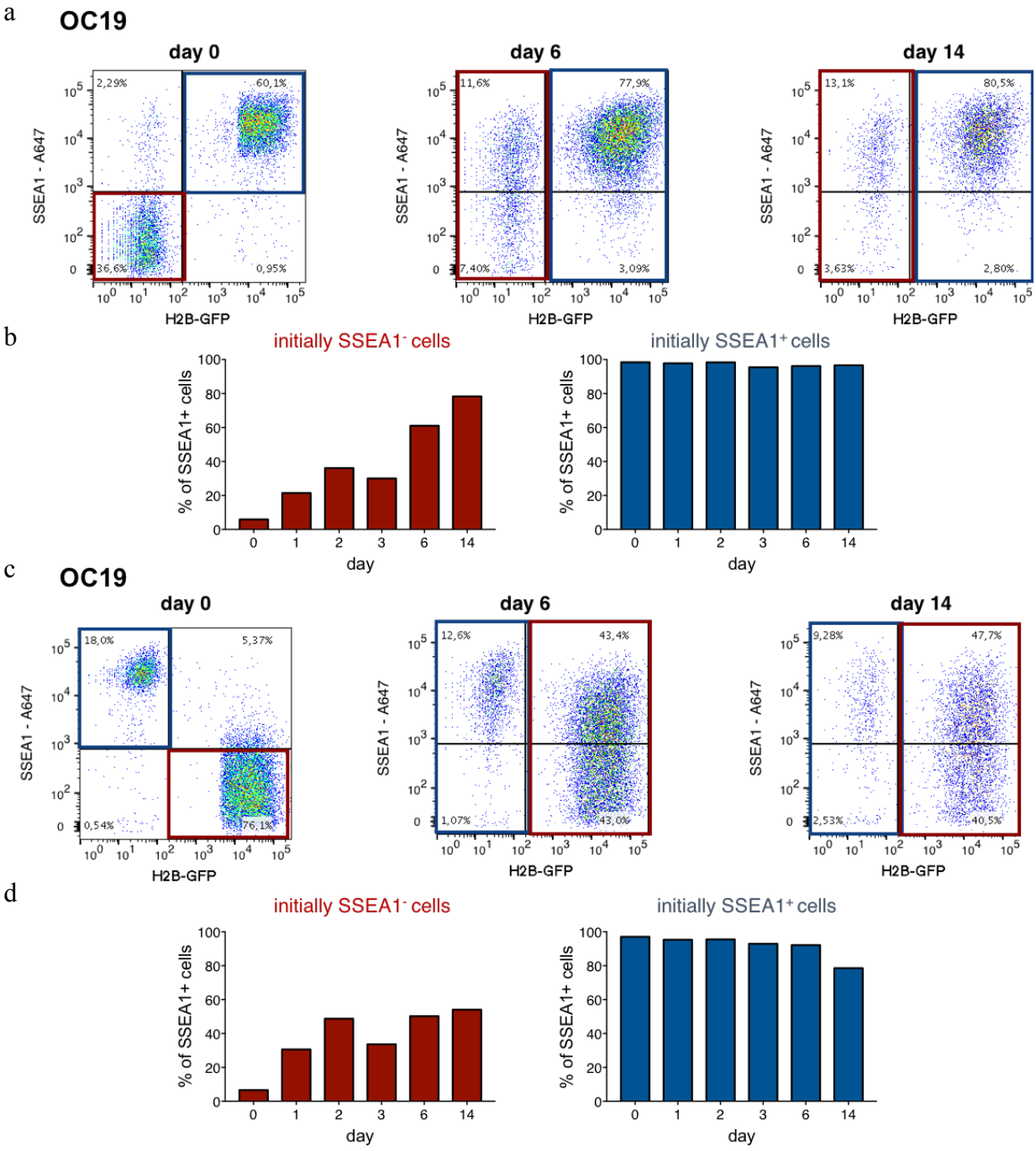

Figure 19: SSEA1$^-$ cells give rise to SSEA1$^+$ cells *in vitro* (OC19).
(a) FACS-sorted, initially 94 % pure SSEA1$^-$ H2BGFP$^-$ (red) and initially 98 % pure SSEA1$^+$ H2BGFP$^+$ (blue) cells of OC19 were mixed in an approximately 50:50 ratio and cultured for 14 days. On day 1, 2, 3, 6 and 14, the cells were stained for SSEA1 and the percentages of SSEA1$^+$ cells in the initially SSEA1$^-$ (red) and initially SSEA1$^+$ (blue) cells analyzed by flow cytometry and quantified (b). (c) FACS-sorted, initially 97 % pure SSEA1$^+$ H2BGFP$^-$ (blue) and initially 93 % pure SSEA1$^-$ H2BGFP$^+$ (red) cells of OC19 were mixed in an approximately 50:50 ratio and cultured for 14 days. On day 1, 2, 3, 6 and 14, the cells were stained for SSEA1 and the percentages of SSEA1$^+$ cells in the initially SSEA1$^-$ (red) and initially SSEA1$^+$ (blue) cells analyzed by flow cytometry and quantified (d). Horizontal lines

in (a and c) depict the isotype staining cutoff. GFP = green fluorescent protein, H2B = histone 2 B

4.2.1.5 SSEA1$^-$ cells are enriched in G_0/G_1 cell cycle phase whereas SSEA1$^+$ cells are enriched in G_2M phase and incorporate more EdU

Since we could show that SSEA1$^-$ cells generate SSEA1$^+$ cells (4.2.1.4), we additionally performed an EdU (5'-ethynyl-2'-deoxyuridine) staining combined with a surface anti-SSEA1 staining in addition to the CTB growth assay in order to assess the proliferation of cells. This allowed us to analyze on single cell level in which cell cycle phase a cell is and correlate it with its surface marker expression at exactly this time point.

Since EdU incorporates into newly synthesized DNA, we pulsed the cells for 1 h with 10 µM EdU and then quantified the number of cells having incorporated EdU within the SSEA1$^-$ and the SSEA1$^+$ population, respectively, via flow cytometry. Therefore, we gated on 2n-4n single cells in a propidium iodide-area versus propidium iodide-height window and then on the SSEA1$^-$ or SSEA1$^+$ cells, respectively. Displaying EdU versus propidium iodide staining then visualized the cell cycle phases $G_0/_1$, S and G_2M (figure 20 a).

SSEA1$^-$ cells were enriched in $G_{0/1}$ cell cycle phase as compared to SSEA1$^+$ cells in OC12, OC14, OC15, OC19 and OC20. On the contrary, SSEA1$^+$ cells were enriched in G_2M and S phase in all 5 OC lines (figure 20 b,c and d).

In addition to quantifying the proportion of cells in different cell cycle phases, we were interested in the amount of actively cycling cells. This was analyzed by comparing the percentage of cells having incorporated EdU (S phase) in SSEA1$^+$ and SSEA1$^-$ cells.

In all 5 OC cell lines, SSEA1$^+$ cells incorporated significantly more EdU than SSEA1$^-$ cells (figure 20 d, e). This difference was biggest in OC14 and OC15 and smallest in OC12 and OC19 (figure 20 d).

Enrichment of SSEA1$^+$ and SSEA1$^-$ cells in the $G_0/_1$, S and G_2M phase, respectively, was statistically significant when comparing the 5 OC cell lines as biological replicates (figure 20 e). Interestingly, the number of cells in G_2M phase correlated with the expression of SSEA1: the more SSEA1 the cells expressed, the more cells were enriched in G_2M phase. And vice versa, the less SSEA1 the cells expressed, the more cells were enriched in $G_0/_1$ phase (figure 20 f, g).

In sum, we concluded that $SSEA1^-$ cells are enriched in $G_0/_1$ and $SSEA1^+$ cells in S and G_2M cell cycle phases and that the two populations differ regarding their *in vitro* proliferation capacity.

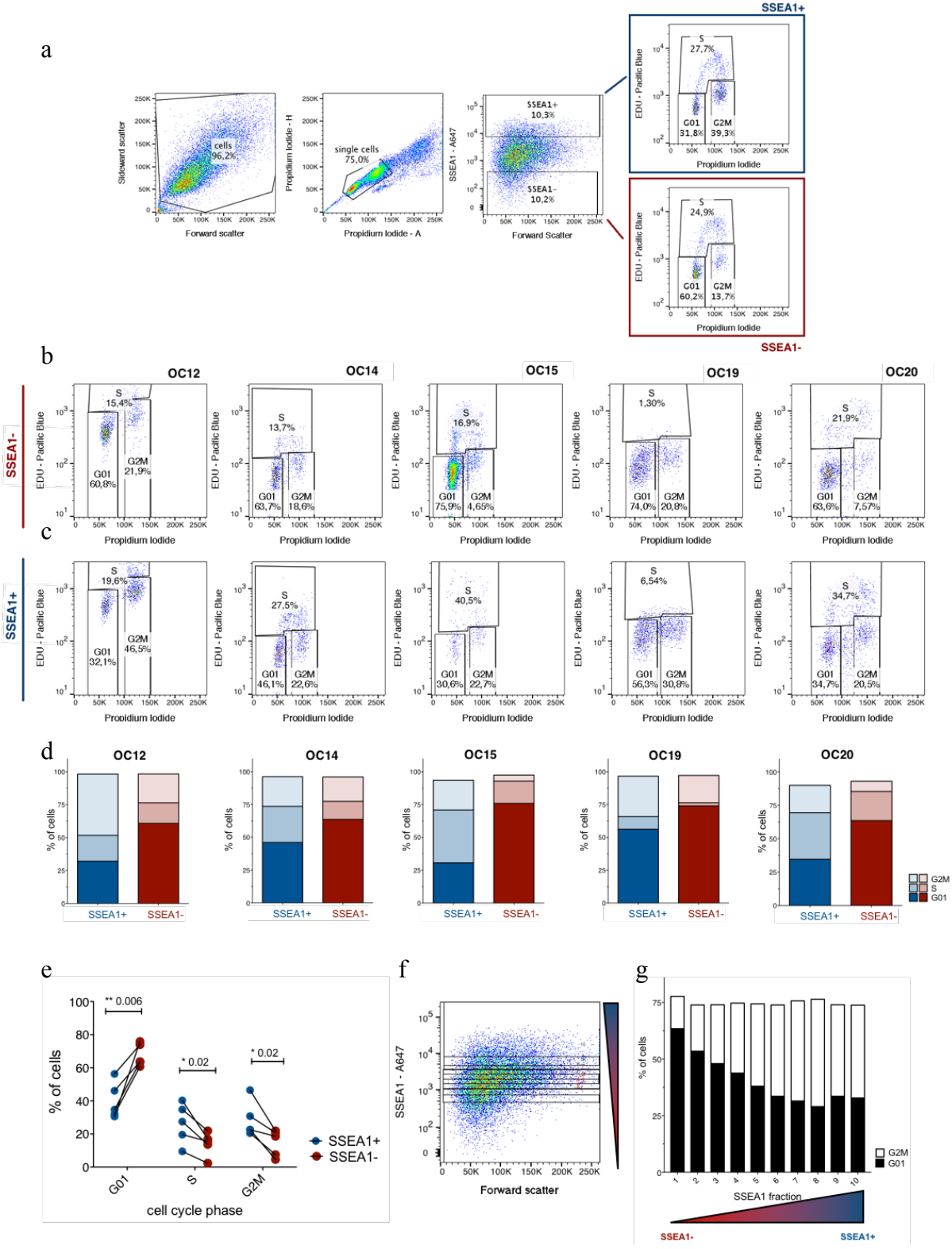

Figure 20: SSEA1$^-$ cells are enriched in the $G_0/_1$ cell cycle phase.
(a) FACS gating scheme of OC cells treated for 1 h with EdU followed by fixation and staining for SSEA1 and detection of EdU. Distribution of the $G_0/_1$, S and G_2M cell cycle phases in SSEA1$^-$ (b) and SSEA1$^+$ (c) cells in the OC cell lines OC12, OC14, OC15, OC19 and OC20. Quantification of the cell cycle phase distribution within SSEA1$^-$ and SSEA1$^+$

cells in each OC line (d) and pooled comparison (e) of all 5 biological replicates (OC12, OC14, OC15, OC19 and OC20). (f) FACS gating scheme to segment cells in 10 %-fractions according to their SSEA1 expression which is used for the analyses shown in (g). (g) The more SSEA1 the cells express (blue), the higher is the number of cells in G_2M cell cycle phase (white). On the contrary, the cells with the least SSEA1 expression (red) are enriched most in $G_0/_1$ phase (black). Data are shown for OC12 cells. * $p < 0.05$, ** $p < 0.01$, paired, parametric, two-tailed t-test.

4.2.1.6 SSEA1$^+$ cells show an enrichment of aneuploid cells

In addition to the cell cycle phases, we analyzed the ploidy of SSEA1$^+$ and SSEA1$^-$ cells.

In a flow cytometric analyses, we quantified the number of cells > 4n by gating on single cells, followed by sub-gating on SSEA1$^+$ / SSEA1$^-$ cells and subsequently based on propidium iodide staining gating, in a propidium iodide-height versus –area window (figure 21 a).

The SSEA1$^+$ cells showed a more than 4-fold increase in the number of cells > 4n in all 5 OC cell lines analyzed (figure 21 b,c and d). The strongest difference in aneuploidy between SSEA1$^+$ and SSEA1$^-$ cells could be detected in OC15 (~12-fold) followed by OC12 (~6-fold). Overall, the SSEA1$^-$ cells were rarely aneuploid at all, whereas the SSEA1$^+$ cells displayed cells > 4n to a greater extent. The enrichment of aneuploid cells in the SSEA1$^+$ population compared to SSEA1$^-$ cells was significant over all 5 biological replicates (figure 21 d).

In sum, SSEA1$^+$ cells displayed more cells > 4n than SSEA1$^-$ cells which were rarely aneuploid at all.

.

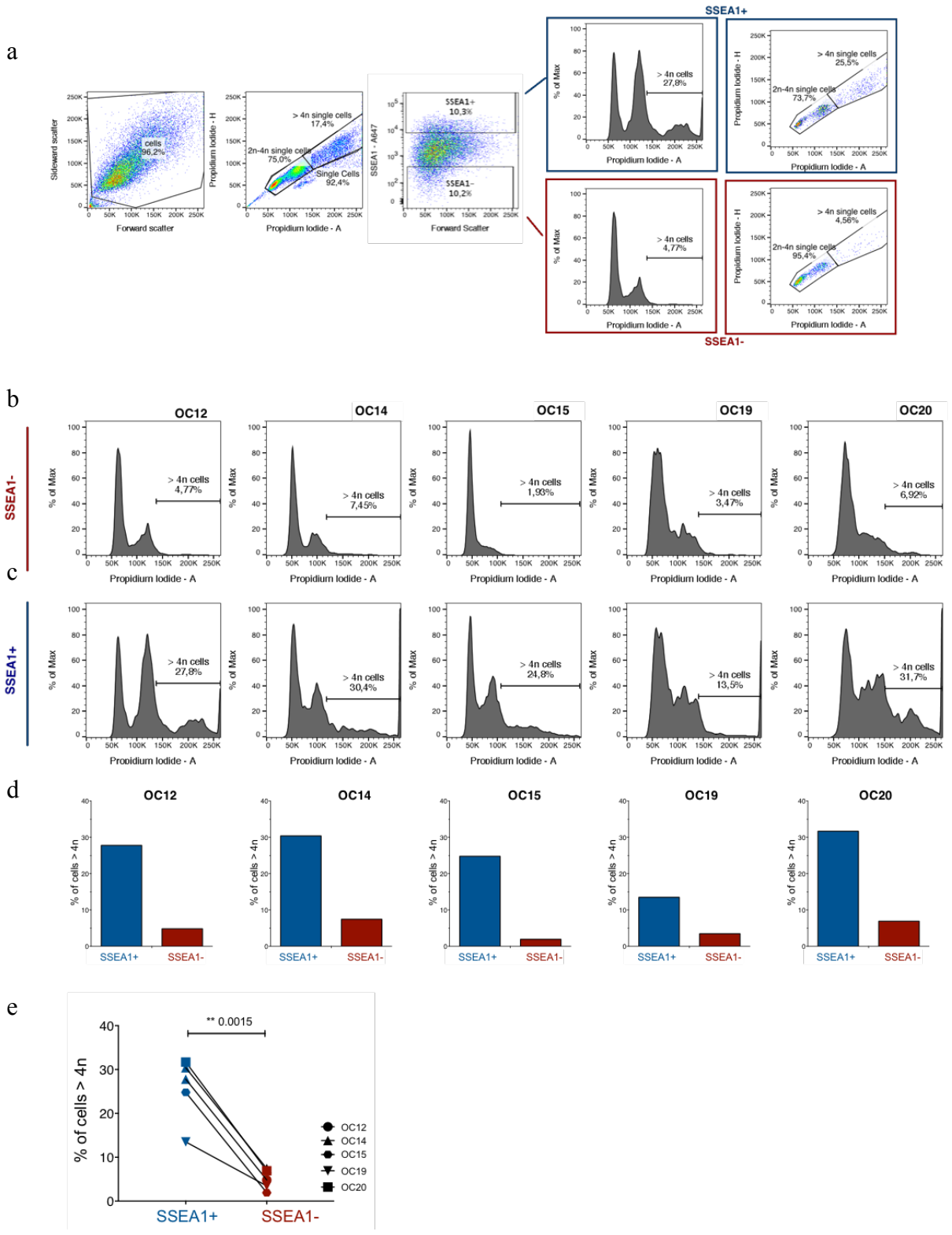

Figure 21: SSEA1$^+$ cells are enriched for cells > 4n.
(a) FACS gating scheme of OC cells treated for 1 h with EdU followed by fixation and staining for SSEA1 and addition of PI. The number of cells > 4n is increased in the SSEA1$^+$ cells (c) as compared to the SSEA1$^-$ cells (b) in the OC cell lines OC12, OC14, OC15, OC19 and OC20. Quantification of the number of cells > 4n within SSEA1$^-$ and SSEA1$^+$ cells in

each OC line (d) and pooled comparison (e) of all 5 biological replicates (OC12, OC14, OC15, OC19 and OC20). ** $p < 0.01$; paired, parametric, two-tailed t-test.

4.2.1.7 SSEA1$^-$ form more and bigger colonies in sphere-forming and adherent conditions

In order to determine the clonogenic potential of SSEA1$^+$ and SSEA1$^-$ cells *in vitro*, we performed sphere-forming assays and colony formation assays in adherent conditions.

Equal numbers of SSEA1$^-$ and SSEA1$^+$ cells were seeded in either 6-well ultra-low attachment (sphere-forming condition) or PRIMARIA plates (adherent conditions). Cells were then allowed to grow for 7 (OC12, OC15) or 14 days (OC18, OC20) and the number of spheres per 6-well were counted manually under a microscope. Regarding the adherent conditions, cells were washed, incubated with a 0.5 % crystal violet / 6 % glutaraldehyde solution for 30 min and the resulting stained colonies automatically counted and analyzed regarding size by a Fiji script (figure 23 a).

SSEA1$^-$ cells formed more spheres than SSEA1$^+$ cells in OC12, OC18 and OC20 cell lines (figure 22 b). In addition, the spheres of OC12 SSEA1$^+$ cells displayed many bubbles, indicative of more cell death occurring (figure 22 a).

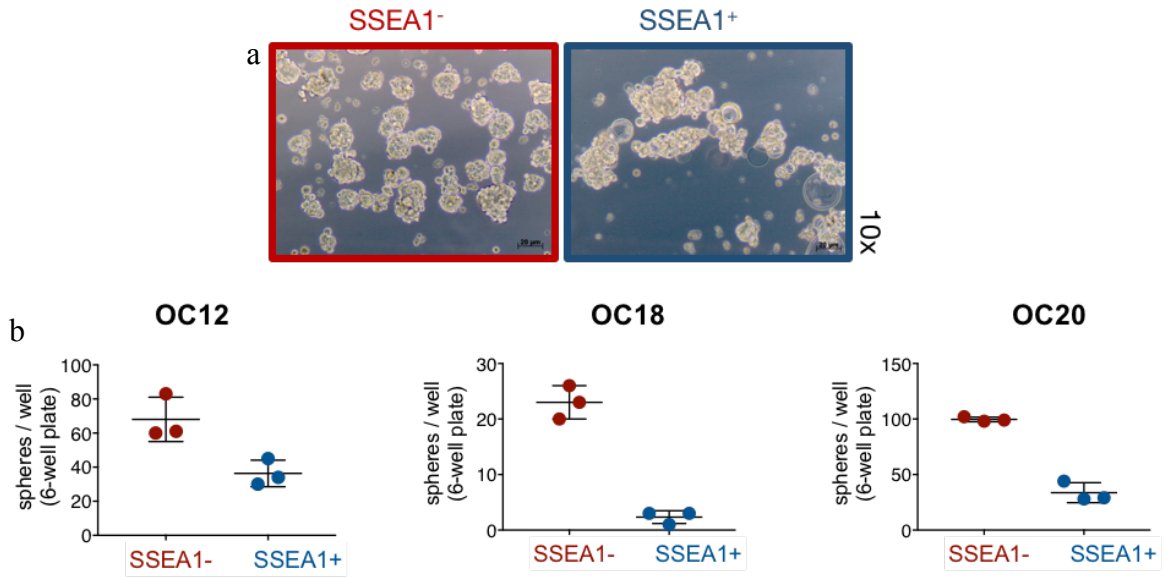

Figure 22: SSEA1$^-$ cells form more spheres in sphere-forming conditions.
(a) Representative images of FACS sorted OC12 SSEA1$^-$ (red) and SSEA1$^+$ (blue) cells cultured in sphere conditions in Ultra Low Attachment (ULA) 6-wells. Scale bar 20 µm, 10x magnification. (b) Quantification of the number of spheres per ULA 6-well. For the OC12 cell line, 3,200 cells were seeded per 6-well, for OC18 12,000 and for OC20 9,000 cells. OC12

cells were cultured for 7 days, OC18 and OC20 for 14 days, respectively. Mean ± SD. n = 3 technical replicates.

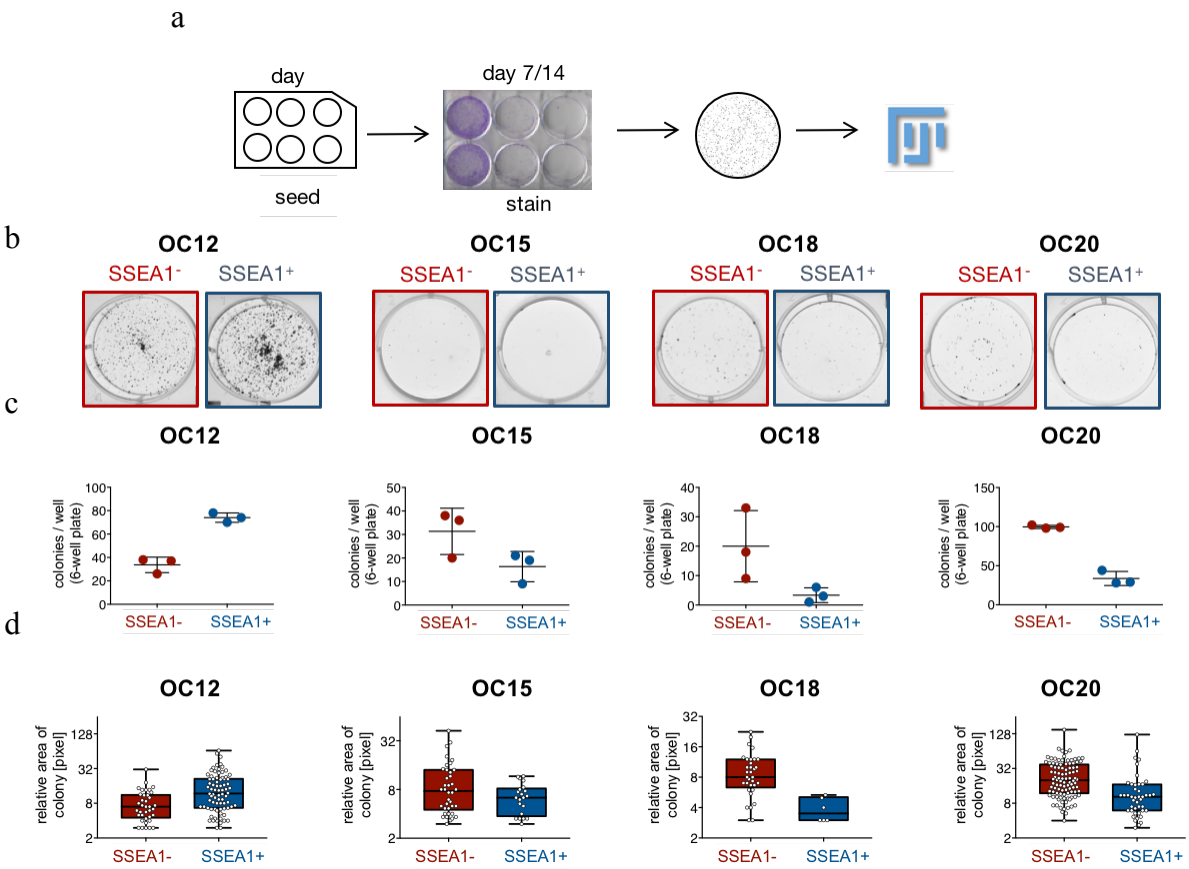

Figure 23: SSEA1$^-$ cells form more colonies in adherent conditions.
(a) Schematic overview of the experimental workflow for quantification of colony number and size. (b) Representative images of the colonies formed by SSEA1$^-$ (red) and SSEA1$^+$ (blue) sorted cells of the respective cell lines. (c) Colony number of FACS sorted SSEA1$^-$ (red) and SSEA1$^+$ (blue) cells cultured in PRIMARIA 6-wells. For the OC12 cell line, 3,200 cells were seeded per 6-well, for OC15 4,000, for OC18 12,000 and for OC20 9,000 cells. OC12 cells were cultured for 7 days, OC15 for 10 days, OC18 and OC20 for 14 days, respectively. (d) Relative area per colony of sorted SSEA1$^-$ (red) and SSEA1$^+$ (blue) cells as quantified by Fiji. Mean ± SD. n = 3 technical replicates. n = 4 biological replicates for OC12 and OC20, n = 1 biological replicate for OC15 and OC18.

In adherent conditions, SSEA1$^-$ cells also tended to form more colonies than SSEA1$^+$ cells (OC15, OC18 and OC20). In OC12, however, SSEA1$^+$ cells formed more colonies than SSEA1$^-$ ones (figure 23 b, c). In addition, the colonies formed by SSEA1$^-$ cells were bigger than those of SSEA1$^+$ cells, except for OC12 which again showed an opposite phenotype (figure 23 d).

Taken together, we showed that SSEA1$^-$ cells form more spheres than SSEA1$^+$ cells in all OC lines analyzed and also form more and bigger colonies in adherent conditions in most OC cell lines.

4.2.1.8 SSEA1$^-$ cells are more clonogenic than SSEA1$^+$ cells in limiting dilution assays *in vitro*

To further analyze in how SSEA1$^+$ and SSEA1$^-$ cells differ regarding their ability to form colonies, we performed an *in vitro* limiting dilution assay. Therefore, FACS-sorted SSEA1$^+$ and SSEA1$^-$ cells were seeded into 96-well plates in 1:2 dilution steps in at least octaplicates, allowed to grow for 7 (OC12, OC15) or 14 days (OC20) and then the wells were scored as positive or negative regarding the outgrowth of a colony (figure 24 a). Colonies were considered as a colony if more than 6 cells formed an epithelial-like colony. Data were then analyzed with the extreme limiting dilution analysis tool ELDA (Hu *et al.,* 2009).

SSEA1$^-$ cells form colonies when seeded at lower cell numbers than SSEA1$^+$ cells (OC15, OC20; figure 24 b). Only OC12 again showed the opposite phenotype: SSEA1$^-$ cells formed less colonies than SSEA1$^+$ cells, similar to the results of the sphere-forming and colony formation assay (figure 22 b, figure 23 c).

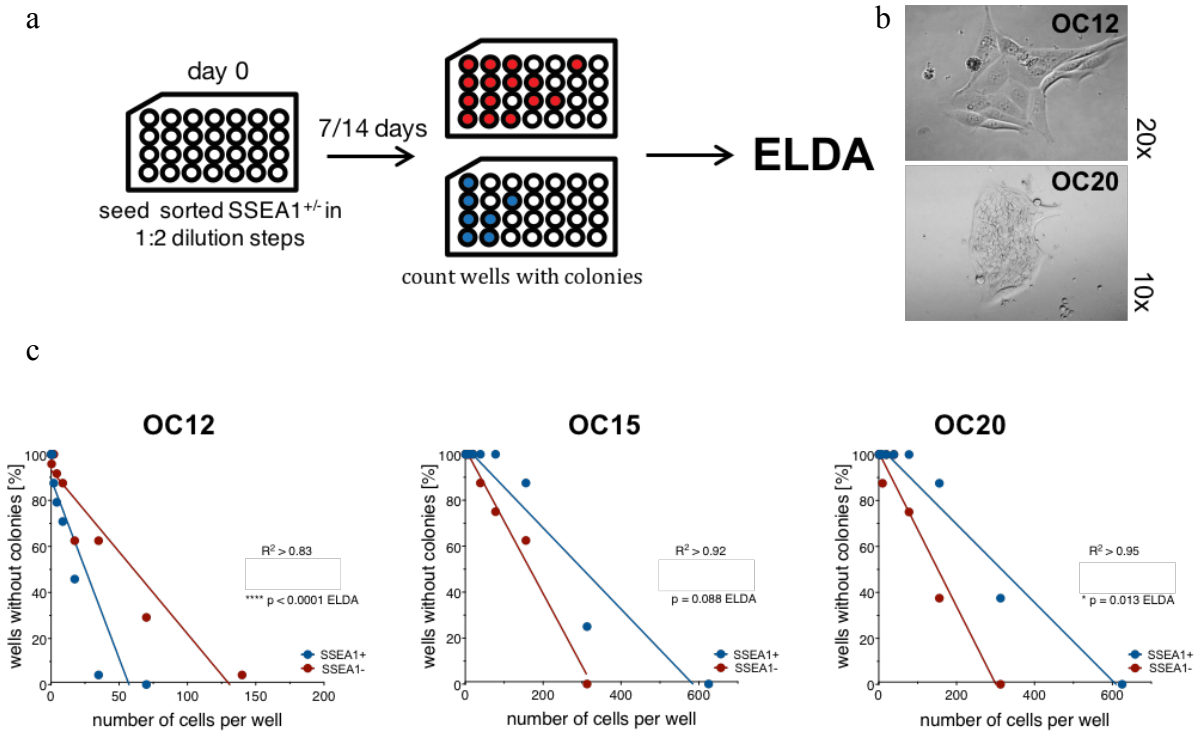

Figure 24: SSEA1$^-$ cells are more clonogenic in limiting dilution analyses *in vitro*.
(a) Schematic overview of the experimental workflow for quantification of wells with colonies. (b) Representative images of colony sizes considered as colonies for the OC12 and

OC20 cell lines. (c) Numbers of wells without colonies of FACS-sorted SSEA1$^-$ (red) and SSEA1$^+$ (blue) cells seeded in limiting dilution analysis were quantified and analyzed using the ELDA tool (Hu *et al.,* 2009). n = 8 (OC15) or 24 (OC12 and OC20) replicates per condition. n = 1 (OC15) or 3 (OC12 and OC20) biological replicates. * $p < 0.05$, **** $p \leq 0.0001$.

4.2.2 Functional characterization of SSEA1$^+$ and SSEA1$^-$ cells *in vivo*

4.2.2.1 SSEA1- initiate tumors *in vivo*

Since SSEA1$^+$ and SSEA1$^-$ cells differed regarding clonogenicity, cell cycle states and various other characteristics *in vitro*, we wondered whether the cells possess a distinct potential to initiate tumors *in vivo.* Thus, we FACS-sorted SSEA1$^+$ and SSEA1$^-$ cells, which have before been lentivirally labeled with a luciferase gene, and injected them into NSG mice and followed tumor growth via bioluminescent imaging.

SSEA1$^-$ cells initiated tumors much earlier than SSEA1$^+$ cells (figure 25 a, c). Both in OC12 and OC20 cell lines, tumor growth of SSEA1$^-$ cells was significantly faster (figure 25 b, c) in all mice injected with SSEA1$^-$ tumor cells (OC12) and in all except one mouse injected with SSEA1$^-$ cells from OC20. Furthermore, injection of SSEA1$^-$ cells led to a higher tumor burden than injection of SSEA1$^+$ cells at the endpoint at week 19 (OC12) or 15 (OC20) as measured by bioluminescence (figure 26). Kaplan-Meier survival analyses indicated that survival of mice injected with SSEA1$^-$ cells was significantly worse than that of mice having been injected with SSEA1$^+$ cells (figure 27). To perform the survival analyses, mice were scored to be dead upon a 100-fold increase in bioluminescence.

In sum, we could show that SSEA1$^-$ cells possess more tumor-initiating potential in an *in vivo* metastasis setting than SSEA1$^+$ cells due to the fact that SSEA1$^-$ cells initiate tumor outgrowth earlier and faster than SSEA1$^+$ cells. Moreover, tumor burden of mice having been injected with SSEA1$^-$ cells was higher than in the group of mice injected with SSEA1$^+$ cells.

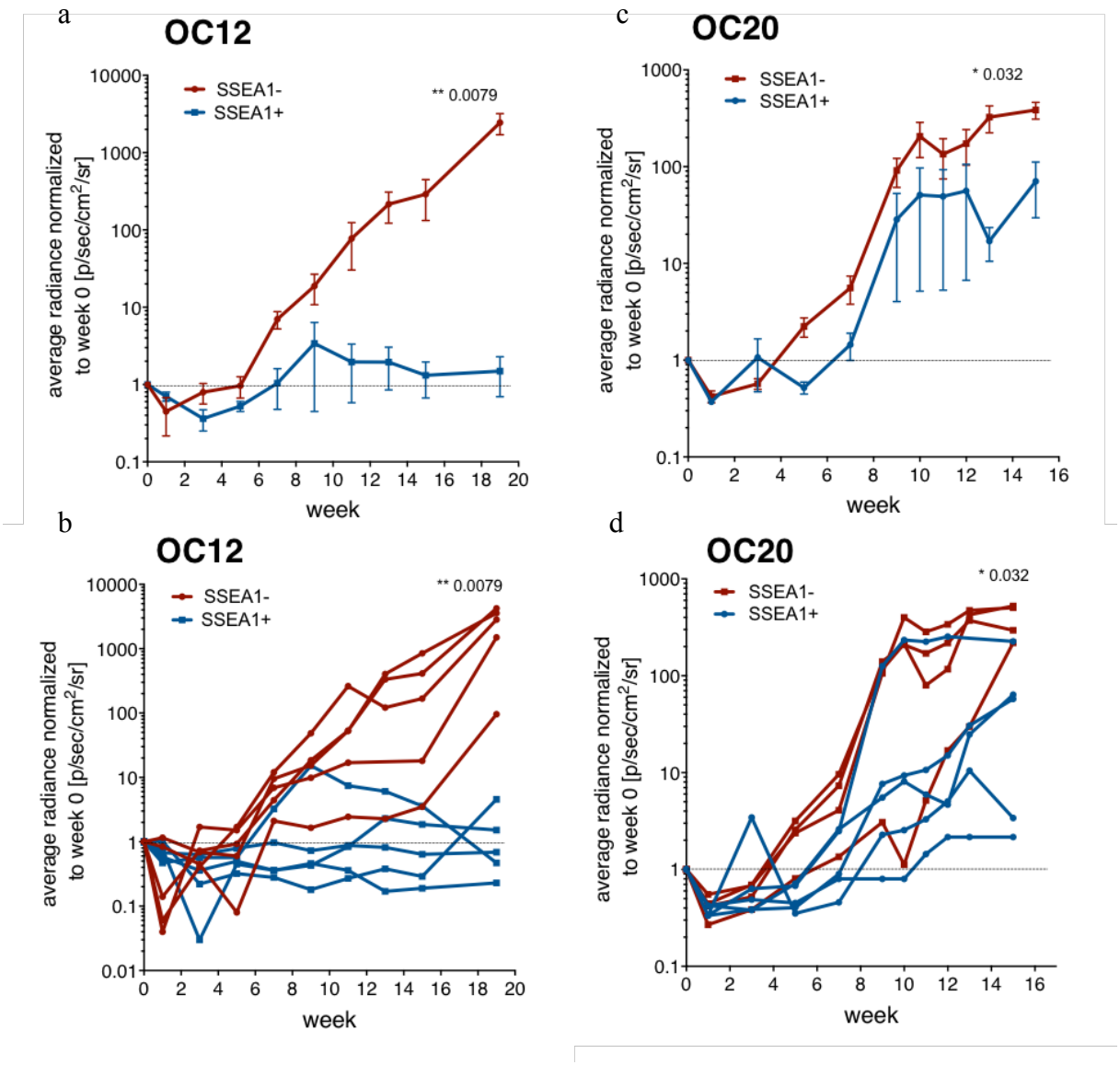

Figure 25: SSEA1$^-$ cells initiate tumors *in vivo*.
Growth curves of FACS-sorted SSEA1$^-$ (red) and SSEA1$^+$ (blue) OC12 (a, b) and OC20 (c, d) cells which have been i.p. injected into NSG mice and which were before lentivirally transduced with a luciferase vector in order to follow tumor growth via bioluminescence. In a and c, the mean ± SEM are shown, in b and d, the growth curves of the tumor cells for each single mouse are depicted. The dashed line denotes the baseline at week 0. n = 5 mice per group, except in OC20 SSEA1$^-$ (4 mice). n = 2 (OC12) or 1 (OC20) biological replicates. * $p < 0.05$, ** $p < 0.01$. Mann-Whitney test.

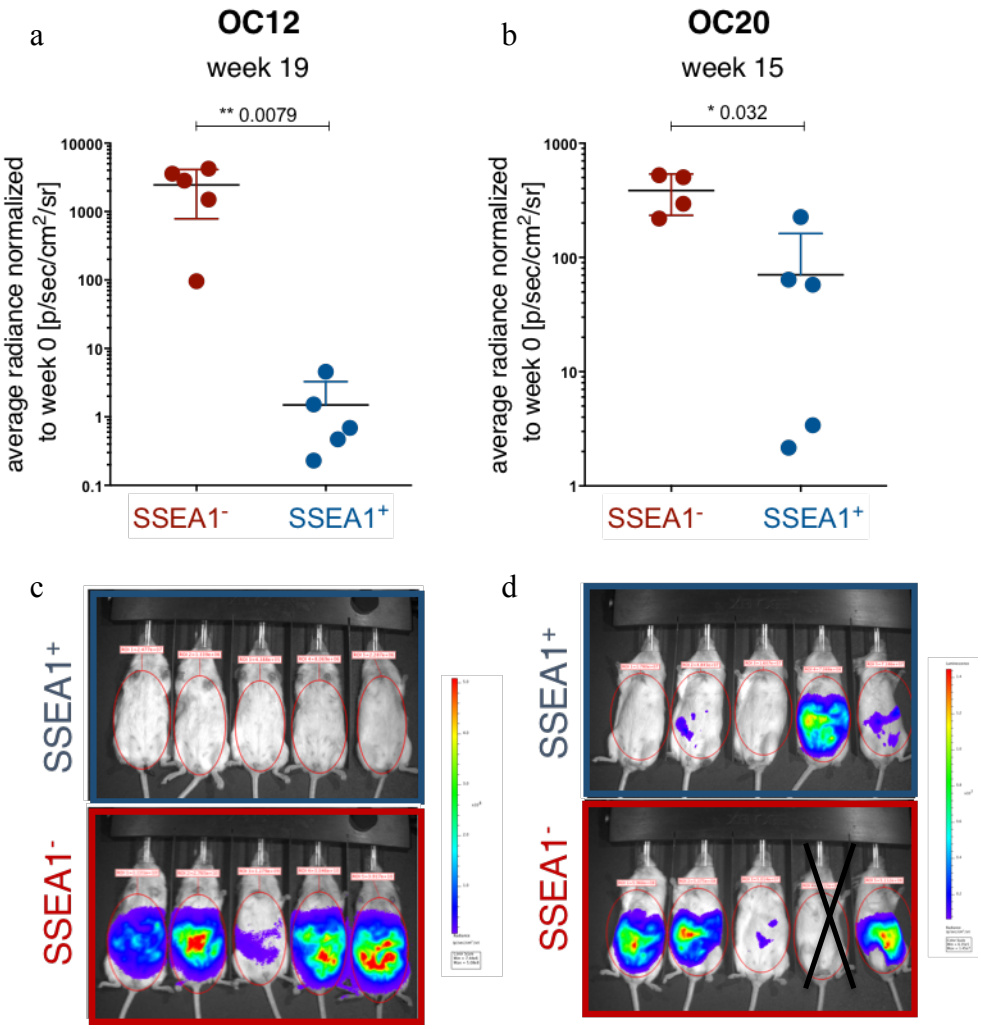

Figure 26: SSEA1$^-$ cells lead to a higher *in* vivo tumor burden in mice than SSEA1$^+$ cells. Tumor burden of mice injected intraperitoneally with FACS-sorted SSEA1$^-$ and SSEA1$^+$ OC12 (a) and OC20 (b) cells at the endpoint of the experiment (week 19 and week 15 for OC12 and OC20, respectively) as measured by the level of bioluminescence normalized to week 0. Images of the *in vivo* bioluminescent signal in mice injected with OC12 (c) and OC20 (d) SSEA1$^-$ (red) and SSEA1$^+$ (blue) cells at the endpoint. n = 4-5 mice per group. Mouse number 4 in (d) was excluded (black cross) since no signal was detected after initial injection at day 0. * $p < 0.05$, ** $p < 0.01$. Mann-Whitney test.

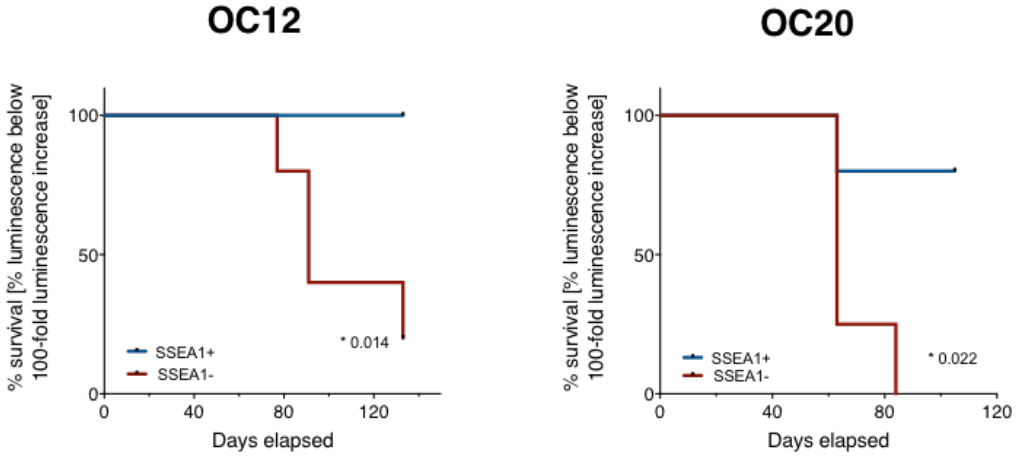

Figure 27: Mice injected with SSEA1$^-$ cells display decreased survival.
Kaplan-Meier survival graphs of NSG mice injected with 10,000 FACS-sorted SSEA1$^-$ (red) or SSEA1$^+$ (blue) OC12 cells (a) and 100,000 SSEA1$^-$ (red) or SSEA1$^+$ (blue) OC20 (b) cells. Mice were scored to be dead upon 100-fold increase in luminescence. * $p < 0.05$. Log-rank (Mantel-Cox) test.

4.2.2.2 SSEA1$^-$ cells are more metastatic, form more ascites and more tumors

In order to verify that the bioluminescent signal was indeed due to tumor cell growth, we opened the mice and analyzed them for tumors or presence of ascites. Thus, tumors were histologically assessed and ascites analyzed via FACS by staining for mH$_2$kd/CD11b$^-$, hEPCAM$^+$ and Venus-Luciferase$^+$.

We injected PBS into the peritoneum of dead mice in order to wash out all ascites including tumor cells. Tumor cells including bigger spheroid clusters were found in the ascites of 7/8 mice injected with SSEA1$^-$ cells but only in 1/8 mice injected with OC12 SSEA1$^+$ cells (figure 28 a, table 11). Furthermore, in 3/8 mice injected with SSEA1$^-$ cells versus 1/8 mice injected with SSEA1$^+$ cells solid tumors could be found (figure 28 b). Metastases even, characterized by the presence of hKI67$^+$ cells, were detected in 6/8 mice injected with SSEA1$^-$ cells. The location of metastasis included uterus, diaphragm, lymph node and liver. No metastases, however, could be found in mice injected with SSEA1$^+$ cells (table 11).

To sum up, SSEA1$^-$ cells form more ascites, tumors and metastases than SSEA1$^+$ cells when injected intraperitoneally into NSG mice.

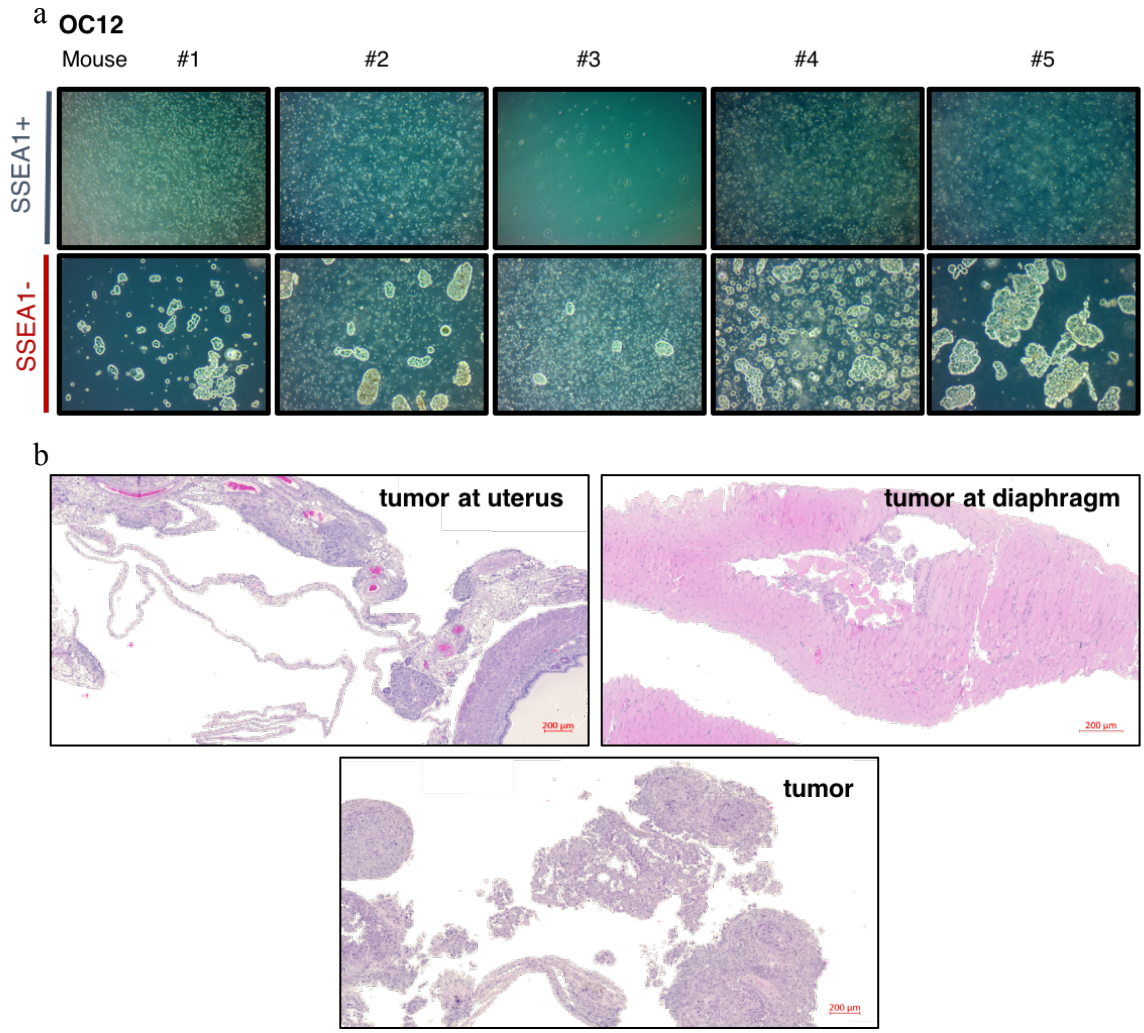

Figure 28: SSEA1$^-$ cells form ascites, tumors and metastases *in vivo*.
(a) Representative images of ascites from NSG mice injected intraperitoneally with FACS-sorted either SSEA1$^-$ (red) or SSEA1$^+$ (blue) OC12 cells. Only the big spheroids in the SSEA1$^-$ ascites are tumor cells. No tumor cells were detected in ascites of mice injected with SSEA1$^+$ cells. (b) H&E stainings of diaphragm, uterus and a tumor taken out from mice injected intraperitoneally with OC12 SSEA1$^-$ cells. The tumor cells have spread to these organs.

Table 11: SSEA1$^-$ cells form more ascites, more tumors and more metastases.
P-values were calculated with the ELDA limiting dilution tool (Hu *et al.,* 2009).

		ascites	tumors	metastases	location of metastases
Experiment 1 OC12	SSEA1$^-$	2/3	2/3	2/3	uterus, diaphragm, lymph node
	SSEA1$^+$	1/3	1/3	0/3	-
Experiment 2 OC12	SSEA1$^-$	5/5	1/5	4/5	Uterus, liver, diaphragm
	SSEA1$^+$	0/5	0/5	0/5	-
Total	SSEA1$^-$	7/8	3/8	6/8	uterus, diaphragm, lymph node, liver
	SSEA1$^+$	1/8	1/8	0/8	-
p-value (total)		** 0.0015	ns	*** 0.0005	

4.2.2.3 SSEA1$^-$ cells give rise to SSEA1$^+$ cells *in vivo*

Since SSEA1$^-$ cells gave rise to SSEA1$^+$ cells *in vitro* but not vice versa (4.2.1.4), we analyzed whether SSEA1$^-$ cells also gave rise to SSEA1$^+$ cells *in vivo.* Therefore, we assessed ascites from mice via FACS by staining for mH$_2$kd/CD11b$^-$, hEPCAM$^+$ and Venus-Luciferase$^+$, as well as SSEA1 (figure 29 a). Cells derived from mice injected with SSEA1$^+$ cells, merely contained tumor cells and if so, the cells were mostly SSEA1$^+$ (figure 29 d). However, the ascites of all five mice injected with SSEA1$^-$ tumor cells consisted of SSEA1$^-$ and SSEA1$^+$ cells (figure 29 d). Tumors derived of initially SSEA1$^-$ sorted cells (figure 29 c) also displayed a positive SSEA1 staining.

Thus, we concluded that SSEA1$^-$ cells sustain *in vivo* tumor growth by generating SSEA1$^-$ and SSEA1$^+$ cells.

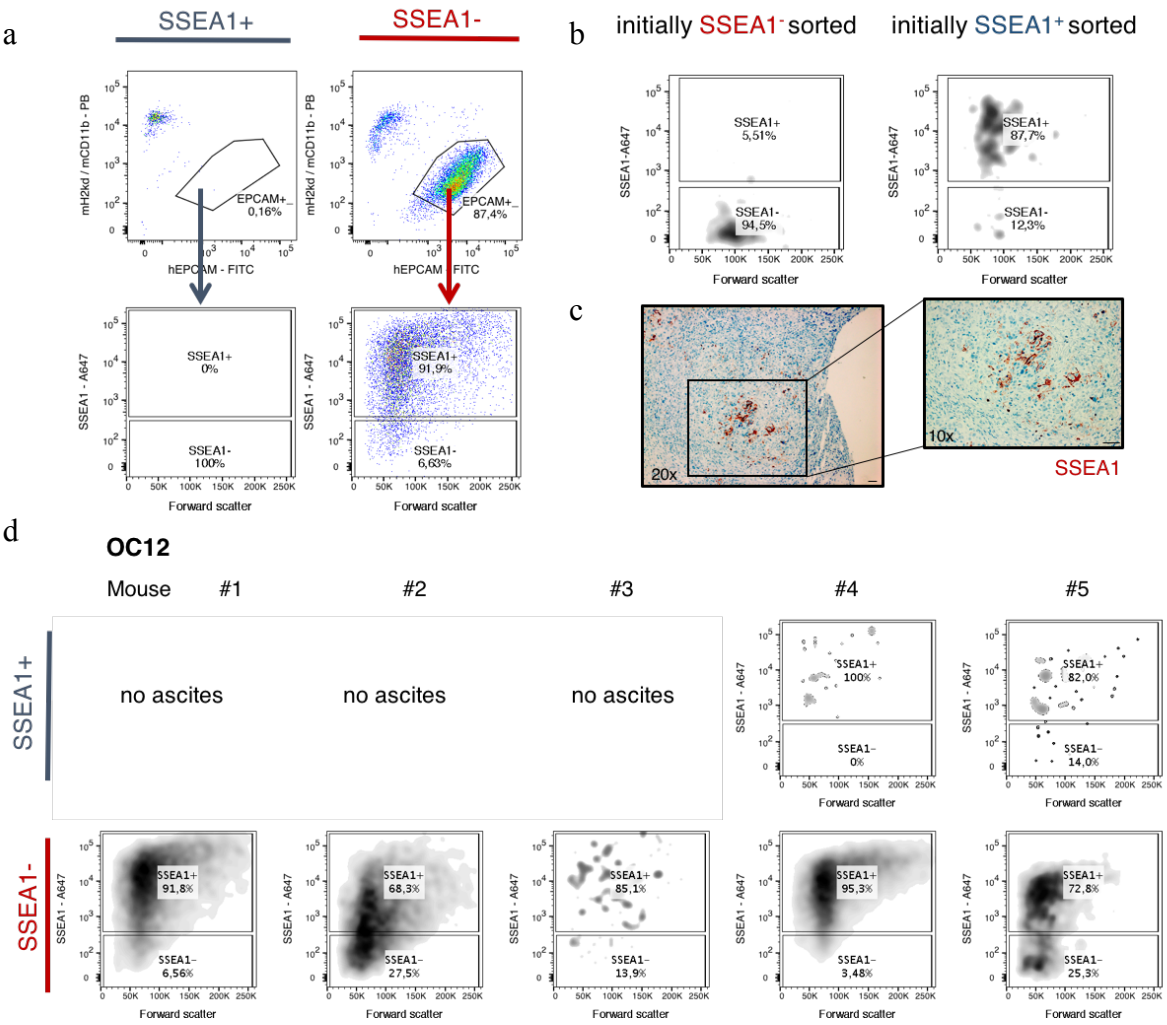

Figure 29: SSEA1$^-$ cells give rise to SSEA1$^+$ cells *in vivo*.
(a) Gating scheme for the detection of SSEA1 expression of ascites harvested from mice intraperitoneally injected with FACS-sorted SSEA1$^-$ and SSEA1$^+$ OC12 cells. Gating was performed by including single cells and excluding PI$^+$ / mH2kd$^+$ / mCD11b$^+$ cells. Within the hEPCAM$^+$ population, the expression of SSEA1 was analyzed. (b) Purity of initially SSEA1$^-$ or SSEA1$^+$ FACS-sorted cells for i.p. injection into mice. (c) Immunohistochemical staining of a tumor derived from initially SSEA1$^-$ FACS-sorted cells. SSEA1 staining is shown in red. Scale bar denotes 100 µm. (d) SSEA1 expression in mouse ascites harvested from mice intraperitoneally injected with initially FACS-sorted SSEA1$^-$ (red) and SSEA1$^+$ (blue) OC12 cells.

4.2.2.4 SSEA1$^-$ cells are more clonogenic in *in vivo* limiting dilution analyses

To further test the tumorigenic potential of SSEA1$^+$ and SSEA1$^-$ cells, we performed *in vivo* limiting dilution analyses of FACS-sorted SSEA1$^-$ and SSEA1$^+$ cells. Therefore, 100, 1,000, 10,000 or 100,000 either SSEA1$^-$ or SSEA1$^+$ cells were subcutaneously injected into NSG mice.

Tumor incidence was higher in all experimental groups of mice injected with SSEA1$^-$ cells than in the group of mice injected with SSEA1$^+$ cells (table 12, figure 30a). The frequency of tumor-initiating cells as estimated by ELDA (Hu *et al.,* 2009) differed significantly from 1:580 (218-1,543) in the SSEA1$^-$ group compared to 1:37,914 (14,187-101,319) in the SSEA1$^+$ group (table 12, figure 30b). Furthermore, tumor volume was significantly bigger in the group of mice injected with 1,000, 10,000 or 100,000 SSEA1$^-$ cells as compared to the group of SSEA1$^+$ cells (figure 30c).

Taken together, SSEA1$^-$ cells formed more and bigger tumors in an *in vivo* limiting dilution analyses, thereby revealing a higher tumor-initiating frequency.

Table 12: Tumor take rate and frequency of tumor-initiating cells in the SSEA1$^-$ and SSEA1$^+$ populations in an *in vivo* limiting dilution analysis. p-value was calculated with the ELDA tool (Hu *et al.,* 2009). TIC = tumor-initiating cell.

FACS-sorted cell population	Number of injected cells	Tumor incidence	Estimated TIC frequency (95% CI)	p-value
OC12 SSEA1$^-$	100,000	5/5 (100%)	1:580 (218 – 1543)	**** < 0.0001
	10,000	5/5 (100%)		
	1,000	4/5 (80%)		
	100	1/5 (20%)		
OC12 SSEA1$^+$	100,000	4/5 (80%)	1:37,914 (14,187 – 101,319)	
	10,000	2/5 (40%)		
	1,000	1/5 (20%)		
	100	0/5 (0%)		

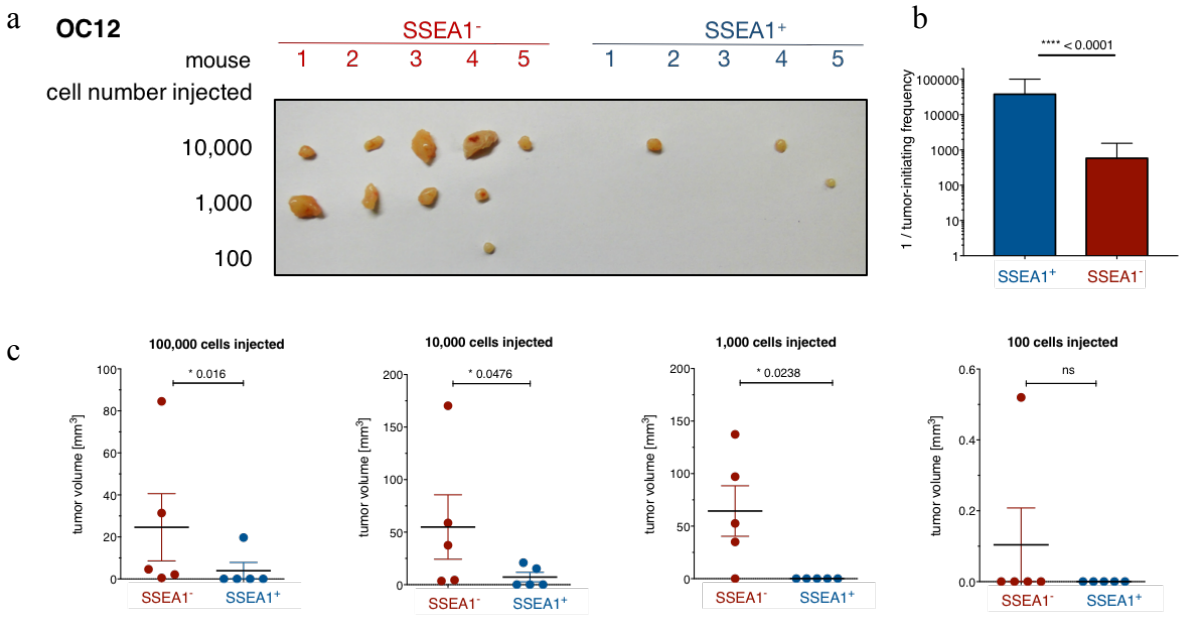

Figure 30: SSEA1$^-$ cells are more clonogenic than SSEA1$^+$ cells in an *in vivo* limiting dilution analyses.
(a) Image of the tumors that were obtained by subcutaneously injecting 100, 1,000 and 10,000 FCAS-sorted OC12 SSEA1$^-$ or SSEA1$^+$ cells into NSG mice at the endpoint of the experiment. (b) Number of tumor-initiating cells within the SSEA1$^-$ and SSEA1$^+$ OC12 cell populations as assessed by ELDA tool based on the number of tumors harvested. (c) Volume of the harvested tumors as calculated by the formula (π/6) x (length x width x heigth). n = 5 mice per group * $p < 0.05$, **** $p < 0.0001$, ns = not significant. Mann-Whitney test.

4.3 Molecular differences between SSEA1$^+$ and SSEA1$^-$ cells

4.3.1 Gene expression profiling analyses show that SSEA1$^-$ and SSEA1$^+$ cells cluster together

Since SSEA1$^-$ and SSEA1$^+$ cells displayed many phenotypic differences, we believed that this is due to molecular differences. In order to analyze the underlying molecular differences between SSEA1$^-$ and SSEA1$^+$ cells, we thus performed transcriptional profiling of FACS- and MACS-sorted SSEA1$^+$ and SSEA1$^-$ cells of 6 OC cell lines by using the Illumina HT12v4 bead Chip technology.

Unsupervised hierarchical clustering of microarray data of 42 samples of 6 OC patient-derived cell lines of SSEA1$^+$ and SSEA1$^-$ FACS- / MACS-sorted cells by clustering the top 100 differentially expressed genes with average-linking method and manhattan distance revealed that the OC cell lines were clustering together instead of the SSEA1$^-$ and SSEA1$^+$ samples (figure 31 a). Principal component analysis (figure 31 b) also showed that samples were clustering according to patient background and not SSEA1 status. Interestingly, the OC12 samples clustered most apart from the other OC cell lines (figure 31 b).

Because OC cell lines were clustering with each other, we performed hierarchical clustering of the microarray data within single patient background (figure 32). After removing batch effects like “chip type” or “sortedMACSed” by the ComBat method (Johnson *et al.,* 2007), we could now detect that the SSEA1$^-$ and SSEA1$^+$ samples clustered together, respectively, in all OC cell lines except OC14 and OC18 which had a single outlier (figure 32). Principal component analyses now also showed that the SSEA1$^-$ and SSEA1$^+$ cells cluster together, respectively, (figure 33) except for OC15 and OC18.

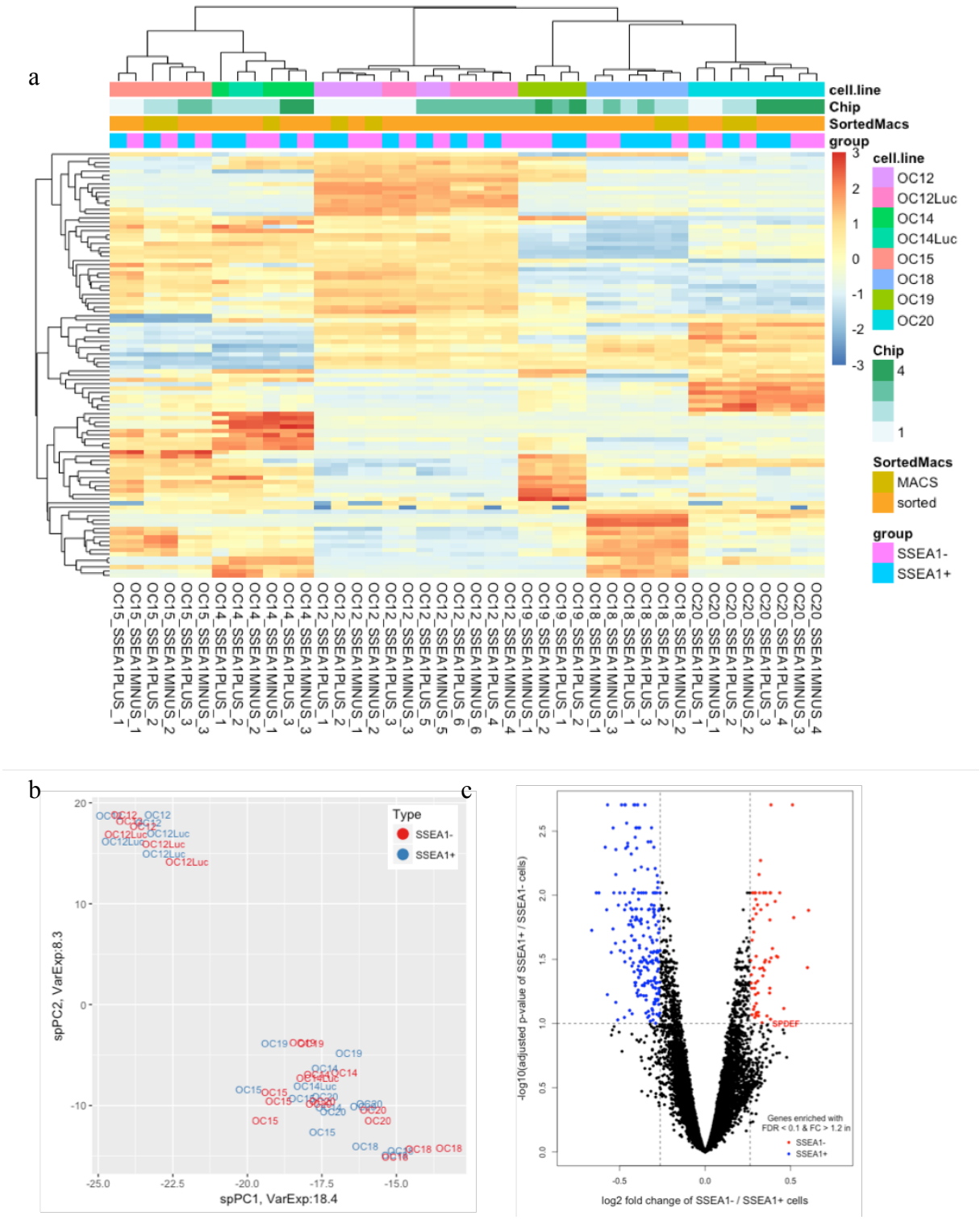

Figure 31: Gene expression profiling of SSEA1$^-$ and SSEA1$^+$ cells unravels differentially expressed genes.
(a) Unsupervised hierarchichal clustering of microarray data of SSEA1$^+$ and SSEA1$^-$ sorted cells of 42 samples of 6 OC patient-derived cell lines. Average-linking method and manhattan distance were applied. Expression data are log2 normalized and the top 100 differentially expressed genes were used for the heatmap. Column colors correspond to cell line (cell.line),

chip number (Chip), whether the cells were sorted or MACSed (SortedMACS) or SSEA1 expression (group). (b) Principal component analysis of the samples used for differential gene expression analysis. $SSEA1^+$ cells are depicted in blue and $SSEA1^-$ ones in red. (c) Volcano plot representing the differential gene expression of the 24,053 genes which passed the coefficient of variation filtering method (CV = 0.5). Genes expressed significantly higher (FDR < 0.1, FC > 1.2) in the $SSEA1^-$ and $SSEA1^+$ cells are depicted in red or blue, respectively. Heatmap, principal component and volcano plot were plotted with the R scripts listed in 7.2. BH = Benjamini-Hochberg, FC = Fold change, FDR = false discovery rate.

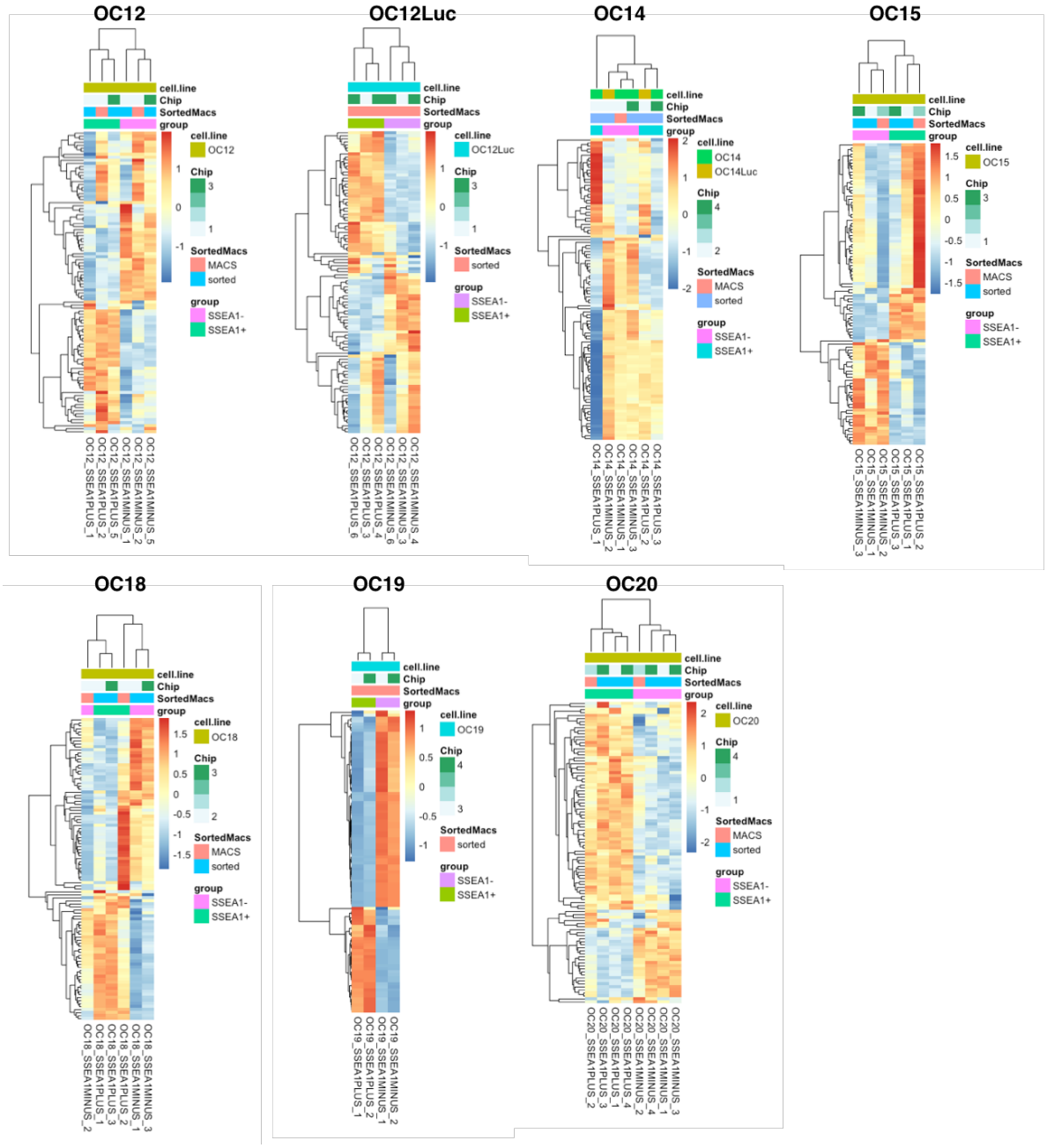

Figure 32: Unsupervised hierarchichal clustering of SSEA1$^-$ and SSEA1$^+$ microarray data according to single patient background.
Microarray data of SSEA1$^-$ and SSEA1$^+$ sorted cells were clustered by unsupervised hierarchichal clustering based on single patient background (OC12, OC12Luc, OC14, OC15, OC18, OC19 and OC20, repectively). Average-linking method and manhattan distance for clustering of the columns were applied. Expression data are log2 normalized and the top 100 differentially expressed genes were used for the heatmap. Based on the data from figure 31 a, the data were computationally batch-corrected with the "ComBat" (Johnson *et al.,* 2007) function in R in order to get rid of the batch effect of the different chips used. Only OC14 and OC18 were additionally batch-corrected for the parameter "SortedMacs". Column colors correspond to cell line (cell.line), chip number (Chip), whether the cells were sorted or MACSed (SortedMacs) or SSEA1 expression (group). Heatmaps were plotted with the R

script listed in 7.2.

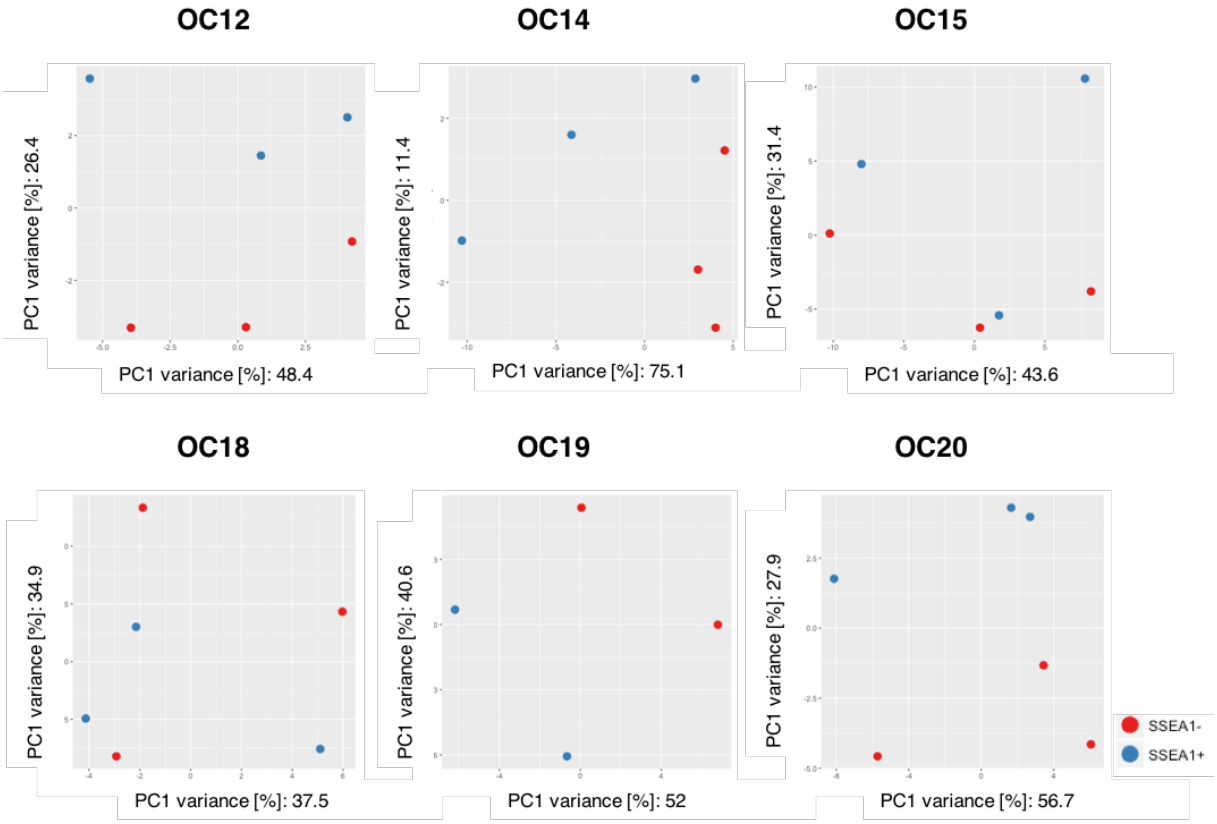

Figure 33: Principal component analysis of SSEA1$^-$ and SSEA1$^+$ microarray data within single patient background.
Principal component analysis of the replicates of each individual OC cell line (OC12, OC14, OC15, OC18, OC19 and OC20, respectively) used for differential gene expression analysis. SSEA1$^+$ cells are depicted in blue and SSEA1$^-$ ones in red. Principal component plots were plotted with the R script listed in 7.2.

4.3.2 Gene expression profiling reveals differentially expressed genes between SSEA1$^-$ and SSEA1$^+$ cells

Testing for statistically differentially expressed genes with Chipster software revealed many differentially expressed genes between SSEA1$^-$ and SSEA1$^+$ cells when analyzing all samples together (table 13) or when analyzing them within single patient background (table 14).
Samples were analyzed in a pooled way with Benjamini-Hochberg method for multiple testing correction and without correction for multiple testing in order to increase the number of genes (table 13). Since the patient background had an impact to the number of statistically significant genes, we also performed the analyses individually, comparing SSEA1$^+$ and SSEA1$^-$ cells within a single patient. Hence, we got many more statistically significantly enriched genes between SSEA1$^+$ and SSEA1$^-$ cells (table 14).

Table 13: Differentially expressed genes between SSEA1$^-$ and SSEA1$^+$ cells when analyzing all 6 OC cell lines in a pooled manner. Genes with a FC > 1.2 were analyzed by different statistical testing methods. (different p-values, BH, none). BH = Benjamini-Hochberg, FC = fold change.

testing method for differentially expressed genes between SSEA1$^+$ and SSEA1$^+$ cells for all 6 OC lines	gene number, FC > 1.2
p-value < 0.05, BH	378
p-value < 0.1, BH	702
p-value < 0.001, none	423
p-value < 0.01, none	1384
p-value < 0.05, none	3561

Table 14: Differentially expressed genes between SSEA1$^-$ and SSEA1$^+$ cells for each OC cell line individually. Replicate numbers as well as respective fold changes (FC) for the statistical testing (p-value < 0.05, BH correction).

	replicates	p- value < 0.05, BH	FC
OC12	3 per SSEA1$^+$/SSEA1$^-$ group	450 genes	> 1.3
OC14	2 per SSEA1$^+$/SSEA1$^-$ group	741 genes	> 1.6
OC15	2 per SSEA1$^+$/SSEA1$^-$ group	17 genes	> 1.9
OC18	2 per SSEA1$^+$/SSEA1$^-$ group	933 genes	> 1.4
OC19	2 per SSEA1$^+$/SSEA1$^-$ group	430 genes	> 1.5
OC20	3 per SSEA1$^+$/SSEA1$^-$ group	1195 genes	> 1.3

4.3.1 Gene expression profiling analyses predict SPDEF to be enriched in SSEA1$^-$ cells

To further unravel the molecular differences between SSEA1$^-$ and SSEA1$^+$ cells, we analyzed the differentially enriched genes in SSEA1$^-$ and SSEA1$^+$ cells in detail. Since SSEA1$^+$ and SSEA1$^-$ cells clustered together in 4 out of 6 OC cell lines (OC12, OC15, OC19 and OC20), respectively, but not in OC14 and OC18 (figure 32), we decided to exclude OC14 and OC18 from the molecular analyses.

In the 4 OC cell lines OC12, OC15, OC19 and OC20, 15 genes were upregulated in the SSEA1$^-$ population. Among these genes, we found SPDEF (Sam-pointed ets-domain containing transcription factor) to be significantly differentially enriched in all SSEA1$^-$ populations (figure 34 a). In the SSEA1$^+$ population, 21 genes were significantly upregulated (figure 34 b). As a cut-off, a p-value < 0.1 was chosen in order to detect more differentially expressed genes because of the heterogeneous patient background.

Differential SPDEF expression as compared to the levels of other differentially expressed genes in SSEA1$^-$ and SSEA1$^+$ cells is shown in the volcano plots in figure 30 c. Normalized $\log_2$-fold change expression of SPDEF as measured by the Illumina array (Illumina probe ILMN_2161330) in replicates of the 6 OC cell line-derived FACS-sorted SSEA1$^+$ and SSEA1$^-$ cells reveals that SPDEF is significantly differentially enriched in OC12, OC15 and OC20 cells (figure 34 c). In OC14 and OC19 sorted SSEA1$^-$ and SSEA1$^+$ cells, there is also a tendency for SPDEF enrichment in SSEA1$^-$ cells. Only in OC18 sorted SSEA1$^-$ and SSEA1$^+$ cells, SPDEF was enriched in the SSEA1$^+$ population.

To sum up, SPDEF was enriched in SSEA1$^-$ cells of all 4 OC cell lines OC12, OC15, OC19 and OC20.

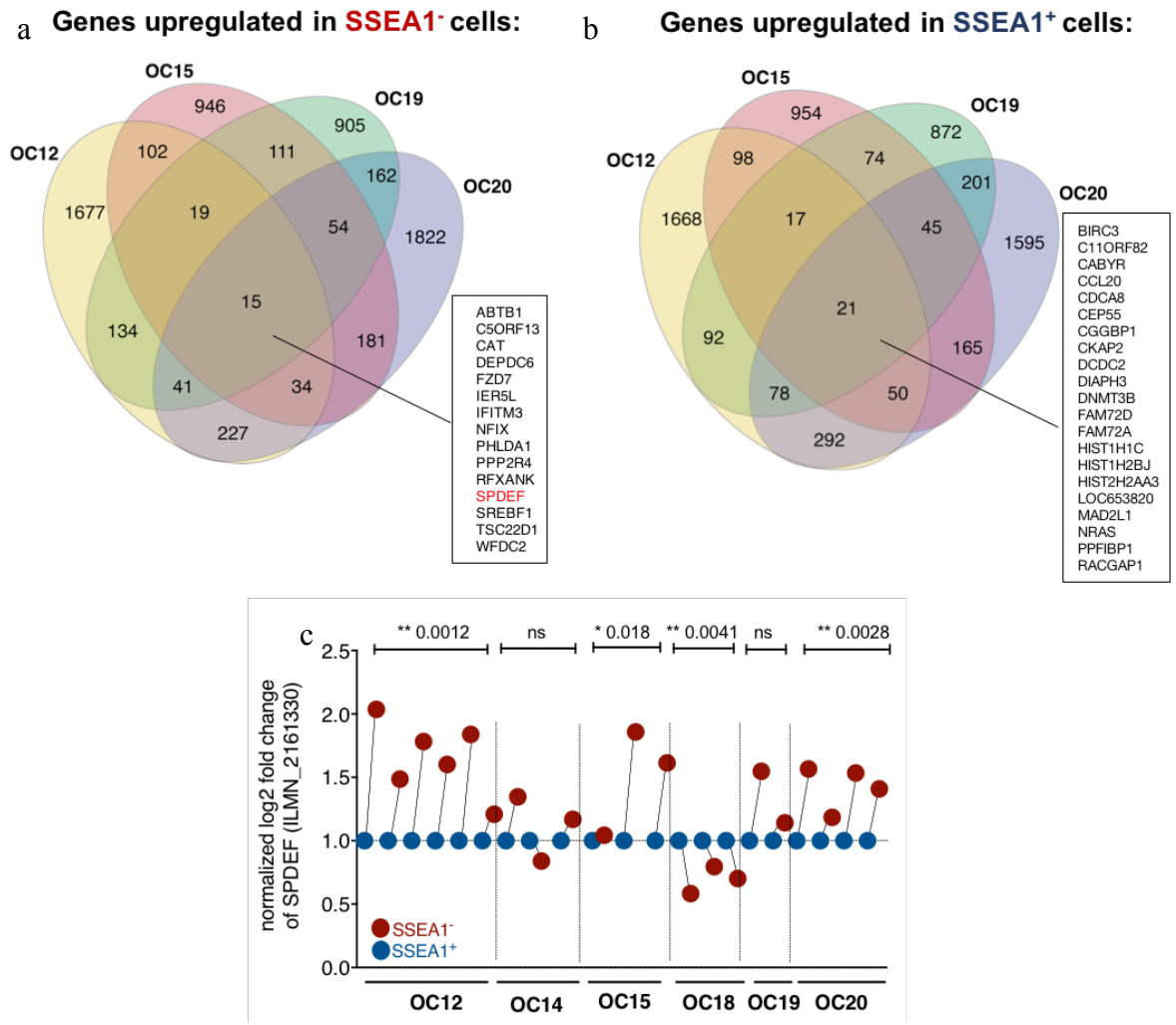

Figure 34: Overlap of differentially enriched genes in the SSEA1$^-$ or SSEA1$^+$ cells of OC12, OC15, OC19 and OC20 cell lines.
Overlap of genes which were differentially upregulated in the SSEA1$^-$ (a) or SSEA1$^+$ (b) cells of OC12, OC15, OC19 and OC20 cells. 15 and 21 genes were differentially enriched in all of the OC cell lines in SSEA1$^-$ and SSEA1$^+$ cells, respectively. For statistical testing, the empirical Bayes test with a p-value of 0.1 was used. (c) Normalized $\log_2$-fold expression of the Illumina probe ILMN_2161330 which is assigned to the SPDEF gene in FACS-sorted SSEA1$^+$ (blue) and SSEA1$^-$ (red) cells of 6 OC cell lines.

4.3.1 GSEA and GO reveal enrichment of different gene signatures in the SSEA1$^-$ cells

To further investigate the molecular differences between SSEA1$^-$ and SSEA1$^+$ cells of the OC cell lines OC12, OC15, OC19 and OC20, we performed GSEA (Gene set enrichment analyses) and GO (Gene ontology analyses) of the mRNA of SSEA1$^-$ and SSEA1$^+$ sorted cells (figure 35 and figure 36).

GSEA analyses of the mRNA of FACS-sorted SSEA1$^+$ and SSEA1$^-$ cells of the OC12, OC15, OC19 and OC20 cell lines again revealed that the transcription factor SPDEF was among the most differentially enriched genes in SSEA1$^-$ cells figure 35 a). The analyses further revealed a significant enrichment of genes assigned to the gene sets "GU_PDEF_TARGETS_UP", as well as to "HUANG_FOXA2_TARGETS_DN" (figure 35d, e). The gene set "GU_PDEF_TARGETS_UP" includes genes up-regulated after knockdown of SPDEF by RNAi and the gene set "HUANG_FOXA2_TARGETS_DN" denotes genes downregulated by induced expression of FOXA2.

Gene sets involved in proliferation and DNA replication were mostly enriched in the SSEA1$^+$ population (FDR < 0.1, figure 35 c). In the SSEA1$^-$ population, GSEA analyses revealed an enrichment of signatures related to metastasis and invasiveness ("VANTVEER_BREAST_CANCER_METASTASIS" and "ANASTASSIOU_ MULTICANCER_INVASIVENESS_SIGNATURE"), stem and progenitor cells ("BOQUEST_STEM_CELL_UP" and "ENGELMANN_CANCER_PROGENITORS_DN"), as well as breast cancer ("LANDIS_BREAST_CANCER_PROGRESSION_DN" and "DOANE_BREAST_CANCER_ESR1_UP"), especially to the luminal type of breast cancer ("SMID_BREAST_CANCER_LUMINAL_B_UP" and "CHARAFFE_BREAST_ CANCER_LUMINAL_VS_BASAL_UP") and to signaling pathways like HES/HEY and HIF1a/hypoxia ("ELVIDGE_HYPOXIA_BY_DMOG_UP", "ELVIDGE_HIF1A_ TARGETS_DN" and "ELVIDGE_HYPOXIA_UP") signaling (FDR < 0.1, figure 35 b).

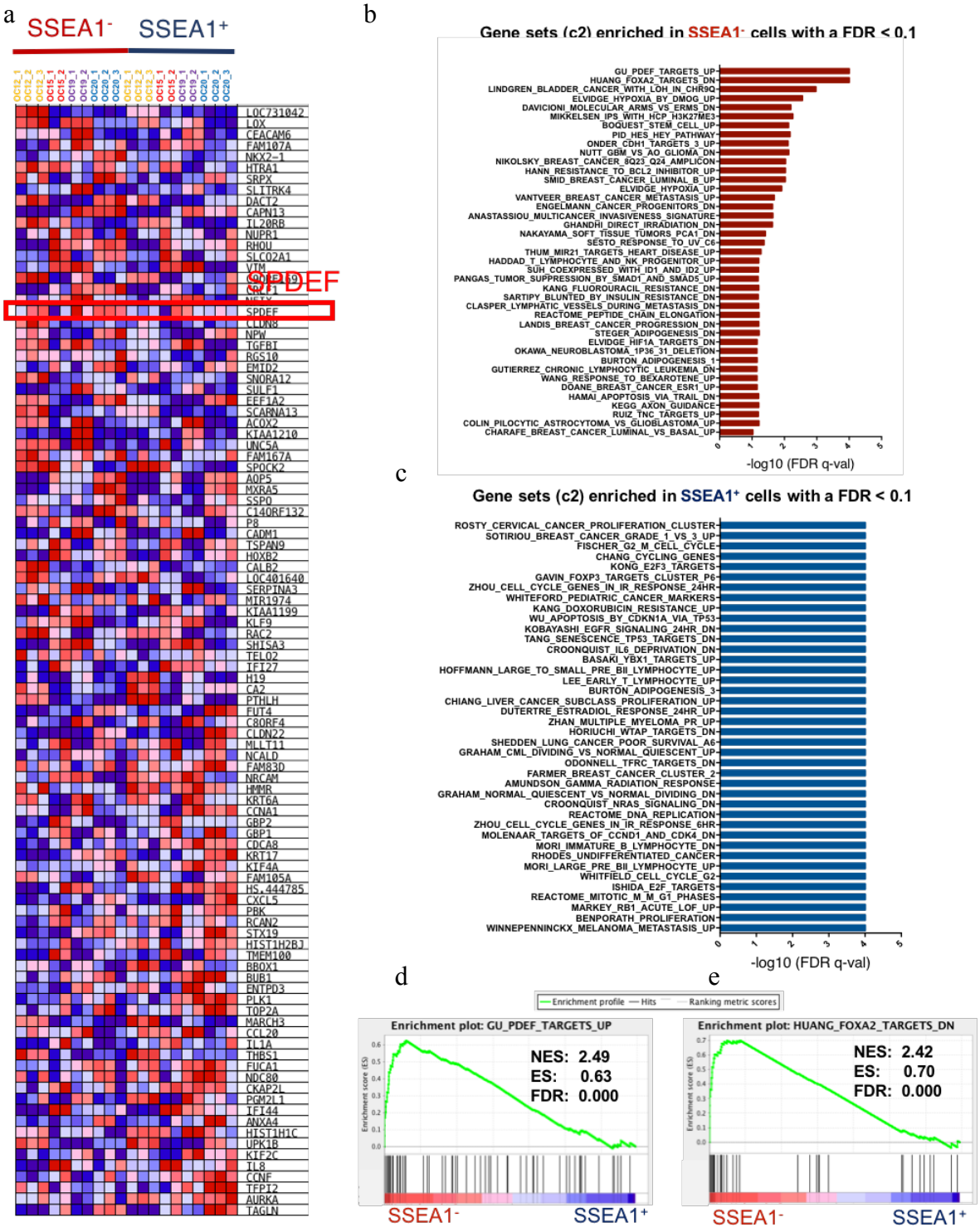

Figure 1: Gene set enrichment analyses (GSEA) predict SPDEF and SPDEF gene signatures to be enriched in SSEA1⁻ cells.
GSEA analyses of mRNA of FACS-sorted SSEA1⁻ and SSEA1⁺ cells of OC12, OC15, OC19 and OC20 cell lines. Among the most differentially enriched genes is SPDEF which is highlighted in red (a). Top significantly (FDR < 0.1) enriched gene signatures derived from genes mostly enriched in the SSEA1⁻ (b) or SSEA1⁺ (c) population. Gene set enrichment plots of gene sets enriched in SSEA1⁻ cells (d, e). ES = enrichment score, FDR = False discovery rate, NES = normalized enrichment score.

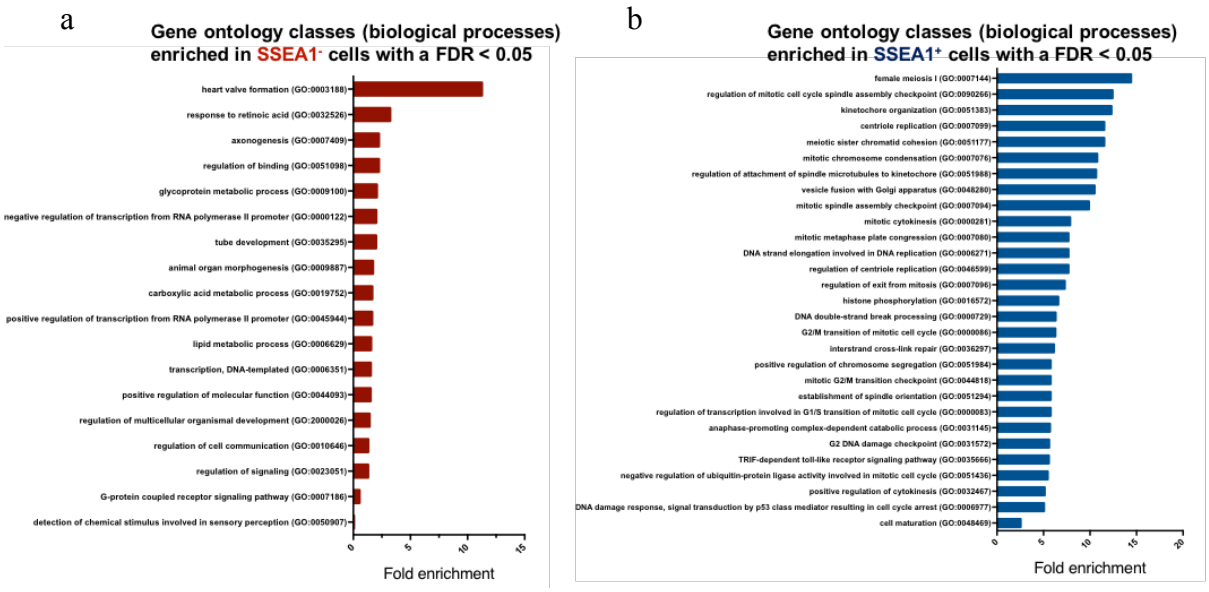

Figure 36: Differentially enriched gene signatures (biological processes) in SSEA1$^-$ and SSEA1$^+$ populations according to gene ontology analyses.
Gene ontology analyses for gene signatures enriched in SSEA1$^-$ (a) and SSEA1$^+$ cells (b) performed with the Gene ontology Consortium web page using the "biological process" choice and a FDR < 0.05.

Regarding GO analyses, the biological processes enriched in SSEA1$^-$ cells were mostly related to development and organ morphogenesis (figure 36 a). The biological processes enriched in the SSEA1$^+$ cells were mainly involved in DNA replication and proliferation (figure 36 b), similar to the results of GSEA (figure 35 b, c).

Taken together, the signatures enriched in SSEA1$^-$ cells predict a more aggressive, stem-like cell type whereas the signatures enriched in SSEA1$^+$ cells describe a more proliferative cell population.

4.4 SPDEF is enriched in the SSEA1$^-$ cells and drives tumor growth

4.4.1 SPDEF is expressed in OC cells and is enriched in SSEA1$^-$ cells

Based on gene expression profiling, we identified SPDEF to be enriched in SSEA1$^-$ cells as compared to SSEA1$^+$ ones.

To verify this, we performed quantitative RT-PCR of FACS-sorted OC12 and OC20 SSEA1$^-$ and SSEA1$^+$ cells. SPDEF was significantly enriched in SSEA1$^-$ cells as compared to SSEA1$^+$ cells (figure 37).

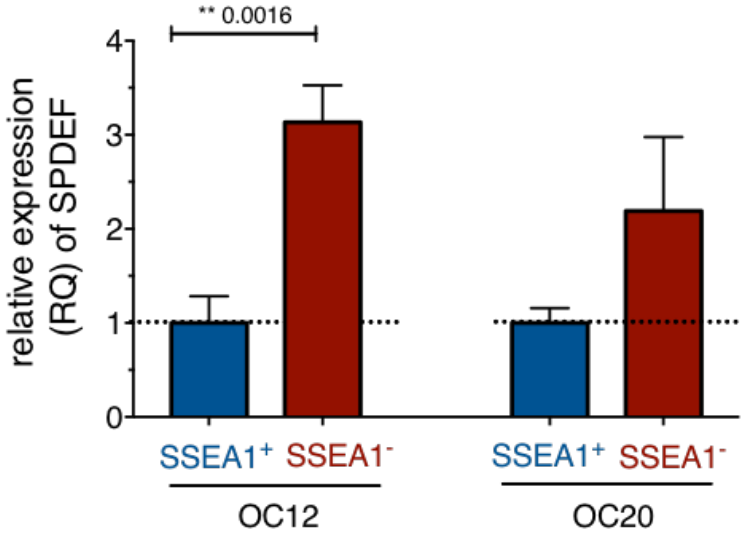

Figure 37: SPDEF is enriched in SSEA1$^-$ cells in several OC cell lines.
(a) SPDEF expression as measured by qRT-PCR in FACS-sorted SSEA1$^+$ and SSEA1$^-$ cells of OC12 and OC20 cell lines. n = 4 (OC12) and n = 1 (OC20) biological replicates(s). n = 3 technical replicates. ** $p < 0.01$, unpaired, parametric, two-tailed t-test.

4.4.2 SPDEF can be efficiently overexpressed and knocked down in OC cells

Previous data showed that SPDEF is overexpressed in SSEA1$^-$ cells compared to SSEA1$^+$ cells. We thus wondered, whether expression of SPDEF is responsible for the phenotype observed in SSEA1$^-$ cells regarding increased tumor growth and clonogenicity.

Hence, we engineered a vector to lentivirally overexpress SPDEF in the OC12 and OC20 cell lines – the ones from which we had previously gained *in vivo* data regarding differential growth. Furthermore, we also generated doxycycline-inducible SPDEF knockdown and non-silencing (NS) control cell lines. SPDEF could be overexpressed more than 10- or 100-fold, respectively (OC20 and OC12), as compared to empty vector iT2 control (figure 38 a). Doxycycline-induced knockdown efficiency of SPDEF was roughly 80 % as compared to doxycycline-treated non-silencing control in both OC12 and OC20 cell lines (figure 38 b). Western blotting further verified the overexpression of SPDEF on protein level. However, knockdown of SPDEF could only be verified on protein level in OC20 but not in OC12 since no basal SPDEF expression could be detected (figure 38 c, d).

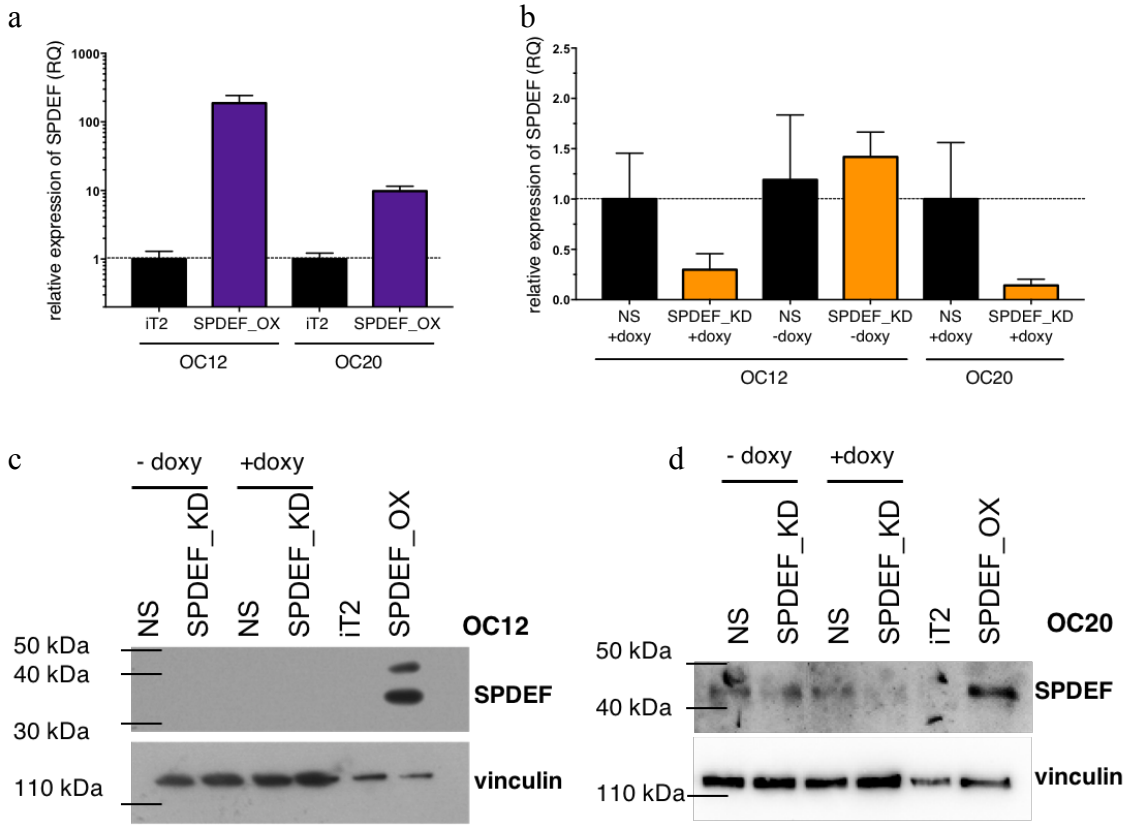

Figure 38: SPDEF can be downregulated by inducible doxycycline-induced knockdown and also overexpressed.

SPDEF expression as measured by qRT-PCR in OC12 and OC20 cells in either the control iT2 (black, (a)) or SPDEF overexpressing cells (purple, (a)) or the SPDEF knockdown (orange, (b)) and respective NS control cells (black, (b)) either with or without doxycycline administration. (c) Verification of SPDEF knockdown and overexpression in OC12 cells (c) and OC20 (d) cells. Vinculin was used as a loading control. iT2 = IRES-tdtomato 2, KD = knockdown, NS = non-silencing, OX = overexpression

4.4.3 SPDEF knockdown and overexpression changes the morphology of the cells

The morphology of cells either overexpressing SPDEF or displaying SPDEF knockdown differed: OC12 cells transduced with a SPDEF shRNA-expressing knockdown construct displayed a less epithelial-like growth when induced with doxycycline (figure 39 a, orange) and instead, grew more mesenchymal-like and more as single cells than in epithelial clusters compared to the NS control cells with and without doxycline and the SPDEF KD cells without doxycycline (figure 39 a, black). All control cells grew like the parental OC12 cell line in epithelial-like clusters. No differences could be observed between OC12 SPDEF OX and control iT2 cells.

However, OC20 cells transduced with SPDEF-overexpressing constructs grew in a more epithelial way than iT2 control cells (figure 39 b). No differences between SPDEF KD and NS control cells in OC20 cells were observed.

Taken together, we observed a more mesenchymal-like growth upon SPDEF KD in the epithelial cell line OC12 and a more epithelial-like growth upon SPDEF overexpression in the OC20 cell line which grows more in spheroid-like, adherent clusters.

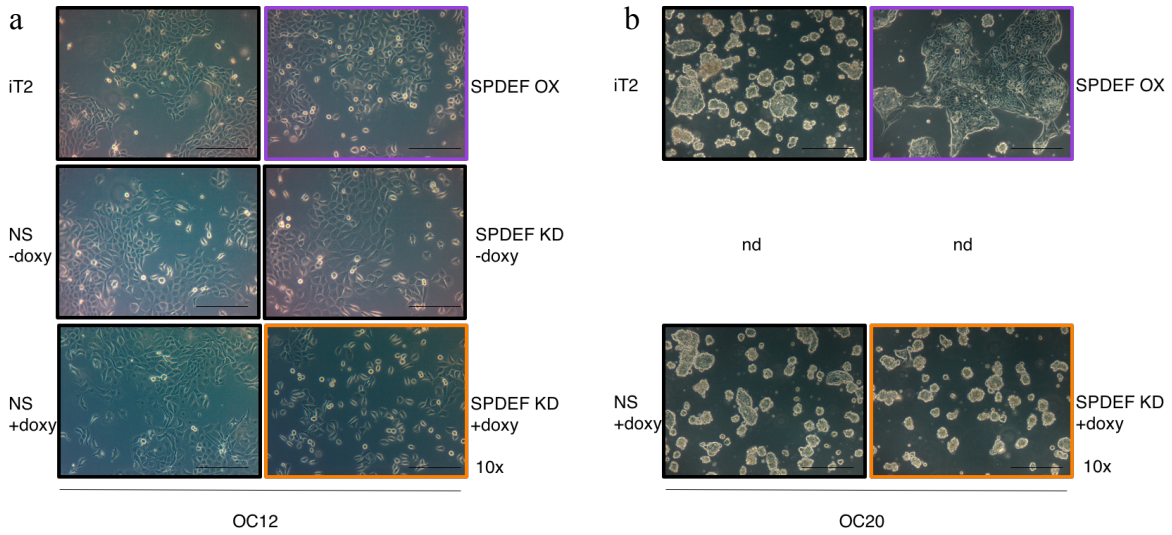

Figure 39: SPDEF knockdown and overexpression change the morphology of cells.
(a) Morphology of OC12 cells transduced with iT2 control (black), SPDEF OX (purple), NS control (black) or SPDEF KD (-doxy: black, +doxy: orange) shRNA-expressing viruses. SPDEF KD + doxy cells grow more as single cells and in a more mesenchymal way as the respective NS ± doxy and SPDEF KD –doxy cells. (b) OC20 cells transduced with iT2 control (black), SPDEF OX (purple), NS control +doxy (black) and SPDEF KD +doxy (orange) shRNA-expressing viruses. SPDEF OX cells grow in a more epithelial way than iT2 control cells. doxy = doxycycline, iT2 = IRES-tdtomato 2, KD = knockdown, nd = not determined, NS = non-silencing, OX = overexpression.

4.4.4 SPDEF-overexpressing cells grow more and knockdown cells display reduced growth *in vitro*

Since SSEA1$^-$ cells grew more *in vivo*, but not *in vitro* – which might be because they gave rise to SSEA1$^+$ cells with time, we wondered whether the SPDEF overexpressing (OX) or knockdown (KD) cells also grow differentially.

Therefore, we cultured SPDEF OX or SPDEF KD cells with their respective iT2 or NS control for up to 8 days *in vitro* and monitored growth indirectly by using the CellTiterBlue assay & measuring the absorbance of resorufin which is the product from the reduction of resazurin in viable cells.

SPDEF overexpressing cells grew significantly more both in OC12 and OC20 cell lines (figure 40 a, b). Knockdown of SPDEF reduced cell growth significantly in OC12 cells but not in OC20 ones as compared to control.

To sum up, lentiviral expression of SPDEF increased proliferation in cells as measured by reduction of resazurin to resorufin.

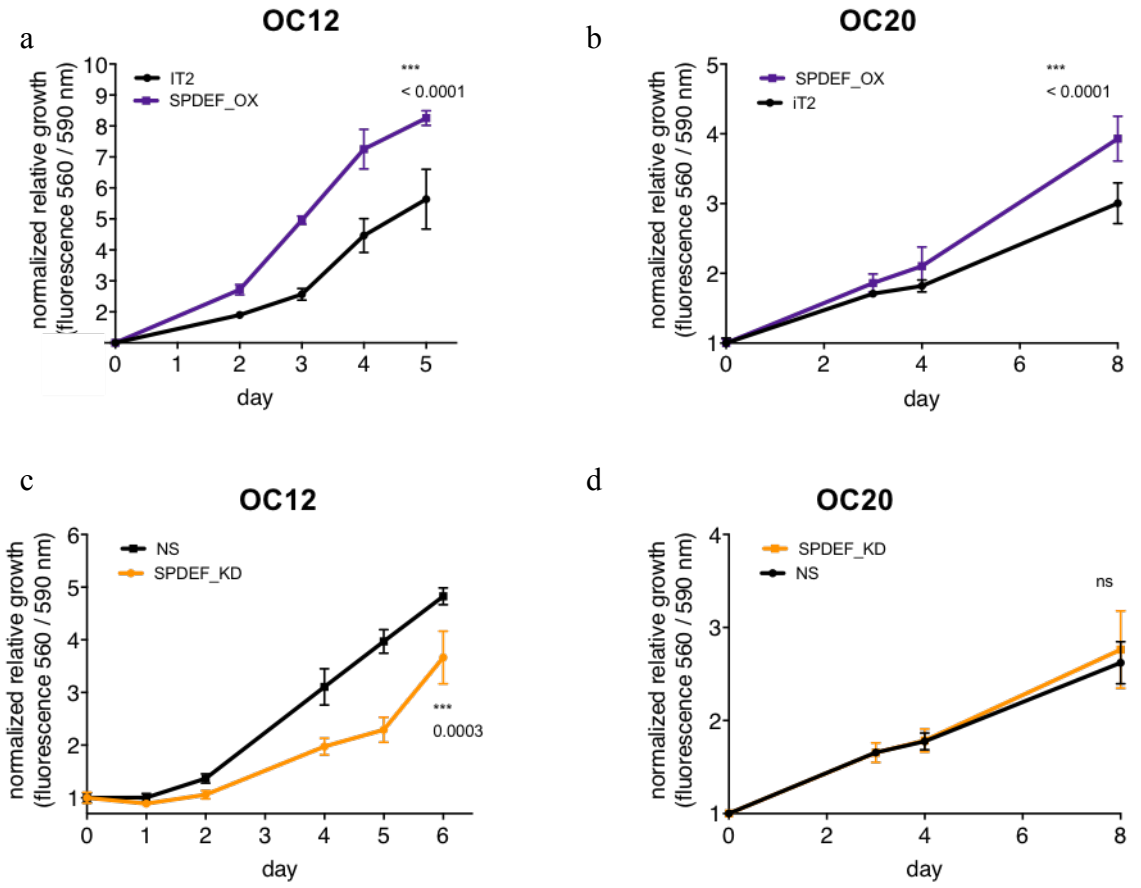

Figure 40: Growth curve of SPDEF overexpressing and knockdown cells.
Growth of SPDEF OX (purple) and iT2 control cells was measured via the CellTiterBlue assay at several time points and normalized to day 0 in OC12 (a) and OC20 (b) cells. Also, growth of SPDEF KD (orange) and NS control (black) cells was compared in OC12 (c) and OC20 (d) cells. For OC12, 750 cells per 96-well PRIMARIA well and for OC20, 4000 cells were seeded, respectively. Cells were grown in CSC-medium depleted for estrogen and supplemented with 0.1 µM tamoxifen. Mean ± SD. *** $p < 0.001$, **** $p \leq 0.0001$, ns = not significant. Two-way ANOVA. OX = overexpression, iT2 = IRES-tdtomato 2, KD = knockdown, NS = non-silencing.

4.4.5 SPDEF overexpression increases colony number and size whereas SPDEF knockdown decreases them

Since SSEA1$^-$ cells formed more and bigger colonies and SPDEF was enriched in this cell population, we consequently asked, whether overexpression of SPDEF also enabled the outgrowth of more and bigger colonies.

In order to determine the clonogenic potential of SPDEF OX and iT2 control cells *in vitro*, we performed colony formation assays in adherent conditions. Both in OC12 and OC20 patient cell lines, SPDEF overexpressing cells formed significantly more and bigger colonies (figure

41) when initially seeding the same number of single cells into 6-wells (OC12: 3,200; OC20: 50,000 cells).

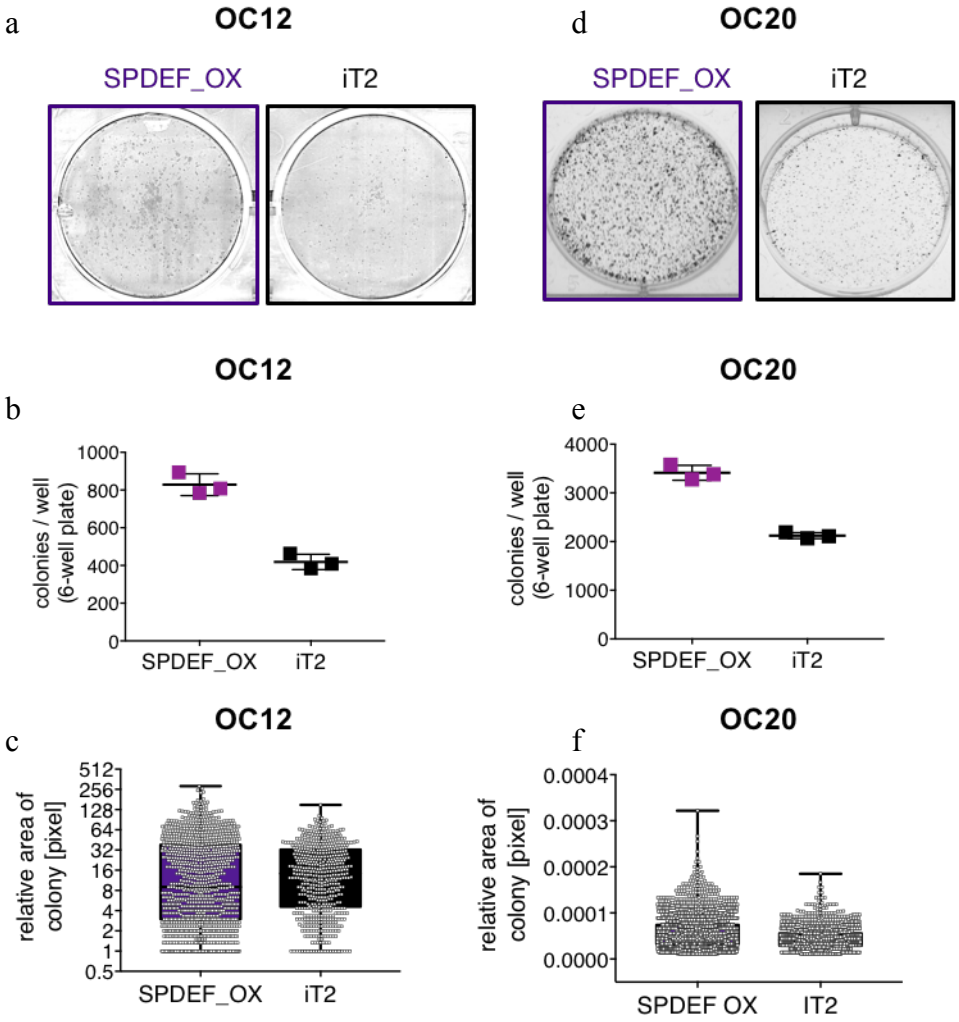

Figure 41: SPDEF overexpressing cells form more and bigger colonies.
Representative images of the colonies formed by SPDEF OX (purple) and iT2 control (black) cells of OC12 (a) and OC20 (d) cell lines. Colony number of SPDEF OX (purple) and iT2 control (black) cells of OC12 (b) and OC20 (e) cells cultured in PRIMARIA 6-wells. For the OC12 cell line, 3,200 cells were seeded per 6-well and for OC20 50,000 cells. OC12 cells were cultured for 7 days and OC20 cells for 14 days, respectively. Relative area per colony of SPDEF OX (purple) and iT2 control (black) cells of OC12 (c) and OC20 (f) cells as quantified by Fiji. Mean ± SD (b). Box and whisker plot, min to max (c, f). n = 3 technical replicates. n = 4 biological replicates for OC12 and 3 for OC20; one exemplary result is shown. OX = overexpression, iT2 = IRES-tdtomato 2

On the contrary, knocking down SPDEF in OC cells led to significantly less and smaller colonies than in NS control cells, again both in OC12 and OC20 cells (figure 42).

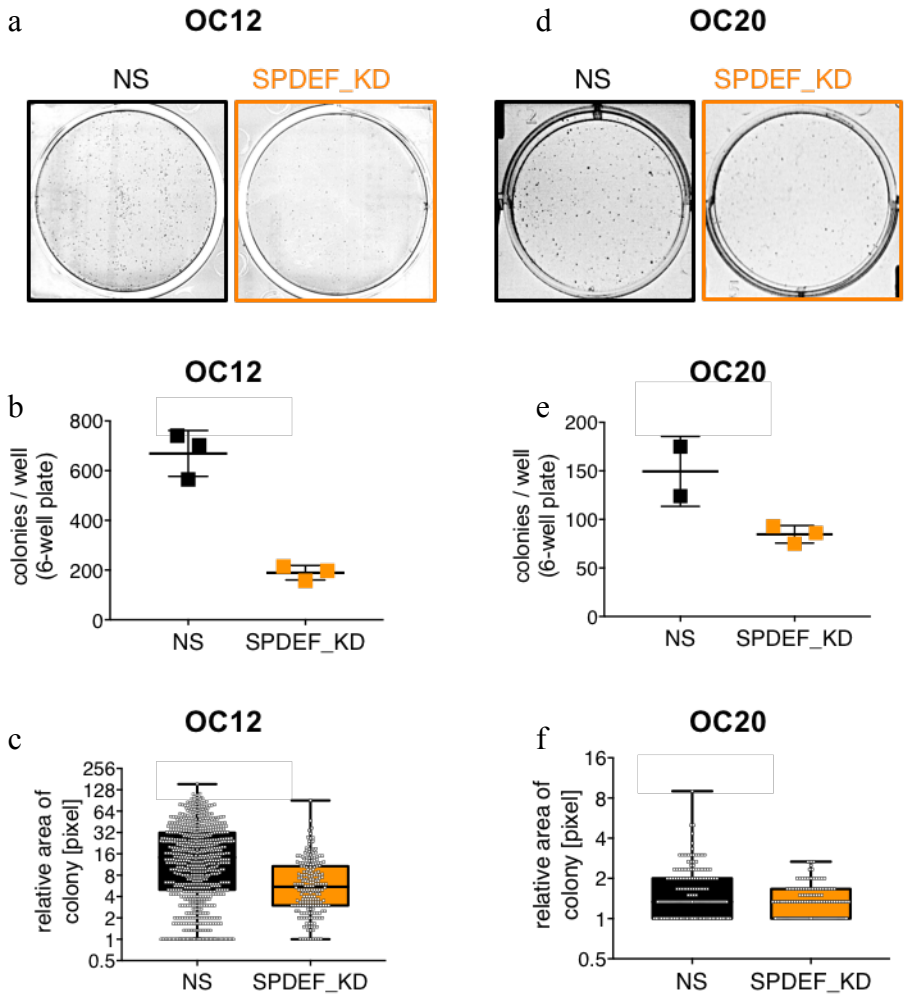

Figure 42: SPDEF knockdown cells form less and smaller colonies.
Representative images of the colonies formed by SPDEF KD (orange) and NS control (black) cells of OC12 (a) and OC20 (d) cell lines. Colony number of SPDEF KD (orange) and NS control (black) cells of OC12 (b) and OC20 (e) cells cultured in PRIMARIA 6-wells. For the OC12 cell line, 3,200 cells were seeded per 6-well and for OC20 16,000 cells. OC12 cells were cultured for 7 days and OC20 cells for 14 days, respectively. Relative area per colony of SPDEF KD (orange) and NS control (black) cells of OC12 (c) and OC20 (f) cells as quantified by Fiji. Mean ± SD (b,e). Box and whisker plot, min to max (c,f). n = 3 technical replicates (OC12) and n=2-3 technical replicates (OC20). n = 4 biological replicates for OC12 and 3 for OC20; one exemplary result is shown. KD = knockdown, NS = non-silencing.

4.4.6 SPDEF knockdown decreases *in vitro* clonogenicity

Since knockdown of SPDEF decreases colony formation potential, we wondered whether SPDEF knockdown cells are less clonogenic than NS control cells. Therefore, we performed *in vitro* limiting dilution analyses.

In the wells cultured with the SPDEF knockdown cells, less colonies were formed than in the wells containing the NS control cells (figure 43). According to ELDA limiting dilution analysis tool, these differences were even statistically significant. In OC12 NS control cells, roughly 1 in 4 cells (range from 2.6 – 6.7 cells) was a colony-forming cell, whereas in SPDEF knockdown cells, only 1 in 13 cells (range from 8.3 – 20.6 cells) were able to form colonies. In the OC20 population, 1 in 128 cells (range from 98.7 – 166 cells) could give rise to colonies in the NS control cell line whereas 1 out of 211 cells (range from 162.7 – 274 cells) only could form colonies in the SPDEF knockdown cells (figure 43 b).

Taken together, knockdown of SPDEF reduced the ability to form colonies in *in vitro* limiting dilution conditions.

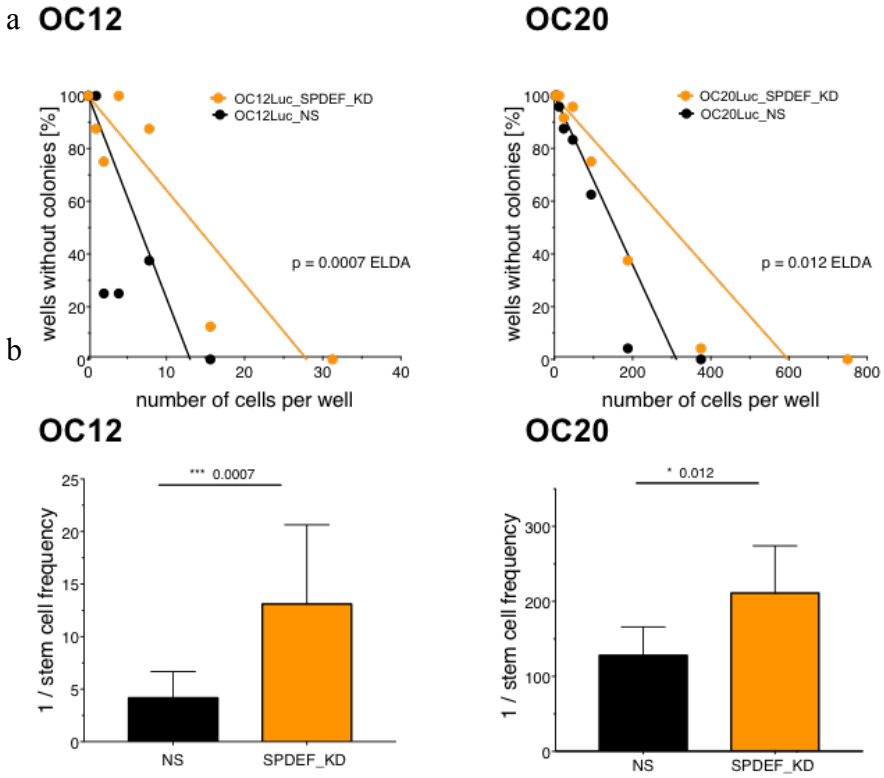

Figure 43: SPDEF knockdown cells are less clonogenic in limiting dilution analyses *in vitro*.

(a) Numbers of wells without colonies of NS (black) and SPDEF KD (orange) OC12 and

OC20 cells seeded in limiting dilution conditions were quantified and analyzed using the ELDA limiting dilution tool. n = 8 (OC12) or 24 (OC20) replicates per condition. (b) Confidence intervals for 1 / stem cell frequencies as assessed by ELDA. n = 1 biological replicate. * $p < 0.05$, *** $p < 0.001$, ns = not significant. NS = non-silencing control, KD = knockdown.

4.4.7 SPDEF overexpressing cells close wounds more rapidly than control cells

To further characterize the effect of increased SPDEF expression on OC cells, we performed a wound closure assay.

Cells were grown to confluence, incubated for 1 h with mitomycin in order to block proliferation and then scratched with a sterile tip to inflict a wound. Monitoring of the cells for up to 19 h, revealed that the SPDEF overexpressing cells close the inflicted scratch faster than the iT2 control cells (figure 44). Already after 8.5 h, the difference in closed wound area was obvious (figure 44 c).

Taken together, we could show that SPDEF overexpressing cells migrate faster than control iT2 ones.

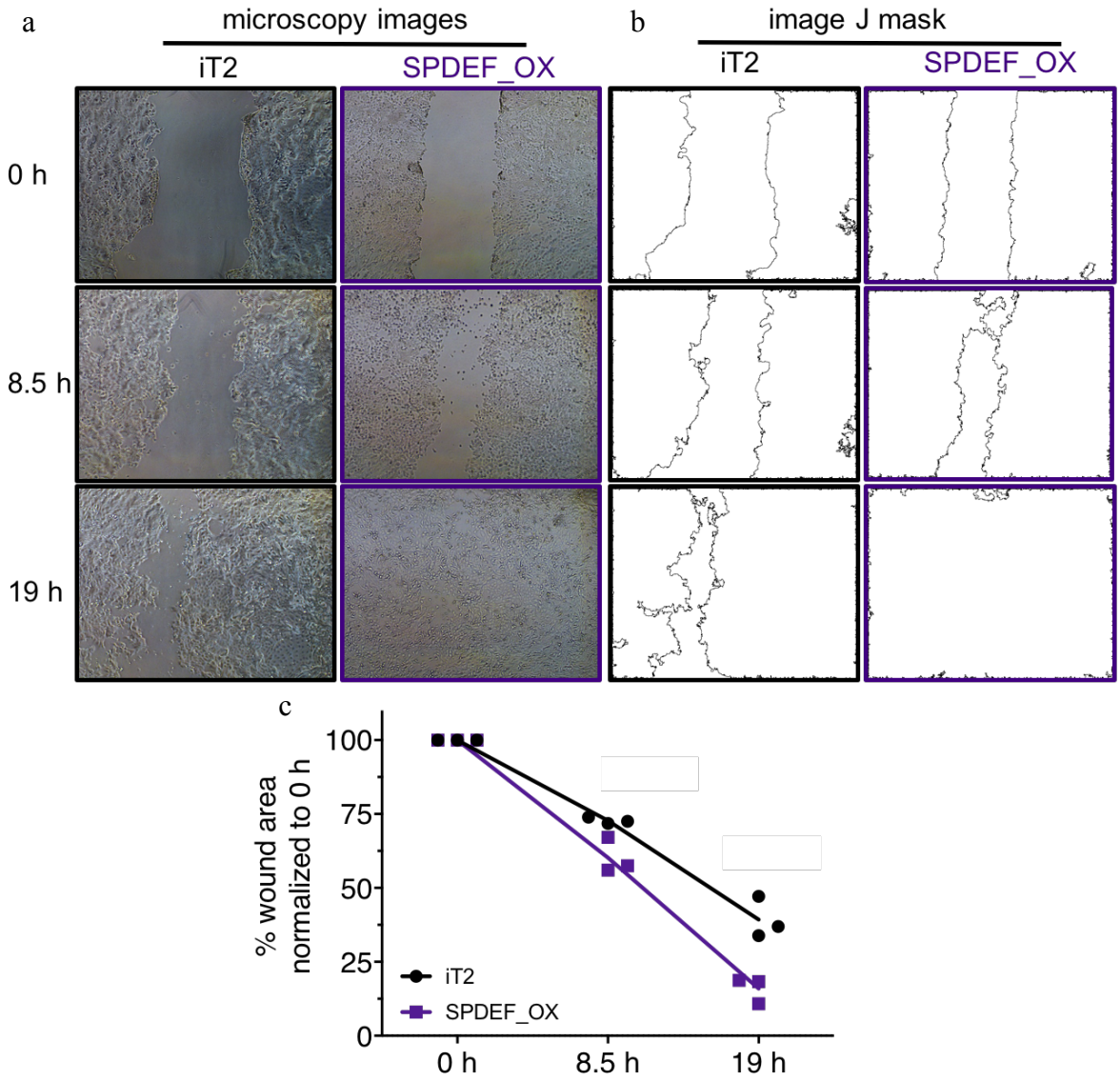

Figure 44: SPDEF overexpression allows cells to close wounds more rapidly.
SPDEF overexpressing (purple) OC12 or iT2 control (black) cells were cultured to confluence, incubated for 1 h with 10 µg/ml mitomycin C, then a scratch was made and the medium changed. Microscopy images were taken in triplicates at time points 0 h, 8.5 h and 19 h (a). The area of the wound was measured by applying a mask via Fiji (b) and the resulting area was normalized to 0 h and quantified (c). iT2 = IRES-tdtomato 2, OX = overexpression.

4.4.8 Knockdown of SPDEF impedes *in vivo* tumor growth

Previous data showed that SSEA1$^-$ cells initiate tumors *in vivo* and lead to a higher tumor burden. Since SPDEF has been shown to be enriched in the SSEA1$^-$ population, we wondered whether SPDEF expression is responsible for the phenotype of increased tumor growth in SSEA1$^-$ cells. Consequently, we aimed at answering the question whether knockdown of SPDEF impairs tumor growth.

Thus, we intraperitoneally injected luciferase-labeled OC20 SPDEF knockdown and NS control cells into NSG mice which were kept under doxycycline treatment. And indeed, the SPDEF knockdown cells initiated tumors later and overall tumor growth was significantly impeded (figure 45 a, b). Furthermore, injection of SPDEF knockdown cells led to a lower tumor burden than injection of NS cells at the endpoint at week 22 (OC20) as measured by bioluminescence (figure 45 c, d). Kaplan-Meier survival analyses indicated that survival of mice injected with SPDEF KD cells was significantly better than that of mice having been injected with control NS cells (figure 45 e). To perform the survival analyses, mice were scored to be dead upon a 100-fold increase in bioluminescence.

Intraperitoneally injected luciferase-labeled OC12 SPDEF knockdown and NS control cells, however, did not show a differential growth. Albeit, there was a huge heterogeneity regarding the growth pattern of SPDEF KD

In sum, we could show that SPDEF KD diminishes tumor growth and reduces the tumor-initiating potential of OC20 cells. Moreover, tumor burden of mice having been injected with SPDEF KD cells was lower than in control cells.

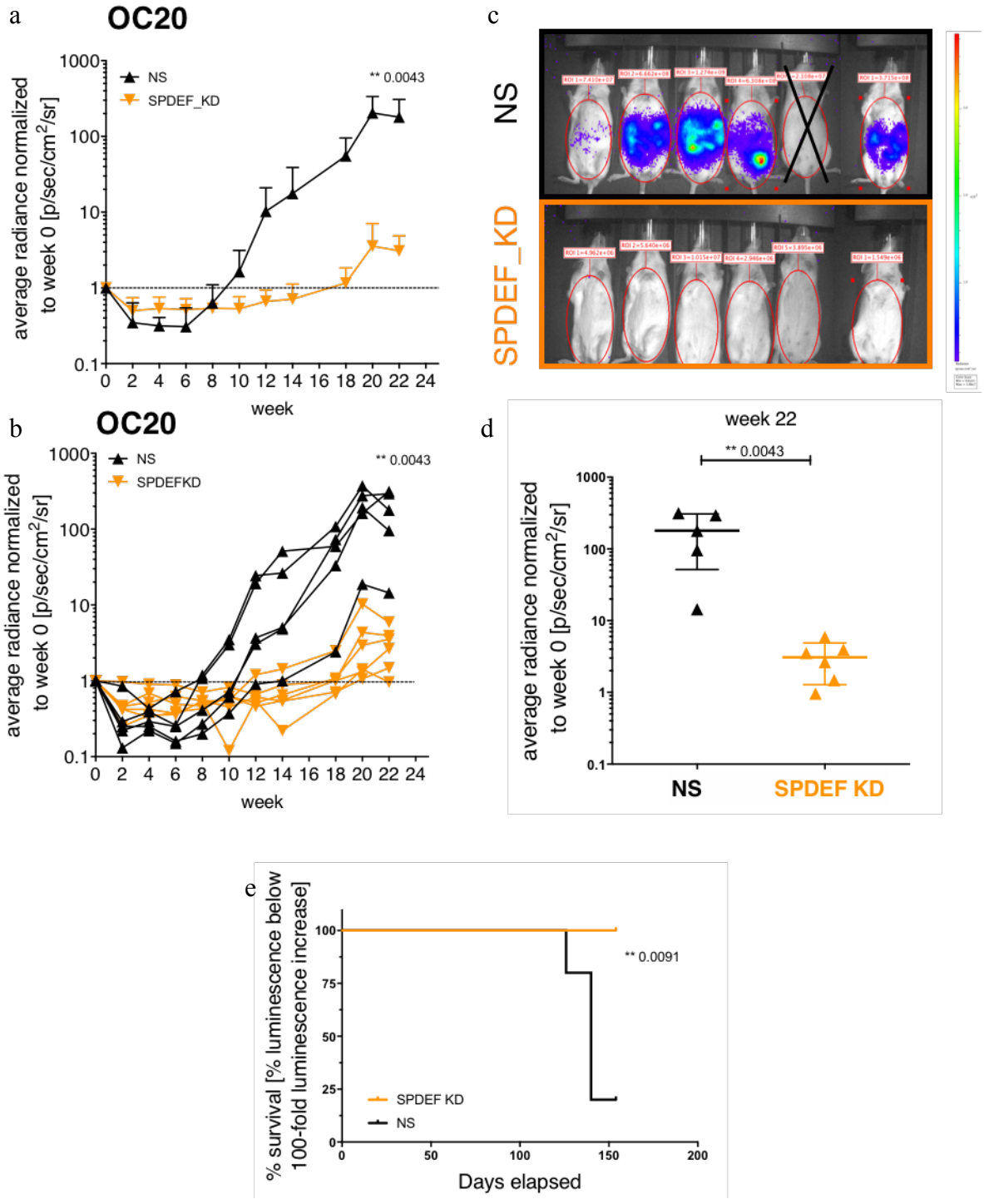

Figure 45: SPDEF knockdown impedes tumor growth *in vivo* (OC20*)*.
Growth curves of SPDEF knockdown (orange) and non-silencing control (black) OC20 cells (a) which have been i.p. injected into NSG mice and which were before lentivirally transduced with a luciferase vector in order to follow tumor growth via bioluminescence. In a, the mean ± SEM of the average radiance is shown, in b, the growth curves of the tumor cells for each single mouse are depicted. The dashed line denotes the baseline at week 0. (c) Images of the *in vivo* bioluminescent signal in mice injected with SPDEF knockdown

(orange) and non-silencing control (black) OC20 cells at the endpoint at week 22. n = 5 (SPDEF knockdown) or 6 mice per group (NS). Mouse number 5 was excluded in the analysis due to no signal at the initial time point. (d) Tumor burden of mice injected intraperitoneally with NS control (black) and SPDEF KD (orange) cells at the endpoint of the experiment (week 22) as measured by the level of bioluminescence normalized to week 0. (e) Kaplan-Meier survival graphs of NSG mice injected with 100,000 NS control (black) or SPDEF KD (orange) cells. Mice were scored to be dead upon 100-fold increase in luminescence. Log-rank (Mantel-Cox) test. ** $p < 0.01$. Mann-Whitney test. NS = non-silencing, KD = knockdown.

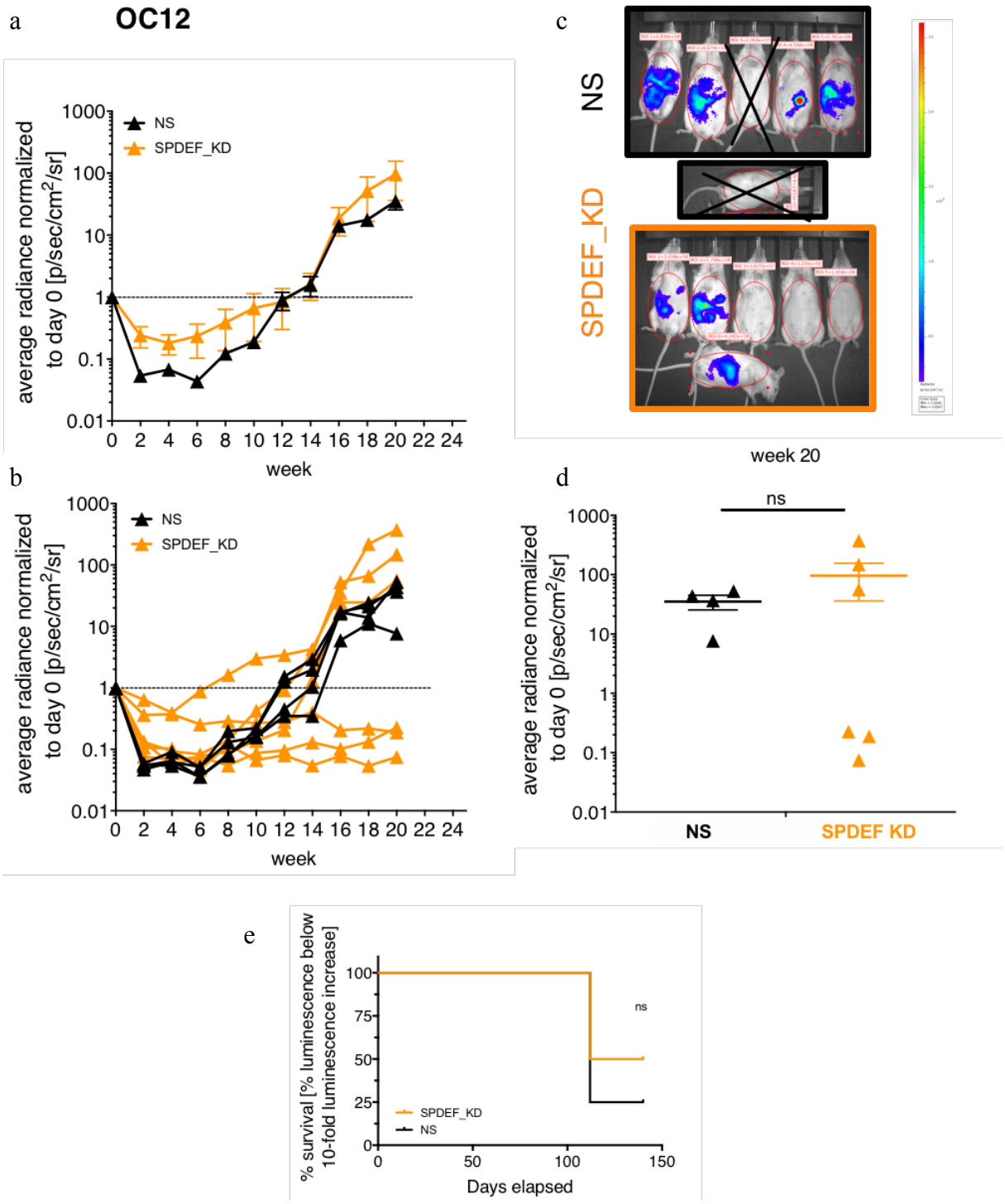

Figure 46: SPDEF knockdown does not impede tumor growth *in vivo* (OC12).
Growth curves of SPDEF knockdown (orange) and non-silencing control (black) OC12 cells (a) which have been i.p. injected into NSG mice and which were before lentivirally transduced with a luciferase vector in order to follow tumor growth via bioluminescence. In a, the mean ± SEM of the average radiance is shown, in b, the growth curves of the tumor cells for each single mouse are depicted. The dashed line denotes the baseline at week 0. (c) Images of the *in vivo* bioluminescent signal in mice injected with SPDEF knockdown

(orange) and non-silencing control (black) OC12 cells at the endpoint at week 20. n = 4 (NS) or 6 mice per group (SPDEF knockdown). Mice number 3 and 6 were excluded in the analysis due to no signal at the initial time point. (d) Tumor burden of mice injected intraperitoneally with NS control (black) and SPDEF KD (orange) cells at the endpoint of the experiment (week 20) as measured by the level of bioluminescence normalized to week 0. (e) Kaplan-Meier survival graphs of NSG mice injected with 10,000 NS control (black) or SPDEF KD (orange) cells. Mice were scored to be dead upon 10-fold increase in luminescence. Log-rank (Mantel-Cox) test ** $p < 0.01$. Mann-Whitney test. NS = non-silencing, KD = knockdown.

4.4.9 SPDEF overexpression leads to more tumors, ascites and metastases

Since knockdown of SPDEF impaired tumor growth *in vivo* in OC20 cells, we wondered whether overexpression of SPDEF increased the tumorigenic potential.

Thus, we injected OC20 SPDEF overexpressing und iT2 control cells intraperitoneally into NSG mice. Five out of six mice injected with SPDEF overexpressing cells developed tumor cell-containing ascites as compared to one in six from the iT2 control group. Regarding tumor formation, also no tumors were detected in the iT2 control group as compared to four out of six tumors in the SPDEF overexpressing group. Metastatic loci were found exclusively in mice injected with SPDEF overexpressing cells at organs such as the uterus, liver, spleen and stomach/colon. Since the luciferase signal was not detectable in these cells, tumor growth could not be monitored over time.

In sum, we could show that SPDEF overexpression increased tumor and ascites formation of OC cells.

Table 15: Tumor formation and development of ascites in NSG mice injected with OC20 SPDEF OX and iT2 control cells.
100,000 either iT2 control or SPDEF overexpressing cells were intraperitoneally injected into mice and tumor growth, ascites, as well as metastasis development were evaluated.

		ascites	tumors	metastases	location of metastases
OC20	IT2	1/6	0/6	0/6	-
	SPDEF OX	5/6	4/6	3/6	uterus, liver, spleen, stomach/colon

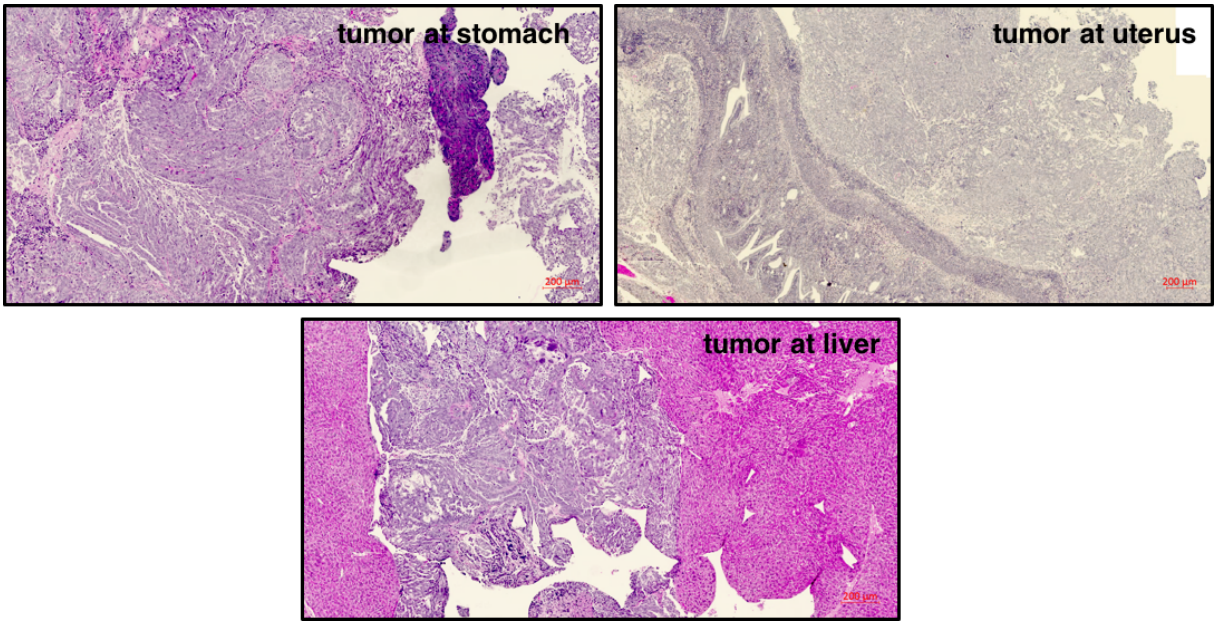

Figure 47: SPDEF overexpressing cells form tumors/metastases at various organs.
H&E stainings of stomach, liver and uterus, as well as tumors at these organs taken out from mice injected intraperitoneally with OC20 SPDEF OX cells.

4.4.10 SPDEF overexpression increases clonogenicity more in SSEA1$^-$ than SSEA1$^+$ cells

Previous observations showed that SPDEF overexpressing cells form more and SPDEF knockdown cells form less colonies. Since SPDEF was enriched in the SSEA1$^-$ cells, we wondered whether we can increase colony number of SSEA1$^+$ cells by inducing expression of SPDEF in these, thereby rescuing the phenotype of the SSEA1$^+$ cells. At the same time, we wanted to ascertain whether knockdown of SPDEF in the SSEA1$^-$ cells decreases their colony-forming capacity.

In order to determine the clonogenic potential of SSEA1$^+$ and SSEA1$^-$ cells possessing either knockdown or overexpression of SPDEF, we FACS-sorted SSEA1$^+$ and SSEA1$^-$ cells within the SPDEF overexpressing and knockdown, as well as iT2 and NS control cells and seeded them in equal numbers in 24-well plates *in vitro* in order to evaluate colony formation.

SPDEF overexpression enabled SSEA1$^-$ but also SSEA1$^+$ cells to form more and bigger colonies than the SSEA1$^-$ and SSEA1$^+$ cells of the iT2 control cell line (figure 48 a, c, e). Overexpression of SPDEF in SSEA1$^+$ cells increased the colony number to an even higher number than in iT2 SSEA1$^-$ cells.

However, overexpression of SPDEF allowed the growth of more colonies in SSEA1$^-$ cells than in SSEA1$^+$ (5-fold more colonies in SSEA1$^-$ SPDEF overexpressing compared to iT2

SSEA1$^-$ control versus 3-fold more colonies in SSEA1$^+$ SPDEF overexpressing cells as compared to iT2 SSEA1$^+$ control, figure 48 g).

Further, doxycycline-induced knockdown of SPDEF also decreased the number and size of colonies in both SSEA1$^-$ and SSEA1$^+$ cells (figure 48 b, d, f). Colony number of SSEA1$^-$ SPDEF KD cells could nearly be decreased to the level of control SSEA1$^+$ cells (figure 48 b).

Taken together, we could show that we can rescue the colony-forming ability of SSEA1$^+$ cells by overexpressing SPDEF in these and in turn, decrease colony formation in SSEA1$^-$ cells by knocking down SPDEF. In total, we could show that SPDEF expression is responsible for mediating clonogenicity in ovarian cancer cells.

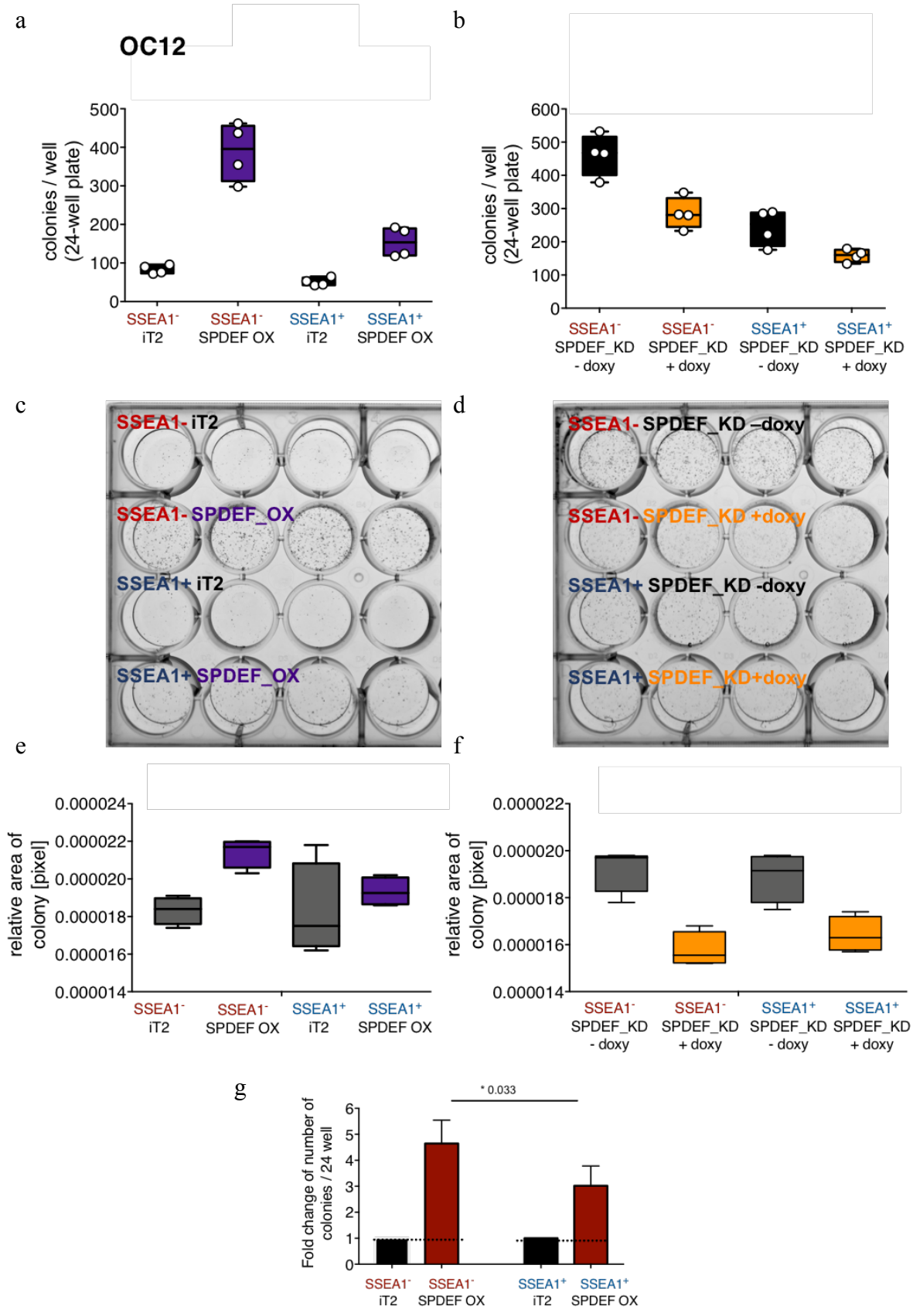
a
OC12
colonies / well (24-well plate)
SSEA1- iT2
SSEA1- SPDEF OX
SSEA1+ iT2
SSEA1+ SPDEF OX
b
colonies / well (24-well plate)
SSEA1- SPDEF_KD - doxy
SSEA1- SPDEF_KD + doxy
SSEA1+ SPDEF_KD - doxy
SSEA1+ SPDEF_KD + doxy
c
SSEA1- iT2
SSEA1- SPDEF_OX
SSEA1+ iT2
SSEA1+ SPDEF_OX
d
SSEA1- SPDEF_KD –doxy
SSEA1- SPDEF_KD +doxy
SSEA1+ SPDEF_KD -doxy
SSEA1+ SPDEF_KD+doxy
e
relative area of colony [pixel]
f
relative area of colony [pixel]
g
* 0.033
Fold change of number of colonies / 24 well

Figure 48: Overexpression of SPDEF rescues clonogenicity of SSEA1$^+$ cells and knockdown of SPDEF in SSEA1$^-$ cells decreases it to the level of SSEA1$^+$ cells.
(a, b) Colony number of OC12 SPDEF OX (purple) or SPDEF KD +doxycycline (orange) and iT2 control or SPDEF KD without doxycycline (black) in SSEA1$^-$ (red) and SSEA1$^+$ (blue) cells. (c, d) Image of the colonies formed by OC12 SPDEF OX (purple) or SPDEF KD +doxycycline (orange) and iT2 control or SPDEF KD without doxycycline (black) within SSEA1$^-$ (red) and SSEA1$^+$ (blue) cells cultured in 24-well PRIMARIA plates. For the OC12 cell line, 800 cells were seeded per 24-well and cultured for 7 days, respectively. (e, f) Relative area of colonies of the respective cell populations as quantified by Fiji. (g) Fold change of colony number of SPDEF overexpressing cells compared to iT2 in SSEA1$^-$ and SSEA1$^+$ cells, respectively. Mean ± SD. Box and whisker plot, min to max. n = 3 technical replicates. * $p < 0.05$, unpaired, parametric, two-tailed t-test. iT2 = IRES-tdtomato, KD = knockdown, OX = overexpression.

4.4.11 SPDEF overexpression within SSEA1$^-$ cells endows them with an initial growth advantage *in vivo* and further increases long-term tumorigenicity

In order to assess whether SPDEF overexpression can also boost tumor growth in SSEA1$^-$ cells *in vivo*, we injected OC12 SPDEF OX SSEA1$^-$ and OC12 iT2 SSEA1$^-$ control cells into mice and monitored initial survival and growth as well as long-term tumor outgrowth. Assessing the initial ability of the cells to cope with the new environment upon intraperitoneal injection mimics the step of metastasis in mice, and thus, allowed us to collect information about the metastatic capacities of these cells.

SPDEF overexpressing SSEA1$^-$ cells survived better during the first 168 h (7 days) as compared to iT2 SSEA1$^-$ cells (figure 49). The signal of the SPDEF overexpressing cells did not decrease but instead rather increased after the initial injection step. The signal of the control iT2 SSEA1$^-$ cells, however, quickly decreased and stayed at a lower level than the baseline at 0 h.

Long-term monitoring of these cell populations in the mice showed that again the SSEA1$^-$ SPDEF OX cells grew but not the iT2 control cells (figure 49).

To sum up, we could show that overexpression of SPDEF in SSEA1$^-$ cells further increases *in* vivo tumorigenicity. The SPDEF OX cells have an initial but also long-term growth advantage.

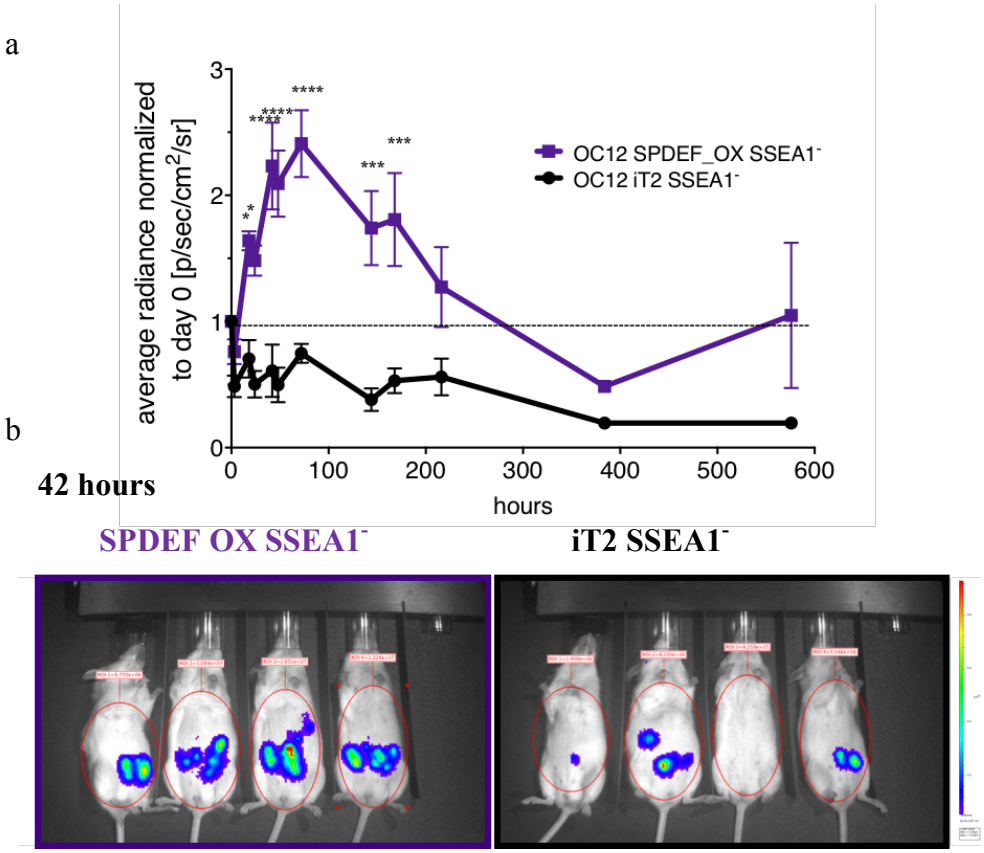

Figure 49: Overexpression of SPDEF within the SSEA1⁻ cells provides them with an initial growth advantage upon transplantation into NSG mice.
(a) Growth curve of SPDEF overexpressing (purple) and iT2 control (black) cells within FACS-sorted SSEA1⁻ OC12 cells that have been i.p. injected into NSG mice and which were before lentivirally transduced with a luciferase vector in order to follow tumor growth via bioluminescence. Mean ± SEM of the average radiance is shown. The dashed line denotes the baseline at 0 hours. (b) Images of the *in vivo* bioluminescent signal in mice injected with SPDEF overexpressing (purple) and iT2 control (black) OC12 cells at 42 hours. n = 4 mice per group. ** $p < 0.01$, *** $p < 0.001$, **** $p < 0.0001$. Mann-Whitney test. iT2 = IRES-tdtomato 2, OX = overexpression.

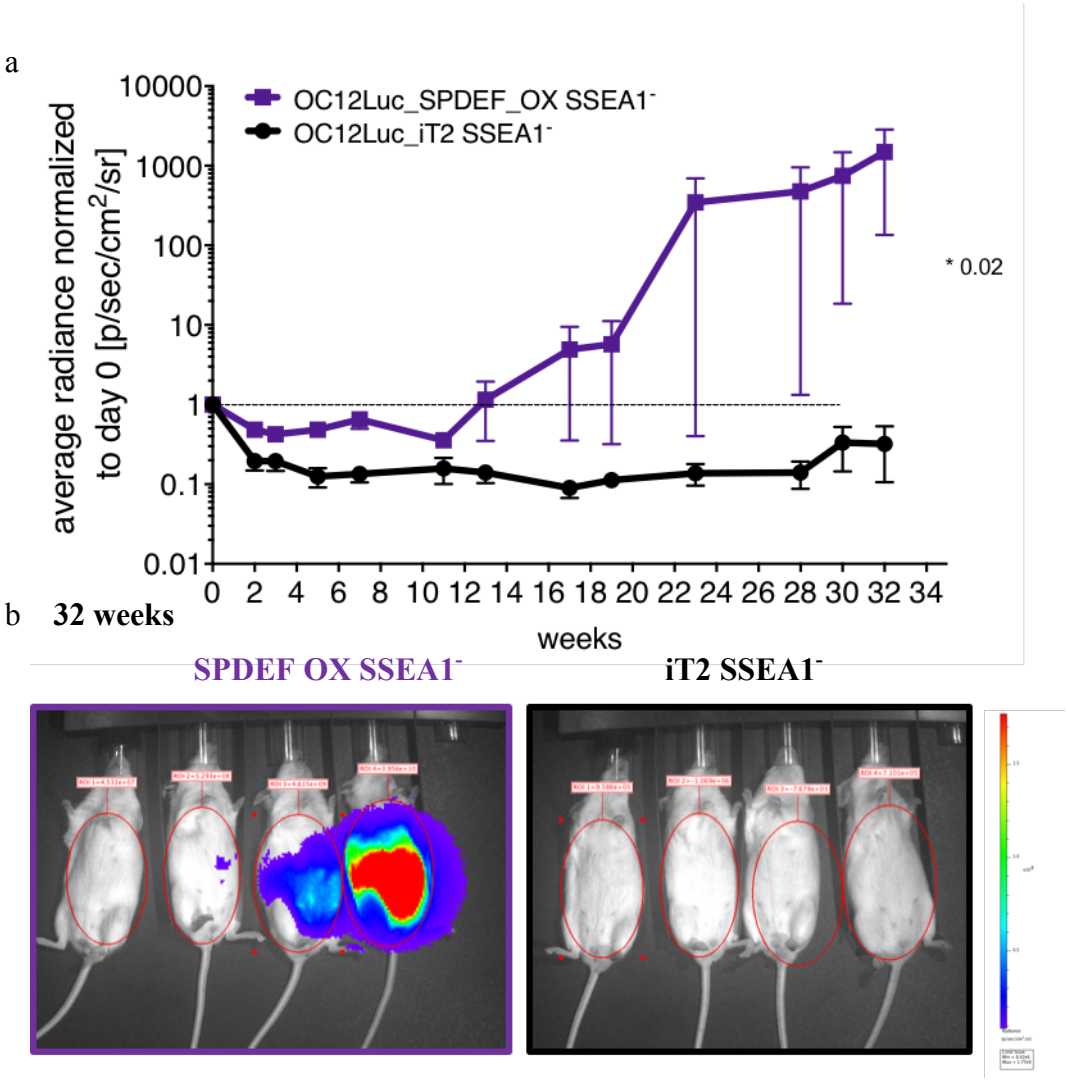

Figure 50: Overexpression of SPDEF increases tumorigenicity of SSEA1⁻ cells *in vivo*.
(a) Growth curve of SPDEF overexpressing (purple) and iT2 control (black) cells within FACS-sorted SSEA1⁻ OC12 cells that have been i.p. injected into NSG mice and which were before lentivirally transduced with a luciferase vector in order to follow tumor growth via bioluminescence. Mean ± SEM of the average radiance is shown. The dashed line denotes the baseline at 0 hours. (b) Images of the *in vivo* bioluminescent signal in mice injected with SPDEF overexpressing (purple) and iT2 control (black) OC12 cells at week 24. n = 4 mice per group. * $p < 0.05$. Mann-Whitney test. iT2 = IRES-tdtomato 2, OX = overexpression.

4.4.12 Overexpression of SPDEF induces more tumors both in SSEA1$^-$ and SSEA1$^+$ cells

Previous observations had shown that SPDEF overexpression in SSEA1$^-$ cells renders tumor cells more metastatic. To further validate this finding, we performed *in vivo* experiments in a second OC line and in addition, overexpressed SPDEF in the SSEA1$^+$ cells in order to analyze whether it rescues their less tumorigenic phenotype and renders them more aggressive.

Since luciferase was lost in these cells, we could only assess tumor formation at the end of the experiment. And indeed, SSEA1$^+$ cells overexpressing SPDEF formed more tumors than SSEA1$^+$ iT2 control cells (table 16). Hence, SPDEF overexpression rescued tumorigenicity of SSEA1$^+$ cells. SSEA1$^-$ SPDEF OX cells also formed more tumors than SSEA1$^-$ iT2 control cells.

Taken together, we could show that SPDEF overexpression increases tumor formation i*n vivo* both in SSEA1$^-$, as well as SSEA1$^+$ cells.

Table 16: Tumor formation in NSG mice injected with OC20 SSEA1$^-$ / SSEA1$^+$ SPDEF OX and iT2 control cells.
100,000 either iT2 control or SPDEF overexpressing, FACS-sorted OC20 SSEA1$^-$ or SSEA1$^+$ cells were intraperitoneally injected into mice and tumor development was evaluated. P-Values were calculated with the ELDA limiting dilution tool (Hu *et al.,* 2009).

mouse group	tumors	p-value
OC20 IT2 SSEA1+	1/3	
		0.05
OC20 SPDEF OX SSEA1$^+$	3/3	
OC20 iT2 SSEA1$^-$	0/3	
		** 0.009
OC20 SPDEF_OX SSEA1-	2/2	

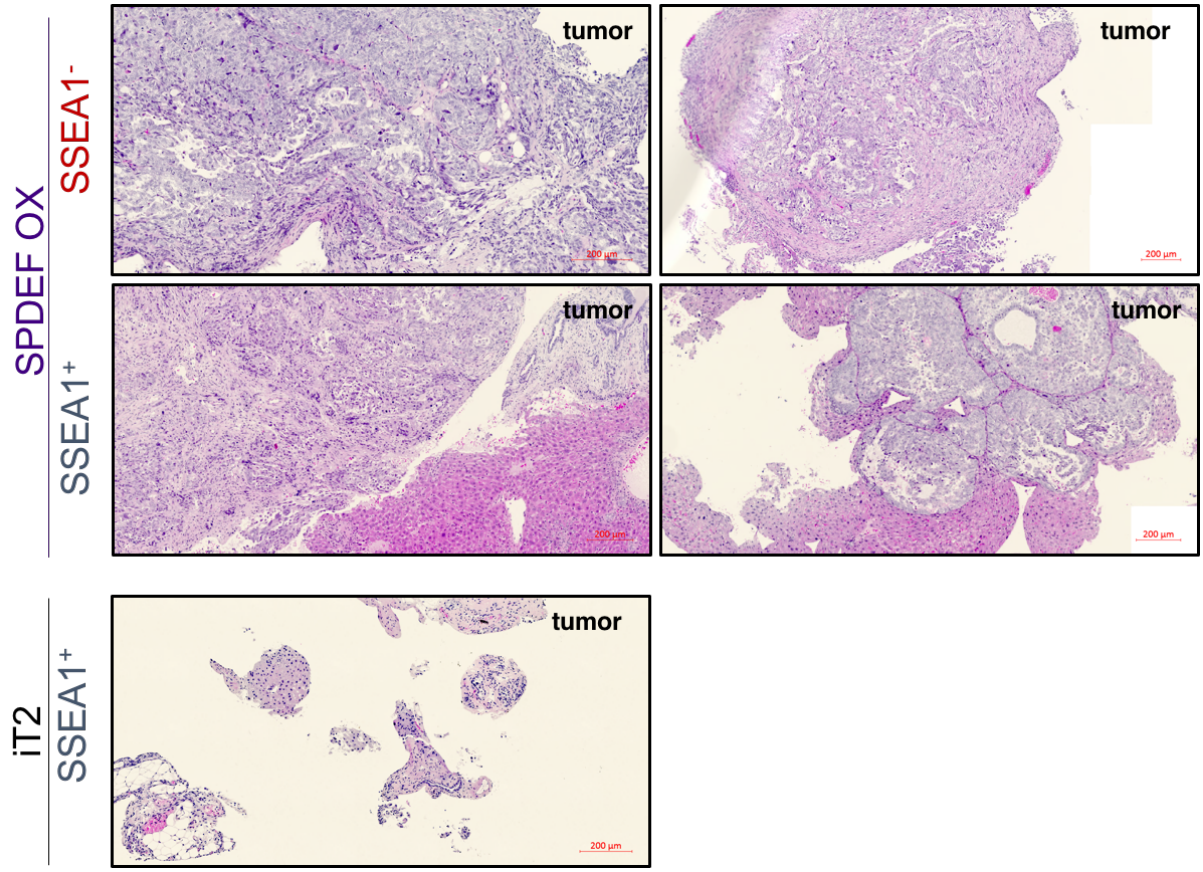

Figure 51: SPDEF overexpresssion induces tumor formation in SSEA1$^+$ and SSEA1$^-$ cells.
H&E stainings of tumors taken out from mice injected intraperitoneally with OC20 SPDEF OX SSEA1$^+$ and SSEA1$^-$ cells (a) as well as iT2 SSEA1$^+$ cells (b).

4.4.13 SPDEF correlates with ESR1 expression and is enriched in ESR1^{high} tumors

Since ovarian cancer is known to be an estrogen-driven cancer (Rao and Slotman 1991, Spillman *et al.,* 2010) we wondered whether there is a link between estrogen receptor and SPDEF expression.

The analysis of ESR1 and SPDEF gene expression with data from the TCGA dataset revealed that ESR1 and SPDEF correlated (figure 52 a). Further, SPDEF was significantly enriched in high grade serous ovarian cancer tumor samples of the TCGA dataset classified to be ESR1^{high} (split according to mean ESR1 expression) as compared to ESR1^{low} tumors (figure 52 b). Finally, ESR1 was more enriched in SSEA1$^-$ samples (and thus SPDEF high expressing ones) of OC15, OC19 and OC20 as compared to SSEA1$^+$ cells (figure 52 c). Only in OC12 SSEA1$^-$ cells, ESR1 was not enriched.

Taken together, we could identify a correlation between ESR1 expression and SPDEF. SPDEF was further significantly enriched in ESR1^{high} ovarian tumors.

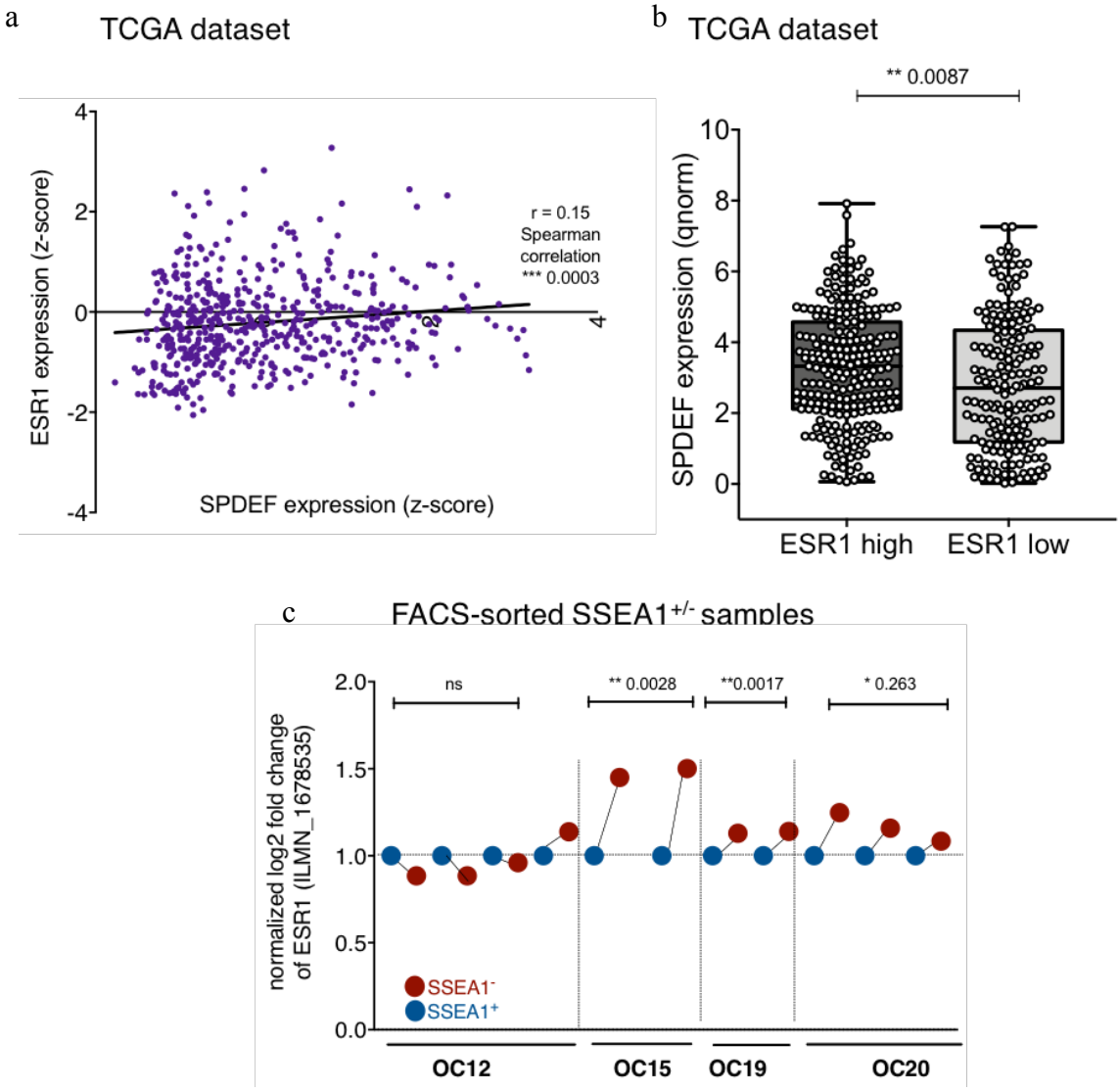

Figure 52: SPDEF is enriched in ESR1^{high} tumors.
(a) SPDEF correlates with ESR1 expression in bulk high grade serous ovarian cancer samples of the TCGA dataset. Spearman correlation. (b) SPDEF is enriched in ESR1^{high} serous ovarian cancer tumors of the TCGA dataset which were allocated to be either ESR1^{high} or low by splitting the groups according to mean ESR1 expression. (c) ESR1 expression is enriched in SSEA1^{-} (and thus SPDEF high) OC15, OC19 and OC20 cells. * $p < 0.01$, ** $p < 0.001$, *** $p < 0.0001$, ns = not significnt.

4.4.14 Gene expression profiling reveals differentially expressed genes between SPDEF overexpressing and iT2 control cells, as well as between SPDEF KD and NS control cells

SPDEF overexpression showed a strong phenotype concerning increased tumorigenicity. To analyze underlying molecular differences, we performed gene expression profiling of SPDEF overexpressing and iT2 control cells, as well as of SPDEF knockdown and NS control cells by using the Illumina HT12v4 bead Chip technology.

Bioinformatic analyses revealed many differentially regulated genes between OC12/OC20 SPDEF OX and iT2 (figure 53 a, table 17) and SPDEF KD and NS cells (figure 53 b, table 17). To further narrow down the number of differentially regulated genes, we analyzed which genes are differentially upregulated in SPDEF OX samples when comparing iT2 and SPDEF OX cells in both OC12 and OC20 cell lines, as well as genes at the same time also downregulated in SPDEF knockdown samples when comparing SPDEF KD versus NS control cells (figure 54). In addition, the signature includes the genes downregulated in SPDEF OX samples when comparing iT2 and SPDEF OX cells and simultaneously upregulated in SPDEF knockdown samples when comparing SPDEF knockdown versus NS control cells. Thus, our bioinformatic analyzes narrowed down the genes differentially regulated to a 144-gene signature which included the gene Forkhead Box A2 (FOXA2) that was enriched in iT2 and SPDEF KD samples of OC12/OC20.

Table 17: Differentially expressed genes between OC12/OC20 SPDEF OX vs. iT2 and SPDEF KD vs. NS cells, respectively. BH = Benjamini-Hochberg, FDR = False discovery rate

testing method for differentially expressed genes	number of genes OC12/OC20 SPDEF_OX vs. iT2	number of genes OC12/ OC20 SPDEF_KD vs. NS
FDR < 0.05, BH	1044	289
p-value < 0.01, none	1857	1418

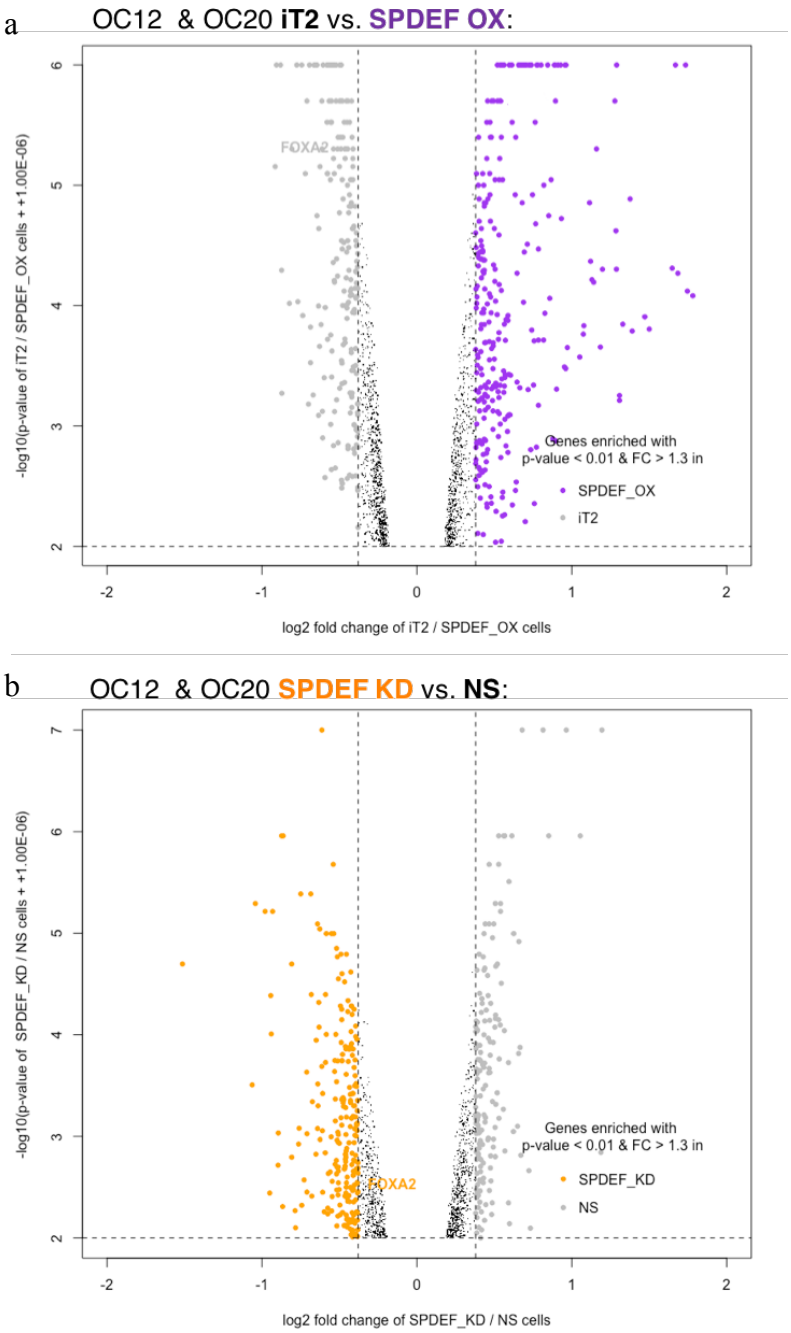

Figure 53: Volcano plot of differentially enriched genes between iT2 and SPDEF OX cells, as well as between SPDEF KD and NS cells.
(a) Genes differentially enriched in SPDEF OX vs. iT2 cells with a p-value > 0.01. Genes enriched with a fold change > 1.3 are labeled in purple (SPDEF OX) or grey (iT2). The differential enrichment of FOXA2 in the iT2 cells is additionally marked. (b) Genes differentially enriched in SPDEF KD vs. NS cells with a p-value > 0.01. Genes enriched with a fold change > 1.3 are labeled in orange (SPDEF KD) or grey (NS). The differential enrichment of FOXA2 in the SPDEF KD cells is additionally marked.

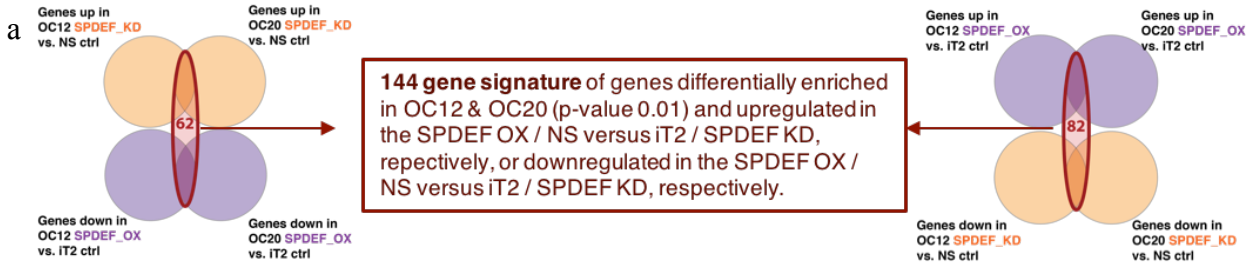
a
Genes up in OC12 SPDEF_KD vs. NS ctrl
Genes up in OC20 SPDEF_KD vs. NS ctrl
62
Genes down in OC12 SPDEF_OX vs. iT2 ctrl
Genes down in OC20 SPDEF_OX vs. iT2 ctrl
144 gene signature of genes differentially enriched in OC12 & OC20 (p-value 0.01) and upregulated in the SPDEF OX / NS versus iT2 / SPDEF KD, repectively, or downregulated in the SPDEF OX / NS versus iT2 / SPDEF KD, respectively.
Genes up in OC12 SPDEF_OX vs. iT2 ctrl
Genes up in OC20 SPDEF_OX vs. iT2 ctrl
82
Genes down in OC12 SPDEF_KD vs. NS ctrl
Genes down in OC20 SPDEF_KD vs. NS ctrl

b

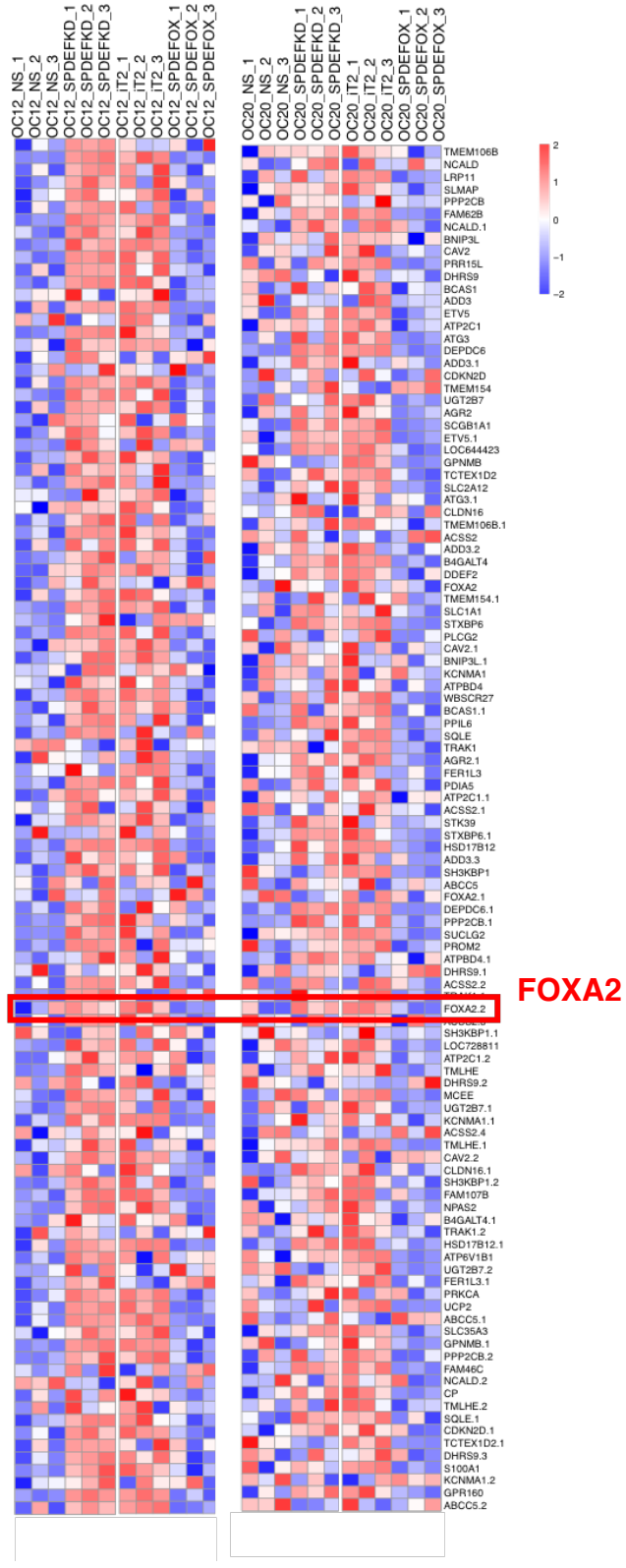
OC12_NS_1
OC12_NS_2
OC12_NS_3
OC12_SPDEFKD_1
OC12_SPDEFKD_2
OC12_SPDEFKD_3
OC12_iT2_1
OC12_iT2_2
OC12_iT2_3
OC12_SPDEFOX_1
OC12_SPDEFOX_2
OC12_SPDEFOX_3
OC20_NS_1
OC20_NS_2
OC20_NS_3
OC20_SPDEFKD_1
OC20_SPDEFKD_2
OC20_SPDEFKD_3
OC20_iT2_1
OC20_iT2_2
OC20_iT2_3
OC20_SPDEFOX_1
OC20_SPDEFOX_2
OC20_SPDEFOX_3
FOXA2

Figure 54: Heatmaps of genes differentially enriched in SPDEF KD or iT2 OC12 and OC20 cells.
(a) Scheme of how the 144-gene signature of differentially enriched genes in OC12/OC20 SPDEF OX vs. iT2 and SPDEF KD vs. NS was generated. The full signature is given in Supplementary figure 1. (b) Genes enriched in SPDEF KD and iT2 samples of OC12/OC20 (SPDEF low samples) when comparing SPDEF KD vs. NS or SPDEF OX vs. iT2 cells. FOXA2 is marked by a red box. red = enriched genes, blue = deriched genes.

Besides enrichment of FOXA2 in the iT2 and SPDEF KD samples, GSEA identified the gene set "BOCHKIS_FOXA2_TARGETS" to be enriched in the SPDEF KD cells compared to NS cells (figure 55) in OC12 and OC20 cells.

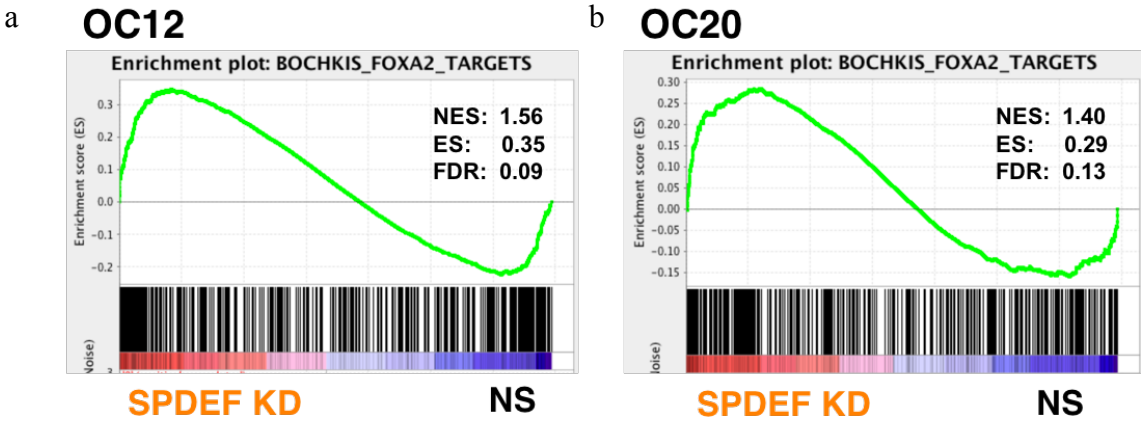

Figure 55: Gene set enrichment plots enriched in SPDEF KD cells of OC12 and OC20.
(a) Gene set enrichment plots "Bochkis_FOXA2_targets" enriched in SPDEF KD cells of OC12 and (b) OC20 cells.ES = enrichment score, FDR = False discovery rate, NES = normalized enrichment score.

According to GSEA, gene sets related to TGF-β signaling, Wnt-signaling, epithelial-to-mesenchymal transition and estrogen response were further enriched in SPDEF OX cells of OC12/OC20 cells. In the SPDEF KD and iT2 cells, gene sets related to fatty acid metabolism, cholesterol homeostasis, glycolysis and oxidative phosphorylation were enriched (figure 56, figure 57).

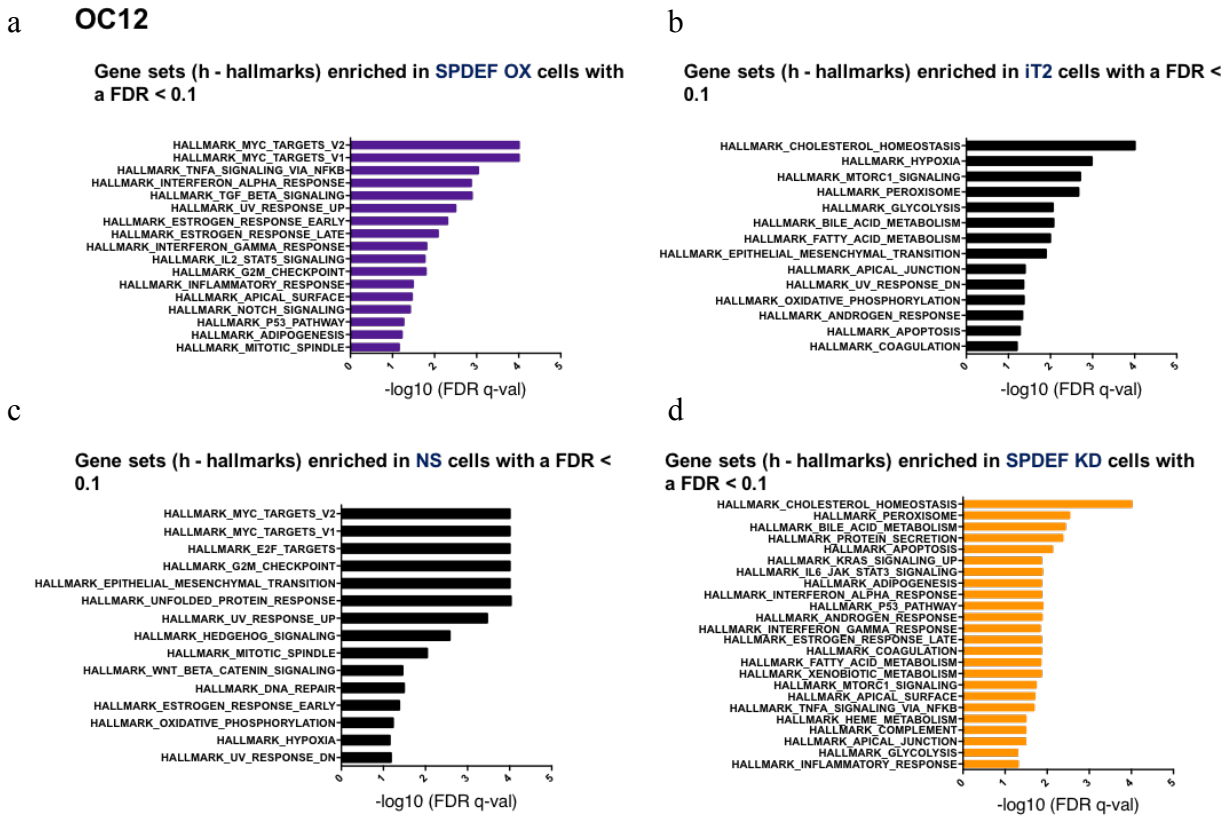

Figure 56: Hallmark gene sets derived from GSEA which are enriched in SPDEF overexpression, knockdown and respective iT2 and NS control cells in OC12.
(a) Hallmark gene sets which are enriched with a FDR < 0.1 in SPDEF OX (purple) and (b) iT2 (black), when comparing SPDEF OX vs. iT2, and which are enriched in (c) NS (black) and (d) SPDEF KD (orange) cells, when comparing SPDEF KD vs. NS.

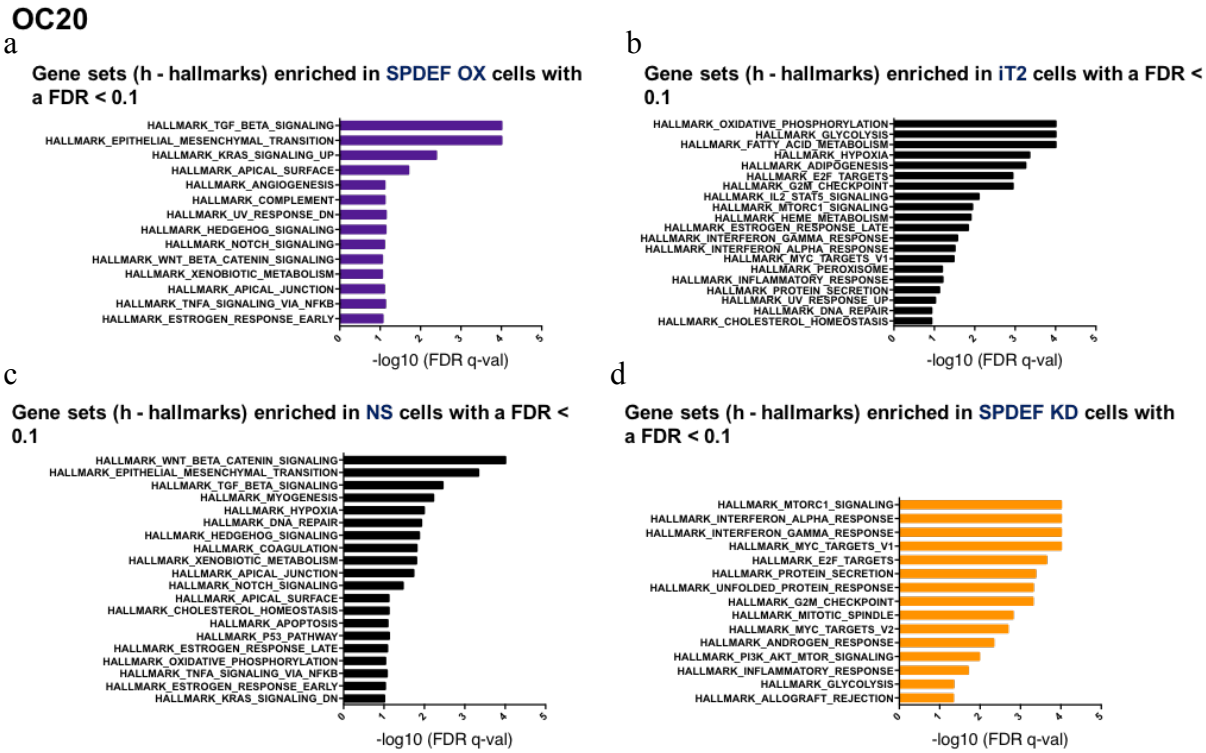

Figure 57: Hallmark gene sets derived from GSEA which are enriched in SPDEF overexpression, knockdown and respective iT2 and NS control cells in OC20.
(a) Hallmark gene sets which are enriched with a FDR < 0.1 in SPDEF OX (purple), and (b) iT2 (black), when comparing SPDEF OX vs. iT2, and which are enriched in (c) NS (black) and (d) SPDEF KD (orange) cells, when comparing SPDEF KD vs. NS.

In order to verify the data obtained from the microarray, we performed qPCR analyses of genes predicted to be differentially enriched between SPDEF OX and iT2, as well as SPDEF KD and NS samples. Quantitative PCR analyses of the selected genes RARRES1, EEF1A2, HIF1α, MUC1, YIPF1 and LRP3 verified their enrichment in the SPDEF overexpressing cells. SREBF1 and HMGCR were shown to be enriched in the SPDEF KD cells (figure 58).

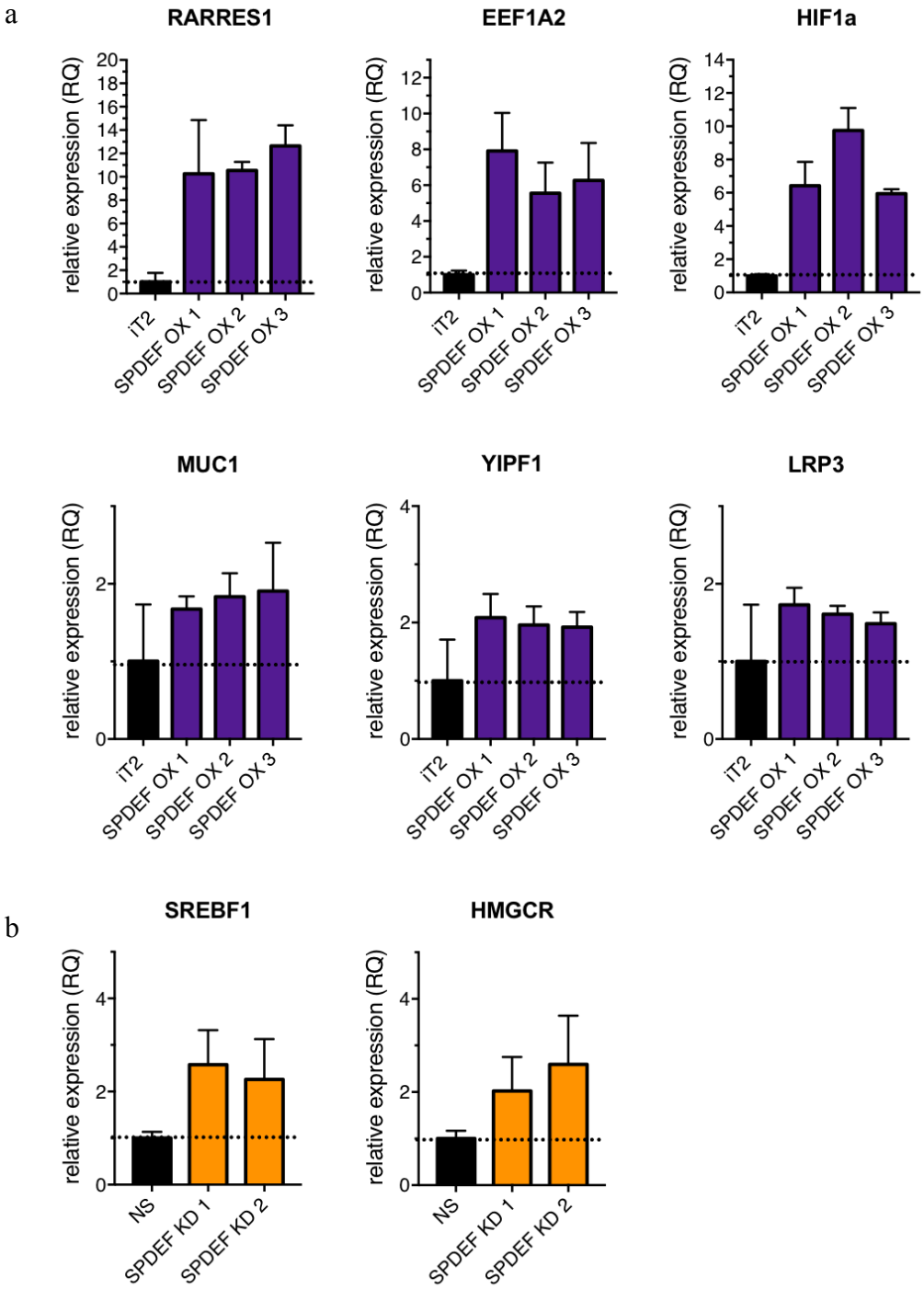

Figure 58: mRNA expression of SPDEF target genes.
Expression of mRNA of SPDEF target genes in the OC12 cell line as predicted by the Illumina HT12v4 microarray was verified via qPCR. (a) Expression of genes predicted to be induced in the SPDEF overexpressing (purple) cell lines as compared to iT2 control (black). (b) Expression of genes predicted to be induced in the SPDEF knockdown (orange) cell lines as compared to NS control (black).

4.4.15 A 15-gene signature derived from the SPDEF overexpressing cells predicts worse overall survival in patients

To analyze whether the expression of the target genes of SPDEF has a predictive value regarding overall survival of HGSOC patients, a gene signature from the top 15 differentially expressed genes between OC12 iT2 and SPDEF OX samples (SLC16A9, HES4, RAB31, LRP3, EEF1A2, BAIAP2L2, UNC5A, RNF39, CRYAB, YIPF1, TSPAN9, PTGER2, RAP1GAP, MLPH, RARRES1) was calculated. Therefore, the z-score expression for these genes over all patients from the TCGA dataset (n = 420 patients) was evaluated and then, the sum over all genes calculated. The lower 25 % and the upper 75 % quantile of the sum of the z-scores was assigned to either death (1) or alive (0) events and a Kaplan-Meier curve calculated.

Overall survival for patients displaying a high expression of the 15-gene SPDEF target gene signature was significantly lower than that of patients displaying lower expression (p = 0.0325, HR = 0.67, CI = 0.46 – 0.97) of the 15 genes (figure 59). Median overall survival of patients expressing low levels of SPDEF target genes was 1329 days versus 1213 days of patients expressing higher levels.

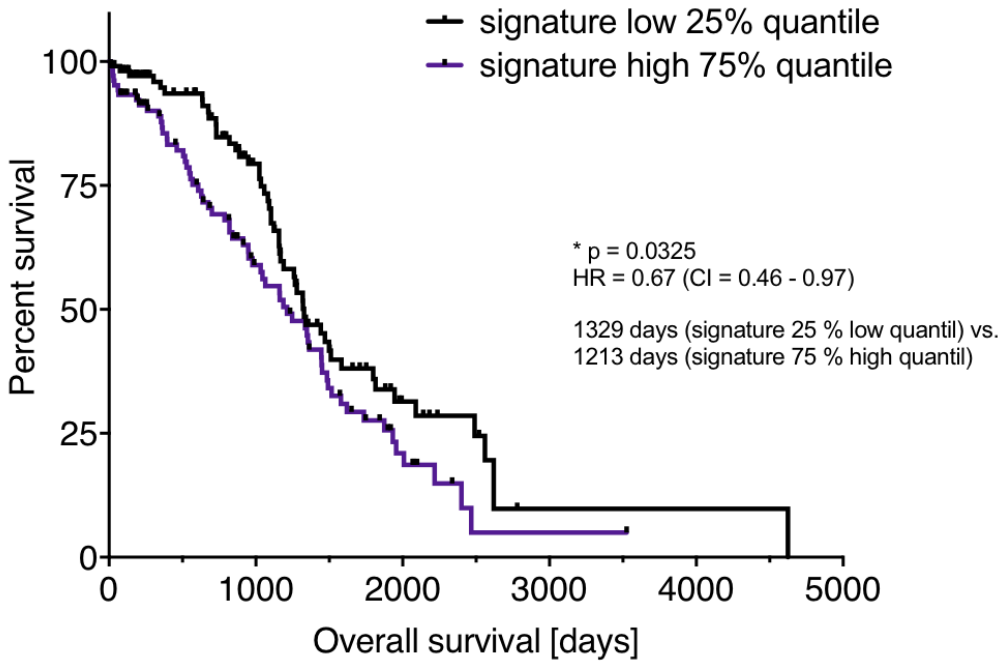

Figure 59: Overall survival of HGSOC patients according to a 15-gene signature derived from the OC12 SPDEF overexpressing gene expression analyses.
Log-rank (Mantel-Cox) test. CI = confidence intervall, HR = hazard ratio.

4.4.16 The 15-gene SPDEF target gene signature is enriched in SSEA1$^-$ cells

To verify whether the 15-gene SPDEF target gene signature is also enriched in SSEA1$^-$ or SSEA1$^+$ cells of the patients, we performed GSEA analyses. Therefore, we analyzed in which cell population the 15-gene SPDEF target gene signature is enriched in either a pooled analysis of OC12, OC15, OC19 and OC20 cells or in single analyses of these OC cells.

The 15-gene signature derived from the SPDEF target genes was highly enriched in the SSEA1$^-$ cells of the OC patients when performing the pooled analysis (figure 60 a). Also, we could verify that in 3 out of 4 patients the signature was also enriched in the SSEA1$^-$ cells when performing the single OC line GSEA analyses (figure 60 b). As expected, the signature was most strongly enriched in OC12 cells, the cell line from which the 15-gene SPDEF target gene signature was generated (figure 60 b).

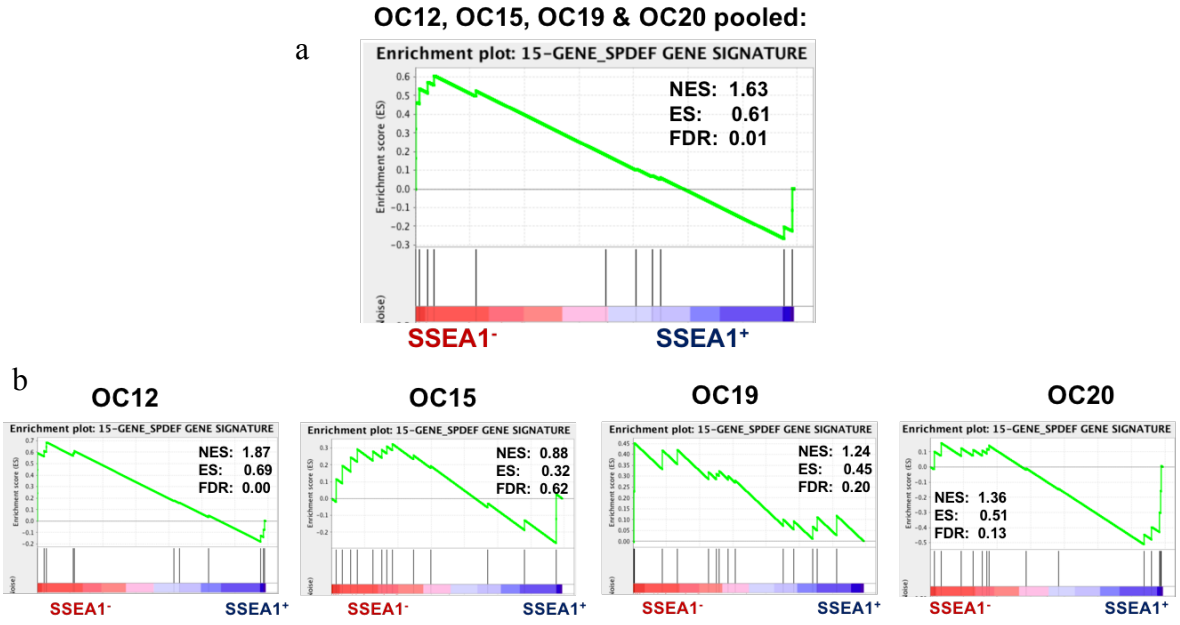

Figure 60: Enrichment of the 15-gene SPDEF target gene signature in SSEA1$^-$ cells according to GSEA.
(a) Gene set of the 15-gene SPDEF target gene signature enriched in SSEA1$^-$ cells in a pooled GSEA analysis of OC12, 15, 19 and 20. (b) Single gene sets of the GSEA analyses of the 15-gene SPDEF target gene signature in OC12, OC15, OC19 or OC20.

4.5 FOXA2 is enriched in the SPDEF knockdown cells and impairs tumor growth

4.5.1 FOXA2 is enriched in the SPDEF knockdown population

We identified FOXA2 to be enriched in the SPDEF knockdown cells when comparing SPDEF KD vs. NS control, as well as in the iT2 control cells when comparing SPDEF OX vs. iT2 control cells (figure 53, figure 54). Further, a FOXA2 target gene set was predicted by GSEA to be also enriched in the SPDEF KD cells (figure 55). Since FOXA2 expression has been described to be a tumor suppressive gene in various cancers (Vorvis *et al.,* 2016, Ding *et al.,* 2017, Li *et al.,* 2017), we wondered whether the increased expression of FOXA2 in SPDEF knockdown cells compared to SPDEF overexpressing ones contributes to the phenotype of impaired *in vivo* growth and colony formation potential in HGSOC.

In both the OC12 and OC20 cell lines engineered for SPDEF overexpression or knockdown, FOXA2 expression was decreased in the SPDEF overexpressing cells as compared to iT2 control ones. (figure 61 a). Beyond, doxycycline-induced SPDEF knockdown cells displayed increased FOXA2 expression in OC cells (figure 61 a). For OC12, this could further be verified via qPCR and on protein level (figure 61 b, c and d).

In sum, SPDEF expression is inversely correlated to FOXA2 expression.

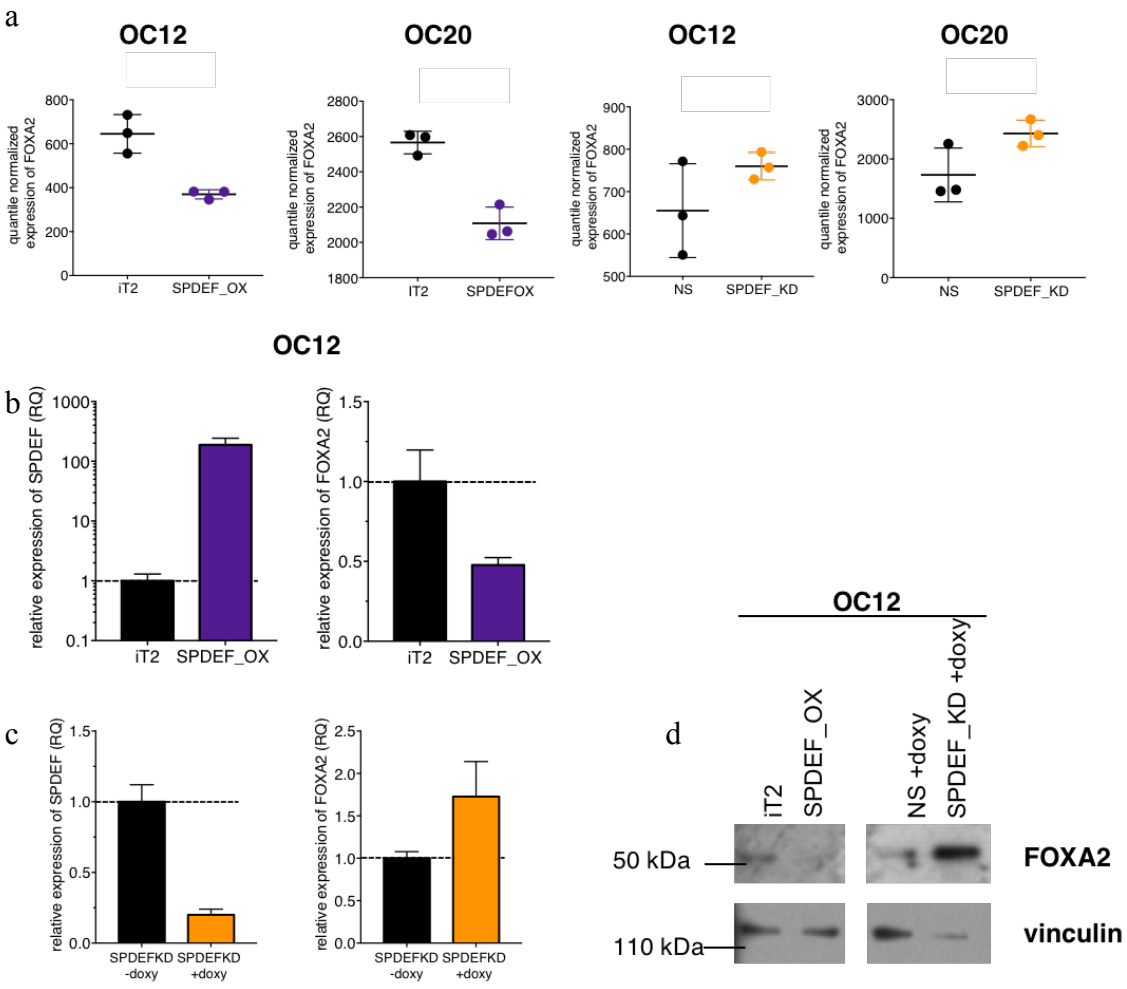

Figure 61: FOXA2 is enriched in the SPDEF knockdown and decreased in the SPDEF overexpressing cells.
(a) Quantile normalized expression of the Illumina probe ILMN_1668052 which is assigned to the FOXA2 gene in SPDEF overexpressing (purple) and SPDEF knockdown (orange) and iT2 and NS control cells, respectively, in OC12 and OC20 cell lines. (b) SPDEF and FOXA2 expression as measured by qRT-PCR in SPDEF overexpressing (purple) and doxycycline-induced SPDEF knockdown (orange) OC12 cells (c). (d) Western blot depicting FOXA2 expression in OC12 SPDEF overexpressing and knockdown, as well as in iT2 and NS control cells. Vinculin was used as a loading control.

4.5.2 FOXA2 can be overexpressed and knocked down in OC cells

In order to prove that FOXA2 expression is indeed functional, we generated doxycycline-inducible FOXA2 knockdown and stable, as well as inducible FOXA2 overexpression cell lines.

FOXA2 could efficiently be knocked down by the combination of two shRNAs and also inducibly overexpressed as verified by qPCR and WB (figure 62).

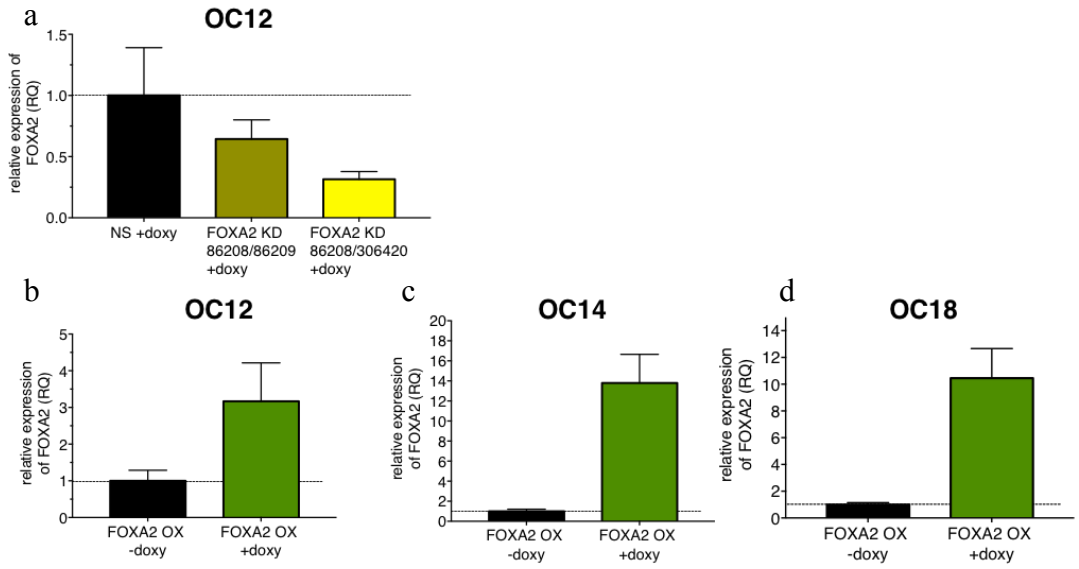

Figure 62: FOXA2 can be upregulated and downregulated by inducible doxycycline-induced overexpression and knockdown, respectively.
FOXA2 expression as measured by qRT-PCR in OC12 cells (a) in either the NS control (black, +doxy) or the two FOXA2 KD cell lines transduced with shRNAS 86208/86209 or 86208/306420 (ochre and yellow, +doxy). (b-d) FOXA2 expression measured by qRT-PCR in the doxycycline-induced FOXA2 overexpressing cell line (green) and the respective non-induced control (black). KD = knockdown, NS = non-silencing, OX = overexpression.

4.5.3 FOXA2 overexpression grow worse while FOXA2 knockdown grow better *in vitro*

Previous data showed that SPDEF overexpressing cells grew better and SPDEF knockdown cells grew worse *in vitro* (4.4.4). Since FOXA2 expression was inversely correlated with SPDEF expression, we consequently tested whether FOXA2 overexpressing cells grew worse and FOXA2 knockdown cells grew better.

Indeed, upon doxycycline-induced FOXA2 overexpression, cells grew worse as measured by the CellTiterBlue assay (figure 63). Induced FOXA2 knockdown showed that cells cultured for 6 days had a growth benefit as compared to NS control cells.

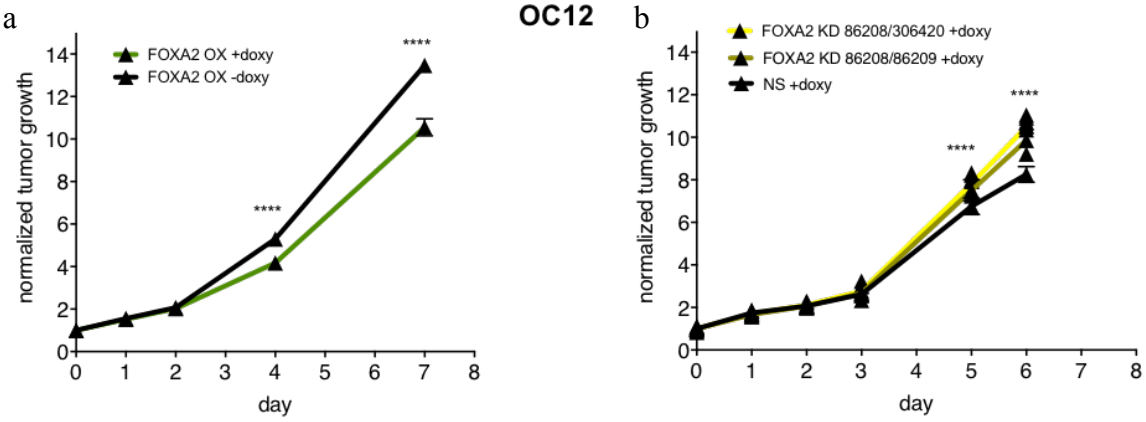

Figure 63: Growth curve of FOXA2 overexpressing and knockdown cells.
(a) Growth of FOXA2 OX (green, +doxy) and non-induced FOXA2 OX control cells (black, -doxy) was measured via the CellTiterBlue assay at several time points and normalized to day 0 in OC12 cells. (b) Also, growth of two FOXA2 KD (yellow and ochre, +doxy) and NS control (black, +doxy) cells was compared in OC12 cells. For OC12, 750 cells per 96-well PRIMARIA well were seeded. Mean ± SD. **** $p \leq 0.0001$, ns = not significant. Two-way ANOVA. OX = overexpression, NS = non-silencing, KD = knockdown.

4.5.4 FOXA2 overexpression decreases colony number and size

To prove whether FOXA2 overexpression has a similar phenotype as SPDEF knockdown regarding the ability to form colonies, we performed colony formation assays.

Induced overexpression of FOXA2 led to a significantly lower number of colonies, both in OC12 and OC20 cell lines (figure 64). Colonies formed by FOXA2-overexpressing cells were also smaller than colonies formed by control cells.

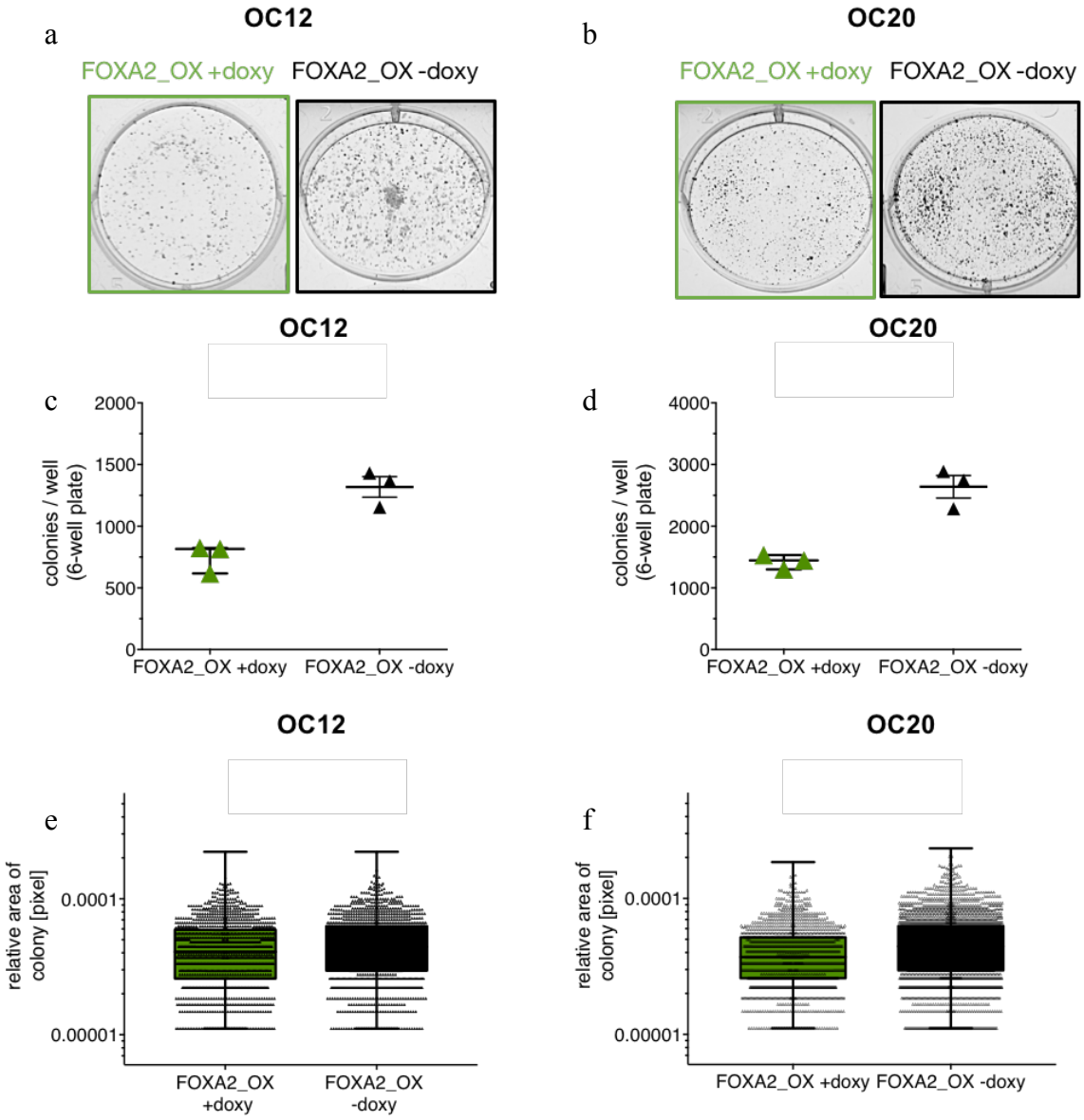

Figure 64: FOXA2 overexpression form less and smaller colonies.
(a) Representative images of the colonies formed by FOXA2 OX (green, +doxy) and non-induced FOXA2 OX control cells (black, -doxy) of OC12 and OC20 cell lines. (b) Colony number of FOXA2 OX (green) and non-induced FOXA2 OX control cells (black) of OC12 and OC20 cells cultured in PRIMARIA 6-wells. For the OC12 cell line, 3,200 cells were seeded per 6-well and for OC20 50,000 cells. OC12 cells were cultured for 7 days and OC20 cells for 14 days, respectively. Mean ± SD. (c) Relative area per colony of FOXA2 OX (green) and non-induced FOXA2 OX control cells (black) of OC12 and OC20 as quantified by Fiji. Box and whisker plot, min to max. n = 3 technical replicates. n = 1 biological replicate for OC12 and OC20. OX = overexpression.

4.5.5 FOXA2 overexpression increases SPDEF and FOXA2 knockdown decreases it

To test whether the inverse correlation between SPDEF and FOXA2 expression is directly linked, we analyzed FOXA2 and SPDEF expression in FOXA2 knockdown and overexpression cell lines by qPCR.

SPDEF was reduced in FOXA2 knockdown cell lines (figure 65 a). The level of SPDEF knockdown in the two cell lines displaying shRNA-induced FOXA2 knockdown correlated with the efficiency of the knockdown (figure 62 a). In the cell lines overexpressing FOXA2, SPDEF was upregulated upon induced expression of FOXA2 (figure 65 b-d). This was true for three OC cell lines analyzed (OC12, OC14 and OC18).

Taken together, FOXA2 overexpression increased SPDEF expression and FOXA2 knockdown decreased it.

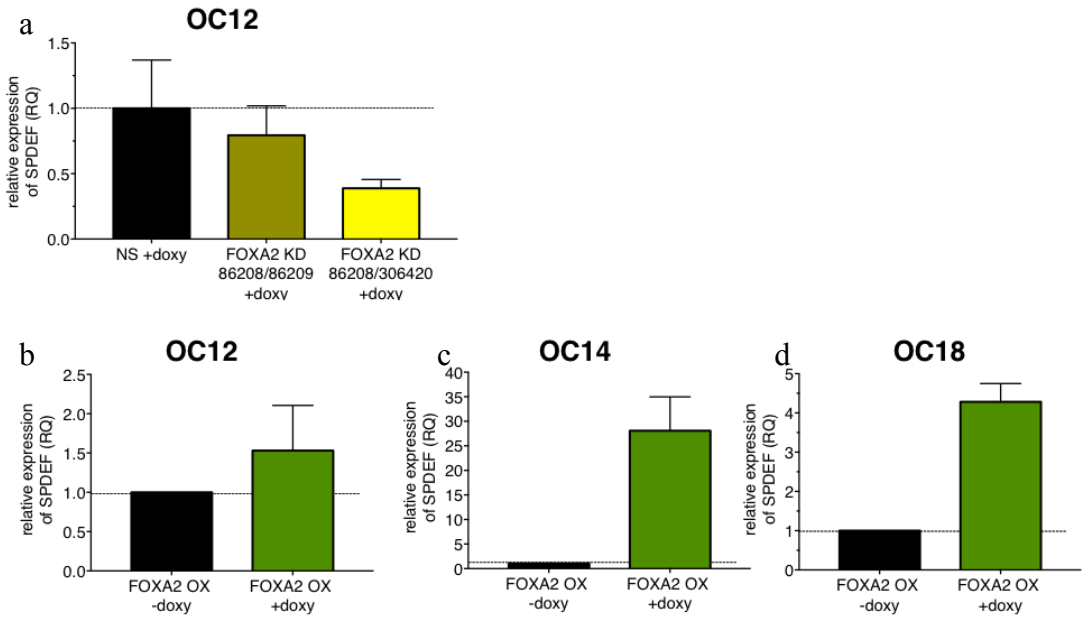

Figure 65: SPDEF is decreased in the FOXA2 knockdown and enriched in the FOXA2 overexpressing cells.

SPDEF expression as measured by qRT-PCR in OC12 (a) in either the NS control (black, +doxy) or the two FOXA2 KD cell lines transduced with shRNAS 86208/86209 or 86208/306420 (ochre and yellow, +doxy). (b-d) SPDEF expression measured by qRT-PCR in the doxycycline-induced FOXA2 overexpressing cell line (green) and the respective non-induced control (black). KD = knockdown, NS = non-silencing, OX = overexpression.

4.5.6 FOXA2 overexpression abolishes tumor growth *in vivo*

FOXA2 overexpression decreased *in* vitro growth and colony formation potential. To analyze whether overexpression of FOXA2 also impaired *in vivo* growth, we injected iT2 control and FOXA2 overexpressing, as well as inducible FOXA2-expressing cells and its control intraperitoneally into NSG mice.

In both experiments, the mice injected with the FOXA2 overexpressing cells showed a delayed initiation of tumors and an overall impaired growth *in vivo*.

Taken together, we concluded that FOXA2 overexpression impairs *in vivo* tumor growth.

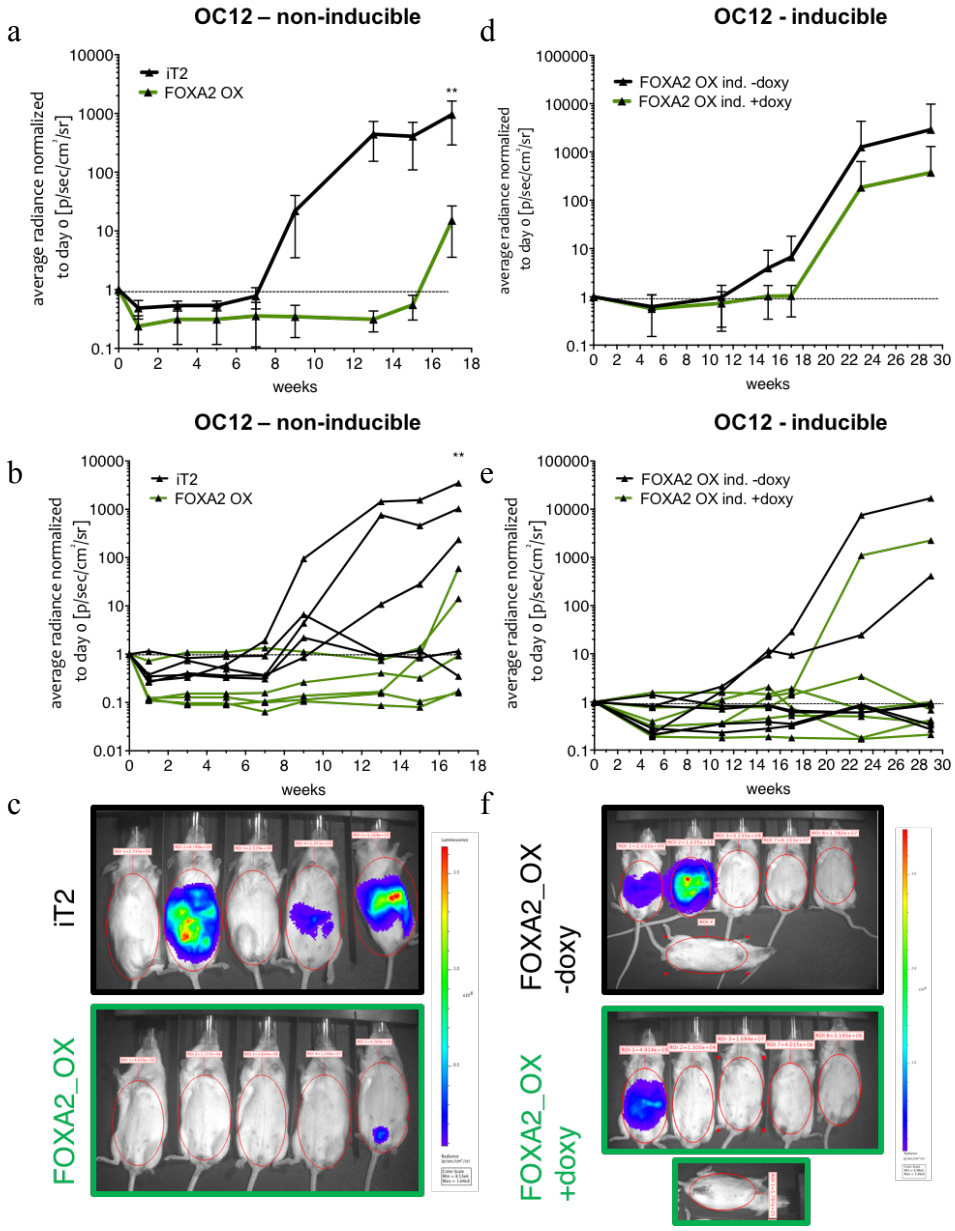

Figure 66: FOXA2 overexpression impedes tumor growth *in vivo.*
(a,c) Growth curves of FOXA2 overexpressing (green) and iT2 control (black) OC12 cells which have been i.p. injected into NSG mice and which were before lentivirally transduced with a luciferase vector in order to follow tumor growth via bioluminescence. (b,d) Growth curves of FOXA2 overexpressing (green, doxycycline-induced) and control (black, not induced) OC12 cells. In a and b, the mean ± SEM of the average radiance is shown, in b and d, the growth curves of the tumor cells for each single mouse are depicted. The dashed line denotes the baseline at week 0. (e, f) Images of the *in vivo* bioluminescent signal in mice injected with FOXA2 overexpressing (green) and iT2 control (black) OC12 cells at the endpoint at week 17 or 13, respectively. n = 5 (a,c) or 6 mice per group (b,d). * $p < 0.05$, ** $p < 0.01$. Two-way ANOVA. iT2 = IRES-tdtomato2, OX = overexpression.

4.5.7 FOXA2 expression correlates with an increased overall survival

Since FOXA2 expression impaired *in vivo* growth of tumors, we wondered whether patients displaying increased expression of FOXA2 had an increased overall survival benefit. Therefore, we analyzed four publicly available datasets. Median overall survival of patients displaying FOXA2 overexpression in their tumors was significantly increased as compared to overall survival of FOXA2 low patients in the datasets GSE23554, GSE9891, GSE26193 and GSE14764

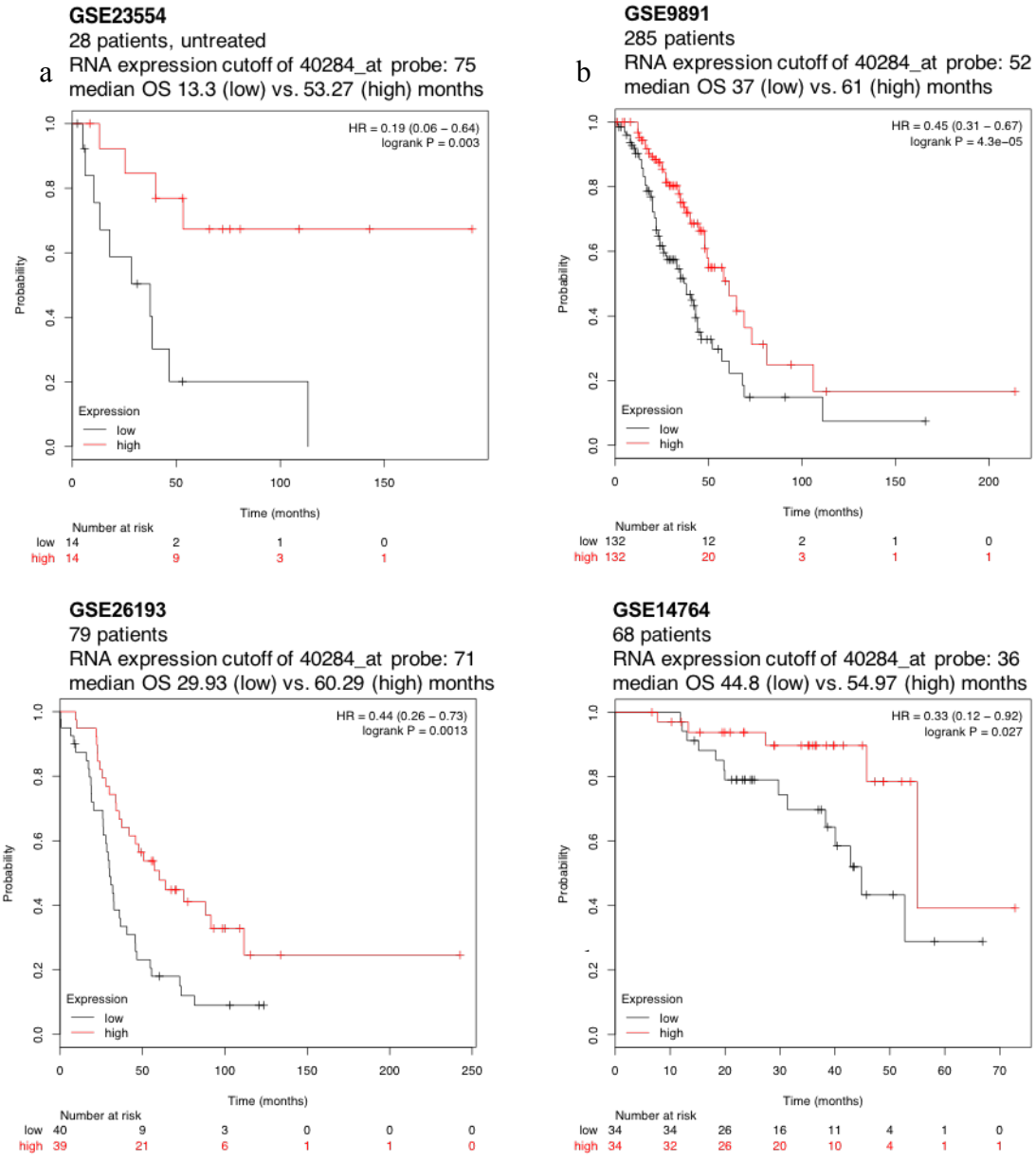

Figure 67: Overall survival of patients stratified according to high or low FOXA2 expression.
Kaplan-Meier analyses showing overall survival of patients stratified according to the RNA

expression of the FOXA2 probe 40284_at of the Affymetrix U133 array. High expression of FOXA2 is depicted in red and low expression in black. The datasets GSE23554 (a), GSE9891 (b), GSE26193 (c) and GSE14764 (d) were used.

5. DISCUSSION

In this study, we demonstrate that SSEA1$^-$ cells from high grade serous ovarian cancer are tumor-initiating cells. Furthermore, the transcription factor SPDEF was shown to be enriched in SSEA1$^-$ cells. SPDEF knockdown decreased the clonogenicity of bulk tumor cells *in vitro* and abolished *in vivo* tumor growth. In contrast, overexpression of SPDEF increased the tumorigenicity of both SSEA1$^-$ and SSEA1$^+$ cells. It could be shown that SPDEF mediates its tumorigenic effects through decreasing FOXA2 expression. The anti-tumorigenic effects of FOXA2 were demonstrated by overexpressing FOXA2 which impaired *in vivo* tumor growth.
Taken together, we identified SSEA1$^-$ cells as tumor-initiating cells in HGSOC whose tumorigenicity is mediated via expression of SPDEF which itself decreases expression of the tumor suppressive transcription factor FOXA2.

5.1 SSEA1$^-$ cells are tumor-initiating cells in HGSOC

SSEA1$^-$ cells initiate tumors

Tumor-initiating cells have been identified in various tumor entities (Bonnet *et al.,* 1997, Al-Hajj *et al.,* 2003, Singh *et al.,* 2003, Collins *et al.,* 2005, Son *et al.,* 2009, Boiko *et al.,* 2010). In ovarian cancer, tumor-initiating cells are considered to be responsible for primary tumor outgrowth, peritoneal spread and metastatic relapse (Lupia *et al.,* 2017). The metastatic spread into the peritoneum occurs during the early stages of the disease and the colonization of the organs in the peritoneum is the major problem regarding curing HGSOC. Thus, identification of the tumor-initiating cells is crucial. However, no conclusive evidence about the markers of tumor-initiating cells in ovarian cancer has been provided. In addition, even less is known about the underlying functionality and the molecular mechanisms of these markers.
In this study, we now demonstrate that SSEA1$^-$ high grade serous ovarian cancer cells possess higher tumor-initiating potential than SSEA1$^+$ cells in intraperitoneally injected *in vivo* xenograft models (figure 25) and in *in vivo* limiting dilution analyses (figure 30). As few as 100 SSEA1$^-$ cells were able to initiate a tumor *in vivo* whereas 10,000 SSEA1$^+$ cells were only able to establish tumors in 2 out of 5 mice (SSEA1$^-$: 5/5 mice). The tumorigenicity of SSEA1$^-$ cells was further verified in the intraperitoneal setting in which 10,000 SSEA1$^-$ cells were tumorigenic but 10,000 SSEA1$^+$ cells were not (OC12). This was also shown for a second patient-derived OC cell line: 100,000 OC20 SSEA1$^-$ tumor cells led to a significantly higher tumor burden than SSEA1$^+$ cells and the mice survived less as measured by a 100-fold

increase in bioluminescence (figure 26 and figure 27). Further, we showed that SSEA1$^-$ cells are more metastatic than SSEA1$^+$ cells. SSEA1$^-$ cells formed metastatic nodules on organs like the liver, diaphragm and uterus (table 11) in 6 out of 8 mice. SSEA1$^+$ cells however did not form any visible metastatic foci.

Markers that have been claimed by others to identify tumor-initiating cells in ovarian cancer include CD44$^+$, CD44$^+$CD24$^-$, CD133$^+$, CD44$^+$CD117$^+$, ALDH1A1$^+$ CD117$^+$ and CD44$^+$MyD88$^+$ (Zhang *et al.,* 2008, Alvero *et al.,* 2009, Meng *et al.,* 2012, Zhang *et al.,* 2012, Gao *et al.,* 2015, Lupia *et al.,* 2017). However, due to heterogeneity of the disease and the limited number of patients assessed, none of these markers could have been conclusively validated. A major problem addressing the heterogeneity of cells is culturing them using serum in the medium. However, only one (Zhang *et al.,* 2012) out of four studies cultured the cells in a defined CSC medium, in the other studies, the tumor cells were cultured in FCS-supplemented medium (Alvero *et al.,* 2009, Meng *et al.,* 2012, Gao *et al.,* 2015, Lupia *et al.,* 2017). Since cell lines cultured under FCS-conditions are known to lose their heterogeneity and morphological characteristics when transplanted into NSG mice (Lee *et al.,* 2006), these studies have to be seen critically since the actual tumor-initiating cells might have been outgrown in culture by proliferative cells. Further, no primary tumor tissue but conventionally cultured cell lines were used in some of the studies that identified tumor-initiating markers (Meng *et al.,* 2012, Gao *et al.,* 2015).

We circumvent this issue by using primary patient-derived cell lines cultured in a defined CSC medium for our analyses instead of conventional cell lines cultured under FCS-conditions. Moreover, we could observe the tumor-initiating potential of the SSEA1$^-$ cells in two independent patient-derived cell lines, strengthening the finding that SSEA1$^-$ cells are indeed tumor-initiating cells in HGSOC.

To verify that the SSEA1$^-$ population is distinct from that of other surface markers, we showed that SSEA1 expression does not overlap with CD24 and C44 expression in a FACS staining (figure 13 and figure 14). Cells were further completely negative for CD133 (data not shown). Although the FACS staining demonstrated that the SSEA1$^-$ population is distinct from the CD44$^+$ population, we found a slight but not significant enrichment for CD44 mRNA in the SSEA1$^-$ samples in our microarray data (data not shown). This could, however, indicate that the SSEA1$^-$ tumor-initiating population could be further narrowed down by sorting for SSEA1$^-$ CD44$^+$ cells. This is also of particular interest since a connection between CD44 and SSEA1 expression has been described. CD44 ligation, which leads to induced

maturation of myeloid cells, resulted in an increase of SSEA1 expression by decreasing sialyl-SSEA1 (SSEA1$^-$) levels (Gadhoum and Sackstein 2008).

In mouse medulloblastoma, SSEA1 (CD15) expression was found to be a marker for tumor-propagating cells (Read *et al.,* 2009). These data are in line with the finding that neural stem and progenitor cells in the mouse adult brain have been shown to express SSEA1 but not their differentiated progeny (Capela *et al.*, 2002, Capela *et al.*, 2006). However, another study by Son *et al.* showed that SSEA1$^+$ cells are also enriched for tumor-initiating cells in human glioblastoma (Son *et al.,* 2009). Though, a study by Kenney-Herbert *et al.* questioned that SSEA1 is a phenotypically distinct marker for tumor-initiating cells in human glioblastoma (Kenney-Herbert *et al.,* 2015).

Since, in humans, SSEA1 is expressed on differentiated cells including epithelial cells (Fox *et al.,* 1983, Arber and Weiss 1993) but not on mouse differentiated cells (Solter *et al.,* 1979), the data of Son *et al.* may be contradictive. However, it may very well be that SSEA1 is also expressed by human neural stem and progenitor cells as it is by mouse ones (Capela *et al.*, 2002, Capela *et al.*, 2006). Our finding that SSEA1$^-$ cells are the tumor-initiating population in ovarian cancer is supported by the data of Arber and Weiss, Fox *et al.*, Solter *et al.* and Wright *et al.* which state that SSEA1 is absent in human embryonic or pluripotent cells but mostly expressed on human differentiated cells (Solter *et al.,* 1979, Fox *et al.,* 1983, Arber *et al.,* 1993, Wright *et al.,* 2009).

Taken together, we identified SSEA1$^-$ cells as tumor-initiating cells in high grade serous ovarian cancer.

SSEA1$^-$ cells form more spheres and colonies and are more clonogenic in vitro

Colony formation assays of single cells in adherent, sphere or soft-agar conditions and limiting dilution analyses are considered to be an indicator of the stemness and differentiation of single cells (Rajendran and Jain 2018). The more colonies are formed from a pre-defined number of cells, the more undifferentiated/stem-like the cells are supposed to be.

We could show that SSEA1$^-$ cells form two- up to five-fold more colonies in sphere-forming conditions from three out of three tested patient OC lines (figure 22). Additionally, in adherent conditions, from four patient OC lines tested, three showed a strong tendency to form more colonies (figure 23). OC20 SSEA1$^-$ cells formed clearly more colonies than SSEA1$^+$ cells.Although OC15 and OC18 SSEA1$^-$ cells had a strong tendency to form more colonies than the respective SSEA1$^+$ cells, the variability between the wells was high. Effects

like the location in the incubator or technical issues like unequal medium volumes or unequal seeding numbers might have contributed to the variability. Repetition of the experiment might eradicate these issues and potentially also give significant results. Other than in the sphere-forming assay, $SSEA1^-$ cells from the OC12 cell line, however, formed less colonies in adherent conditions than $SSEA1^+$ cells. This result was reproducible in four independent experiments and could be attributable to the adherent conditions. It might be that the $SSEA1^+$ cell population of OC12 cells carries some mutations or displays increased activity in signaling pathways which enable them to grow better on the adherent PRIMARIA plates. Further, the fact that the OC12 cell line was the only OC line established in estrogen-free conditions might have selected for different cell populations of $SSEA1^+$ and $SSEA1^-$ cells.

Besides the number of colonies, the $SSEA1^-$ cells also formed bigger colonies than the $SSEA1^+$ cells in three out of four patient-derived cell lines (figure 23). Only $SSEA1^+$ cells of the OC12 cell line formed bigger colonies than $SSEA1^-$ cells.

The increased colony formation potential was also reflected in the *in vitro* limiting dilution analyses of $SSEA1^+$ and $SSEA1^-$ cells. In the OC15 and OC20 cell lines tested, the $SSEA1^-$ cells were significantly more clonogenic than the $SSEA1^+$ cells, thus, $SSEA1^-$ cells gave rise to colonies already at very low cell numbers. Again, the $SSEA1^-$ cells of the OC12 cell line showed in the adherent *in vitro* limiting dilution conditions the same result as in the adherent colony formation assay: they were less clonogenic than the $SSEA1^+$ cells.

The data of Son *et al.* which show that $SSEA1^+$ cells are enriched for tumor-initiating cells also demonstrate that the colony-forming and *in vitro* limiting dilution potential of $SSEA1^+$ cells is higher than that of $SSEA1^-$ cells (Son *et al.,* 2009). This seems contradictive, however, Son *et al.* show this for a different tumor entity in which the healthy stem cells are considered to be $SSEA1^+$ [Capela, 2006 #455;Capela, 2002 #456]. Further, they show that the $SSEA1^+$ cells are the tumorigenic population. We, however demonstrate that the $SSEA1^-$ cells are the tumor-initiating population and it is also this cell type which forms increased colonies compared to $SSEA1^+$ cells.

Taken together, we could show that $SSEA1^-$ cells have a strong tendency to form more colonies than $SSEA1^+$ cells in adherent conditions and that they also form more spheres compared to $SSEA1^+$ cells.

SSEA1$^-$ give rise to SSEA1$^+$ cells

By genetically labeling the cells with H2B-GPF, we could show that SSEA1$^-$ cells establish a cellular hierarchy by giving rise to SSEA1$^+$ cells *in vitro* and *in vivo*. SSEA1$^+$ cells, however, do not give rise to SSEA1$^-$ ones (figure 18, figure 19 and figure 29). The low number of SSEA1$^-$ cells in mouse number 5 of initially SSEA1$^+$ FACS-sorted and intraperitoneally injected cells (figure 29), might be due to the initial sort purity which was about 88 % pure for SSEA1$^+$ cells. Thus, some SSEA1$^-$ cells might have also been injected, grown out and given rise to SSEA1$^+$ cells.

Initially SSEA1$^-$ cells can divide asymmetrically and give rise to a SSEA1$^+$ and a SSEA1$^-$ cell as demonstrated by time-lapse imaging (data not shown). These findings illustrate that SSEA1$^-$ cells are on top of the cellular hierarchy and further, that SSEA1$^+$ do not change their phenotype and become SSEA1$^-$.

Asymmetrical division in addition to symmetrical division has been considered to be a hallmark of stem cells and also cancer stem cells (Knoblich 2008, Beck *et al.,* 2013). Hence, the fact that SSEA1$^-$ cells give rise to SSEA1$^-$ but also SSEA1$^+$ cells further supports our conclusion of SSEA1$^-$ cells being tumor-initiating cells in HGSOC.

Further, the frequency of asymmetric division has been shown to correlate negatively with the proliferative behavior of cells: the more they proliferate, the fewer asymmetric division they do (Bu *et al.,* 2013). This is in line with our finding that SSEA1$^+$ cells incorporate significantly more EdU than SSEA1$^-$ cells and thus, seem to proliferate more (figure 20).

The appearance of the SSEA1 epitope from SSEA1$^-$ cells may be due to several explanations. As potential mechanisms for the generation of the SSEA1 epitope, several glycosidases and glycosyltransferases, including fucosyltransferases 4 and 9 have been considered (Knowles *et al.,* 1982, Nakayama *et al.,* 2001, Nishihara *et al.,* 2003). However, recent evidence was provided that SSEA1 expression is regulated by sialidase activity. In human myeloid cells, it was shown that cleavage of sialyl-SSEA1 by α(2-3)-sialidase activity yields SSEA1. Besides, increased expression of SSEA1$^+$ was correlated with increased differentiation in this cell type (Gadhoum *et al.,* 2008). Interestingly, sialidase genes are significantly enriched in OC12 (NEU1), OC14 (NEU1), OC18 (NEU3, NEU4) and OC20 (NEU4) SSEA1$^+$ cells according to our microarray data (data not shown).

Since SSEA1 negativity can be either explained by the complete or partial absence of the SSEA1 epitope or by masking the epitope with other sugar moieties like sialyl residues, SSEA1$^-$ cells can also be potentially sialyl-SSEA1 cells. Sialyl-SSEA1 cells have, for

example, been implicated in driving breast cancer metastasis of hormone-dependent cancers (Julien *et al.,* 2011).

Since $SSEA1^+$ expression has been correlated to differentiation processes in various human cell types (Fox *et al.,* 1983, Arber *et al.,* 1993, Gadhoum *et al.,* 2008) and SSEA1 negativity with a less differentiated phenotype (Gadhoum *et al.,* 2008, Wright *et al.,* 2009), the asymmetrical division of a $SSEA1^-$ cell and the subsequent appearance of SSEA1 might give rise to a less differentiated, tumor-initiating cell ($SSEA1^-$ cell) that is potentially a sialyl-SSEA1 cell and a differentiated $SSEA1^+$ cell.

In ovarian cancer, it has further been shown, that $SSEA1^+$ tumor cells arise from initially $SSEA1^-$ ovarian tissue (Fox *et al.,* 1983).

Son *et al.* show that $SSEA1^+$ cells are enriched for tumor-initiating cells in a model of human glioblastoma and that these $SSEA1^+$ cells establish a cellular hierarchy by giving rise to $SSEA1^-$ cells (Son *et al.,* 2009). Again, since neural stem an progenitor cells have been shown to be also $SSEA1^+$ in mice [Capela, 2006 #455;Capela, 2002 #456], it can be that in this tumor entity the $SSEA1^+$ cells are the more stem-like tumor-initiating cells, different from our model. Scaffidi *et al.* demonstrate that cells generated by *in vitro* somatic reprogramming of human fibroblasts contain CSC features and that these cells are $SSEA1^+$. They further show that $SSEA1^+$ cells can initiate tumors and generate heterogeneous lineages by giving rise to both $SSEA1^+$ and differentiated $SSEA1^-$ cells with less tumorigenic potential (Scaffidi *et al.,* 2011). However, Scaffidi *et al.* did not use primary cells from tumors but rather fibroblasts which they transformed into tumorigenic cells. Thus, the results are not contradictive to our data.

Overall, a differential expression of various glycosyltransferases, glycosidases, sialyltransferases and sialidases driven by oncogenic drivers may result in phenotypic differences between cell types. Ovarian cancers, for example, might express an oncogenic transcription factor which highly induces expression of sialyltransferases and thus, may display tumorigenic $SSEA1^-$ cells. In glioblastoma then, another oncogenic transcription factor might preferentially induce sialidase genes and hence, the more tumorigenic cells may be phenotypically $SSEA1^+$.

To sum up, we show that $SSEA1^-$ cells give rise to both $SSEA1^-$ and $SSEA1^+$ cells, thereby giving rise to a heterogeneous cellular hierarchy.

SSEA1$^+$ cells incorporate more EdU and are enriched in G_2M cell cycle phase

Although we could not detect growth differences between SSEA1$^+$ and SSEA1$^-$ cells *in vitro* in a CellTiter Blue assay (figure 17), we demonstrated that these cells are significantly differentially enriched in distinct cell cycle phases. Whereas SSEA1$^-$ cells were strongly enriched in $G_{0/1}$ phase of all 5 OC lines tested, SSEA1$^+$ cells were enriched in G_2M cell cycle phase (figure 20). Further, the level of SSEA1 expression correlated with the number of cells in G_2M phase. In addition, the SSEA1$^+$ cells incorporated significantly more EdU than the SSEA1$^-$ cells, indicating that they proliferated more (figure 20). The low number of cells in S phase of OC19 SSEA1$^+$ and SSEA1$^-$ cells is probably due to a too short labeling time with EdU since the OC19 cell line growth rate is very slow and thus, EdU incorporation is also more slowly.

The differences between the CellTiter Blue growth assay and the EdU experiment might be explained by our finding that SSEA1$^-$ cells give rise to SSEA1$^+$ cells (figure 18). Thus, the SSEA1$^-$ cells analyzed over a time period of 6 (OC12) or 18 (OC20) days in the CellTiter Blue assay (figure 17) had already given rise to SSEA1$^+$ progeny in the wells, and hence, we did not really measure growth of the initially FACS-sorted SSEA1$^-$ population but rather of a heterogeneous mixture of cells. The percentage of obviously still present SSEA1$^-$ cells in $G_{0/1}$ cell cycle phase did not contribute to a differential growth velocity, indicating that SSEA1$^-$ cells had generated SSEA1$^+$ cells rapidly and in great numbers.

Adult stem cells are considered to have long cell cycle phases or to be quiescent, indicating an enrichment in $G_{0/1}$ phase (Knoblich 2008). This is similar to the SSEA1$^-$ cells in our study from which we thus believe that they resemble more stem-like cells than the SSEA1$^+$ which itself are considered as more proliferative progenies.

Another study has already implicated SSEA1 in proliferation: By silencing fucosyltransferase 9, an enzyme implicated in the generation of SSEA1 (Nakayama *et al.,* 2001), Yagi *et al.* show that SSEA1 expression is involved in the proliferation of neural stem cells via modulation of the Notch pathway (Yagi *et al.,* 2012).

Besides the interpretation that SSEA1$^+$ cells proliferate more due to increased EdU incorporation, we also speculate that a greater portion of the SSEA1$^+$ than the SSEA1$^-$ cells might be arrested at G_2M cell cycle phase. Since the G_2M cell cycle checkpoint is known to arrest proliferation of damaged cells or to provide the possibility of repair (Stark and Taylor 2004), the SSEA1$^+$ cells would consequently not divide but rather arrest or go into apoptosis (DiPaola 2002) within time as could be seen by time-lapse imaging (data not shown).

Further, SSEA1$^+$ cells are bigger (figure 15) and show a significantly greater amount of aneuploidy, defined as cells > 4n, than SSEA1$^-$ cells in all five OC lines tested (figure 21). Cancer cells are known to possess a huge amount of genomic instability including aneuploidy (Lengauer *et al.,* 1998, Rajagopalan and Lengauer 2004). Aneuploidy usually occurs due to a weakened mitotic checkpoint (Cahill *et al.,* 1998, Rajagopalan *et al.,* 2004). Thus, the increased amount of aneuploidy in SSEA1$^+$ cells as compared to SSEA1$^-$ cells might be due to the increased proliferation as measured by EdU incorporation. Increased number of mitotic cycles in SSEA1$^+$ cells may have led to increased chromosomal instability and aneuploidy.
However, aneuploidy has also been considered to be necessary for tumor development (Duesberg *et al.,* 1999). Nevertheless, according to our *in vitro* assays and *in vivo* tumorigenicity assays, the SSEA1$^-$ cells are more tumorigenic although they show nearly no aneuploidy. It has also been shown that tumor cells without aneuploidy, that were still diploid/near-diploid, displayed a deficiency in mismatch repair. At the same time, these cells had a mutation rate which was two to three times higher than that of normal cells (Lengauer *et al.,* 1997, Rajagopalan *et al.,* 2004) enabling them to acquire the necessary genetic changes to progress tumorigenesis. It has to be further shown in more experiments how SSEA1$^-$ cells differ from SSEA1$^+$ cells on the genetic level.
The expression of SSEA1$^+$ might, however, also be a side effect and thus, a marker for more aneuploid or stressed cells and cells enriched in G_2M cell cycle.
In sum, we believe that SSEA1$^-$ cells are more quiescent / stem-like than SSEA1$^+$ cells because they are enriched in $G_{0/1}$ cell cycle phase. SSEA1$^+$ cells, however, replicate more often based on EdU incorporation. At the same time, they seem to be more arrested in G_2M phase compared to SSEA1$^-$ cells and be the more damaged cell type as demonstrated by the increased amount of aneuploidy in these cells.

Molecular differences between SSEA1$^+$ and SSEA1$^-$ cells

In order to identify the underlying molecular mechanisms responsible for the phenotypic and functional differences of SSEA1$^-$ and SSEA1$^+$ cells, we performed gene expression profiling of duplicates/triplicates of six FACS-sorted SSEA1$^+$ and SSEA1$^-$ OC cell lines. Unsupervised hierarchical clustering revealed that the six OC lines clustered together (figure 31). Thus, we analyzed the samples according to single patient background. This showed that 4 out of 6 OC lines clustered according to SSEA1 status when performing unsupervised hierarchichal clustering (figure 32). For all further analyses, we decided to exclude the two samples which

did not cluster according to SSEA1 status (OC14, OC18), especially since one sample that did not cluster according to SSEA1 status was processed with MACS instead of FACS-sorting (OC18) and the other sample did not have a matched SSEA1$^-$ sample due to too low RNA quantity (OC14).

Differential gene expression analyses revealed many significantly differentially expressed genes between SSEA1$^+$ and SSEA1$^-$ cells, even when all OC cell lines were analyzed in a pooled manner (378 genes, $p < 0.05$, BH, FC > 1.2). When analyzing according to single patient background, even more differentially expressed genes were identified (up to 1195 genes in OC20, $p < 0.05$, BH, FC > 1.3). Gene set enrichment analyses (GSEA) further showed an enrichment of more than 350 or more than 900 gene sets significantly enriched ($p < 0.05$) in the SSEA1$^-$ or SSEA1$^+$ samples, respectively, in a pooled analysis of OC12, OC15 OC19 and OC20.

From this, we concluded that SSEA1$^+$ and SSEA1$^-$ cells indeed differ significantly on a molecular level based on their gene expression.

5.2 SPDEF is enriched in SSEA1$^-$ TIC and drives tumor growth

SPDEF is enriched in SSEA1$^-$ cells

Besides the differences found when analyzing the OC lines in a pooled manner, we took the different patient backgrounds into account and decided to apply a threshold of $p < 0.1$ for these for differential testing of gene expression. Venn diagram analyses then showed that 15 and 21 genes were upregulated in SSEA1$^-$ or SSEA1$^+$ cells, respectively, in OC12, OC15, OC19 and OC20 (figure 34). Among these, we identified SAM-pointed ETS-domain containing transcription factor (SPDEF) to be enriched in SSEA1$^-$ cells of all samples of OC12, OC15, OC19 and OC20. Enrichment of SPDEF in FACS-sorted SSEA1$^+$ and SSEA1$^-$ cells was verified via qPCR. However, we could only verify endogeneous SPDEF expression on protein level of bulk OC20 but not OC12 cells. All antibodies tested did not detect basal SPDEF levels in OC12 but did detect SPDEF levels from the overexpression. This could be either due to too low or no protein expression of SPDEF in OC12 cells or the fact that the antibodies were not working well. Also, for immunohistochemistry, several antibodies were tested but no working antibody was identified.

SPDEF knockdown and overexpression changes the morphology of cells

In order to analyze the function of SPDEF, we performed lentiviral knockdown and overexpression of SPDEF. Knockdown of SPDEF changed the morphology of the OC cells. In the epithelial OC12 cell line, SPDEF KD cells grew as single cells and in a more mesenchymal way, different from the parental OC12 cell line which grows in a more epithelial way (figure 39). Overexpression of SPDEF, however, also changed the morphology of OC20 cells in that they grew more epithelial-like. This was observed for OC20 only, which under normal conditions grows in more spheroid-like, adherent clusters (figure 39).

In mice, SPDEF knockout has also been shown to change the morphology of goblet and Paneth cells (Gregorieff *et al.,* 2009). Furthermore, overexpression of SPDEF in mice in Clara cells induced differentiation of these cells into goblet cells (Chen *et al.,* 2009).

In sum, we showed that SPDEF knockdown and overexpression changes the phenotype of OC cells by shifting their morphology to a more mesenchymal (SPDEF KD) or epithelial (SPDEF OX) type, respectively.

SPDEF overexpressing cells grow more in vitro

To test for a functional phenotype of SPDEF overexpressing and knockdown cells, we performed *in vitro* growth analyses via the CellTiter Blue assay. Overexpression of SPDEF increased growth of OC12 and OC20 cells in CSC-medium depleted for estrogen. Knockdown of SPDEF impaired growth of OC12 cells, but not of OC20 cells. The growth experiment for OC20 was, however, only performed once. Thus, repeating it might give more information regarding whether knockdown of SPDEF also decreases growth in OC20. Further, the observed growth effect might also be a combination of growth and a more efficient (SPDEF OX) less efficient (SPDEF KD) plating and subsequent colony formation since we showed that SPDEF overexpressing cells form more and SPDEF knockdown cells form less colonies (4.4.5).

Knockdown of SPDEF has also been described to decrease growth of the breast cancer-derived MCF7 cells (Buchwalter *et al.,* 2013). In other tumor entities, however, overexpression of SPDEF decreased growth of prostate cancer, colon cancer and bladder cancer cells (Moussa *et al.,* 2009, Steffan *et al.,* 2012, Tsui *et al.,* 2016, Lo *et al.,* 2017, Tsai *et al.,* 2018). The different roles of SPDEF in various cancer cells has to be further explored. Since SPDEF has been shown to be regulated by estradiol (Buchwalter *et al.,* 2013), it might

be that SPDEF exerts different roles and drives distinct gene expression profiles depending on hormone levels including estrogens or androgens.
Taken together, we show that SPDEF overexpressing cells grow more *in vitro* as compared to iT2 control cells.

SPDEF knockdown cells form less and smaller colonies and are less clonogenic in vitro

To further investigate the phenotype of SPDEF overexpression and knockdown, we performed colony-formation assays *in vitro.* SPDEF overexpressing cells formed significantly more and bigger colonies than control cells (figure 41). Vice versa, SPDEF knockdown cells formed less and smaller colonies than the respective NS control cells (figure 42). By demonstrating that SPDEF knockdown cells compared to NS control cells were less clonogenic in *in vitro* limiting dilution analyses we further supported this finding (figure 43). Similar results were observed for the breast cancer cell line MCF7: Knockdown of SPDEF significantly reduced the colony numbers compared to control cells (Buchwalter *et al.,* 2013). In prostate cancer, colony formation of SPDEF overexpressing cells was reduced in soft agar, however, no difference was observed in anchorage-dependent conditions (Johnson *et al.,* 2010). In another study in prostate cancer, colony formation of SPDEF overexpressing cells was also reduced in soft agar (Cheng *et al.,* 2014). These data demonstrate conflicting roles of SPDEF in various tumor types but may again indicate that a hormonal background might play a role, especially since prostate cancer is mostly an androgen-driven cancer (Feldman and Feldman 2001) and ovarian and breast are estrogen-regulated tissues (Rao *et al.,* 1991, Spillman *et al.,* 2010, Yaghjyan and Colditz 2011).
Taken together, we demonstrate that SPDEF overexpression increases the colony-forming potential of cells in adherent conditions and, vice versa, knockdown of SPDEF reduces the colony formation ability and clonogenicity *in vitro.*

Cells overexpressing SPDEF respond faster in a wound closure assay

To further characterize the phenotype of SPDEF *in vitro*, we performed a wound scratch assay. SPDEF overexpressing cells closed the wound more rapidly than iT2 control cells (figure 44). Since we used mitomycin C to block proliferation, our result indicates that the more rapid closure of the wound was only due to increased migratory potential of SPDEF overexpressing cells. The opposite data, namely decreased speed of migration, were again obtained for prostate tumor cells in three independent studies (Cheng *et al.,* 2014, Chen *et al.,*

2017, Tsai *et al.,* 2018). Again, the data from our study in ovarian tumors and these of prostate cancer seem conflicting, however, considering the different hormonal background of prostate and ovarian tissues (Rao *et al.,* 1991, Feldman *et al.,* 2001, Spillman *et al.,* 2010, Yaghjyan *et al.,* 2011), this could be an explanation for the different results.
To conclude, SPDEF overexpressing cells migrate faster than iT2 control cells.

SPDEF knockdown impairs in vivo tumor growth and SPDEF overexpression leads to more ascites, tumors and metastases

Since SSEA1$^-$ cells initiated tumors *in vivo* and SPDEF was enriched in this population, we wondered whether SPDEF expression is responsible for the phenotype of increased tumor growth in mice injected with SSEA1$^-$ cells. Thus, we knocked down SPDEF in OC cells and compared the tumor growth potential *in vivo* with that of control cells.
Indeed, SPDEF knockdown impeded tumor growth in OC20 cells *in vivo* (figure 45). In OC12 cells no differential tumor growth was observed (figure 46). However, a huge variance regarding tumor burden in the mice injected with OC12 SPDEF KD cells was observed. A possible explanation might be loss of knockdown in some cells which might had a growth advantage compared to SPDEF KD cells. Further, more tumor cells might have been injected into the mice which showed an outgrowth of the SPDEF knockdown population as compared to those which did not grow. Another explanation might be, that the result is correct and there is just no difference between the SPDEF knockdown and NS control cells. The differences which were then observed might be due to the different patient backgrounds: OC12 was derived from a solid tumor and OC20 was established from a pleural effusion sample. Further, the OC12 cell line was assigned to the mesenchymal HGSOC subtype and OC20 to the proliferative one, both transcriptional different from each other. Besides these differences regarding origin of cell line and transcriptional program, the levels of the *ESR1* gene might play a role: The expression of the *ESR1* gene is low to absent in the OC12 cell line, but rather high in OC20 according to our microarray data (data not shown). In breast cancer, it has been described that the hormonal background of the cells is important for the SPDEF-induced cell fate (Buchwalter *et al.,* 2013). SPDEF has been identified as a mediator of mammary luminal epithelial lineage-specific gene expression. In luminal breast cancer tumors, SPDEF knockdown decreased tumor growth. In basal-like ones, however, overexpression of SPDEF decreased tumor growth. Consequently, it was proposed that SPDEF acts as a survival factor for estrogen receptor-positive tumors only (Buchwalter *et al.,* 2013). These data are in line

with our results obtained from SPDEF knockdown in OC12 and OC20 cell lines: It might very well be that the SPDEF knockdown did only impair *in vivo* tumor growth in OC20 because these cells express high levels of ESR1 and not in OC12 which express low levels of ESR1 (data not shown). Further, the OC12 cell line was established without estrogen in the cell culture medium indicating that these cells underwent selection and might grow independent of estradiol.

From these data, one might speculate that SPDEF might act as a survival factor for ESR1-positive ovarian tumors and that this subpopulation of patients in the clinic might benefit from inhibition of SPDEF. However, to further support this hypothesis, a bigger number of $ESR1^{high}$ and $ESR1^{low}$ OC lines should be lentivirally transduced with SPDEF knockdown shRNAs and analyzed regarding tumor growth. If this can be verified in a larger cohort of patient-derived OC lines, SPDEF might be a potential therapeutic target for $ESR1^{+}$ HGSOC patients and the development of SPDEF inhibitors might ultimately help to improve survival of $ESR1^{+}$ HGSOC patients.

We further found that SPDEF levels correlate with ESR1 expression and that SPDEF is also significantly enriched in $ESR1^{high}$ tumors (figure 52). The weak correlation might be due to contamination of the tumor with normal tissue. The finding that SPDEF correlates with ESR1 expression was further supported by the results obtained from GSEA analyses which predicted the hallmark gene set "HALLMARK_ESTROGEN_RESPONSE_EARLY" to be enriched in both OC12 and OC20 SPDEF OX cells as compared to iT2 cells (figure 56 and figure 57). Besides, expression of ESR1 as assessed by our microarray data showed an enrichment of ESR1 in $SSEA1^{-}$ cells in 3 out of 4 patient-derived cell lines (OC15, OC19, OC20, figure 52) but not in OC12. This, however, might be attributable to the fact that OC12 was the only cell line established without estradiol, and thus, another subset of cells might have been selected than in the other cell lines. Further, overall expression of ESR1 in OC12 was low according to the microarray, which indicates that ESR1 might not at all be expressed in this cell line.

Enrichment of *ESR1* gene expression in $SSEA1^{-}$ cells is also in line with the result from GSEA analyses of $SSEA1^{-}$ and $SSEA1^{+}$ cells which predict gene sets like "SMID_BREAST_CANCER_LUMINAL_B_UP" and "DOANE_BREAST_CANCER _ESR1_UP" to be enriched in $SSEA1^{-}$ cells. This led us to the hypothesis that $SSEA1^{-}$ cells may be more luminal-like cells and resemble the luminal type of breast cancers as compared to $SSEA1^{+}$ cells. However, further analyses on protein level like immunohistochemical

stainings have to prove this correlation between SSEA1$^-$ cells and ESR1 expression. Further, the correlation of SPDEF (which is also enriched in SSEA1$^-$ cells) with ESR1 and our functional data showing that knockdown of SPDEF in ESR1^{high} OC lines impairs tumor growth, led us to the hypothesis that SPDEF may act as a survival factor in ESR1^{high} cells. It has to be further proven that knockdown of SPDEF in SSEA1$^-$ cells in ESR1^{high} OC lines also impairs tumor growth.

Since knockdown of SPDEF in OC20 cells impaired tumor growth *in vivo,* we wondered whether overexpression of SPDEF increased tumorigenicity. And indeed, overexpression of SPDEF in OC20 cells led to increased tumor and ascites formation, as well as to more metastases.

In bladder cancer, overexpression of SPDEF has been shown to suppress tumorigenesis (Tsui *et al.,* 2016). In breast cancer, however, the tumor weight of xenografted tumors was less in the SPDEF KD group compared to the control group (Buchwalter *et al.,* 2013). Again, we speculate that estradiol might play a role in the different outcomes of SPDEF OX and KD cells in xenografts regarding tumor growth.

Interestingly, the OC20 SPDEF OX cells display a more epithelial morphology (figure 39), have a growth advantage in the *in vivo* xenograft model and give rise to tumors while the SPDEF KD cells, which have a more mesenchymal phenotype, do not.

This challenges the epithelial-to-mesenchymal transition model which states that cells transition from epithelial cells to mesenchymal cells during cancer progression due to activation of EMT-transcription factors like SNAIL, ZEB and TWIST (Brabletz *et al.,* 2018). Our study challenges this point of view. We show that it is the more epithelial-like, SPDEF overexpressing cells, that are more tumorigenic in HGSOC as compared to their SPDEF knockdown, morphologically more mesenchymal, counterpart. However, it might also be that the more epithelial-like SPDEF overexpressing cells undergo EMT upon intraperitoneal injection into the mice.

Similar data have been observed in other tumor entities. In breast cancer, EPCAM^{high} cells, which are more epithelial-like than EPCAM^{low} cells have been identified to be more tumorigenic than their EPCAM^{low} counterpart (Saini 2017). Interestingly, we could also show that SPDEF overexpression upregulates EPCAM on protein level (supplementary figure 3).

The finding that the SPDEF OX cells are morphologically more epithelial-like cells was also supported by the results from GSEA analyses which predicted the hallmark gene sets

"HALLMARK_EPITHELIAL_TO_MESENCHYMAL_TRANSITION" to be enriched in both OC12 and OC20 NS control cells as compared to SPDEF KD cells (figure 56 and figure 57) and the gene set "HALLMARK_TGF_BETA_SIGNALING"_to be enriched in OC12 and OC20 SPDEF OX cells as compared to iT2 control cells (figure 56 and figure 57). Further, gene ontology analyses predicted the gene ontology terms "regulation of epithelial cell proliferation" to be enriched in OC12 (FDR = 4.50E-04) and OC20 (FDR = 9.70E-04) SPDEF OX cells (data not shown). Since TGFβ signaling is known to induce EMT (Xu *et al.,* 2009, Katsuno *et al.,* 2013), we also analyzed our microarray data regarding expression of TGFβ signaling promoting and inhibiting genes. We could identify several genes involved in TGFβ signaling that were differentially enriched between SPDEF OX and iT2 control cells. Whereas the TGFβ signaling promoting genes TGFBR2 and TGBR3 were enriched in the iT2 cells, the TGFβ signaling inhibiting genes SMAD6, PMEPA1 and FST were enriched in the SPDEF OX cells (supplementary figure 3). Interestingly, SPDEF expression itself has been shown to be repressed through TGFβ signaling (Gu *et al.,* 2007).

These findings further support our hypothesis that SPDEF OX cells are more epithelial-like and nevertheless, the more tumorigenic population.

In agreement with our data, it has been shown that reduced expression of SPDEF stimulates epithelial-to-mesenchymal transition (EMT) through increased expression of CCL2 in prostate cancer (Tsai *et al.,* 2018). Another study by Gu *et al.* supports the finding that knockdown of SPDEF increases genes involved in EMT (Gu *et al.,* 2007). Further, in bladder carcinoma, SPDEF was demonstrated to modulate the expression of EMT-associated genes (Tsui *et al.,* 2016). In breast cancer, overexpression of SPDEF has been demonstrated to suppress EMT by negatively regulating SLUG (Findlay *et al.,* 2011).

Taken together, we show that knockdown of SPDEF impairs tumor growth in OC20 cells and overexpression of SPDEF increases tumor and ascites formation, as well as number of metastases.

5.3 SPDEF OX increases tumorigenicity in SSEA1$^+$ and SSEA1$^-$ cells

SPDEF OX increases tumorigenicity and colony formation in SSEA1$^+$ and SSEA1$^-$ cells

Since SSEA1$^-$ cells initiated tumors *in vivo* and SPDEF was enriched in this population, we wondered whether we can increase the colony number of SSEA1$^+$ cells by inducing expression of SPDEF in these, thereby rescuing the phenotype of the SSEA1$^+$ cells. At the

same time, we wanted to ascertain whether knockdown of SPDEF in the SSEA1$^-$ cells decreases their colony-forming capacity. Further, we wondered whether we can boost tumor growth *in vivo* in SSEA1$^-$ cells by overexpressing SPDEF.

In the adherent plaque forming assay, overexpression of SPDEF led to an increased colony-formation, both in the SSEA1$^-$ and SSEA1$^+$ cells. The effect, however, was significantly stronger in the SSEA1$^-$ cells. Thus, we speculated that the SSEA1$^-$ cells have a higher intrinsic potential to form colonies upon SPDEF overexpression compared to SSEA1$^+$ cells due to their molecular features. The SSEA1$^+$ cells, however, seem to have a lower potential to form colonies due to a different molecular background. Nevertheless, expression of SPDEF in SSEA1$^+$ cells rescued their phenotype and allowed them to form a similar number of colonies as the control iT2 SSEA1$^-$ cells (figure 48).

The increased colony-forming potential was also reflected in the size of the colonies: SPDEF overexpressing colonies formed bigger colonies in SSEA1$^-$ and SSEA1$^+$ cells. In SSEA1$^+$ cells, however, the difference between iT2 and SPDEF OX was not that big due to one outlier in the iT2 group (figure 48).

When inducing the SPDEF KD in SSEA1$^-$ and SSEA1$^+$ cells, we could decrease the colony-forming potential of the SSEA1$^-$ cells to that of control SSEA1$^+$ cells, thereby demonstrating that SPDEF is indeed responsible for the phenotype of increased colony formation in SSEA1$^-$ cells.

In line with the *in vitro* data of the colony formation assay, overexpression of SPDEF increased tumor growth in SSEA1$^-$ cells *in vivo* as compared to iT2 SSEA1$^-$ cells. However, the iT2 SSEA1$^-$ cells did not start growing out until week 30, which is later than the parental SSEA1$^-$ cells did. This, however, might be due to *in vitro* culture and lentiviral transduction. The cells were at a later passage than the parental SSEA1$^-$ cells when injected into NSG mice. Thus, they might have changed during passaging and lost some of their tumorigenicity. This is further supported by the SPDEF OX SSEA1$^-$ cells which also started growing out later than the parental SSEA1$^-$ cells.

Interestingly, overexpression of SPDEF in SSEA1$^-$ cells equipped them with an initial seeding advantage at the early time points after injection. The SPDEF overexpression might thus be of advantage for the cells during early metastatic spreading from the ovaries to the peritoneum and responsible for the colonization of organs at distant sites.

We further used a second cell line (OC20) to prove that SPDEF OX increases tumorigenicity in SSEA1$^-$ and SSEA1$^+$ cells. And indeed, significantly more tumors formed in the mice

injected with SPDEF OX cells, both in SSEA1$^+$ and SSEA1$^-$ cells.

To ultimately support these data, knockdown of SPDEF in SSEA1$^-$ cells has to be done to prove that the phenotype of increased tumor growth in the SSEA1$^-$ cells is because of SPDEF. Taken together, we showed that SPDEF overexpression can increase colony formation in SSEA1$^-$ and SSEA1$^+$ cells, but is stronger in SSEA1$^-$ cells. Further, SPDEF OX also increased growth of tumor cells and tumor formation *in vivo* both in SSEA1$^+$ and SSEA1$^-$ cells. Thus, the tumorigenic potential of SSEA1$^+$ cells can be rescued by overexpressing SPDEF.

A 15-gene SPDEF target gene signature predicts worse overall survival and is enriched in SSEA1$^-$ cells

We generated a 15-gene signature derived from the top 15 differentially expressed genes between OC12 SPDEF overexpressing and iT2 cells. Overall survival was significantly lower for patients displaying a high expression of the 15-gene SPDEF target gene signature. The verification of the signature in SSEA1$^+$/SSEA1$^-$ cells showed that it was enriched in SSEA1$^-$ cells when performing pooled analysis. Analyzing the enrichment of the signature in a single way, showed that it was clearly enriched in SSEA1$^-$ OC12 and also OC19 cells but not enriched in OC15 and OC20 SSEA1$^-$ cells. Thus, we concluded that the signature has to be optimized. Since the signature was only derived from the OC12 cells, the patient background might be one reason why it is not enriched in all SSEA1$^-$ cells from the other OC cell lines. The generation of a signature from differentially expressed genes of SPDEF overexpressing cells from more than OC cell line might optimize the signature itself and maybe be an even better predictor of survival.

5.4 FOXA2 is enriched in the SPDEF KD cells and impairs tumor growth

FOXA2 is enriched in the SPDEF knockdown population

We identified the transcription factor FOXA2 to be negatively regulated by SPDEF. SPDEF knockdown increased the expression of FOXA2 and overexpression of SPDEF decreased FOXA2 gene and protein expression (figure 61). In line with these data, it has also been shown that SPDEF inhibits FOXA2 expression in other tissues like goblet cells (Chen *et al.,* 2009). Another study also showed that SPDEF knockdown enhanced expression of FOXA2 in human airway epithelial cells (Yu *et al.,* 2010). However, regarding cancer, there are no data

so far demonstrating that SPDEF knockdown increases FOXA2 expression. Thus, we are the first establishing a correlation between SPDEF knockdown and increased expression FOXA2 in cancer.

FOXA2 overexpression decreases colony number in vitro and impairs in vitro and in vivo growth

Since FOXA2 has been described to have tumor suppressive capacities in various cancers including pancreatic and gastric cancer, as well as gliomas (Vorvis et al., 2016, Ding et al., 2017, Li et al., 2017), we hypothesized that the upregulation of FOXA2 due to SPDEF knockdown has tumor suppressive functions and that FOXA2 upregulation in SPDEF knockdown cells is responsible for the impaired tumor growth of these cells.

Indeed, inducible FOXA2 overexpression impaired *in vitro* tumor cell proliferation of OC12 cells and vice versa, knockdown of FOXA2 with two shRNAs increased cell proliferation (figure 63). Although the differences were not huge, they were significant. Regarding the two FOXA2 knockdown cell lines, greater differences might be obtained by optimizing the knockdown efficiencies which were about 30 % (shFOXA2 86208/86209) and 60 % (shFOXA2 86208/306420) only.

Further, inducible overexpression of FOXA2 significantly decreased colony number and size in OC12 and OC20 cells (figure 64). Moreover, *in vivo* tumor growth was significantly impaired in cells overexpressing FOXA2. This effect could be clearly observed when comparing FOXA2 OX and iT2 control cells, however, in the inducible setting, the difference was not significant (figure 66). A big variance between the mice regarding tumor outgrowth might have accounted for this. Further, an insufficient induction of the overexpression via doxycycline in the drinking water of the mice might also have added to the non-significant effect. Moreover, the big variance between the mice might also be caused by the fact that we injected a number of cells which is close to the lowest clonogenic number of cells still giving rise to tumors. Thus, increasing the number of cells injected per mouse, as well as repetition of the experiment with a greater number of mice might give better results with less variance between mice.

Forced expression of FOXA2 has been shown to impair tumorigenicity of glioma cells (Ding et al., 2017). Besides, in pancreatic cancer, FOXA2 deletion increased *in vivo* tumor growth (Vorvis et al., 2016), thereby again demonstrating the tumor suppressive functions of FOXA2 which is in agreement with our data. Interestingly, FOXA2 has also been suggested to be a

target of TGF-β1 and to inhibit EMT in lung cancer thereby acting as a tumor metastasis suppressor (Tang *et al.,* 2011).

Taken together, we concluded that the SPDEF KD cells do not grow *in vivo* because they express increased levels of the tumor suppressor FOXA2.

FOXA2 expression may regulate SPDEF in a feedback loop

Besides identifying FOXA2 expression to be increased upon SPDEF knockdown and to be decreased upon SPDEF overexpression, we observed that FOXA2 overexpression upregulates SPDEF in three OC lines tested. Further, FOXA2 KD decreased SPDEF expression. These data suggest that there might be a negative feedback loop between SPDEF and FOXA2.

FOXA2 expression correlates with increased survival

The analysis of transcriptomic data of serous ovarian cancer patients from four different studies revealed that FOXA2 expression correlated with overall survival (figure 67). Patients displaying high FOXA2 levels had a significantly better overall survival than patients with low FOXA2 expression levels. Median overall survival data showed a great difference ranging from 13 months (FOXA2 low-expressing patients) to 53 months (FOXA2 high expressing patients). These data are in line with findings from other tumor entities: In lung adenocarcinoma, high FOXA2 expression was also correlated to better survival (Basseres *et al.,* 2012). Further, high FOXA2 expression predicted for a significantly better overall survival than low FOXA2 expression in gastric cancer (Zhu *et al.,* 2015).

Since increased FOXA2 expression correlated with an increased overall survival, ovarian cancer patients might either benefit from treatment with agents inducing FOXA2 expression or – since SPDEF was shown to negatively regulate FOXA2 - from SPDEF inhibitors.

Taken together, high FOXA2 expression correlates with better overall survival of HGSOC patients and these might benefit from FOXA2-inducing agents or SPDEF inhibitors.

5.5 Conclusion and model

In this study, we propose a model of tumor-initiating cells in HGSOC and the mechanism how their tumorigenicity is maintained (figure 68). Our findings suggest that SSEA1$^-$ cells are tumor- / metastasis-initiating cells in HGSOC that can give rise to both SSEA1$^-$ and SSEA1$^+$ cells while SSEA1$^+$ cannot. Whereas SSEA1$^+$ cells are supposed to be more transit-amplifying cells that proliferate but die within time, SSEA1$^-$ cells are suggested to be the more stem-like population. In SSEA1$^-$ cells, the transcription factor SPDEF is enriched. SPDEF knockdown decreased the clonogenicity of bulk tumor cells *in vitro* and abolished metastatic tumor growth *in vivo*. Further, overexpression of SPDEF increased the tumorigenicity of SSEA1$^-$ and SSEA1$^+$ cells *in vivo*. SPDEF itself suppresses expression of the transcription factor FOXA2. The anti-tumorigenic effects of FOXA2 were demonstrated by overexpressing FOXA2 which impaired *in vivo* tumor growth. We propose that the transcriptional luminal/epithelial-like programs induced or repressed by SPDEF, as well as those genes changed due to suppressed FOXA2 target gene transcription, lead to an increased survival, clonogenicity and metastatic spread of SSEA1$^-$ SPDEF^{high} FOXA2^{low} cells and thus, ovarian cancer tumor initiation and metastasis.

Taken together, we identified SSEA1$^-$ cells as a tumor-initiating population in HGSOC whose tumorigenicity is mediated via expression of SPDEF which itself decreases expression of the tumor suppressive transcription factor FOXA2.

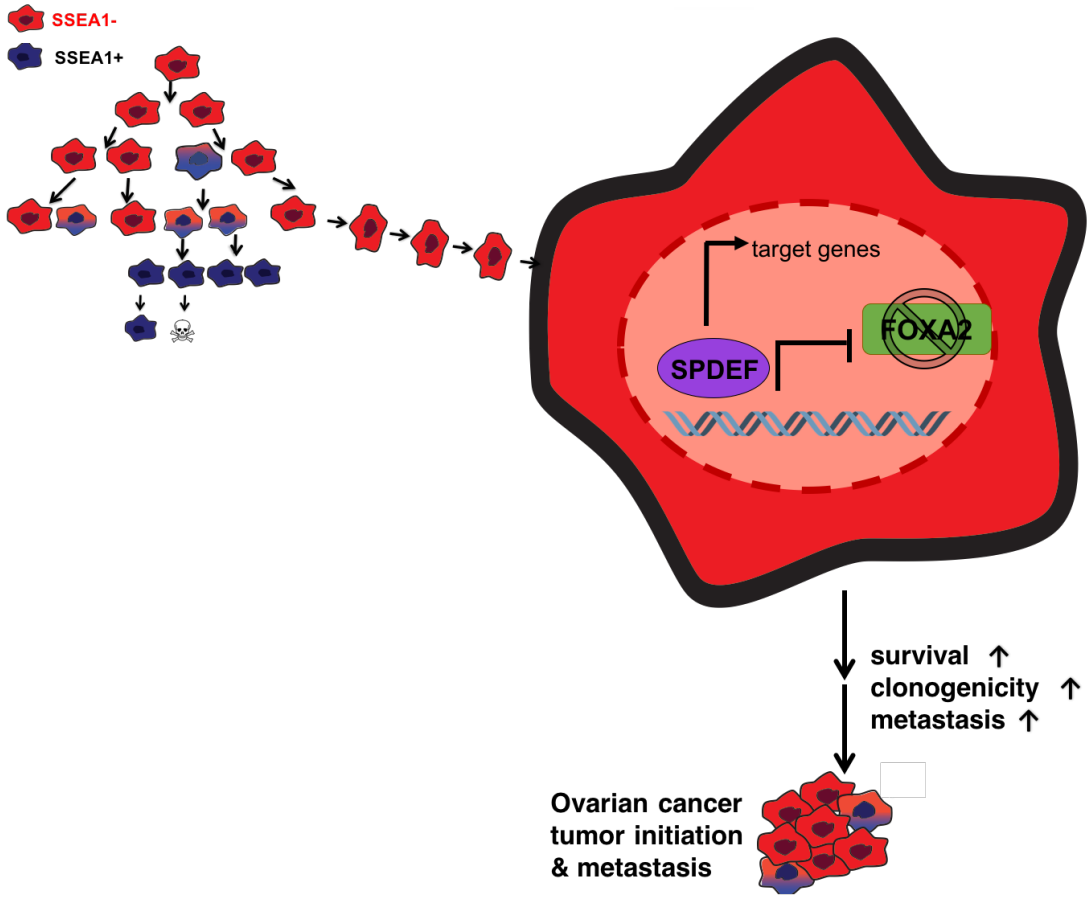

Figure 68: Model: SSEA1$^-$ cells drive tumor initiation and metastasis in high grade serous ovarian cancer due to upregulation of SPDEF and subsequent inhibition of FOXA2.
While SSEA1$^+$ cells are more transit-amplifying cells, which do proliferate but may die within time, SSEA1$^-$ cells can give rise to SSEA1$^+$ cells but also to SSEA1$^-$ ones. In these SSEA1$^-$ cells, the transcription factor SPDEF is enriched which itself decreases FOXA2 expression. The transcriptional programs induced or repressed by SPDEF and FOXA2 target genes lead to an increased survival and clonogenicity of SSEA1$^-$ SPDEF^{high} FOXA2^{low} cells and thus, ovarian cancer tumor initiation and metastasis.

6. BIBLIOGRAPHY

1. Al-Hajj, M., *et al.* (2003). "Prospective identification of tumorigenic breast cancer cells." Proc Natl Acad Sci U S A 100(7): 3983-3988.

2. Allendoerfer, K. L., *et al.* (1999). "Morphological domains of Lewis-X/FORSE-1 immunolabeling in the embryonic neural tube are due to developmental regulation of cell surface carbohydrate expression." Dev Biol 211(2): 208-219.

3. Alvero, A. B., *et al.* (2009). "Molecular phenotyping of human ovarian cancer stem cells unravels the mechanisms for repair and chemoresistance." Cell Cycle 8(1): 158-166.

4. Arber, D. A. and L. M. Weiss (1993). "CD15: A review." Applied Immunohistochemistry 1(1): 17-30.

5. Ashburner, M., *et al.* (2000). "Gene ontology: tool for the unification of biology. The Gene Ontology Consortium." Nat Genet 25(1): 25-29.

6. Balog, C. I., *et al.* (2010). "Mass spectrometric identification of aberrantly glycosylated human apolipoprotein C-III peptides in urine from Schistosoma mansoni-infected individuals." Mol Cell Proteomics 9(4): 667-681.

7. Basseres, D. S., *et al.* (2012). "Frequent downregulation of the transcription factor Foxa2 in lung cancer through epigenetic silencing." Lung Cancer 77(1): 31-37.

8. Bast, R. C., Jr., *et al.* (2009). "The biology of ovarian cancer: new opportunities for translation." Nat Rev Cancer 9(6): 415-428.

9. Basu, M., *et al.* (2015). "Invasion of ovarian cancer cells is induced byPITX2-mediated activation of TGF-beta and Activin-A." Mol Cancer 14: 162.

10. Beck, B. and C. Blanpain (2013). "Unravelling cancer stem cell potential." Nat Rev Cancer 13(10): 727-738.

11. Boiko, A. D., *et al.* (2010). "Human melanoma-initiating cells express neural crest nerve growth factor receptor CD271." Nature 466(7302): 133-137.

12. Bonnet, D. and J. E. Dick (1997). "Human acute myeloid leukemia is organized as a hierarchy that originates from a primitive hematopoietic cell." Nat Med 3(7): 730-737.

13. Brabletz, T., *et al.* (2018). "EMT in cancer." Nat Rev Cancer 18(2): 128-134.

14. Britain, C. M., *et al.* (2018). "Sialylation of EGFR by the ST6Gal-I sialyltransferase promotes EGFR activation and resistance to gefitinib-mediated cell death." J Ovarian Res 11(1): 12.

15. Bu, P., *et al.* (2013). "Asymmetric division: a marker for cancer stem cells in early stage tumors?" Oncotarget 4(7): 950-951.

16. Buchwalter, G., *et al.* (2013). "PDEF promotes luminal differentiation and acts as a survival factor for ER-positive breast cancer cells." Cancer Cell 23(6): 753-767.

17. Cahill, D. P., *et al.* (1998). "Mutations of mitotic checkpoint genes in human cancers." Nature 392(6673): 300-303.

18. Cancer Genome Atlas Research, N. (2011). "Integrated genomic analyses of ovarian carcinoma." Nature 474(7353): 609-615.

19. Capela, A. and S. Temple (2006). "LeX is expressed by principle progenitor cells in the embryonic nervous system, is secreted into their environment and binds Wnt-1." Dev Biol 291(2): 300-313.

20. Chen, G., *et al.* (2009). "SPDEF is required for mouse pulmonary goblet cell differentiation and regulates a network of genes associated with mucus production." J Clin Invest 119(10): 2914-2924.

21. Chen, W. Y., *et al.* (2017). "Loss of SPDEF and gain of TGFBI activity after androgen deprivation therapy promote EMT and bone metastasis of prostate cancer." Sci Signal 10(492).

22. Cheng, W., *et al.* (2005). "Lineage infidelity of epithelial ovarian cancers is controlled by HOX genes that specify regional identity in the reproductive tract." Nat Med 11(5): 531-537.

23. Cheng, X. H., *et al.* (2014). "SPDEF inhibits prostate carcinogenesis by disrupting a positive feedback loop in regulation of the Foxm1 oncogene." PLoS Genet 10(9): e1004656.

24. Chodankar, R., *et al.* (2005). "Cell-nonautonomous induction of ovarian and uterine serous cystadenomas in mice lacking a functional Brca1 in ovarian granulosa cells." Curr Biol 15(6): 561-565.

25. Clark-Knowles, K. V., *et al.* (2007). "Conditional inactivation of Brca1 in the mouse ovarian surface epithelium results in an increase in preneoplastic changes." Exp Cell Res 313(1): 133-145.

26. Coleman, R. L., *et al.* (2017). "Rucaparib maintenance treatment for recurrent ovarian carcinoma after response to platinum therapy (ARIEL3): a randomised, double-blind, placebo-controlled, phase 3 trial." Lancet 390(10106): 1949-1961.

27. Collins, A. T., *et al.* (2005). "Prospective identification of tumorigenic prostate cancer stem cells." Cancer Res 65(23): 10946-10951.

28. Connolly, D. C., *et al.* (2003). "Female mice chimeric for expression of the simian virus 40 TAg under control of the MISIIR promoter develop epithelial ovarian cancer." Cancer Res 63(6): 1389-1397.

29. Ding, B., *et al.* (2017). "Forkhead Box A2 (FOXA2) Inhibits Invasion and Tumorigenesis in Glioma Cells." Oncol Res 25(5): 701-708.

30. Dinulescu, D. M.*, et al.* (2005). "Role of K-ras and Pten in the development of mouse models of endometriosis and endometrioid ovarian cancer." Nat Med 11(1): 63-70.

31. DiPaola, R. S. (2002). "To arrest or not to G(2)-M Cell-cycle arrest : commentary re: A. K. Tyagi et al., Silibinin strongly synergizes human prostate carcinoma DU145 cells to doxorubicin-induced growth inhibition, G(2)-M arrest, and apoptosis. Clin. cancer res., 8: 3512-3519, 2002." Clin Cancer Res 8(11): 3311-3314.

32. Dubeau, L. (1999). "The cell of origin of ovarian epithelial tumors and the ovarian surface epithelium dogma: does the emperor have no clothes?" Gynecol Oncol 72(3): 437-442.

33. Duesberg, P.*, et al.* (1999). "How aneuploidy may cause cancer and genetic instability." Anticancer Res 19(6A): 4887-4906.

34. Dvorak, P.*, et al.* (1998). "Embryoglycan ectodomains regulate biological activity of FGF-2 to embryonic stem cells." J Cell Sci 111 (Pt 19): 2945-2952.

35. El-Naggar, S. M.*, et al.* (2007). "Development of cystic glandular hyperplasia of the endometrium in Mullerian inhibitory substance type II receptor-pituitary tumor transforming gene transgenic mice." J Endocrinol 194(1): 179-191.

36. Feeley, K. M. and M. Wells (2001). "Precursor lesions of ovarian epithelial malignancy." Histopathology 38(2): 87-95.

37. Feldman, B. J. and D. Feldman (2001). "The development of androgen-independent prostate cancer." Nat Rev Cancer 1(1): 34-45.

38. Feldman, R. J.*, et al.* (2003). "Pdef expression in human breast cancer is correlated with invasive potential and altered gene expression." Cancer Res 63(15): 4626-4631.

39. Ferrandina, G.*, et al.* (2008). "Phase III trial of gemcitabine compared with pegylated liposomal doxorubicin in progressive or recurrent ovarian cancer." J Clin Oncol 26(6): 890-896.

40. Findlay, V. J.*, et al.* (2011). "Prostate-Derived ETS Factor Regulates Epithelial-to-Mesenchymal Transition through Both SLUG-Dependent and Independent Mechanisms." Genes Cancer 2(2): 120-129.

41. Fingleton, B. (2017). "Making Cancer Quiescent: SPDEF De-Cycles Beta-Catenin." Gastroenterology 153(1): 10-12.

42. Flesken-Nikitin, A.*, et al.* (2003). "Induction of carcinogenesis by concurrent inactivation of p53 and Rb1 in the mouse ovarian surface epithelium." Cancer Res 63(13): 3459-3463.

43. Fogel, A. I.*, et al.* (2010). "N-glycosylation at the SynCAM (synaptic cell adhesion molecule) immunoglobulin interface modulates synaptic adhesion." J Biol Chem 285(45): 34864-34874.

44. Fong, M. Y. and S. S. Kakar (2009). "Ovarian cancer mouse models: a summary of current models and their limitations." J Ovarian Res 2(1): 12.

45. Foulds, L. (1954). "The experimental study of tumor progression: a review." Cancer Res 14(5): 327-339.

46. Fox, N.*, et al.* (1983). "Immunohistochemical Localization of the Mouse Satge-specific Embryonnic Antigen 1 in Human Tissues and Tumors." Cancer Research 43: 669-678.

47. Fox, N.*, et al.* (1983). "Immunohistochemical localization of the mouse stage-specific embryonic antigen 1 in human tissues and tumors." Cancer Res 43(2): 669-678.

48. Friedman, J. R. and K. H. Kaestner (2006). "The Foxa family of transcription factors in development and metabolism." Cell Mol Life Sci 63(19-20): 2317-2328.

49. Frietsch, J. J.*, et al.* (2010). "Nuclear localisation of LASP-1 correlates with poor long-term survival in female breast cancer." Br J Cancer 102(11): 1645-1653.

50. Gadhoum, S. Z. and R. Sackstein (2008). "CD15 expression in human myeloid cell differentiation is regulated by sialidase activity." Nat Chem Biol 4(12): 751-757.

51. Gallego-Ortega, D.*, et al.* (2015). "ELF5 Drives Lung Metastasis in Luminal Breast Cancer through Recruitment of Gr1+ CD11b+ Myeloid-Derived Suppressor Cells." PLoS Biol 13(12): e1002330.

52. Gao, Y.*, et al.* (2015). "Up-regulation of CD44 in the development of metastasis, recurrence and drug resistance of ovarian cancer." Oncotarget 6(11): 9313-9326.

53. Ghadersohi, A.*, et al.* (2004). "Prostate derived Ets transcription factor shows better tumor-association than other cancer-associated molecules." Oncol Rep 11(2): 453-458.

54. Ghadersohi, A.*, et al.* (2008). "Prostate-derived Ets transcription factor as a favorable prognostic marker in ovarian cancer patients." Int J Cancer 123(6): 1376-1384.

55. Ghadersohi, A.*, et al.* (2007). "Prostate-derived Ets transcription factor (PDEF) downregulates survivin expression and inhibits breast cancer cell growth in vitro and xenograft tumor formation in vivo." Breast Cancer Res Treat 102(1): 19-30.

56. Gooi, H. C.*, et al.* (1981). "Stage-specific embryonic antigen involves alpha 1 goes to 3 fucosylated type 2 blood group chains." Nature 292(5819): 156-158.

57. Gordon, A. N.*, et al.* (2001). "Recurrent epithelial ovarian carcinoma: a randomized phase III study of pegylated liposomal doxorubicin versus topotecan." J Clin Oncol 19(14): 3312-3322.

58. Gregorieff, A.*, et al.* (2009). "The ets-domain transcription factor Spdef promotes maturation of goblet and paneth cells in the intestinal epithelium." Gastroenterology 137(4): 1333-1345 e1331-1333.

59. Greiner, D. L.*, et al.* (1995). "Improved engraftment of human spleen cells in NOD/LtSz-scid/scid mice as compared with C.B-17-scid/scid mice." Am J Pathol 146(4): 888-902.

60. Gu, X.*, et al.* (2007). "Reduced PDEF expression increases invasion and expression of mesenchymal genes in prostate cancer cells." Cancer Res 67(9): 4219-4226.

61. Gunawardane, R. N.*, et al.* (2005). "Novel role for PDEF in epithelial cell migration and invasion." Cancer Res 65(24): 11572-11580.

62. Gyorffy, B.*, et al.* (2012). "Implementing an online tool for genome-wide validation of survival-associated biomarkers in ovarian-cancer using microarray data from 1287 patients." Endocr Relat Cancer 19(2): 197-208.

63. Hakomori, S.*, et al.* (1981). "The hapten structure of a developmentally regulated glycolipid antigen (SSEA-1) isolated from human erythrocytes and adenocarcinoma: a preliminary note." Biochem Biophys Res Commun 100(4): 1578-1586.

64. Haltiwanger, R. S. (2002). "Regulation of signal transduction pathways in development by glycosylation." Curr Opin Struct Biol 12(5): 593-598.

65. Hennen, E. (2011). Diversity and function of Lewis-type glycans in central nervous system development. , Ruhr University Bochum.

66. Hennen, E.*, et al.* (2011). "Structurally distinct LewisX glycans distinguish subpopulations of neural stem/progenitor cells." J Biol Chem 286(18): 16321-16331.

67. Heo, S. H.*, et al.* (2015). "ELK3 Expression Correlates With Cell Migration, Invasion, and Membrane Type 1-Matrix Metalloproteinase Expression in MDA-MB-231 Breast Cancer Cells." Gene Expr 16(4): 197-203.

68. Hirakawa, M.*, et al.* (2014). "Fucosylated TGF-beta receptors transduces a signal for epithelial-mesenchymal transition in colorectal cancer cells." Br J Cancer 110(1): 156-163.

69. Hu, Y. and G. K. Smyth (2009). "ELDA: extreme limiting dilution analysis for comparing depleted and enriched populations in stem cell and other assays." J Immunol Methods 347(1-2): 70-78.

70. International Cancer Genome, C.*, et al.* (2010). "International network of cancer genome projects." Nature 464(7291): 993-998.

71. Ito, M.*, et al.* (2002). "NOD/SCID/gamma(c)(null) mouse: an excellent recipient mouse model for engraftment of human cells." Blood 100(9): 3175-3182.

72. Jabs, J.*, et al.* (2017). "Screening drug effects in patient-derived cancer cells links organoid responses to genome alterations." Mol Syst Biol 13(11): 955.

73. Jang, H.*, et al.* (2012). "O-GlcNAc regulates pluripotency and reprogramming by directly acting on core components of the pluripotency network." Cell Stem Cell 11(1): 62-74.

74. Johnson, T. R.*, et al.* (2010). "Loss of PDEF, a prostate-derived Ets factor is associated with aggressive phenotype of prostate cancer: regulation of MMP 9 by PDEF." Mol Cancer 9: 148.

75. Johnson, W. E.*, et al.* (2007). "Adjusting batch effects in microarray expression data using empirical Bayes methods." Biostatistics 8(1): 118-127.

76. Julien, S.*, et al.* (2011). "Selectin ligand sialyl-Lewis x antigen drives metastasis of hormone-dependent breast cancers." Cancer Res 71(24): 7683-7693.

77. Kallio, M. A.*, et al.* (2011). "Chipster: user-friendly analysis software for microarray and other high-throughput data." BMC Genomics 12: 507.

78. Katoh, M. and M. Katoh (2004). "Human FOX gene family (Review)." Int J Oncol 25(5): 1495-1500.

79. Katsuno, Y.*, et al.* (2013). "TGF-beta signaling and epithelial-mesenchymal transition in cancer progression." Curr Opin Oncol 25(1): 76-84.

80. Kenney-Herbert, E.*, et al.* (2015). "CD15 Expression Does Not Identify a Phenotypically or Genetically Distinct Glioblastoma Population." Stem Cells Transl Med 4(7): 822-831.

81. Kim, C. A.*, et al.* (2001). "Polymerization of the SAM domain of TEL in leukemogenesis and transcriptional repression." EMBO J 20(15): 4173-4182.

82. Kim, I. J.*, et al.* (2014). "HOXB13 regulates the prostate-derived Ets factor: implications for prostate cancer cell invasion." Int J Oncol 45(2): 869-876.

83. Kim, S.*, et al.* (2004). "Maspin expression is transactivated by p63 and is critical for the modulation of lung cancer progression." Cancer Res 64(19): 6900-6905.

84. Kindelberger, D. W.*, et al.* (2007). "Intraepithelial carcinoma of the fimbria and pelvic serous carcinoma: Evidence for a causal relationship." Am J Surg Pathol 31(2): 161-169.

85. Knoblich, J. A. (2008). "Mechanisms of asymmetric stem cell division." Cell 132(4): 583-597.

86. Knowles, B. B.*, et al.* (1982). "Murine embryonic antigen (SSEA-1) is expressed on human cells and structurally related human blood group antigen I is expressed on mouse embryos." Dev Biol 93(1): 54-58.

87. Konstantinopoulos PA*, et al.* (2018). TOPACIO: preliminary activity and safety in patients (pts) with platinum-resistant ovarian cancer in a phase 1/2 study of niraparib in combination with pembrolizumab, SGO Annual Meeting, New Orleans.

88. Kotsopoulos, I. C.*, et al.* (2014). "Serous ovarian cancer signaling pathways." Int J Gynecol Cancer 24(3): 410-417.

89. Kruger, A., *et al.* (2000). "Reduction of breast carcinoma tumor growth and lung colonization by overexpression of the soluble urokinase-type plasminogen activator receptor (CD87)." Cancer Gene Ther 7(2): 292-299.

90. Kurman, R. J. and M. Shih Ie (2008). "Pathogenesis of ovarian cancer: lessons from morphology and molecular biology and their clinical implications." Int J Gynecol Pathol 27(2): 151-160.

91. Lacronique, V., *et al.* (1997). "A TEL-JAK2 fusion protein with constitutive kinase activity in human leukemia." Science 278(5341): 1309-1312.

92. Lanctot, P. M., *et al.* (2007). "The glycans of stem cells." Curr Opin Chem Biol 11(4): 373-380.

93. Lee, J., *et al.* (2006). "Tumor stem cells derived from glioblastomas cultured in bFGF and EGF more closely mirror the phenotype and genotype of primary tumors than do serum-cultured cell lines." Cancer Cell 9(5): 391-403.

94. Lengauer, C., *et al.* (1997). "Genetic instability in colorectal cancers." Nature 386(6625): 623-627.

95. Lengauer, C., *et al.* (1998). "Genetic instabilities in human cancers." Nature 396(6712): 643-649.

96. Li, C., *et al.* (2017). "MicroRNA-187 promotes growth and metastasis of gastric cancer by inhibiting FOXA2." Oncol Rep 37(3): 1747-1755.

97. Liang, S., *et al.* (2009). "Expression of activated PIK3CA in ovarian surface epithelium results in hyperplasia but not tumor formation." PLoS One 4(1): e4295.

98. Lieberoth, A., *et al.* (2009). "Lewis(x) and alpha2,3-sialyl glycans and their receptors TAG-1, Contactin, and L1 mediate CD24-dependent neurite outgrowth." J Neurosci 29(20): 6677-6690.

99. Lin, Y. G., *et al.* (2007). "Curcumin inhibits tumor growth and angiogenesis in ovarian carcinoma by targeting the nuclear factor-kappaB pathway." Clin Cancer Res 13(11): 3423-3430.

100. Liu, Y. C., *et al.* (2011). "Sialylation and fucosylation of epidermal growth factor receptor suppress its dimerization and activation in lung cancer cells." Proc Natl Acad Sci U S A 108(28): 11332-11337.

101. Lo, Y. H., *et al.* (2017). "Transcriptional Regulation by ATOH1 and its Target SPDEF in the Intestine." Cell Mol Gastroenterol Hepatol 3(1): 51-71.

102. Lo, Y. H., *et al.* (2017). "SPDEF Induces Quiescence of Colorectal Cancer Cells by Changing the Transcriptional Targets of beta-catenin." Gastroenterology 153(1): 205-218 e208.

103. Lupia, M. and U. Cavallaro (2017). "Ovarian cancer stem cells: still an elusive entity?" Mol Cancer 16(1): 64.

104. Mahajan, N. (2016). "Signatures of prostate-derived Ets factor (PDEF) in cancer." Tumour Biol 37(11): 14335-14340.

105. Mahajan, N.*, et al.* (2013). "Tumor-suppressive maspin functions as a reactive oxygen species scavenger: importance of cysteine residues." J Biol Chem 288(16): 11611-11620.

106. Marth, J. D. and P. K. Grewal (2008). "Mammalian glycosylation in immunity." Nat Rev Immunol 8(11): 874-887.

107. Matulonis, U. A.*, et al.* (2016). "Ovarian cancer." Nat Rev Dis Primers 2: 16061.

108. Meng, E.*, et al.* (2012). "CD44+/CD24- ovarian cancer cells demonstrate cancer stem cell properties and correlate to survival." Clin Exp Metastasis 29(8): 939-948.

109. Moloney, D. J.*, et al.* (2000). "Fringe is a glycosyltransferase that modifies Notch." Nature 406(6794): 369-375.

110. Moloney, D. J.*, et al.* (2000). "Mammalian Notch1 is modified with two unusual forms of O-linked glycosylation found on epidermal growth factor-like modules." J Biol Chem 275(13): 9604-9611.

111. Morin, P. J. and A. T. Weeraratna (2016). "Genetically-defined ovarian cancer mouse models." J Pathol 238(2): 180-184.

112. Moussa, O.*, et al.* (2009). "PDEF is a negative regulator of colon cancer cell growth and migration." J Cell Biochem 108(6): 1389-1398.

113. Murph, M.*, et al.* (2006). "Of spiders and crabs: the emergence of lysophospholipids and their metabolic pathways as targets for therapy in cancer." Clin Cancer Res 12(22): 6598-6602.

114. Nakayama, F.*, et al.* (2001). "CD15 expression in mature granulocytes is determined by alpha 1,3-fucosyltransferase IX, but in promyelocytes and monocytes by alpha 1,3-fucosyltransferase IV." J Biol Chem 276(19): 16100-16106.

115. Nishihara, S.*, et al.* (2003). "Alpha1,3-fucosyltransferase IX (Fut9) determines Lewis X expression in brain." Glycobiology 13(6): 445-455.

116. Nishiwaki, T.*, et al.* (1998). "Characterization and developmental regulation of proteoglycan-type protein tyrosine phosphatase zeta/RPTPbeta isoforms." J Biochem 123(3): 458-467.

117. Nowell, P. C. (1976). "The clonal evolution of tumor cell populations." Science 194(4260): 23-28.

118. Oettgen, P.*, et al.* (2000). "PDEF, a novel prostate epithelium-specific ets transcription factor, interacts with the androgen receptor and activates prostate-specific antigen gene expression." J Biol Chem 275(2): 1216-1225.

119. Oikawa, T. and T. Yamada (2003). "Molecular biology of the Ets family of transcription factors." Gene 303: 11-34.

120. Orsulic, S.*, et al.* (2002). "Induction of ovarian cancer by defined multiple genetic changes in a mouse model system." Cancer Cell 1(1): 53-62.

121. Oza, A. M.*, et al.* (2015). "Standard chemotherapy with or without bevacizumab for women with newly diagnosed ovarian cancer (ICON7): overall survival results of a phase 3 randomised trial." Lancet Oncol 16(8): 928-936.

122. Ozols, R. F.*, et al.* (2003). "Phase III trial of carboplatin and paclitaxel compared with cisplatin and paclitaxel in patients with optimally resected stage III ovarian cancer: a Gynecologic Oncology Group study." J Clin Oncol 21(17): 3194-3200.

123. Park, J. J.*, et al.* (2012). "Sialylation of epidermal growth factor receptor regulates receptor activity and chemosensitivity to gefitinib in colon cancer cells." Biochem Pharmacol 83(7): 849-857.

124. Perren, T. J.*, et al.* (2011). "A phase 3 trial of bevacizumab in ovarian cancer." N Engl J Med 365(26): 2484-2496.

125. Polyak, K.*, et al.* (2009). "Co-evolution of tumor cells and their microenvironment." Trends Genet 25(1): 30-38.

126. Pujade-Lauraine, E.*, et al.* (2017). "Olaparib tablets as maintenance therapy in patients with platinum-sensitive, relapsed ovarian cancer and a BRCA1/2 mutation (SOLO2/ENGOT-Ov21): a double-blind, randomised, placebo-controlled, phase 3 trial." Lancet Oncol 18(9): 1274-1284.

127. R Core Team (2017). "R: A language and environment for statistical computing. R Foundation for Statistical Computing, Vienna, Austria.". from https://www.r-project.org/.

128. Rajagopalan, H. and C. Lengauer (2004). "Aneuploidy and cancer." Nature 432(7015): 338-341.

129. Rajendran, V. and M. V. Jain (2018). "In Vitro Tumorigenic Assay: Colony Forming Assay for Cancer Stem Cells." Methods Mol Biol 1692: 89-95.

130. Rao, B. R. and B. J. Slotman (1991). "Endocrine factors in common epithelial ovarian cancer." Endocr Rev 12(1): 14-26.

131. Read, T. A.*, et al.* (2009). "Identification of CD15 as a marker for tumor-propagating cells in a mouse model of medulloblastoma." Cancer Cell 15(2): 135-147.

132. Rho, J. H., *et al.* (2014). "Discovery of sialyl Lewis A and Lewis X modified protein cancer biomarkers using high density antibody arrays." J Proteomics 96: 291-299.

133. Rodabaugh, K. J., *et al.* (2007). "Prostate-derived Ets factor is overexpressed in serous epithelial ovarian tumors." Int J Gynecol Pathol 26(1): 10-15.

134. Romero, I. and R. C. Bast, Jr. (2012). "Minireview: human ovarian cancer: biology, current management, and paths to personalizing therapy." Endocrinology 153(4): 1593-1602.

135. Rose, P. G., *et al.* (1998). "Prolonged oral etoposide as second-line therapy for platinum-resistant and platinum-sensitive ovarian carcinoma: a Gynecologic Oncology Group study." J Clin Oncol 16(2): 405-410.

136. Rosen, D. G., *et al.* (2006). "The role of constitutively active signal transducer and activator of transcription 3 in ovarian tumorigenesis and prognosis." Cancer 107(11): 2730-2740.

137. Rudd, P. M., *et al.* (2001). "Glycosylation and the immune system." Science 291(5512): 2370-2376.

138. Sabherwal, Y., *et al.* (2012). "PDEF downregulates stathmin expression in prostate cancer." Int J Oncol 40(6): 1889-1899.

139. Sabherwal, Y., *et al.* (2013). "Epigenetic modifications of prostate-derived Ets transcription factor in breast cancer cells." Oncol Rep 30(4): 1985-1988.

140. Saini, M. (2017). Propagation in vivo and in vitro and Molecular Characterization of Metastasis-initiating Cells from Liquid Biopsies of Breast Cancer Patients, University of Heidelberg.

141. Samanta, A. K., *et al.* (2004). "Overexpression of MEKK3 confers resistance to apoptosis through activation of NFkappaB." J Biol Chem 279(9): 7576-7583.

142. Sasaki, H., *et al.* (1997). "A binding site for Gli proteins is essential for HNF-3beta floor plate enhancer activity in transgenics and can respond to Shh in vitro." Development 124(7): 1313-1322.

143. Scaffidi, P. and T. Misteli (2011). "In vitro generation of human cells with cancer stem cell properties." Nat Cell Biol 13(9): 1051-1061.

144. Schaefer, J. S., *et al.* (2010). "Transcriptional regulation of p21/CIP1 cell cycle inhibitor by PDEF controls cell proliferation and mammary tumor progression." J Biol Chem 285(15): 11258-11269.

145. Schindelin, J., *et al.* (2012). "Fiji: an open-source platform for biological-image analysis." Nat Methods 9(7): 676-682.

146. Schmid, S., *et al.* (2011). "Wnt and hedgehog gene pathway expression in serous ovarian cancer." Int J Gynecol Cancer 21(6): 975-980.

147. Sharrocks, A. D. (2001). "The ETS-domain transcription factor family." Nat Rev Mol Cell Biol 2(11): 827-837.

148. Siegel, R. L.*, et al.* (2018). "Cancer statistics, 2018." CA Cancer J Clin 68(1): 7-30.

149. Singh, S. K.*, et al.* (2003). "Identification of a cancer stem cell in human brain tumors." Cancer Res 63(18): 5821-5828.

150. Sizemore, G. M.*, et al.* (2017). "The ETS family of oncogenic transcription factors in solid tumours." Nat Rev Cancer 17(6): 337-351.

151. Solter, D. and B. B. Knowles (1978). "Monoclonal antibody defining a stage-specific mouse embryonic antigen (SSEA-1)." Proc Natl Acad Sci U S A 75(11): 5565-5569.

152. Solter, D.*, et al.* (1979). "The induction of antigenic changes in a teratocarcinoma stem cell line (F9) by retinoic acid." Dev Biol 70(2): 515-521.

153. Son, M. J.*, et al.* (2009). "SSEA-1 is an enrichment marker for tumor-initiating cells in human glioblastoma." Cell Stem Cell 4(5): 440-452.

154. Spillman, M. A.*, et al.* (2010). "Tissue-specific pathways for estrogen regulation of ovarian cancer growth and metastasis." Cancer Res 70(21): 8927-8936.

155. Stark, G. R. and W. R. Taylor (2004). "Analyzing the G2/M checkpoint." Methods Mol Biol 280: 51-82.

156. Steffan, J. J.*, et al.* (2012). "The transcription factor SPDEF suppresses prostate tumor metastasis." J Biol Chem 287(35): 29968-29978.

157. Steffan, J. J.*, et al.* (2016). "The transcription factor SPDEF suppresses prostate tumor metastasis." J Biol Chem 291(39): 20826.

158. Streit, A.*, et al.* (1990). "Isolation and biochemical characterization of a neural proteoglycan expressing the L5 carbohydrate epitope." J Neurochem 55(5): 1494-1506.

159. Streit, A.*, et al.* (1993). "Interaction of astrochondrin with extracellular matrix components and its involvement in astrocyte process formation and cerebellar granule cell migration." J Cell Biol 120(3): 799-814.

160. Streit, A.*, et al.* (1996). "The Le(x) carbohydrate sequence is recognized by antibody to L5, a functional antigen in early neural development." J Neurochem 66(2): 834-844.

161. Subramanian, A.*, et al.* (2005). "Gene set enrichment analysis: a knowledge-based approach for interpreting genome-wide expression profiles." Proc Natl Acad Sci U S A 102(43): 15545-15550.

162. Szkandera, J.*, et al.* (2013). "Hedgehog signaling pathway in ovarian cancer." Int J Mol Sci 14(1): 1179-1196.

163. Tang, Y.*, et al.* (2011). "FOXA2 functions as a suppressor of tumor metastasis by inhibition of epithelial-to-mesenchymal transition in human lung cancers." Cell Research 21(2): 316-326.

164. Tang, Y.*, et al.* (2011). "FOXA2 functions as a suppressor of tumor metastasis by inhibition of epithelial-to-mesenchymal transition in human lung cancers." Cell Res 21(2): 316-326.

165. ten Bokkel Huinink, W.*, et al.* (1997). "Topotecan versus paclitaxel for the treatment of recurrent epithelial ovarian cancer." J Clin Oncol 15(6): 2183-2193.

166. The Gene Ontology, C. (2017). "Expansion of the Gene Ontology knowledgebase and resources." Nucleic Acids Res 45(D1): D331-D338.

167. Thompson, H. G.*, et al.* (2003). "p62 overexpression in breast tumors and regulation by prostate-derived Ets factor in breast cancer cells." Oncogene 22(15): 2322-2333.

168. Tlsty, T. D. and L. M. Coussens (2006). "Tumor stroma and regulation of cancer development." Annu Rev Pathol 1: 119-150.

169. Tsai, Y. C.*, et al.* (2018). "Androgen deprivation therapy-induced epithelial-mesenchymal transition of prostate cancer through downregulating SPDEF and activating CCL2." Biochim Biophys Acta 1864(5 Pt A): 1717-1727.

170. Tsui, K. H.*, et al.* (2016). "Prostate-derived ets factor represses tumorigenesis and modulates epithelial-to-mesenchymal transition in bladder carcinoma cells." Cancer Lett 375(1): 142-151.

171. Turner, D. P.*, et al.* (2008). "Global gene expression analysis identifies PDEF transcriptional networks regulating cell migration during cancer progression." Mol Biol Cell 19(9): 3745-3757.

172. Turner, D. P.*, et al.* (2011). "Mechanisms and functional consequences of PDEF protein expression loss during prostate cancer progression." Prostate 71(16): 1723-1735.

173. U.S. National Library of Medicine (2018). "https://clinicaltrials.gov/." Retrieved May 16, 2018.

174. Varki, A.*, et al.* (2015). Glycosylation Changes in Cancer. Essentials of Glycobiology. rd, A. Varki, R. D. Cummings et al. Cold Spring Harbor (NY)**:** 597-609.

175. Varki, A.*, et al.* (2009). Glycosylation Changes in Cancer. Essentials of Glycobiology. nd, A. Varki, R. D. Cummings et al. Cold Spring Harbor (NY).

176. Visvader, J. E. (2011). "Cells of origin in cancer." Nature 469(7330): 314-322.

177. Visvader, J. E. and G. J. Lindeman (2012). "Cancer stem cells: current status and evolving complexities." Cell Stem Cell 10(6): 717-728.

178. Vorvis, C.*, et al.* (2016). "Transcriptomic and CRISPR/Cas9 technologies reveal FOXA2 as a tumor suppressor gene in pancreatic cancer." Am J Physiol Gastrointest Liver Physiol 310(11): G1124-1137.

179. Wagner, S. (2013). Identification of tumor-initiating cells in a patient-matched model of serous ovarian carcinoma. Heidelberg, Ruperto Carola University of Heidelberg.

180. Wang, S.*, et al.* (2011). "Synapsin I is an oligomannose-carrying glycoprotein, acts as an oligomannose-binding lectin, and promotes neurite outgrowth and neuronal survival when released via glia-derived exosomes." J Neurosci 31(20): 7275-7290.

181. Wang, Y. C.*, et al.* (2014). "Protein post-translational modifications and regulation of pluripotency in human stem cells." Cell Res 24(2): 143-160.

182. Weigel, D. and H. Jackle (1990). "The fork head domain: a novel DNA binding motif of eukaryotic transcription factors?" Cell 63(3): 455-456.

183. Wolfrum, C.*, et al.* (2004). "Foxa2 regulates lipid metabolism and ketogenesis in the liver during fasting and in diabetes." Nature 432(7020): 1027-1032.

184. Wolfrum, C.*, et al.* (2003). "Insulin regulates the activity of forkhead transcription factor Hnf-3beta/Foxa-2 by Akt-mediated phosphorylation and nuclear/cytosolic localization." Proc Natl Acad Sci U S A 100(20): 11624-11629.

185. Wright, A. J. and P. W. Andrews (2009). "Surface marker antigens in the characterization of human embryonic stem cells." Stem Cell Res 3(1): 3-11.

186. Wu, R.*, et al.* (2007). "Mouse model of human ovarian endometrioid adenocarcinoma based on somatic defects in the Wnt/beta-catenin and PI3K/Pten signaling pathways." Cancer Cell 11(4): 321-333.

187. Xu, J.*, et al.* (2009). "TGF-beta-induced epithelial to mesenchymal transition." Cell Res 19(2): 156-172.

188. Yaghjyan, L. and G. A. Colditz (2011). "Estrogens in the breast tissue: a systematic review." Cancer Causes Control 22(4): 529-540.

189. Yagi, H.*, et al.* (2012). "Lewis X-carrying N-glycans regulate the proliferation of mouse embryonic neural stem cells via the Notch signaling pathway." J Biol Chem 287(29): 24356-24364.

190. Yagi, H.*, et al.* (2010). "Lysosome-associated membrane protein 1 is a major SSEA-1-carrier protein in mouse neural stem cells." Glycobiology 20(8): 976-981.

191. Yan, Q.*, et al.* (2010). "O-fucose modulates Notch-controlled blood lineage commitment." Am J Pathol 176(6): 2921-2934.

192. Yanagisawa, M. (2011). "Stem cell glycolipids." Neurochem Res 36(9): 1623-1635.

193. Yanagisawa, M.*, et al.* (2005). "Characterization of glycoconjugate antigens in mouse embryonic neural precursor cells." J Neurochem 95(5): 1311-1320.

194. Yang, D.*, et al.* (2013). "Integrated analyses identify a master microRNA regulatory network for the mesenchymal subtype in serous ovarian cancer." Cancer Cell 23(2): 186-199.

195. Yang, L. T.*, et al.* (2005). "Fringe glycosyltransferases differentially modulate Notch1 proteolysis induced by Delta1 and Jagged1." Mol Biol Cell 16(2): 927-942.

196. Yu, H.*, et al.* (2010). "Interleukin-13 induces mucin 5AC production involving STAT6/SPDEF in human airway epithelial cells." Cell Commun Adhes 17(4-6): 83-92.

197. Zhang, J.*, et al.* (2012). "CD133 expression associated with poor prognosis in ovarian cancer." Mod Pathol 25(3): 456-464.

198. Zhang, S.*, et al.* (2008). "Identification and characterization of ovarian cancer-initiating cells from primary human tumors." Cancer Res 68(11): 4311-4320.

199. Zhu, C. P.*, et al.* (2015). "The transcription factor FOXA2 suppresses gastric tumorigenesis in vitro and in vivo." Dig Dis Sci 60(1): 109-117.

7. APPENDIX

7.1 Supplementary figures

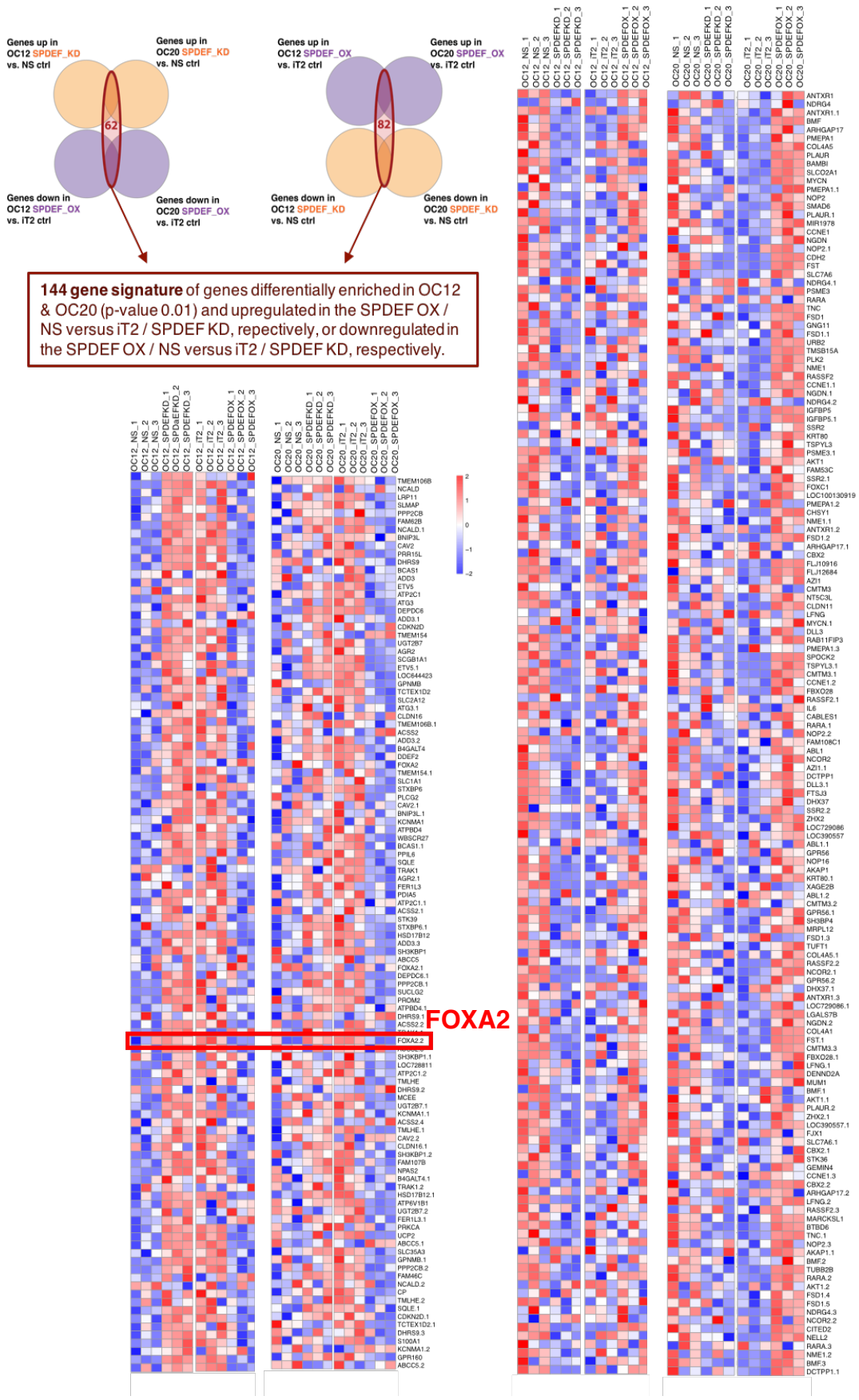

Supplementary figure 1: Heatmaps of the 144-gene signature of differentially enriched genes in OC12 and OC20 cells of SPDEF OX vs. iT2 and SPDEF KD vs. NS.
a) Scheme of how the 144-gene signature of differentially enriched genes in OC12/OC20 SPDEF OX vs. iT2 and SPDEF KD vs NS was generated. (b) Genes enriched in SPDEF KD and iT2 samples of OC12/OC20 (SPDEF low samples). FOXA2 is marked by a red box. (c) Genes enriched in NS and SPDEF OX samples of OC12 / OC20 (SPDEF high samples). red = enriched genes, blue = deriched genes.

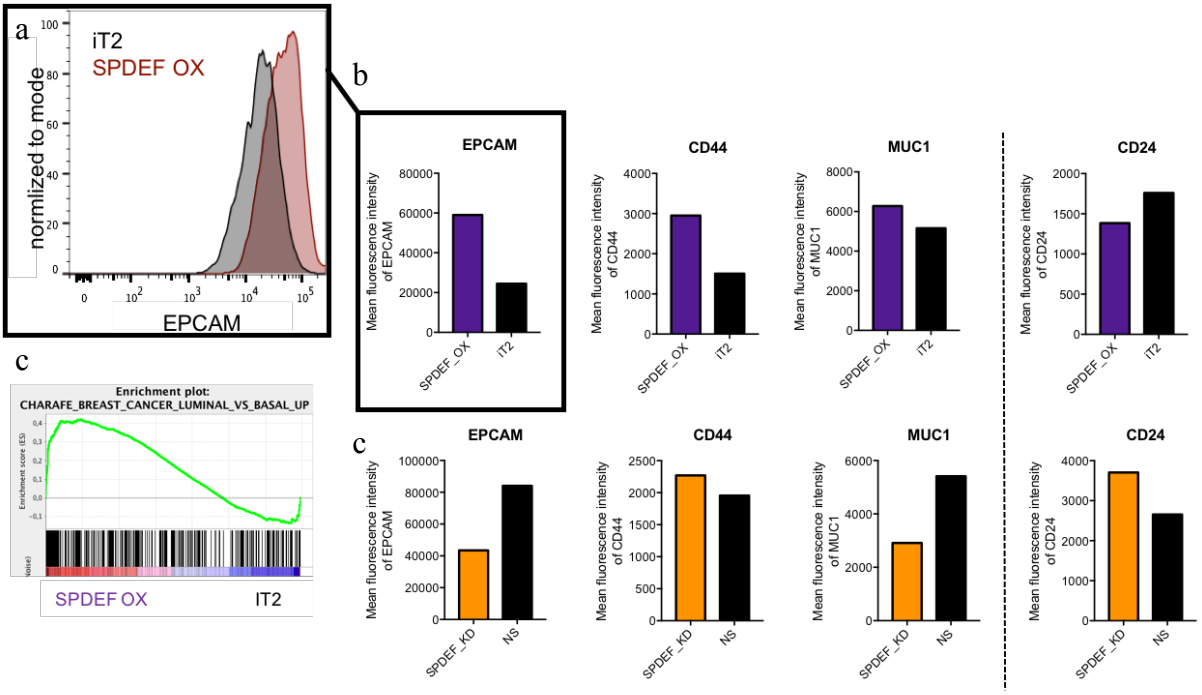

Supplementary figure 2: SPDEF overexpression increases expression of EPCAM, CD44, MUC1 and diminshes CD24 expression while SPDEF knockdown has the opposite effect.
(a) Representative overlay of a FACS staining for EPCAM (red) of SPDEF OX and iT2 control cells (black). (b) Mean fluorescence intensities of SPDEF OX (purple) and iT2 control cells (black) FACS-stained for EPCAM, CD44, MUC1 and CD24. (c) Gene set enrichment plot for genes enriched in SPDEF OX cells compared to iT2 control ones. (d) Mean fluorescence intensities of SPDEF KD (orange) and NS control cells (black) FACS-stained for EPCAM, CD44, MUC1 and CD24. The experiment was performed together with M. Saini.

7. APPENDIX

7.1. Supplementary data

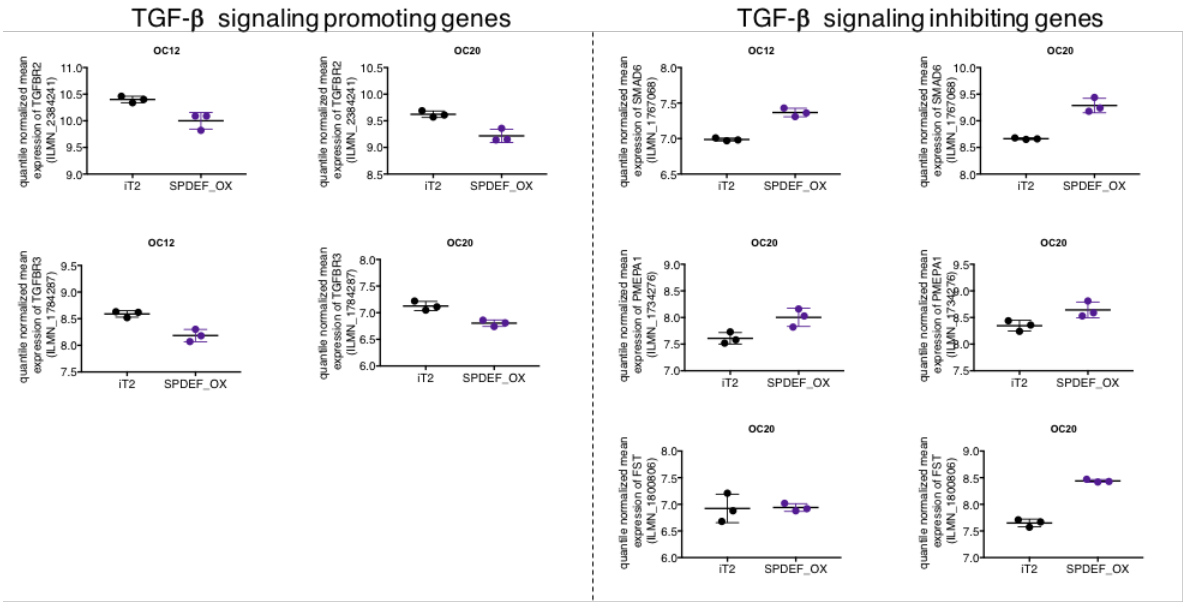

Supplementary figure 3: Expression of TGF-β signaling promoting and inhibiting genes in SPDEF overexpressing and iT2 control cells.
Quantile normalized expression of TGF-β signaling promoting (TGFBR2 and TGRBR3) and inhibiting genes (SMAD6, PMEPA1 and FST) in SPDEF OX (purple) and iT2 control (black) OC12 and OC20 cells.

7.2 Supplementary data

Fiji Macro used for the quantification of adherent colonies.

```
folder = getDirectory("Choose an OUTPUT Directory");
waitForUser("Dear Franzy, please choose the ROIs by pressing t and don't
forget to save ROI set");
NRoi=roiManager("count");
roiManager("Combine");
run("Clear Outside");
run("Subtract Background...", "rolling=1 light");
run("8-bit");
run("Invert");
setAutoThreshold("Default dark");
setThreshold(16, 255);
waitForUser("Dear Franzi, change the threshold if you wish");
for (i=0; i<NRoi; i++)
{
roiManager("Select", i);
run("Analyze Particles...", "size=0.00001-Infinity circularity=0.50-1.00 show=Nothing display exclude
clear summarize");
x=i+1;
saveAs("Measurements", folder+"Results 0"+x+".txt");
wait(100);
}
selectWindow("Summary");
saveAs("text", folder+"Sum"+".txt");
run("Select None");
run("Analyze Particles...", "size=0.00001-Infinity circularity=0.50-1.00 show=Masks");
```

R script for computation of volcano plots

```
> source("https://bioconductor.org/biocLite.R")
> library(plyr)
> library(dplyr)
> library(stringr)
> library(LSD)
> library(tidyr)
> library(reshape2)
> library(Biobase)
> library(genefilter)
> library(geneplotter)
> library(vsn)
> library(ggplot2)
> library(PMA)
> library(gplots)
> library(illuminaHumanv4.db)
> library(stringr)
> library(RColorBrewer)
> library(crossval)
> library(sda)
> library(randomForest)
> library(sva)
> library(pheatmap)
> library(gridExtra)
```

```
> files <- list.files(dataDir, full.names = TRUE, pattern = ".csv" )
> files
> volcanofile <-
read.csv("/Users/zickgraf/Documents/DoktorarbeitFZ/Illumina_Data/SPDEF_OX_KD/R/OC1220/OC1220_SP
DEFKDNS_none001_.csv", header=TRUE)
> head(volcanofile)
> with(volcanofile, plot(log2.FC, -log10(p.value.adjusted), pch=".",  main="Volcano plot", xlim=c(-2,2),
xlab="log2 fold change of SPDEF_KD / NS cells", ylab="-log10(p-value of  SPDEF_KD / NS cells + +1.00E-
06)"))
> with(subset(volcanofile, p.value.adjusted<.01 & log2.FC>0.379), points(log2.FC, -log10(p.value.adjusted),
pch=20, col="grey"))
> with(subset(volcanofile, p.value.adjusted<.01 & log2.FC< -0.379), points(log2.FC, -log10(p.value.adjusted),
pch=20, col="orange"))
> library(calibrate)
> with(subset(volcanofile, p.value.adjusted ==0.0030651 & log2.FC == -0.371666667), textxy(log2.FC, -
log10(p.value.adjusted), labs="FOXA2",offset=0.3, font=2,cex=1.0, pos=4,col="orange"))
> with(subset(volcanofile, p.value.adjusted == 2.00E-06 & log2.FC == 0.521666667), textxy(log2.FC, -
log10(p.value.adjusted), labs="HIF1A",offset=0.3, font=2,cex=1.0, pos=4,col="purple"))

> legend("bottomright", inset=.04, title="Genes enriched with \np-value < 0.01 & FC > 1.3 in",
+        c("SPDEF_KD", "NS"), box.col = "transparent", bty ="n", bg = "transparent", pch=20,
col=c("orange","grey"),horiz=FALSE)
> abline(h = 2, col = "black", lty = 2, lwd = 1) # FDR 0.1 = 1 ; FDR 0.05=1.301029996 p-value 0.01 =2
> abline(v = c(-0.379,0.379), col = "black", lty = 2, lwd = 1)
```

R script for computation of heatmaps

```
>dataDir <- "/Users/zickgraf/Documents/DoktorarbeitFZ/Illumina_Data/GSEA_all42_data/"
>glog2 <- function(x) ((asinh(x)-log(2))/log(2))
>files <- list.files(dataDir, full.names = TRUE, pattern = ".csv" ) #list files of directory
>files
>rawData <- sapply(files, read.csv, USE.NAMES = TRUE)
>str(rawData)
>keytypes(illuminaHumanv4.db)
>phenoData <-na.exclude(rawData$`/Users/zickgraf/Documents/DoktorarbeitFZ/
Illumina_Data/GSEA_all42_data//Phenodata_SSEA1_42_all.csv`)
>expData <- rawData$`/Users/zickgraf/Documents/DoktorarbeitFZ/Illumina_Data/
GSEA_all42_data//SSEA1_all121415181920_42samplesALL.csv`
>View(phenoData)
>View(head(expData))
>rownames(phenoData) <- phenoData$Sample
>featureData <- data.frame(Probe_Id = expData$Probe_Id)
>featureData$Probe_Id <- as.character(featureData$Probe_Id)
>featureSymbols <- select(illuminaHumanv4.db, keys = featureData$Probe_Id,
                    columns = c("SYMBOL", "GENENAME"), keytype = "PROBEID")
>table(duplicated(featureSymbols$PROBEID))
>featureSymbols <- subset(featureSymbols, !duplicated(featureSymbols$PROBEID))
>featureSymbols  <- na.exclude(featureSymbols)
>featureData <- semi_join(featureSymbols, featureData, by = c("PROBEID" = "Probe_Id"))
>rownames(featureData) <- featureData$PROBEID
>rownames(expData) <- expData$Probe_Id
>expData$Probe_Id <- NULL
>expData <- expData[featureData$PROBEID, ]
>sapply(expData, function(x) sum(is.na(x))) #looks for NA in each column
>expData[is.na(expData)] <- 1 #replace them by 1 or 0
>expDataglog2 <- as.matrix(glog2(expData))
>expDataglog2 <- expDataglog2[, rownames(phenoData)]
>HI15XEset <- ExpressionSet(expDataglog2,
```

```
                    phenoData = AnnotatedDataFrame(phenoData),
                    featureData = AnnotatedDataFrame(featureData))
>validObject(HI15XEset)
>Pvars <- rowVars(exprs(HI15XEset))
>HI15XEset <- subset(HI15XEset, !is.na(Pvars))
>topGenes = order(rowVars(exprs(HI15XEset)), decreasing = TRUE)[ seq_len(100) ]
>pheatmap( (exprs(HI15XEset)[topGenes, ] ),
        scale="row",
        cellheight=3,
        cellwidth=12,
        border_color = "NA",
        breaks = NA,
        clustering_method = 'average',
        clustering_distance_cols = 'manhattan',
        show_rownames = F, show_colnames = T,
        labels_col = as.character(pData(HI15XEset)[,"Sample"]),
        annotation_col = pData(HI15XEset)[, c("group","SortedMacs", "Chip",  "cell.line") ]
        )
```

for batch correction:

```
batch = pData(HI15XEset)$SortedMacs
edata <- exprs(HI15XEset)
modCombat = model.matrix(~1, data=pData(HI15XEset))
combat_edata = ComBat(dat=edata, batch=batch, mod=modCombat, par.prior=TRUE, prior.plots=F)
exprs(HI15XEset) <- combat_edata
pData(HI15XEset)
```

for grepping of a specific cell line:

```
HI15XEset_OC12_2 <- HI15XEset[, grep("OC12", pData(HI15XEset)$cell.line)]
pData(HI15XEset_OC12_2)
HI15XEset <- HI15XEset_OC12_2
```

R script for computation of PCA

```
> dataDir <-
"/Users/zickgraf/Documents/DoktorarbeitFZ/Illumina_Data/GSEA_all42_data/SSEA1_all121415181920_42sa
mplesALL"
> glog2 <- function(x) ((asinh(x)-log(2))/log(2))
> files <- list.files(dataDir, full.names = TRUE, pattern = ".csv" ) #list files of directory
> files
> rawData <- sapply(files, read.csv, USE.NAMES = TRUE)
> str(rawData)
> keytypes(illuminaHumanv4.db)
> phenoData <-
na.exclude(rawData$`/Users/zickgraf/Documents/DoktorarbeitFZ/Illumina_Data/GSEA_all42_data/Phenodata_
SSEA1_42_all.csv`)
> expData <-
rawData$`/Users/zickgraf/Documents/DoktorarbeitFZ/Illumina_Data/GSEA_all42_data/SSEA1_all1214151819
20_42samplesALL.csv`
> View(phenoData)
> rownames(phenoData) <- phenoData$Sample
> featureData <- data.frame(Probe_Id = expData$Probe_Id)
> featureData$Probe_Id <- as.character(featureData$Probe_Id)
> featureSymbols <- select(illuminaHumanv4.db, keys = featureData$Probe_Id,
                    columns = c("SYMBOL", "GENENAME"), keytype = "PROBEID")
> featureData <- semi_join(featureSymbols, featureData, by = c("PROBEID" = "Probe_Id"))
> expDataglog2 <- expDataglog2[, rownames(phenoData)]
```

```
> HI15XEset <- ExpressionSet(expDataglog2,
                      phenoData = AnnotatedDataFrame(phenoData),
                      featureData = AnnotatedDataFrame(featureData))
> validObject(HI15XEset)
> HI15XEset_OC12_2 <- HI15XEset[, grep("OC12", pData(HI15XEset)$cell.line)]
> pData(HI15XEset_OC12_2)
> HI15X_CBT <- HI15XEset_OC12_2
> ntop <- 100
> Pvars <- rowVars(exprs(HI15X_CBT))
> select <- order(Pvars, decreasing = TRUE)[seq_len(min(ntop,length(Pvars)))]
> PCA <- (prcomp(t(exprs(HI15X_CBT)[select, ]), scale = F))
> percentVar <- round(100*PCA$sdev^2/sum(PCA$sdev^2),1)
> summary(PCA)
> dataGG = data.frame(PC1 = PCA$x[,1], PC2 = PCA$x[,2],
                PC3 = PCA$x[,3], PC4 = PCA$x[,4],
                Type = pData(HI15X_CBT)$group,
                Cell.line = pData(HI15X_CBT)$cell.line)
> PCA1 = (qplot(PC1, PC2, data = dataGG, color =  Type,
           main = "PC1 vs PC2, top Var, H015 PDAC Xenografts", size = I(4), label=Cell.line, geom = "point")
      + labs(x = paste0("PC1, VarExp:", round(percentVar(Pujade-Lauraine et al., ),4)),
           y = paste0("PC2, VarExp:", round(percentVar(Pujade-Lauraine et al., ),4)))
      + scale_colour_brewer(type="qual", palette=6))
> PCA2 = (qplot(PC1, PC2, data = dataGG, color =  Type,
           main = "PC1 vs PC2, top Var, H015 PDAC Xenografts", size = I(3), label=Cell.line, geom = "text")
      + labs(x = paste0("PC1, VarExp:", round(percentVar(Pujade-Lauraine et al., ),4)),
           y = paste0("PC2, VarExp:", round(percentVar(Pujade-Lauraine et al., ),4)))
      + scale_colour_brewer(type="qual", palette=6))
> grid.arrange(PCA1, PCA2, ncol = 2)
```

7.3 List of Abbreviations

A	
A	Area
A647	Alexa Fluor 647
AdCre	adenovirus cyclization recombination
APC	allophycocyanin
Asc	ascites
ATOH1	atonal basic-helix-loop-helix transcription factor 1
B	
BH	Benjamini-Hochberg
BIS-TRIS	di-tris(hydroxymethyl)aminomethane
BRCA1/2	breast cancer type 1/2 susceptibility gene
BSA	bovine serum albumin
C	
Ca_2Cl	calcium chloride
CA125	cancer antigen 125
CCL2	chemokine C-C ligand 2
CD11b	cluster of differentiation 11b
CD15	cluster of differentiation 15
CD151	cluster of differentiation 151
CD24	cluster of differentiation 24
CD44	cluster of differentiation 44
CI	confidence interval
c-Met	tyrosine-protein kinase Met
CSC	cancer stem cell
D	
DNA	deoxyribonucleic acid
DMEM/F12	Dulbecco's Modified Eagle Medium / Nutrient mixture F12
E	
EDTA	ethylenediaminetetraacetic acid
EdU	5-ethynyl-2'deoxyuridine
EGF	epidermal growth factor
ELDA	extreme limiting dilution analyses
EMT	epithelial-to-mesenchymal transition
EPCAM	epithelial cell adhesion molecule
ETS	E-twenty-six family
F	
FACS	fluorescence-activated cell sorting
FC	fold change
FDR	false discovery rate
FGF	fibroblast growth factor 2
FIGO	International Federation of Gynecology and Obstetrics

FITC	fluorescein isothyocyanate
FSC-A	forward scatter area
FSC-W	forward scatter width
FSHR	follicle-stimulating hormone receptor
FOXA2	Forkhead box protein A2

G

GFP	green fluorescent protein
GSEA	gene set enrichment analysis
GSH	glutathione

H

h	human / hours
H	Height
H2B – GFP	histone H2B – green fluorescent protein
H2kd	class I major histocompatibility antigen H2kd
HBS	HEPES-buffered saline
HCL	hydrochloride
HEK	human embryonic kidney cells 293
HEPES	4-2-hydroxyethyl-1-piperazineethanesulfonic acid
HGSOC	high-grade serous ovarian cancer
HR	hazard ratio
HRP	horseradish peroxidase

I

IGFR3	insulin-like growth factor receptor 3
i.p.	intraperitoneal
IRES	internal ribosome entry site
iT2	IRES-tdtomato 2

J

JAK2	Janus kinase 2

K

KD	knockdown
Ki67	antigen Ki67

L

l	liter
LB	lysogeny brooth

M

m	mouse
MACS	magnetic activated cell sorting
MAPK	mitogen-activated protein kinase
MES	2-(N-morpholino)ethanesulfonic acid

mg	milligram
MISIIR	Müllerian inhibiting substance type II receptor
ml	milliliter
mM	millimolar
MOPS	3-(N-morpholino)propanesulfonic acid
mTOR	mammalian target of rapamycin

N

N_2	nitrogen
Na_2HPO_4	disodium phosphate
NaCl	sodium chloride
NaOH	sodium hydroxide
NF-κB	nuclear factor kappa B
NS	non-silencing
NSG	NOD.Cg-Prkdc^{scid} *Il2rg*^{tm1Wjl}

O

OC	ovarian cancer
O-GlcNac	O-linked β-N-acetylglucosamine
OSE	ovarian surface epithelium
OX	overexpression

P

PARP	poly ADP-ribose polymerase
PB	Pacific Blue
PBS	phosphate buffered saline
PEB	PBS-EDTA-BSA buffer
PCR	Polymerase chain reaction
PD-1	programmed cell death protein 1
PI	propidium iodide
PNT	pointed domain

Q

qPCR	Quantitative polymerase chain reaction

R

RIPA	radioimmunoprecipitation assay buffer
RNA	ribonucleic acid
RQ	relative quantification
RT	room temperature

S

SAM	sterile alpha motif
SD	standard deviation
SDS	sodium dodecyl sulfate
SDS-PAGE	sodium dodecyl sulfate polyacrylamide gel electrophoresis
SEM	standard error of the mean

SOC	serous ovarian cancer
SPDEF	SAM-pointed domain ETS-containing factor
SSC	sideward scatter
SSEA1	Stage-specific embryonic antigen 1
SSEA3/4	Stage-specific embryonic antigen 3/4
STIC	serous intraepithelial carcinoma lesions
SV40 Tag	Simian Vacuolating 40 T antigen

T

TAE	Tris-acetate-EDTA
TBS	Tris-buffered saline
TBS-T	Tris-buffered saline with tween
tdtomato	tandem dimer tomato
TIC	tumor-initiating cell
TNM	classification of malignant tumors: tumor (T), lymph node (N), metastasis (M)
TP53	tumor protein 53
TRIS	tris(hydroxymethyl)aminomethane
TRA-1-60	tumor resistance antigen 1-60
TRA-1-81	tumor resistance antigen-1-81

U

µg	microgram
µl	microliter
ULA	ultra low attachment
µM	micromolar

V

VEGF	vascular endothelial growth factor
VEGFR2	vascular endothelial growth factor receptor 2

W

WT1	Wilms Tumor 1

7.4 List of figures

7.5 List of tables

7.6 List of supplementary figures

CONTRIBUTIONS

R computing was performed with the kind help of Felix Geist and Manuel Reitberger.

Immunohistochemical stainings were performed by Vanessa Vogel and Ornella Kossi.

Mouse experiments were performed together with and mostly measured by Corinna Klein.

The experiment in supplementary figure 3 was performed together with Massimo Saini.

ACKNOWLEDGEMENTS

My biggest thank you goes to **Dr. Martin Sprick:** Thank you for always believing in me and my ideas and allowing me to persuade my research independently! I am so happy that you allowed me to join your group and to take up this project. Thanks for all the times I knocked on your door and you had an open ear for discussions - no matter how much we got lost in detail or tried to convince each other of our opinions. It was always fun and I learned so much about how to think in a scientific way and how to be critical towards data. Most importantly, we shared our love for science which resulted in many exciting experiments. Thank you for your supervision, trust but also the freedom to develop and follow my own scientific ideas which helped me becoming the scientist I am now.

I would also like to thank **Prof. Andreas Trumpp** for giving me the opportunity to pursue my thesis in his lab. Thank you for your trust and freedom to develop my own project and push my own ideas. It was a pleasure to discuss science with you and to get inspired by your ideas. I am very grateful for your support and encouragement. The DKFZ and especially HI-STEM were the best working environment I could imagine for performing my Ph.D. work, both scientifically and regarding the international environment.

I would also like to thank **Dr. Thomas Hofmann** for being my second referee and **Prof. Thomas Holstein** and **Prof. Karin Müller-Decker** for being part of my thesis committee.

Further, I would like to thank **Dr. Thomas Hofmann** and **Dr. Christoph Springfeld** for having been members of my TAC committee.

I would like to thank the METICS: **Lisa Becker, Elisa Espinet-Hernandez, Felix Geist, Corinna Klein, Ornella Kossi, Sarah-Jane Neuberth, Elisa Noll, Manuel Reitberger, Massimo Saini, Vera Thiel, Vanessa Vogel and Roberto Würth.** Thank you for being our METICS family – without you this thesis would not have been possible! Thank you for the humor with which we took good and bad days, thanks for always having an open ear for questions and thank you to all of you who supported me in any way.
Special thanks I would like to express to **Corinna Klein** for having put so much effort into taking care of and measuring my mouse experiments. Also for all the other technical help and just being who you are! I would also like to express my gratitude to **Felix Geist** and **Manuel Reitberger** for helping me out with R programming and teaching me the basics of the scripts they wrote. Thanks a lot! **Dr. Elisa Espinet-Hernandez** thank you for teaching me my first spanish words with our notepads and for

making me proud by winning the german course competition! I would also like to thank you for always having an open ear and being eager to discuss ideas or experimental questions. **Sarah-Jane Neuberth**, thank you for joining our group and taking over parts of the SPDEF project - I am sure we will get further inspiring data from you! Thank you **Lisa Becker, Elisa Noll, Vera Thiel** and **Roberto Würth** for always discussing science with me and having a smile on your faces! Thank you **Ornella Kossi** and **Vanessa Vogel** for taking care of all the immunohistochemical stainings.

I would also like to express my happiness about having been in the best office and working together with the most amazing colleagues and friends I could imagine. Thank you, **Jacob Insua-Rodriguez**, **Maren Pein** and **Tsunaki Hongu** for making the last years so colorful, thank you for all the amusing lunch and coffee - as well as "bakery" breaks we had and thank you for all the "just chatting". Your contributions to this thesis go far beyond sharing office and lab space.
Maren Pein thank you for standing by my side when I needed it most! **Jacob-Insua-Rodriguez**, thank you for being one of the funniest persons I have ever met (Scrunchy ;))! **Tsunaki Hongu**, it was a pleasure to meet you and I hope to see you some day in Japan!

I would also especially like to thank **Natasha Anstee, Thomas Berger, Kristin Decker, Megan Druce, Mattia Falcone, Julius Gräsel**, **Pablo Hernández-Malmierca, Chris Hirche**, **Camille Lowy** and **Angela Riedel** in addition to all the people already mentioned for having so much fun together and sharing some special evenings and party nights in Heidelberg. It was a pleasure to meet you, hang out with you and become friends!

I would also like to thank the former lab members **Dr. Steve Wagner** and **Corinna Köhler** for having been working on the ovarian cancer project before and for all the effort you put into it.

Carsten Bahr, I will never forget our trip to Lucca, Italy. Traveling together with you, missing trains, kind of bribing taxi drivers, nearly missing airplanes and then being suspected to be a terrorist in the plane made this conference very special for me ☺.

I would like to thank all other people in HI-STEM for making the laboratory such a pleasureful environment to work in. It was always fun to discuss science with you and have relaxing lunch get-togethers. Also thank you for sharing reagents! You are a great crowd – both scientifically and personally!

I would also like to thank **Marina Gilke**, **Erika Krückel** and **Dagmar Wolf** for all their administrative support.

Finally, I would like to thank my family: I am exceptionally grateful to have a brother like **Alexander** who always cheers me up and makes me laugh when I need it most. Thank you for being yourself. Most importantly, I want to thank my parents, **Ilona** and **Klaus**, for their constant support and their encouragement! You always helped me in reaching my goals. With your love, you backed me up in times I needed it most. Thanks for always believing in me!